Effect of ausforming on the microstructure and transformation kinetics of a medium carbon carbide-free bainitic steel

by

Muftah ZORGANI

MANUSCRIPT-BASED THESIS PRESENTED TO ÉCOLE DE TECHNOLOGIE SUPÉRIEURE IN PARTIAL FULFILLMENT FOR THE DEGREE OF DOCTOR OF PHILOSOPHY Ph.D.

MONTREAL, 17 NOVEMBER 2021

ÉCOLE DE TECHNOLOGIE SUPÉRIEURE
UNIVERSITÉ DU QUÉBEC

BOARD OF EXAMINERS (THESIS PH.D.)

THIS THESIS HAS BEEN EVALUATED

BY THE FOLLOWING BOARD OF EXAMINERS

Mr. Mohammad Jahazi, Thesis Supervisor
Department of Mechanical Engineering, École de technologie supérieure

Mr. Carlos Garcia-Meteo, Thesis Co-supervisor
National Center for Metallurgical Research (CENIM-CSIC)

Mr. Ammar B. Kouki, President of the Board of Examiners
Department of Electrical Engineering, École de technologie supérieure

Mr. Vladimir Brailovski, Member of the jury
Department of Mechanical Engineering, École de technologie supérieure

Mr. Ricardo Zednik, Member of the jury
Department of Mechanical Engineering, École de technologie supérieure

Mr. Thomas Sourmail, External Evaluator
Ascometal (CREAS), Swiss Steel Group

THIS THESIS WAS PRESENTED AND DEFENDED

IN THE PRESENCE OF A BOARD OF EXAMINERS AND PUBLIC

<DEFENCE DATE OF THE THESIS>

AT ÉCOLE DE TECHNOLOGIE SUPÉRIEURE

ACKNOWLEDGMENT

EFFET DE L'AUSFORMATION SUR LA MICROSTRUCTURE ET LA CINÉTIQUE DE TRANSFORMATION D'UN ACIER BAINITIQUE SANS CARBURE

Muftah ZORGANI

RESUME

Les aciers à haute résistance, caractérisés par une excellente combinaison de propriétés Les aciers à haute résistance, caractérisés par une excellente combinaison de propriétés mécaniques, telles que la ductilité et la formabilité, avec une soudabilité et un coût satisfaisant sont en demande continue dans la plupart des industries, en particulier l'industrie automobile, où la réduction du poids des véhicules est un moyen important d'améliorer à la fois la consommation du carburant ainsi que l'efficacité et la sécurité des passagers. Une nouvelle génération d'aciers bainitiques nanostructurés à haute teneur en carbone-silicium, connue sous le nom d'aciers bainitique sans carbure (CFB), a été développée pour répondre à la demande ci-dessus. Cependant, l'acier CFB nanostructuré à haute teneur en carbone doit être traité thermiquement, parfois pendant plusieurs jours, pour atteindre les caractéristiques structurelles microscopiques requises. En outre, les inconvénients d'une teneur élevée en carbone sont des problèmes de soudabilité, où des fissures peuvent se développer dans les zones affectées par la chaleur en raison de la formation de martensite non trempée. Dans ce contexte, l'acier CFB nanostructuré à faible ou moyen carbone pourrait être une excellente alternative car il pallie les lacunes des aciers CFB nanostructurés à haut carbone. Cependant, l'obtention de CFB nanostructurés dans de l'acier à faible et moyen carbone peut être difficile car la réduction de la teneur en carbone de l'acier augmente la température de démarrage de la martensite et diminue la différence entre les températures de démarrage de la bainite et de la martensite, ce qui entraîne finalement la perte des avantages de la transformation de la bainite préformée à basse température.

Parmi les paramètres importants qui contrôlent l'épaisseur des lamelles de la ferrite bainitique, il y a la résistance de l'austénite à partir de laquelle la bainite se développe et la force motrice de la transformation austénite-bainite. Par conséquent, les traitements thermomécaniques tels que l'ausformage peuvent être une solution possible pour surmonter les limitations de l'utilisation d'un acier à haute teneur en carbone. L'écrouissage de l'austénite, dû à la déformation avant la transformation bainitique, résiste à l'épaississement des lamelles de ferrite bainitique. En outre, la cinétique de transformation bainitique, la morphologie de la microstructure et la stabilité de l'austénite résiduelle peuvent être affectées. Par conséquent, afin d'atteindre les objectifs ci-dessus, une compréhension plus fondamentale des mécanismes impliqués dans l'évolution de la microstructure résultant du processus d'ausformage dans les aciers à teneur moyenne en carbone élevé est nécessaire. En particulier, l'impact de l'ausformage sur la transformation bainitique et les caractéristiques des lattes bainitiques doivent être compris et liés aux paramètres d'ausformage.

Le présent projet de thèse vise à répondre à la question ci-dessus en vue de déterminer à terme les conditions d'ausformage optimales afin d'obtenir des plaques bainitiques de taille

nanométrique dans un acier à teneur moyenne en carbone et à haute teneur en Si. À cette fin, trois objectifs majeurs ont été identifiés : La première partie de l'étude détaille comment la stabilité de l'austénite résiduelle déformée est modifiée en fonction de l'importance de la déformation à 600°C avant la transformation bainitique isotherme à 325 à 400°C. L'analyse a montré que le principal facteur contribuant à la stabilité de l'austénite conservée était la choix de la température isotherme bainitique, quel que soit le pourcentage de déformation. Pour l'acier étudié, la transformation bainitique au-dessus de Ms et en dessous de 350°C était la température seuil au-dessus de laquelle l'austénite résiduellee dans la matrice CFB se décomposait en martensite de façon importante à mesure que le pourcentage de déformation augmentait. La microstructure CFB obtenue à 325°C avait la stabilité thermique d'austénite conservée la plus élevée parmi les autres températures de transformation bainitique.

Dans la deuxième partie de l'étude, l'anisotropie dans la morphologie de la CFB est corrélée à la déformation de plasticité de transformation (TP) en fonction de la température d'ausforming (au-dessus ou en dessous de la température de début de bainite, (Bs). Le changement microstructural observé par SEM et l'analyse EBDS a été comparé à l'évolution des déformations TP calculées par les déformations axiales et radiales pendant la transformation bainitique à 325°C après déformation de l'austénite à 600, 400 et 325°C. L'ausforming à 600°C a eu un effet limité sur les changements microstructuraux et les déformations TP et comparable l'état isotherme pur. Un alignement dans les plaques de ferrite bainitique a été observé lorsqu'une déformation plastique compressive a été appliquée en dessous de Bs. La déformation TP s'est intensifiée avec un alignement sévère dans la microstructure lorsque l'ausforming a été appliqué à la température de transformation isothérmique (325°C). morphologie avec ~100 nm d'épaisseur de plaques de ferrite bainiitc a été obtenue et la dureté a atteint un niveau similaire à celui d'un état martensitique (~550 HV).

Enfin, la réponse de la microstructure CFB au processus de revenu, obtenue via des conditions non ausformées et ausformées, a été étudiée. Cela a été fait afin de déterminer les mécanismes sous-jacents des changements dilatométriques et microstructuraux observés pour le revenu non isotherme à 600°C, et revenu isotherme à 400 et 500°C pendant 1 heure. La microstructure avec une morphologie plus épaisse, qui a été produite par une transformation isotherme pure, c'est-à-dire sans ausformage préalable, a montré des changements dilatométriques minimes pour toutes les températures de revenu examinées. De plus, l'examen MEB a révélé un épaississement dans les lamelles de ferrite bainitique qui a conduit à une réduction de la dureté. D'autre part, une contraction du signal dilatométrique a été observée dans la microstructure bainitique ausformée au début de l'étape de chauffage de la trempe isotherme à environ 400°C. Cette contraction était associée au début des précipitation de la cémentite. Après que la température de revenu ait atteint 500°C, la contraction était plus perceptible et était liée à la formation de précipités de cémentite résultant de la décomposition de la ferrite bainitique et/ou de l'austénite conservée sous forme de film qui pourraient être révélés par des examens MEB et XRD. La présence de ces précipités empêche le grossissement de la ferrite bainitique, produisant ainsi des niveaux de dureté similaires à ceux de l'état non revenu.

EFFECT OF AUSFORMING ON THE MICROSTRUCTURE AND TRANSFORMATION KINETICS OF A MEDIUM CARBON CARBIDE-FREE BAINITIC STEEL

Muftah ZORGANI

ABSTRACT

High-strength steels, characterized by an excellent combination of mechanical properties, such as ductility and formability, with satisfactory weldability and cost, are in continuous demand in most industries, especially the automotive industry, where reducing vehicle weight is an important means of improving both fuel efficiency and passenger safety. A new generation of nanostructured bainitic steels with high carbon-silicon content, known as carbide-free bainitic ferrite (CFB), has been developed to meet the above demand. However, high-C nanostructured CFB steel needs to be heat-treated, sometimes for several days, to attain the required microscopic structural features. Furthermore, the drawbacks of high carbon content are weldability problems, where cracks can be developed in the heat-affected zones due to the formation of untempered martensite. In this context, low- or medium-C nanostructured CFB steel could be an excellent alternative as it overcomes the shortcomings of high-C nanostructured CFB steels. However, obtaining nanostructured CFB in low- and medium-C steel can be challenging because reducing the steel's carbon content increases the martensite start temperature and diminishes the difference between bainite and martensite start temperatures, ultimately resulting in losing the benefits of performing bainite transformation at a low temperature.

Among the prominent parameters that control the bainitic ferrite plate thickness is the strength of the austenite from where the bainite grows and the driving force of the transformation. Therefore, thermomechanical treatments such as ausforming can be a possible solution to overcome the limitations of using high carbon steel. The work hardening of supercooled austenite, owing to deformation prior to bainite transformation, resists the thickening growth of bainitic ferrite plates. Besides, the kinetics of bainite transformation, microstructure morphology, and retained austenite stability can be affected. Therefore, in order to achieve the above objectives, a more fundamental understanding of the mechanisms involved in the evolution of the microstructure as a result of the ausforming process in medium-C high Si steels is required. In particular, the impact of ausforming on bainitic transformation and the characteristics of bainitic laths needs to be understood and related to the ausforming parameters.

The present Ph.D. project aims to address the above question with the view to ultimately determine optimum ausforming conditions in order to obtain nanosized bainitic plates in a medium carbon high Si steel. To this end, three major objectives were identified: The first part of the study provides the details of how the stability of deformed retained austenite was modified according to the amount of deformation at 600 °C prior to isothermal bainitic

transformation at 325 to 400 °C. The analysis showed that the main factor contributing to retained austenite's stability was bainitic isothermal temperature regardless of percent deformation. For the studied steel, bainitic transformation above M_S and below 350 °C was the threshold temperature above which the retained austenite within the CFB matrix decomposed dramatically to martensite as percent deformation increased. CFB microstructure obtained at 325 °C had the highest retained austenite thermal stability among other bainite transformation temperatures.

In the second part of the study, the anisotropy in the morphology of CFB is correlated to the transformation plasticity strain (TP) as a function of ausforming temperature (above or below bainite start temperature, (B_S). The microstructural change observed by SEM and EBDS analysis were compared with TP strains evolution calculated by axial and radial strains during bainite transformation at 325 °C after deforming supercooled austenite at 600, 400, and 325 °C. Ausforming at 600 °C had a limited effect on microstructural changes and TP strains and comparable with the pure isothermal condition. An alignment in bainitic ferrite plates was observed when a compressive plastic deformation was applied below B_S. The TP strain intensified with severe alignment in the microstructure when the ausforming was applied at the isothermal transformation temperature (325 °C). Moreover, nanostructured morphology with ~100 nm bainitic ferrite plate thickness was obtained, and the hardness reached a level similar to that of a martensitic state (~550 HV).

Finally, the response of the CFB microstructure to tempering process, obtained via pure isothermal transformation (P-bainite), i.e., no deformation applied prior to bainitic transformation, and ausforming followed by isothermal transformation (A-bainite), was investigated. The aim of this study was done in order to determine the underlying mechanisms of observed dilatometric and microstructural changes during isothermal tempering at 400 and 500 °C. The outcome of this investigation showed that the P-bainite condition had minimal dilatometric changes for all examined tempering temperatures. In addition, no microstructural changes, such as cementite precipitation, revealed either by metallography or XRD examination, expect a mild increase in bainitic ferrite plats by about 20%. Consequently, the hardness level before and after tempering has not changed much (6% decrease). Likewise, ausformed sample (A-bainite) showed minimum dilatometric and microstructural change during tempering at 400 °C.

On the other hand, a large contraction in dilatometric signal was observed in the ausformed bainitic microstructure that tempered at 500 °C. The change in dilatation started at the early stage of the heating step at around 400 °C. The observed contraction was linked to cementite precipitation due to either decomposition of bainitic ferrite and/or film-like retained austenite. The cementite precipitates could be revealed by SEM and XRD techniques with an amount of about 6%. The presence of these precipitates prevents the large coarsening of bainite ferrite, thereby producing hardness levels similar to that of non-tempered conditions (14% decrease). Moreover, the calculation of carbon content in bainitic ferrite showed a remarkable decrease, from 0.19 to 0.08 wt.% after tempering at 500 °C, compared with other investigated conditions. This can be related to altering the supersaturated bainitic ferrite crystal (BCT) to its equilibrium

state (BCC). The significant effect of tempering in the A-bainite sample is due to the enhancement of carbon diffusion through the existence of high dislocation density.

TABLE OF CONTENTS

LIST OF TABLES

LIST OF FIGURES

LIST OF ABBREVIATIONS

APT	Atom Probe Tomography\
BCC	Body-center cubic
BCT	Body-center tetergonal
CFB	Carbide-free bainite
CCT	Continuous cooling transformation
EBSD	Electron Back Scattered Diffraction
FCC	Face-center cubic
Fe_3C	Cementite
FE-SEM	Field emission scanning electron microscopy
GB	Stored energy due to the shape deformation
HV	Vickers Hardness
IPS	Invariant plain strain
LVDT	Linear variable differential transformer
LOM	Light optical microscopy
M/A	Martensite/Austenite
PAGB	Prior austenite grain boundary
RCL	Relative change in length
RCD	Relative change in diameter
RA	Retained austenite
RA_{block}	Blocks of retained austenite
RA_{film}	films of retained austenite

TRIP   Transformation-induced plasticity

TMT   Thermomechanical treatment

T_{NR} Non-recrystallization temperature

TTT   Time-temperature-transformation

TP   Transformation plasticity

IT   Isothermal tempering

NIT   Non-isothermal tempering

IBT   Isothermal bainitic trasformation

LIST OF SYMBOLS

ΔG_m	Maximum free-energy change
ΔG_N	Minimum free-energy change for the nucleation of bainite in any steel
$\Delta G^{\gamma \rightarrow \alpha}$	Free-energy change for the transformation of austenite to ferrite
M_S	Martensite start temperature
B_S	Bainite start temperature
σ	Stress
σ_γ	Austenite yield strength
$\sigma_{\alpha b}$	Bainite yield strength
Z	Zener – Hollomon parameter
Q	Activation energy
R	Universal gas constant
ε	Strain
$\dot{\varepsilon}$	Strain rate
μ	Shear modulus
b	Burgers vector
ρ	Dislocation density
$t_{\alpha b}$	Thickness of bainitic ferrite plate
U	Immobilization parameter
Ω	Remobilization parameter
I_α	Integrated intensities of ferrite
I_γ	Integrated intensities of austenite

λ	Wavelength of the radiation
hkl	Miller indices
θ	Bragg angle
γ_R	Retained austenite
γ_{Rf}	Film-like retained austenite
γ_{Rb}	Blocky-shape retained austenite
α_b	Bainitic ferrite
α_m	Martensite

INTRODUCTION

Low-cost steel with high strength, toughness, formability, and weldability are in continuous demand in most industrial sectors, especially in the automotive industry. The fundamental goal is to reduce the vehicle weight to improve fuel efficiency while simultaneously improving passenger safety. This combination can be achieved by controlling the microstructure via the alloy's chemical composition, heat treatment, and thermomechanical processing (Hossein Beladi, 2012). To achieve this goal, grain refinement strengthening is one of the most beneficial techniques to produce strong steel (H. K. D. H. Bhadeshia, 2009; Maalekian, Lendinez, Kozeschnik, Brantner, & Cerjak, 2007; Tsuji & Maki, 2009).

In recent years, a new generation of nanostructured bainitic steels with a high carbon (> 0.7%) and silicon (> 1%) content known as carbide-free bainite CFB) has been obtained by low-temperature isothermal transformation (austempering). The CFB microstructure is free from carbide precipitates due to the presence of an adequate content of silicon (Si), which suppresses the formation of these precipitates. Therefore, the microstructure mainly comprises fine bainitic ferrite platelets surrounded by retained austenite films (Hossein Beladi, Timokhina, Hodgson, & Adachi, 2012). The tensile strength of some CFB steels (1600–2300 MPa) matches those of commercial quenched and tempered alloys with higher toughness (130 MPa $m^{1/2}$) and ductility (20%). Furthermore, in some cases, CFB steels can replace margining steels, which are at least 90 times more expensive. The excellent combination of these properties originates from the unique microstructure, which consists of thin bainitic ferrite plates (20–40 nm); these plates provide strength, and thin films of retained austenite enhance the toughness and ductility (H. K. D. H. Bhadeshia, 2009).

However, the use of high-C CFB steels in several industrial sectors is limited due to their poor weldability and formability because of the high carbon content and the very long transformation time at low temperatures, requiring days to complete. Hence, the development

of nanostructured bainitic steels with low or medium carbon content, which would not have the above shortcomings are excellent candidate alloys for most automotive applications. However, it is challenging to produce nanostructured bainite in steel with a carbon content of less than 0.6% as the martensite start temperature (M_S) increases with the decrease in the steel carbon content. Furthermore, the difference between the bainite and martensite start temperatures decreases (Harshad K. D. H. Bhadeshia, 2005; H. K. D. H. Bhadeshia, 2009, 2013). As a result, a thickening of the bainitic ferrite plates occurs due to transformation at a high temperature. The plate thickness of bainitic ferrite has been reported to be primarily dependent on the strength of austenite at the transformation temperature and transformation driving force, which both decrease as the temperature increases (Garcia-Mateo & Caballero, 2014). Several attempts have been made to produce nanostructured bainitic steels with a low carbon content, which is of significance in the automotive industry. Yang and Bhadeshia (Yang & Bhadeshia, 2008) reported that the use of substitutional solutes to reduce M_S to produce nanostructured bainite in low-carbon steel is not promising, as the microstructure coarsens due to the coalescence of fine bainite laths.

Hence, to solve this issue, ausforming is conducted to generate nanostructured bainite in low-carbon steels, where the strength of austenite before bainite transformation can be enhanced by work hardening resulting from plastic deformation. Identifying the result of the impact of deformation on the transformation of CFB steel in terms of transformation kinetics and microstructure morphology, as well as the necessity of information and quantitative data in some respects in this field, is the backbone of this investigation. Understanding the relationships between ausforming parameters, heat treatment conditions, and associated microstructural features of CFB will facilitate the use of nanostructured CFB in different industrial applications.

The aims of this research are as follows:

- Develop further understanding of the influence of ausforming prior to bainitic isothermal transformation on the stability of retained austenite that exists within the carbide-free

bainitic matrix. In particular, to quantify the decomposition of retained austenite to martensite at ambient temperature, a data which is rarely available in the literature.

- Evaluate the effectiveness of utilizing ausforming to modify the CFB microstructures toward nano-scaled features.

- To better understand the mechanisms of microstructural anisotropy due to ausforming and its relation to the evolution of transformation plasticity phenomena.

- Investigate and understand the mechanisms involved in the evolution of dilatometric behavior and microstructure changes during isothermal tempering of non-ausformed and ausformed bainite structure of a medium carbon CFB steel.

This thesis is divided into five chapters, as detailed below.

Chapter 1 provides a background of the project, as well as the base for the necessary knowledge of relevant topics, e.g., phase transformation of steel during the quenching and isothermal treatment; formation mechanisms of nanostructured CFB and their relationship with ausforming processes; and development of dislocations during bainite transformation and deformation steps. Key metallurgical aspects are covered in this section.

Chapter 2 describes the experimental procedures, including different subsections; the first section introduces the examined material and characteristics of as-received material. The second section discusses dilatometry equipment and the difference in using quenching and deformation modules.

Chapter 3 provides quantitative data regarding the connection between the percent deformation and the stability of retained austenite in the CFB microstructure during cooling to room temperature. Based on this study, the thermal and mechanical stability of retained austenite, which is related to its decomposition to fresh martensite, during cooling to room temperature is investigated qualitatively and quantitatively by dilatometry analysis,

4

microstructural observation, and hardness evolution. A model is presented to illustrate the competition between bainite sheave growth resistance due to the introduction of dislocations by deformation and the enhancement of bainite transformation at different isothermal temperatures.

Chapter 4 discusses the kinetics of bainite transformation and microstructure evolution of CFB and their relation to transformation plasticity strains due to deformation at three temperatures: above the bainite start temperature (B_S); at a specified isothermal transformation temperature (325 °C); and at a temperature between B_S and isothermal temperature. The study results demonstrate that the transformation rate and the microstructure refinement of CFB are notably promoted by deformation at 325 °C compared to non-ausformed and other ausformed conditions. The morphology is significantly modified under low-temperature ausforming conditions, whereas it is nearly indistinguishable between the non-ausformed and high-temperature ausformed conditions. By utilizing a low-temperature ausforming condition, the thickness of the bainitic ferrite plate shifts to almost nanoscale (~100 nm); hence, the hardness of CFB steel attains that of tempered martensitic steel.

Chapter 5 focuses on the microstructural response of two types of CFB microstructures to tempering treatments. Submicron bainitic ferrite plates were obtained by pure isothermal (no prior deformation) transformation at 325 °C, while nano-scale level CFB was produced by ausforming and isothermal holding of the supercooled austenite at 325 ºC. The analysis of the results showed that the softening that occurred after tempering was caused by the thickening of bainitic ferrite plates in the pure isothermal transformation, a mechanism that was absent in the ausformed samples. On the other hand, cementite precipitates at α_b/γ_{Rf} The interface was produced as a result of decomposition of either bainite or film-like retained austenite due to tempering at 500 ºC in ausformed CFB microstructure; thereby, preventing the thickening of bainitic plates. Moreover, the volume fraction of retained austenite for all conditions did not change from its original levels after tempering at all temperatures.
.

CHAPTER 1

LITERATURE REVIEW

1.1   Phase changes of steel during heat treatment

The heat treatment of steel involves the combination of heating to an appropriate temperature and maintaining that temperature for a particular time (i.e., holding time), followed by cooling to room temperature via the control of the cooling rate depending on the desired properties; typically, it is the last thermal process in the manufacturing procedure. Thus, caution should be exercised. The heat-treatment process of steel, as well as the required properties, are strongly affected by the type and percentage of the alloying elements in the steel, such as carbon (C), manganese (Mn), silicon (Si), chromium (Cr), molybdenum (Mo), nickel (Ni), vanadium (V), tungsten (W), aluminum (Al), and others. The main heat-treatment process of steel, which typically contains a carbon content of less than 2 weight percent (wt.%), significantly affects its metallurgical behavior; as a result, its mechanical properties are modified. At very slow cooling rates, the time is enough to allow the system to reach a near-equilibrium condition, as shown in the iron-carbon phase diagram for steel, Figure 1-1 (International & Handbook, 1991). As shown in this diagram, the solubility of carbon in the face-centred cubic (FCC) region or austenite (γ) region is greater than that in the body-centred cubic (BCC) or ferrite (α) region. Alloying elements modify the Fe–C phase diagram depending on the type of the elements. For example, Mn and Ni stabilize the austenite phase, i.e., the austenite–ferrite critical temperatures (A_1 and A_3) are decreased by their addition, whereas Si and Mo are the primary ferritic phase stabilizers (A_1 and A_3 are increased) (Ashby & Jones, 1998). Figure 1-2 shows different alloying elements that affect the Fe–C phase diagram, specifically the change in the γ-phase field. It can be seen that those alloying elements such as Cr, Ti, and Mo shrink the γ region, where the A_1 and A_2 temperatures rise, and the carbon content at eutectoid temperature decreases. In contrast, Mn has an inverse effect on the γ-phase zone when added to steel.

In practical heat treatment situations, the cooling rates vary through the thickness of the part, and a non-equilibrium transformation takes place. For instance, martensite and bainite transformations occur as a result of the rapid cooling from the austenite region above A_3 temperature. It is essential to point out that alloying elements, such as Cr, Mo, and Ni, can prompt martensite or bainite transformation even with a slower cooling rate, i.e., enhancing the hardenability of steel (Radionov, 2019).
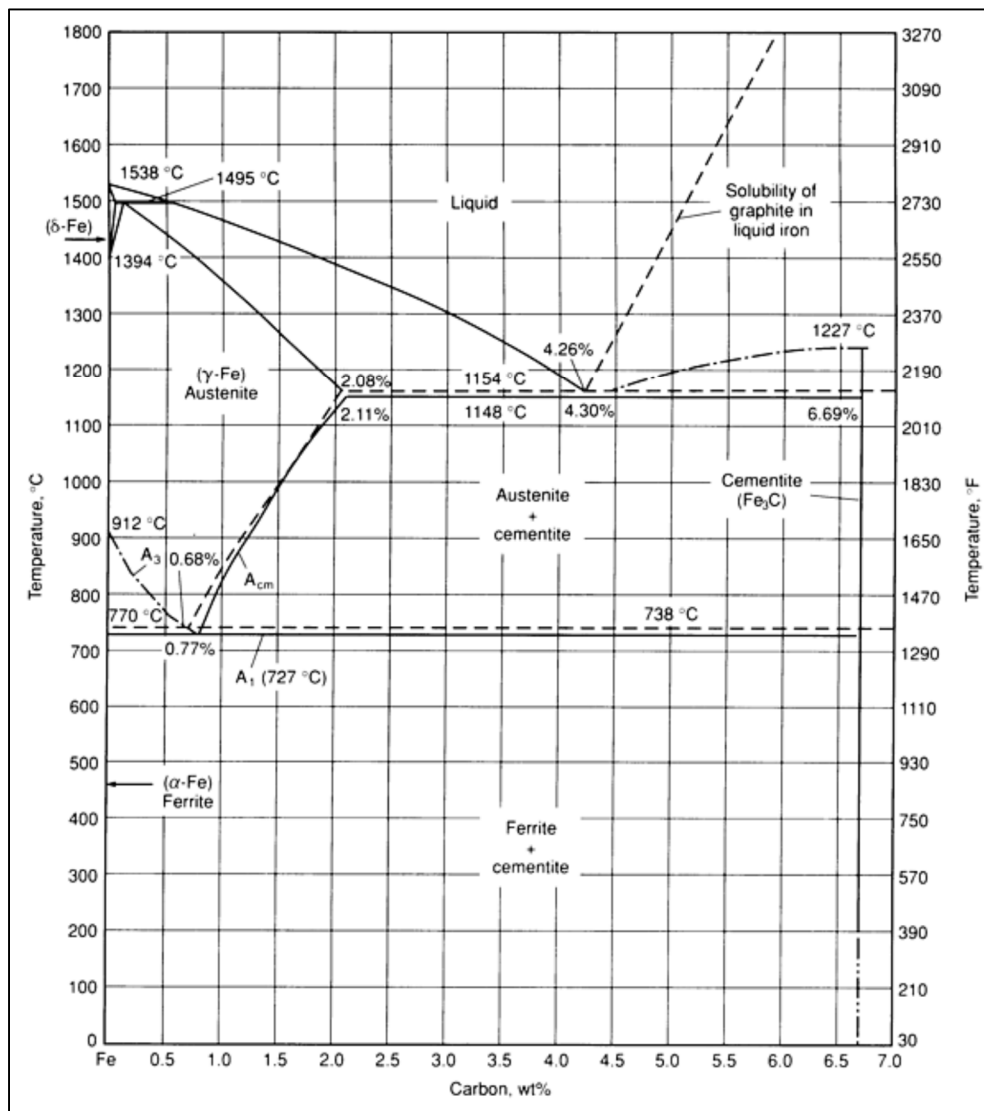
Figure 1-1 The Fe–C equilibrium diagram for steel, depicting carbon in wt.%
Taken from ASM Handbook volume 4 (1991, p 17)
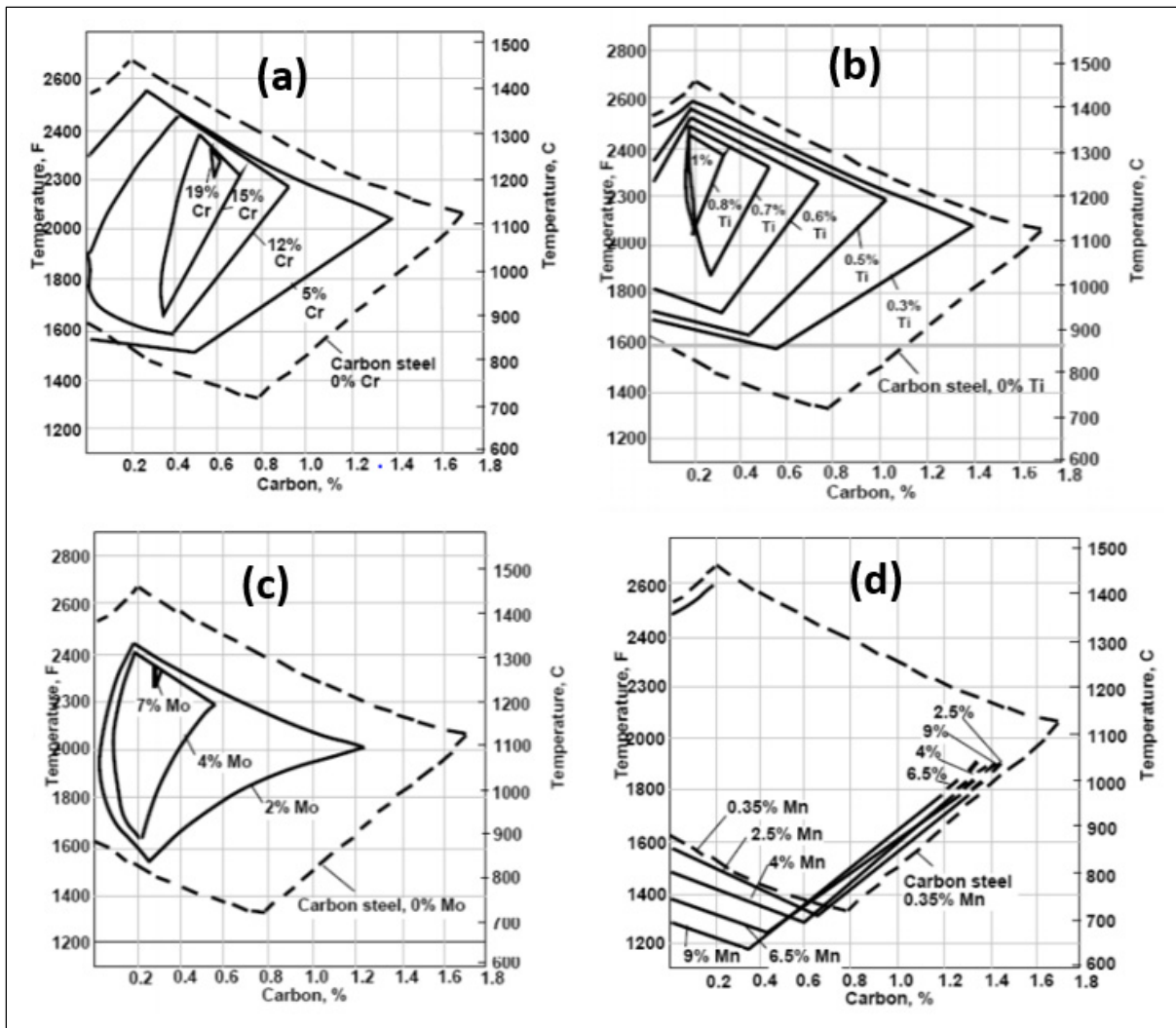
Figure 1-2 Effect of the addition of the alloying element on the γ-phase zone: (a) Cr; (b)Ti
(d) Mn
Adopted from Mehran Maalekian (2007, p. 8)

Accordingly, the microstructure evolution of steel during heat treatment, i.e., heating, cooling, and isothermal holding at a specific temperature, can be described as a function of its transformation mechanisms. In this context, Bhadeshia (H. K. D. H. Bhadeshia, 2001) introduced a classification method for steel microstructures according to the mechanisms of transformation, Reconstructive and displacive transformation, as shown in Figure 1-3.
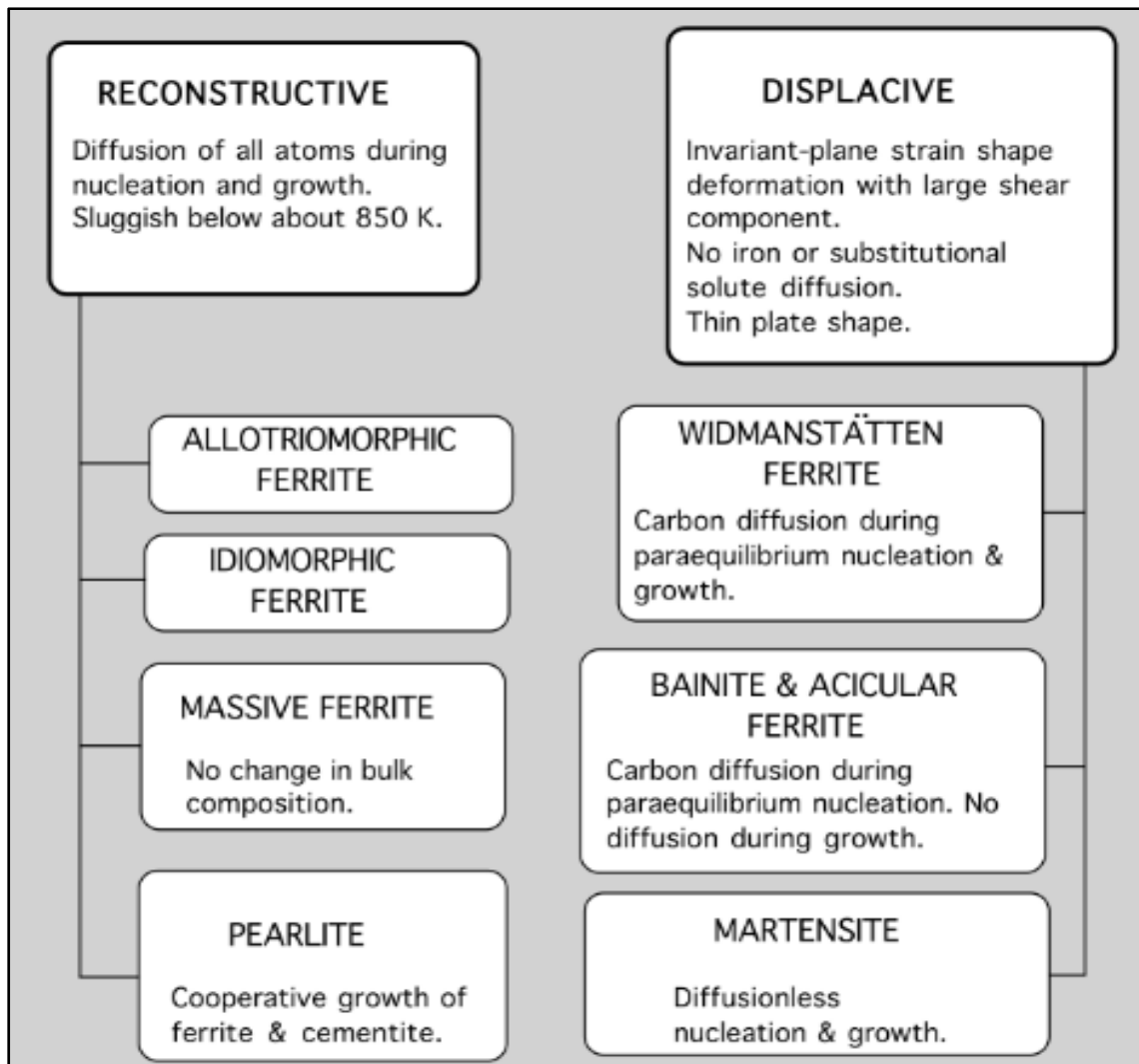
Figure 1-3 Classification of the different mechanisms of austenite transformation
Taken from H.K.D.H. Bhadeshia (2010, p. 256)

1.2   Reconstructive transformation (Diffusion)

This type of transformation involves the movement of atoms in the crystal structure, which necessitates the dissociation of all atomic bonds to rearrange the atoms in a different pattern that requires diffusion. As a result of diffusion, the chemical composition changes because some atoms preferentially remain in the parent phase, whereas others preferentially remain in the product phase. Temperature and time, which affect the diffusion process, play a significant role in transformation. Typically, reconstructive transformation is difficult to take place at a

temperature below eutectoid temperature, A₁ (Bhadeshia & Honeycombe, 2003; Francisca G. Caballero, 2014). Figure 1-4 illustrates the diffusion transformation (e.g., $\gamma\rightarrow\alpha$), where the parent atoms (austenite) change their position (diffusion) to form a new phase, ferrite (α). The reconstructive transformation products include allotriomorphic (grain boundary) ferrite, idiomorphic (intergranular) ferrite, massive ferrite, and pearlite.
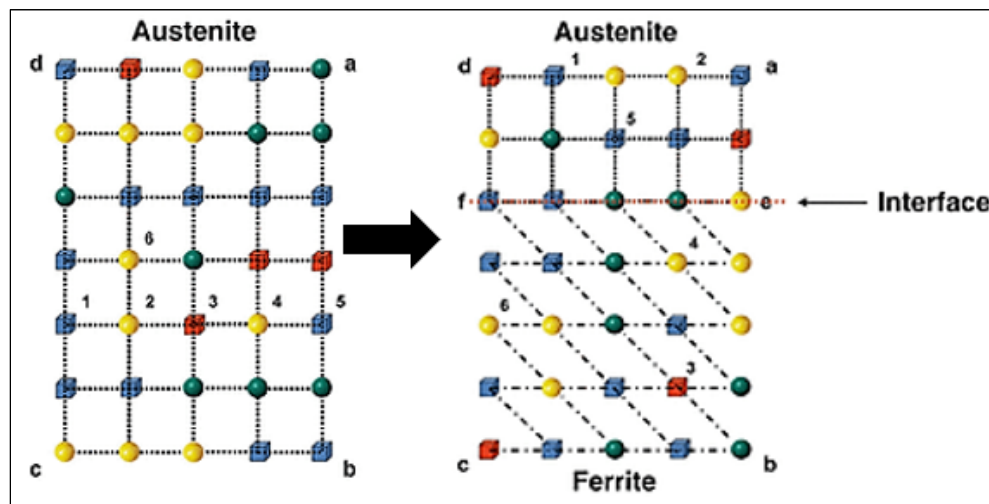
Figure 1-4 Reconstructive austenite–ferrite transformation
Adapted from Caballero F.G (2014, p. 3056-3065)

1.3   Displacive transformation

Displacive transformation is a change in the parent crystal structure to the product crystal structure via crystal deformation, i.e., rearrangement of atoms, without diffusion (Fielding, 2013), as seen in Figure 1-5. Transformation dominated by considerable strain energy as a result of atomic volume change between γ(FCC) and α(BCC). Therefore, the morphology of phases of displacive transformation is growing as thin plates to minimize the system strain energy. Moreover, austenite grain boundaries act as a barrier to plate growth, while in diffusion transformation (reconstructive), growth can exceed the grain boundaries. The growth causes the shape of the transformed region to change, the change being an invariant–plane strain, IPS, which has a strong shear component (s), that varies according to the type of transformation product, and a smaller dilatation component (δ) (Swallow & Bhadeshia, 2013), see Table 1-1.

Transformation temperature affects the transformation type, as shown in Figure 1-3 (right side), top represents higher temperature than at the bottom. At high temperatures, carbon diffuses (paraequilibrium) during nucleation and growth processes, as in widmanstatten ferrite transformation. While, during bainite transformation, carbon diffusion occurs only during the nucleation step. At low temperatures, i.e., martensite transformation, carbon atoms cannot diffuse during nucleation and growth.
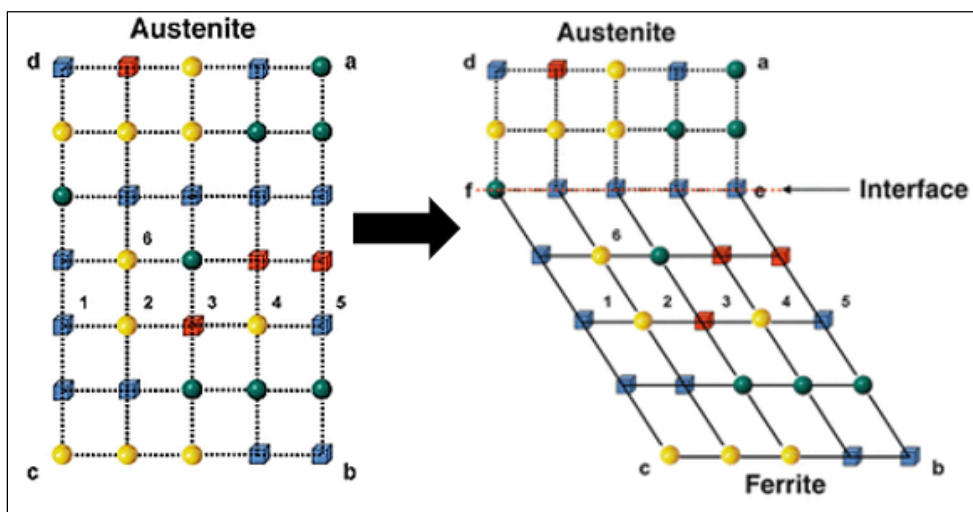
Figure 1-5 Schematic of the displacive mechanism
Adapted from Caballero F.G (2014, p. 3056-3065)

Table 1-1 Approximate values of shear (s) and dilatation (δ) for a displacive
transformation in steels
Adapted from H.K.D.H. Bhadeshia (2002)

Transformation	s	δ	Morphology
Widmanstatten ferrite	0.36	0.03	Thin plates
Bainite	0.22	0.03	Thin plates
Martensite	0.24	0.03	Thin plates
Acicular ferrite	0.22	0.03	Thin plates

1.3.1   Martensite transformation

Martensite can be obtained at different temperatures, but in steels, it typically forms at a relatively low temperature depending on the chemical composition of the steel. Since the transformation is diffusionless and carbon is trapped in the lattice, the BCC lattice turns into a body center tetragonal (BCT), and the amount of carbon in the steel determines the degree of tetragonality (Ashby & Jones, 1998). Martensite forms as thin plates or laths due to the constrained formation by surrounding grains and subdivided the prior austenite grain into packets, which consists of blocks of laths. Hence, the mechanical properties of transformed martensite are controlled by the size of these packets and blocks and the mode in which these microstructural features partition the austenite grain (Nambu et al., 2013). Figure 1-6 shows the crystallographic hierarchy of martensitic microstructure schematically.
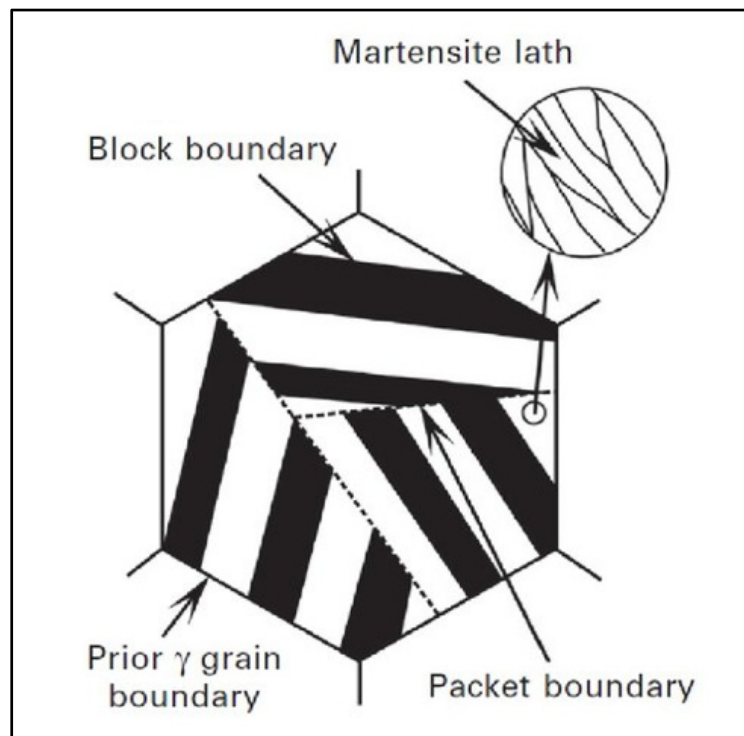
Figure 1-6 Schematic diagram showing characteristic
morphology of lath martensite in an austenite grain
Taken from Maki (2012, p. 38)

Martensite transformation occurs athermally at a particular temperature range, regarded as martensite start temperature (M_S) and martensite finish temperature (M_f), dependent mainly on the chemical composition of the steel. The martensite volume fraction is dependent only on temperature, and time cannot change the transformed amount of martensite. Carbon is found to be the primary element that strongly affects M_S (Bhadeshia & Honeycombe, 2003). Furthermore, all mathematical models used to predict M_S consider a large factor for the effect of C compared to the other alloying elements (Granger & Stewart, 1946; Krauss, 2014), as shown in the equation (1-1), M_S is the martensite start temperature in °C, and X_i is the alloying element amount in wt.% of steel. (S.-J. Lee & Van Tyne, 2011; van Bohemen, 2013).

$$M_s\ (\text{°C}) = 561 - \mathbf{474.2}x_C - 33x_{Mn} - 17x_{Ni} - 17x_{Cr} - 21x_{Mo} \tag{1-1}$$

The morphology of martensite in steel changes from lath in a low and medium C-steel (<0.6% C) to plate in high-C steel (>0.6%C). Mixed morphologies (lenticular) are observed between 0.6% C and 1.0% C. Figure 1-7a, 1-7b, and 1-7c show the different morphologies of the martensitic structure (Maki, 2012).
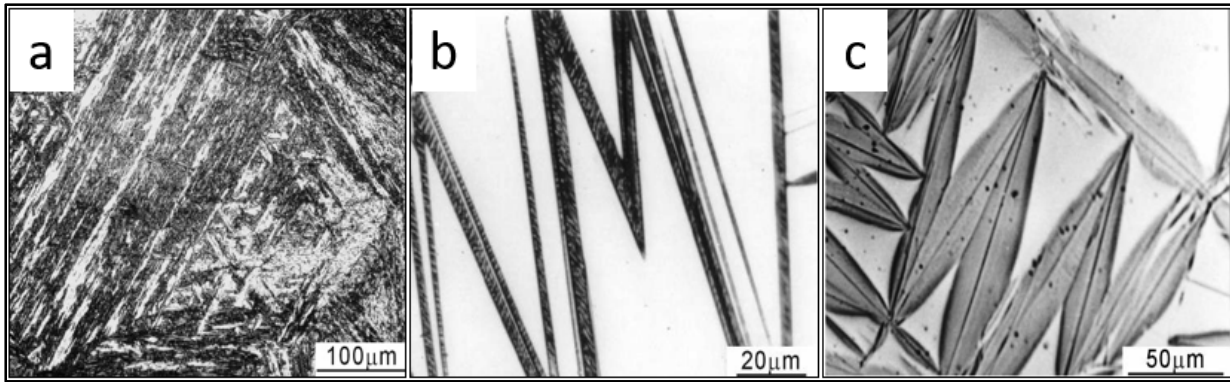
Figure 1-7 Martensite morphologies; (a) lath, (b) plate, and (c) lenticular
Adapted from Maki (2012, p. 34-58)

1.3.2   Bainite transformation

Bain and Davenport were the first to identify the bainite microstructure (α_b), which was obtained by the transformation of steel at a constant temperature (austempering) (Bain & Davenport, 1930). When the temperature was low enough, ferrite and cementite do not grow as parallel lamellae (such as that observed in pearlite) but instead exhibit an irregular lath-like shape. The nucleation and growth of bainite proceeds only when two thermodynamic requirements are fulfilled (Garcia-Mateo & Caballero, 2014), and the temperature at which both criteria are fulfilled, is called the bainite start temperature (B_S):

- nucleation condition ($\Delta G_m < G_N$)

- growth condition ($\Delta^{\gamma \to \alpha} < - G_B$)

Where (ΔG_m) is the maximum free-energy change that accompanies nucleation under para-equilibrium conditions, ($\Delta^{\gamma \to \alpha}$) is the free-energy change for the transformation of austenite without any change in chemical composition, and (G_N) is the minimum free-energy change for the nucleation of bainite in any steel.

$$\Delta G_N = 3.5463 \cdot T(K) - 3499.4 \tag{1-2}$$

When the temperature reaches the B_S, an embryo of ferrite primarily nucleates at the austenite grain boundary due to the free-energy change and then grows, within the sheaf, to a particular length known as "subunit." The subunit has uniform dimensions because each subunit grows to a limiting size which can be much smaller than that of the austenite grain. For the transformation to continue, new platelets nucleate and grow, giving rise to clusters of parallel sub-units with identical crystallographic orientation, habit plane, and size, as shown schematically in Figure 1-8a and SEM micrograph in Figure 1-8b (F. G. Caballero, Bhadeshia, Mawella, Jones, & Brown, 2013).
.
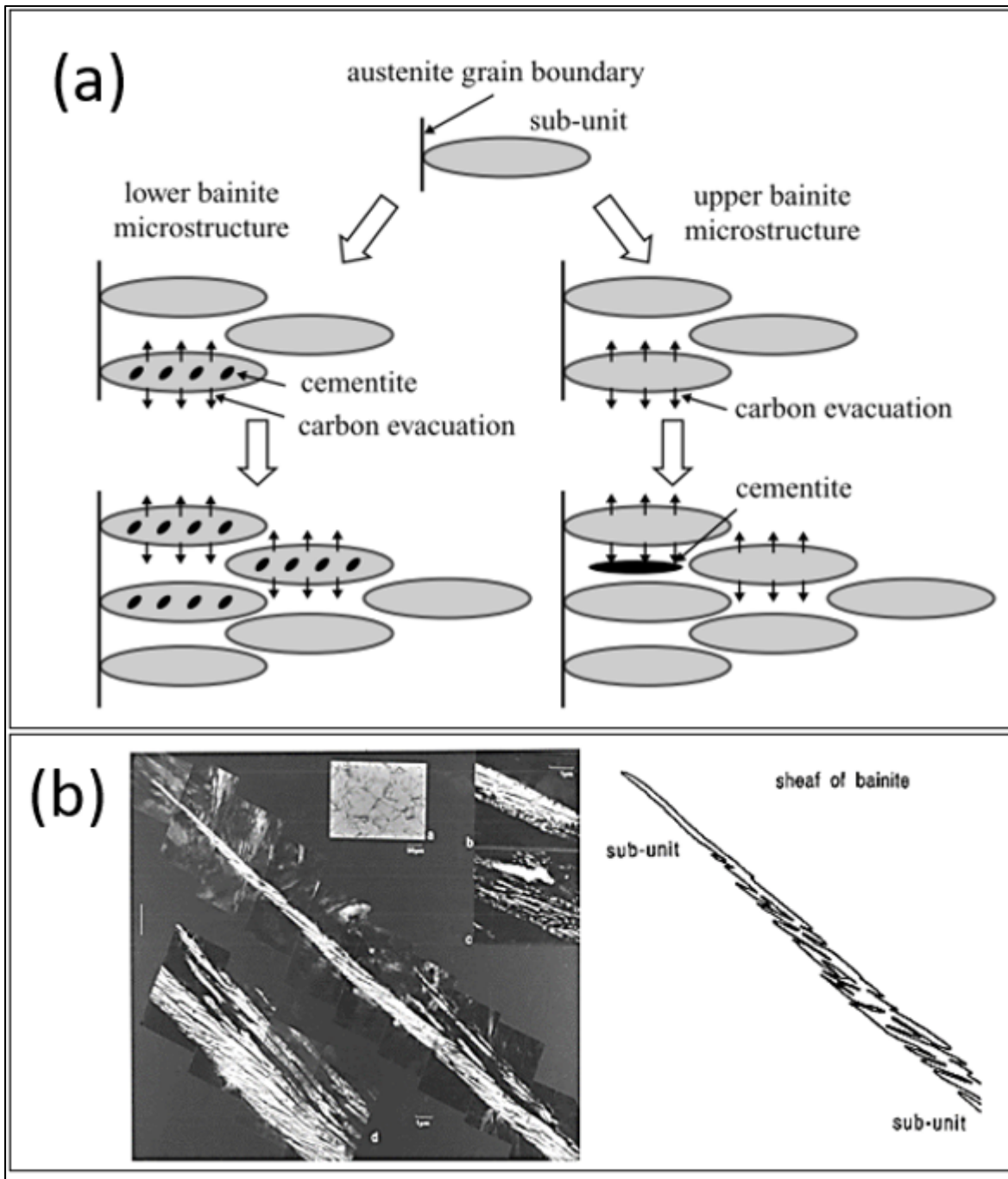
Figure 1-8 (a) Schematic of bainite subunit and sheaf formation in well-known bainite morphologies, i.e., upper and lower bainite; (b) TEM micrograph of bainite sheaf, and a sketch of the subunit near the sheaf tip
Taken from Azuma et al. (2005, p 222); H. K. D. H. Bhadeshia (2015, p 19)

Bainite transformation is well known to occur via para-equilibrium nucleation and displacive growth, as mentioned previously. In this type of transformation, substitutional alloying elements, such as Cr, Mn, and Si, cannot redistribute between the parent (austenite) and the product (bainite) phases during bainitic transformation. Only interstitial alloying elements, such as carbon, can diffuse out of the supersaturated bainitic ferrite plate. This phenomenon has been experimentally proven in several studies by atom probe tomography (APT), which permits the tracing of the atoms of elements after the end of the para-equilibrium transformation (F. G. Caballero, Miller, & Garcia-Mateo, 2010; Hofer, Winkelhofer, Clemens, & Primig, 2016; I. Timokhina, Beladi, Xiong, & Hodgson, 2011; I. B. Timokhina et al., 2016). There are three possibilities for carbon redistribution (H. K. D. H. Bhadeshia, 2009):

- Carbon partitions into austenite (γ); then, excess carbon is not present in the ferrite plate.

- Carbon is trapped by the advancing interface due to diffusionless growth.

- Some carbon atoms diffuse, while the remainder is trapped, leading to partially supersaturated ferrite.

The activity of carbon partition continues until austenite reaches its T_o carbon content, which is the locus of all the points at which the chemical composition and free energy of austenite and ferrite are identical. Therefore, austenite is not reached its equilibrium composition (Ae$_3$), which is called incomplete reaction, as illustrated in Figure 1-9 (H. K. D. H. Bhadeshia, 2002). Since bainite is displacive, there is energy stored inside the steel, as a consequence of their transformation, in the form of elastic strains. This stored energy is usually accounted for in steel design, and in the case of bainite, this is given as $G_B \approx 400$ J mol^{-1} (Takahashi & Bhadeshia, 1991).
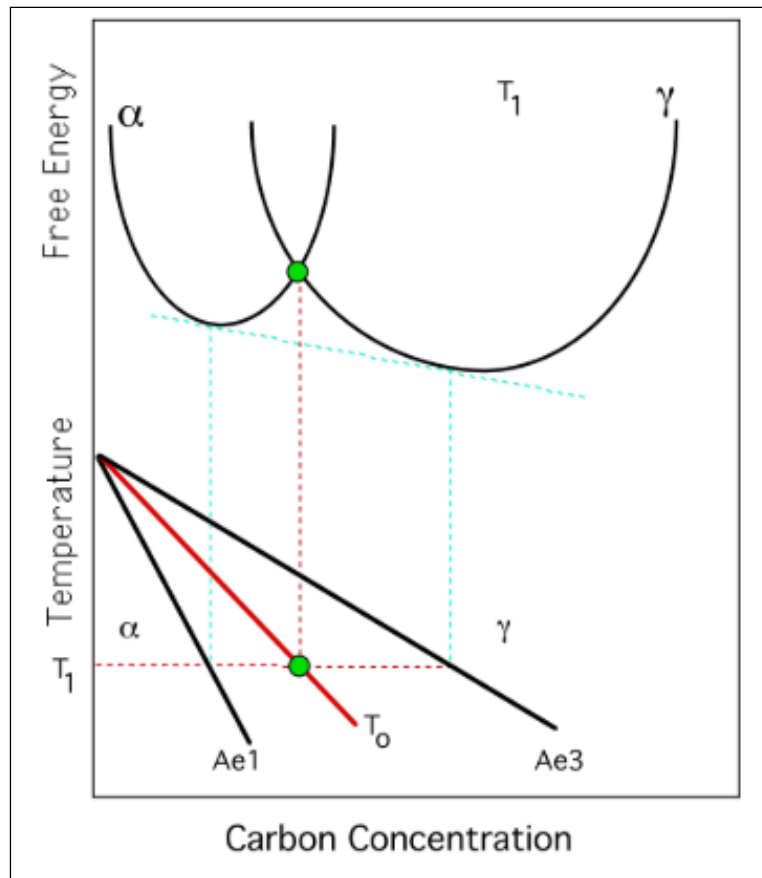
Figure 1-9 Schematic of the origin of the T_o curve
Taken from H. K. D. H. Bhadeshia (2005, p65)

Bainite grows at temperatures where the austenite is mechanically weak and unable to elastically accommodate the shape deformation accompanying displacive transformation, unlike martensite transformation. The shape deformation is accompanied by IPS, with large shear (s) and dilatation (δ) components having magnitudes of 0.26 and 0.03, respectively, as illustrated in (Figure 1-10a). This large strain is accommodated by plastic relaxation of the surrounding austenite, Figure 1-10b, leading to a displacement (tent shape) to the bainite sheave, as in Figure 1-10c (H. K. D. H Bhadeshia, 2013; Swallow & Bhadeshia, 2013). Of course, the occurrence of such plastic distortion leads to increased dislocations generation at the α_b/γ interface, which halts the growth of the bainite platelets before it encounters any hard obstacle such as austenite grain boundary (H. Bhadeshia, 2010).
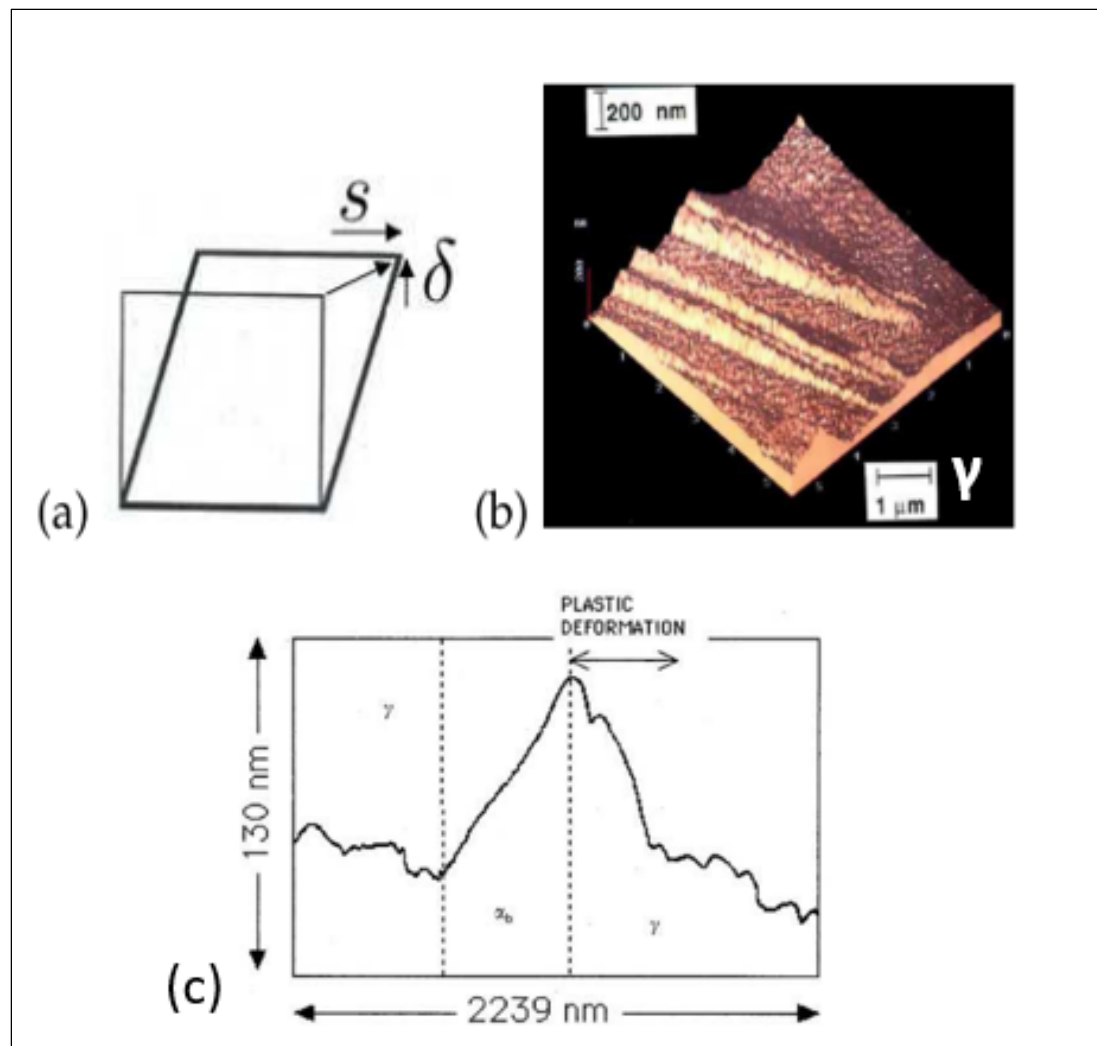
Figure 1-10 (a) Illustrations of IPS, (b) AMF image of shape change; (c)
displacement of the plastic deformation in austenite
Adopted from H. K. D. H Bhadeshia (2013, p2-4)

Bainite can be classified into different forms according to its appearance under microscopic examination; upper and lower bainite are the most well-known forms of bainite morphologies. The former is obtained at transformation temperatures (greater than 400 °C), depending on the chemical composition of steel, while the latter is obtained at a lower transformation temperature. Transformation at a higher temperature (upper bainite) permits the diffusion of carbon out of the growing bainitic ferrite lath and cementite precipitates in the boundary between the growing ferrite plates. On the other hand, low transformation temperature limits

the carbon diffusion in ferrite. Therefore, as all the carbon cannot diffuse out of ferrite, small cementite precipitates are also formed inside the bainite laths or plates (Azuma et al., 2005; Yin, Hillert, & Borgenstam, 2017). The model in Figure 1-8a illustrates the mechanisms of the two aforementioned bainitic transformations. Globular bainite (granular) is another form of bainite that appears as blocks of bainite and austenite (equiaxed bainite morphology) under an optical microscope resulting from the slow cooling in low-carbon steel, leading to the massive growth of sheaves. The transformation mechanism of globular bainite is identical to that of ordinary bainite. The nucleation and growth kinetics of cementite is almost the same as those of bainitic ferrite (Spanos, Fang, Sarma, & Aaronson, 1990). In her chapter book, (F. G. Caballero, 2012) reported a classification diagram of the differences in bainite morphologies representing low- and high-carbon bainite. The description is based on the appearance of the bainitic phase (Figure 1-11). Recently, bainitic steel was developed with simple chemical composition, C, Mn, Cr, and Si alloying elements. The hardenability of these steels' compositions is controlled so that the transformation temperature is dramatically suppressed, giving slender plates of bainitic ferrite, under isothermal conditions (H. K. D. H. Bhadeshia, 2013; F. G. Caballero & Bhadeshia, 2004; F. G. Caballero, Bhadeshia, Mawella, Jones, & Brown, 2002). This bainitic steel is named in the literature as nanostructured bainite, super bainite, novel bainite, and nano-bain steel (H. Beladi, Adachi, Timokhina, & Hodgson, 2009; H. K. D. H. Bhadeshia, 2009; F. G. Caballero, Bhadeshia, Mawella, Jones, & Brown, 2001; F. Hu, Hodgson, & Wu, 2014; Huang et al., 2013)
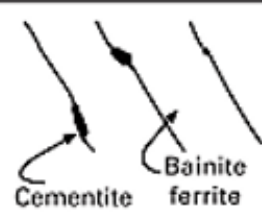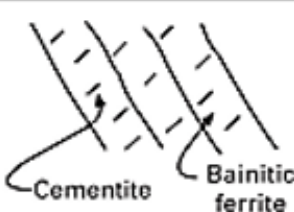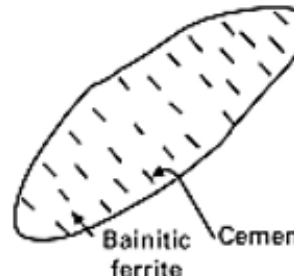
Bainite	Morphology	Bainite description
Granular bainite	Irregular ferrite with M/A	Martensite/ MA ... Bainite ferrite
Lath-like upper bainite	Lath-like ferrite with cementite on lath boundaries	Bainite ferrite ... Cementite
Cementite-free lath-like bainite	Lath-like ferrite with M/A on lath boundaries	Bainite ferrite ... Martensite (M)/ austenite (A)/MA
Lath-like lower bainite	Lath-like ferrite with cementite inside the ferrite laths	Cementite ... Bainitic ferrite
Plate-like lower bainite	Plate-like ferrite with cementite inside the ferrite plates	Bainitic ferrite ... Cementite

Figure 1-11 Morphological classification of bainite in steel
Taken from Caballero, F. G. (2012, p. 438)

1.4 Development of nanostructured carbide-free bainite (CFB)

Typically, cementite (Fe$_3$C) or other carbide particles are present in ordinary bainitic steels. These particles typically occupy either the area between the bainitic ferrite sheave (upper

bainite) or even inside the bainite subunits (lower bainite). Carbides are extremely brittle compounds, and they exhibit a brittle fracture mechanism (cleavage), which occurs very rapidly. Therefore, eliminating carbides from the microstructure leads to the enhancement of mechanical properties, particularly fracture resistance (toughness) (H. K. D. H. Bhadeshia, 2013; Yang & Bhadeshia, 2008). Adding alloying elements in steel, such as silicon (Si > 1.0%) and/or aluminum (Al), suppresses the precipitation of carbides during bainite transformation due to their low solubility in cementite. Therefore, austenite remains enriched in C, which finally leads to its stabilization. The resulting microstructure is known as carbide-free bainite (CFB). Generally speaking, CFB morphology is almost no different from the upper bainite; the only difference is the presence of carbon-enriched retained austenite as films, i.e., film-like (γ_{Rf}) interwoven between the subunits and blocky-shape (γ_{Rb}) located between the bainitic sheave instead of the carbides. The two different morphologies of retained austenite are related to differences in carbon contents, i.e., the film-like are much richer in carbon than the blocky-shape (H. K. D. H. Bhadeshia, 2015). Figure 1-12a illustrates the schematic of CFB formation with inserted TEM images, depicting the difference between CFB and upper bainite microstructures at room temperature as shown in Figure 1-12b and 1-12c.

1.4.1 Microstructure Morphology

The crystallographic features hierarchy of bainitic structure is similar to the one in martensite, and the main difference is that the smallest feature is a plate-like shape, as shown in Figure 1-6. The bainitic plate has the commonly Kurdjumov–Sachs (K-S) or Nishiyama-Wassermann (N-W) orientation relationship (OR) with respect to the austenite matrix. In the case of the K-S OR relationship, there are 24 variants (24 bainitic ferrite orientations), while in the N-W OR, 12 variants could be grown in one austenite grain (Y. Guo et al., 2017; Kaneshita, Miyamoto, & Furuhara, 2017; Rivas, 2016; B. B. Wu, Wang, X. L., Wang, Z. Q., Zhao, J. X., Jin, Y. H., Wang, C. S., Shang, C. J., Misra, R. D. K., 2018; Yin, 2017).
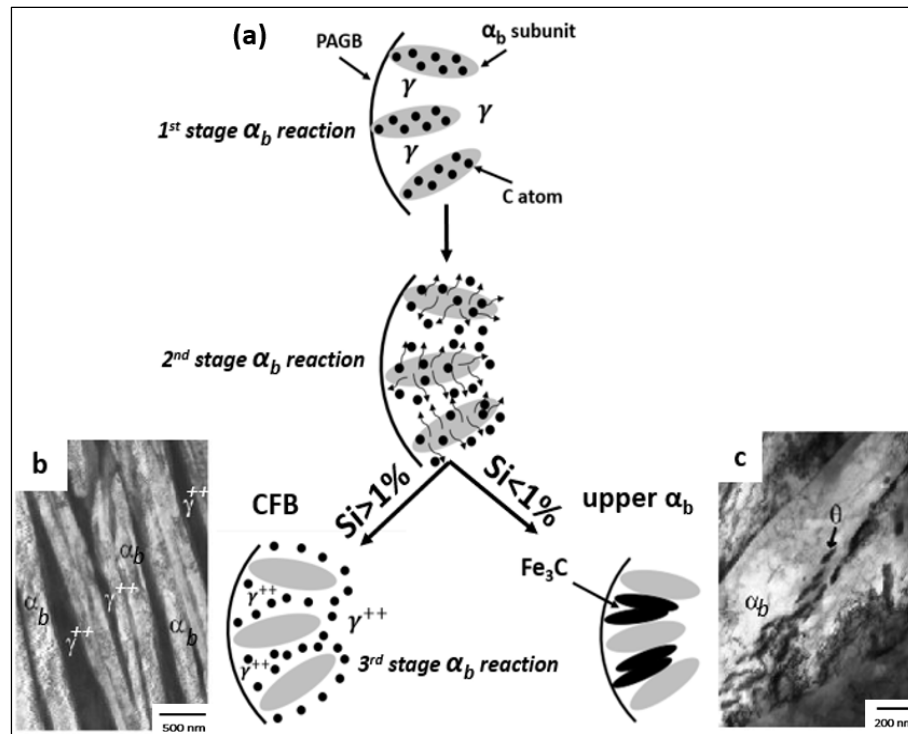
Figure 1-12 Schematic of the difference in the formation of CFB and upper bainite (a) TEM images for CFB (b) and upper bainite(c). γ and γ^{++} are retained austenite and carbon-enriched retained austenite, respectively, α_b is bainitic ferrite, and θ is Fe₃C

Adapted from Caballero, F. G. et al. (2012, p. 443-452)

Bainitic ferrite plates (α_b) with film-like retained austenite (γ_{Rf}) in the nano-scale range (<100 nm) constitute an important feature of nanostructured bainitic steels. This unique structure's behavior is similar to that of a composite structure (C. Garcia-Mateo et al., 2012). The excellent combination of strength, toughness, and ductility of nanostructured bainitic steel is related to bainitic ferrite plates (hard phase) and retained austenite (ductile phase). Figure 1-13 shows the SEM micrograph depicting the features of the nanostructured bainite in high-carbon steel. However, several factors can affect the thickness of the bainitic ferrite plate and the size of retained austenite, which needs to be comprehensively studied better to understand the interdependence between microstructure and mechanical properties. Three main factors could have a direct effect on bainitic ferrite plates thickness: 1) strength of the austenite phase during transformation, which is thought to be the main affecting factor; 2) dislocation density at the

bainite/austenite interface; 3) the chemical free-energy change accompanying transformation (Cornide, Garcia-Mateo, Capdevila, & Caballero, 2013; S. B. Singh & Bhadeshia, 1998).

The strengthening mechanism of nano-bainitic steel is known to depend on the size of the bainitic plate and also on the existence of the amount, shape, and distribution of the second phase, which commonly retained austenite (film-like or blocky-shape) and/or martensite. With the decrease in bainite plate thickness, the strength enhancement increases (C. Garcia-Mateo & F. G. Caballero, 2005; C. Garcia-Mateo, Caballero, & Bhadeshia, 2003). The yield strength of bainite ($\sigma_{Y\alpha b}$) can be identified by the strength of pure annealed iron (σ_{Fe}), solid solution strengthening contribution from the alloying elements (σ_{ss}^i), and strengthening due to carbon in the solid solution (σ_C), as well as other factors (H. K. D. H. Bhadeshia, 2015; Young & Bhadeshia, 1995), as follows:

$$\sigma_{Y\alpha b} = \sigma_{Fe} + \sum \sigma_{ss}^i + \sigma_C + 115 L_{\alpha b}^{-1} + 7.341 x 10^{-6} \rho_D^{0.5} + K_P \Delta^{-1} \qquad (1\text{-}3)$$

where, $L_{\alpha b}$ [μm] is the mean intercept line of the ferrite plate measured in a direction normal to the plate length; ρ_D is the dislocation density; kp is a constant; and Δ the distance between two carbide particles.
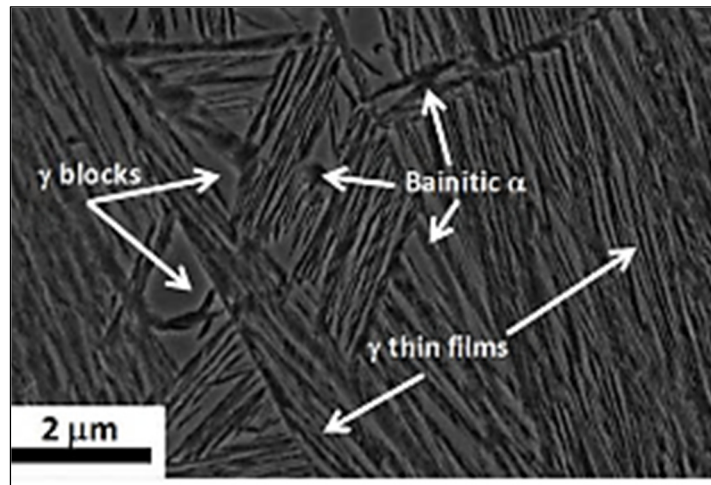
Figure 1-13 SEM image of nanostructured CFB
austempered at 250 °C
Taken from Morales-Rivas et al. (2018, p. 507)
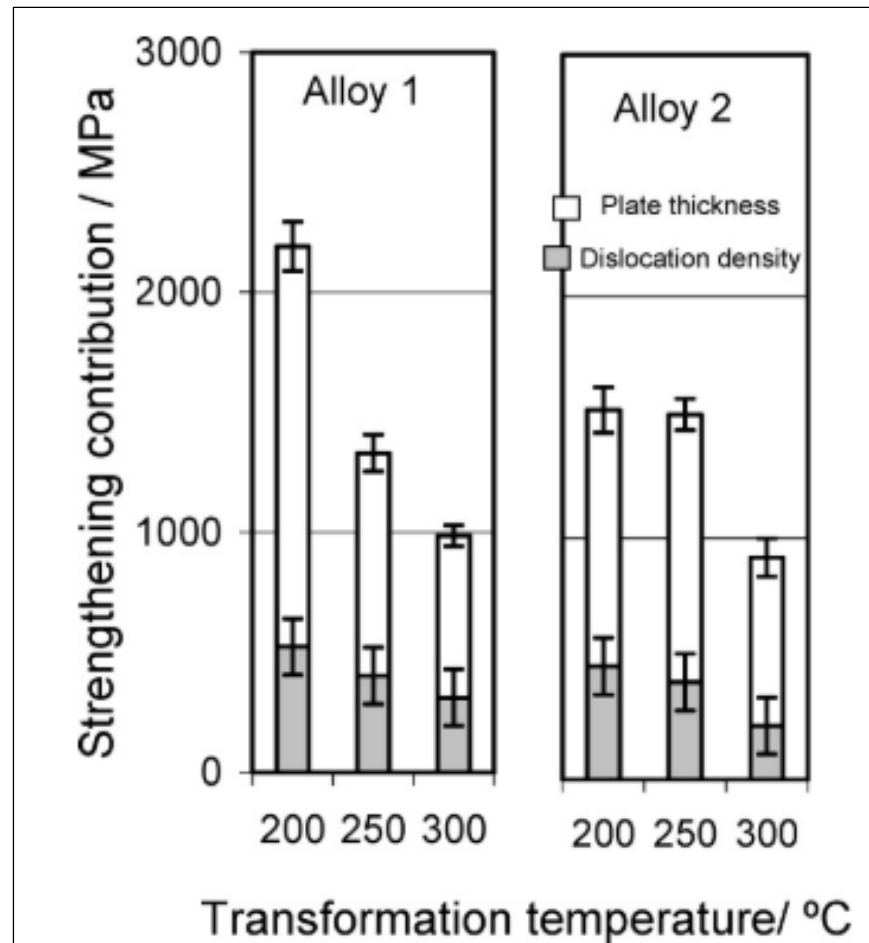
Figure 1-14 Strengthening contribution factors as a function of
the isothermal transformation temperature
Taken from C. Garcia-Mateo & Caballero (2005, p. 1739)

Recently, it has been reported that the tensile strength of some CFB steels could match those of commercial quenched and tempered alloys, $\sigma_{UTS} > 2000\ MPa$, with a higher toughness ($130\ MPa\ m^{0.5}$) and 20% ductility (H. K. D. H. Bhadeshia, 2009). Garcia-Mateo et al. (C. Garcia-Mateo & F. G. Caballero, 2005) investigated the factors affecting the strength of CFB steels and reported that the thickness (width) of the bainitic ferrite plate is the primary contributor to the strength of bainite (Figure 1-14). Examples of the existence of nanostructured bainitic alloy steels are shown in Table 1-2.

Table 1-2 Examples of existing nanostructured bainitic steel
Taken from (V. Igwemezie, 2014)

	C	Si	Mn	Mo	Cr	V	Co	Al
Steel 1	0.98	1.46	1.89	0.26	1.26	0.09	--	--
Steel 2	0.83	1.57	1.98	0.24	1.02	--	1.54	--
Steel 3	0.78	1.49	1.95	0.24	0.97	--	1.60	0.99

1.4.2   Stability of retained austenite

As mentioned in section 1.3, the retained austenite in bainitic steel commonly presents two different morphologies, γ_{Rf} and γ_{Rb}. The austenite films which have a higher carbon content are more stable (higher M_S) than the blocky morphology, which held much lower carbon content. The amount of carbon in both types mainly depends on the alloy's chemical composition and the kinetics of bainitic transformation. The film-like retained austenite interspersed between ferrite plates plays a significant role in ductility as the steel's work hardening capacity will be enhanced when these films undergo stress and transform to martensite through the Transformation-Induced plasticity (TRIP) mechanism. Moreover, the presence of retained austenite, whether film-like or blocky, improves the stress corrosion cracking resistance (SCC) due to the low hydrogen diffusivity in austenite (H. K. D. H. Bhadeshia, 2009; F. G. Caballero & Bhadeshia, 2004).

The stability of the retained austenite (γ_R) can be determined by estimating the amount of transformed martensite either thermally, i.e., due to temperature change, or mechanically (applied strain) (Edmonds, 1983). The formation of untempered martensite must be avoided as it could serve as crack initiation sites (Grajcar, Skrzypczyk, & Kozłowska, 2018; A. S. Podder, 2011; Xie et al., 2014). The stability of γ_R is reported to be affected by its carbon content, morphology, and size (S. Lee, Lee, & De Cooman, 2011; Luo et al., 2011; X.C. Xiong, 2013). On the other hand, the bainitic transformation temperature and the state of supercooled austenite can also alter the above factors and affect the (γ_R) stability (Chiou, Yang, & Huang, 2001; Leijie Zhao, 2019). Therefore, to exploit the complete benefits of the TRIP effect for

ductility enhancement, the stability of retained austenite must be improved. While, if the stability of γ_R is too low, it rapidly transforms to martensite under minimal strain or temperature change resulting in the formation of fragile fresh martensite. Figure 1-15 schematically illustrates the change in the stability of retained austenite based on the different deformation conditions according to M_S and M_d, where M_d is the temperature at which the austenite to martensite transformation does not occur regardless of the applied strain. Sheriff proposed a model that calculates the fraction of retained austenite as a function of the plastic strain, chemical composition, deformation temperature, and starting amount of austenite (Sherif, Mateo, Sourmail, & Bhadeshia, 2004):

$$\ln(V_{\gamma R}^0) - \ln(V_{\gamma R}) = K_1 . \Delta G_{chem}^{\gamma \to \alpha} . \varepsilon, \tag{1-4}$$

Where K_1 is an independent constant, and ε is the strain. M_d is then defined as the temperature at which the driving force for the transformation due to chemical composition ($\Delta G_{chem}^{\gamma \to \alpha}$) equals zero.

It is worth noting that the nanostructured CFB microstructure may include a different amount of blocky-shaped retained austenite (γ_{Rb}) which may transform to fresh martensite depending on its chemical composition. Therefore, nanostructured bainite properties can be affected by the size, distribution and fraction of the above constituents.
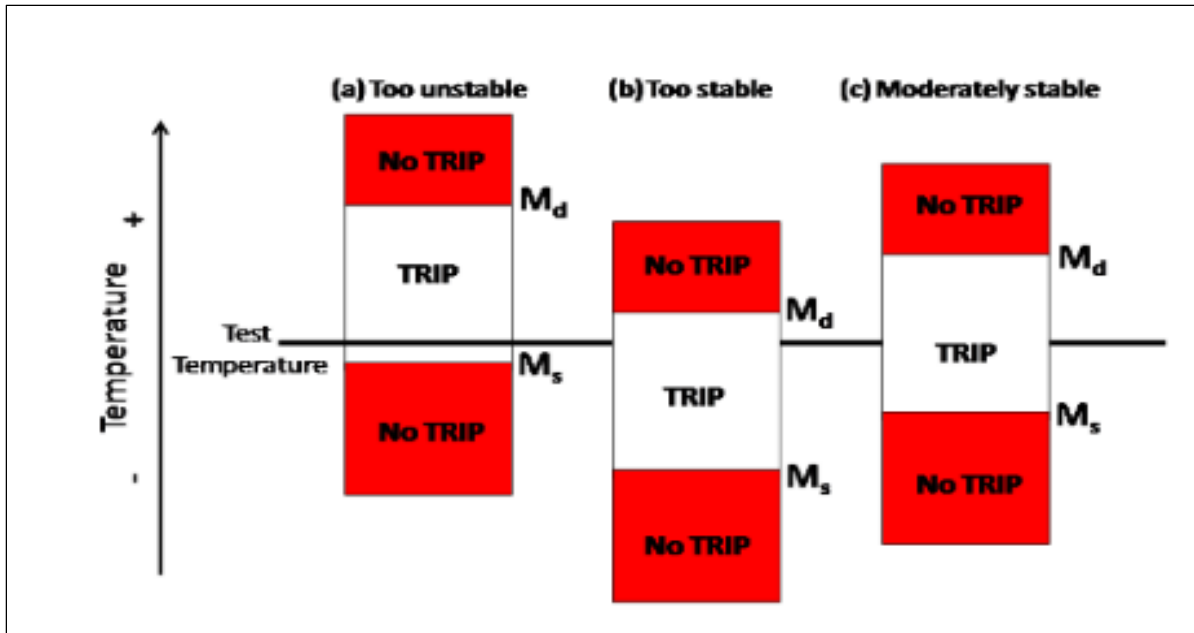
Figure 1-15 Schematic of the test temperature compared to different M_s and M_d values under three scenarios for the mechanical stability of austenite
Taken from Rivas (2016, p.37)

1.4.3   Tempering of nanostructured CFB

CFB steels are used in applications such as rails, casting frogs, bearing, and automobile body panels. Such application needs further processing steps, such as coating, galvanizing, welding, and tempering, to enhance some specific properties (F. C. Zhang, Yang, & Kang, 2013; Jing Zhao et al., 2020). These extra processing steps are applied at a temperature high enough to alter the features of CFB microstructure; for instance, coalescence and coarsening of the bainitic ferrite plates, decomposition of retained austenite, and precipitation of fine cementite could be a consequence of such processing, which can alter the mechanical properties (C. Garcia-Mateo, Peet, Caballero, & Bhadeshia, 2013; Park, Seol, Lim, Kim, & Park, 2015). Therefore, applying tempering treatment can stimulate what might happen during these applications.

Tempering heat treatments occur at temperatures where austenite decomposes, and the metastable microstructure of steel approaches the equilibrium structure. The mechanisms

associated with the structural changes produced by tempering can be divided into three stages, which might be overlapped and happened concurrently (Cheng, Brakman, Korevaar, & Mittemeijer, 1988; Morra, Böttger, & Mittemeijer, 2001; A. S. Podder, 2011; Primig & Leitner, 2011):

- Segregation of carbon atoms to these lower energy sites and pre-precipitation clustering in the iron matrix and cementite precipitation or transition carbides in high–carbon steels.
- Decomposition of retained austenite into equilibrium condition, i.e., formation of cementite and ferrite.

- Spheroidization/coarsening of carbides and recovery of dislocation structure followed by recrystallization of ferrite.

It worth noting that the stages mentioned above can take place during quenching of relatively high-M_S steels (austempering). Consequently, the auto tempering could happen more likely in bainite because $B_S > M_S$ which leads to the faster partition of carbon from α_b into γ_R and carbides precipitations. The expected microstructural changes in bainitic steel during tempering for different periods at 500 ℃ are explained by Bhadeshia (H. K. D. H. Bhadeshia, 2015) in Figure 1-16Figure 1-16.

In nanostructured bainite, strength relies to a lesser extent on carbon in solid solution, and it is the ferrite plate thickness, which is the dominant factor that controls the strength. Thus, significant changes in strength do only occur as a result of the plate thickness coarsening (Hala Salman Hasan, 2014; Mathew J. Peet, Babu, Miller, & Bhadeshia, 2017; M. A. Santajuana et al., 2018). The experimental results showed that the drop in hardness of a high C-Si nanostructured bainite obtained at 190 ℃ for two weeks was very limited below tempering of 500 ℃, as shown in Figure 1-17..
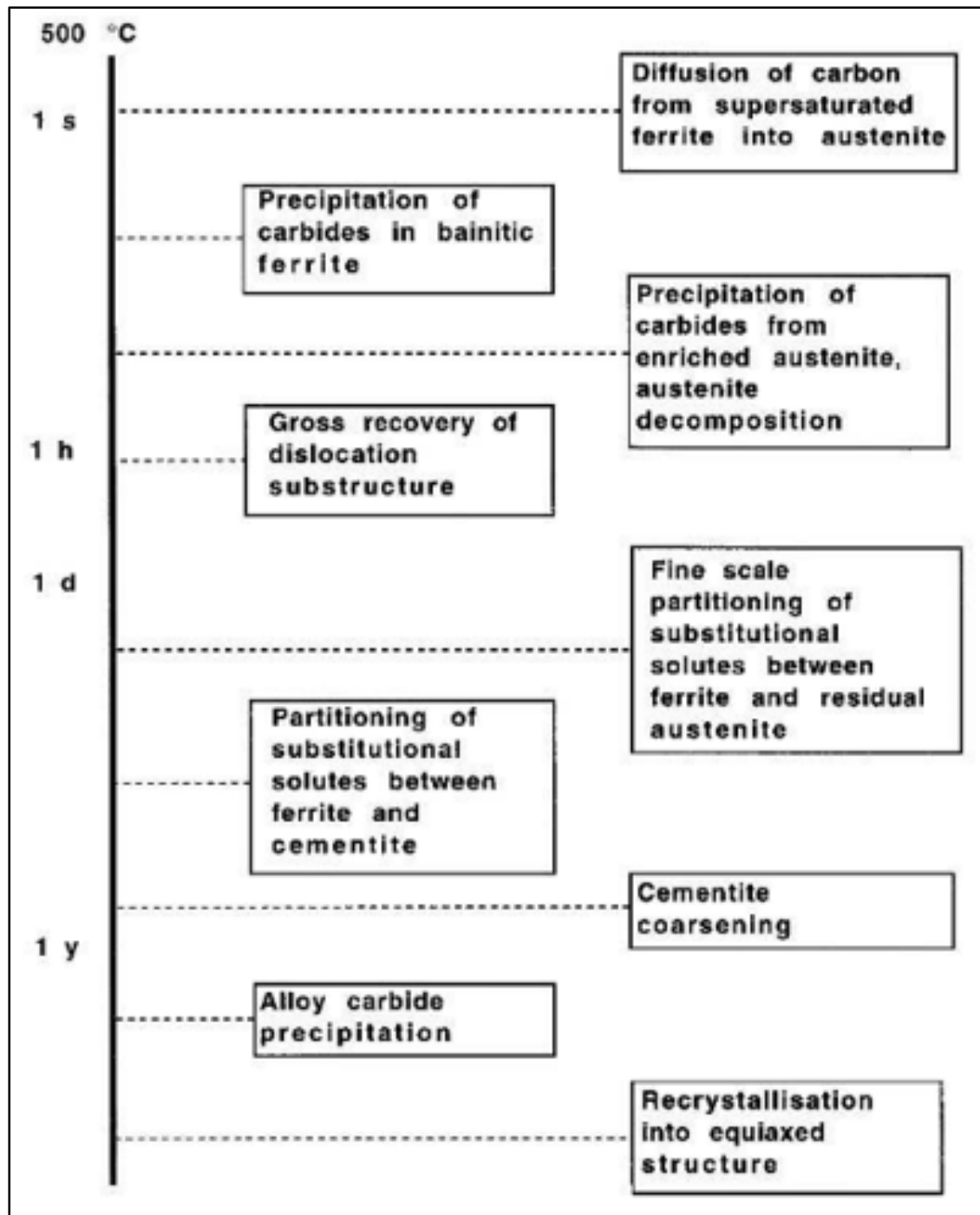
Figure 1-16 Microstructural changes vs. time during tempering of bainite at 500 ºC
Taken from H. K. D. H. Bhadeshia (2015, p88)
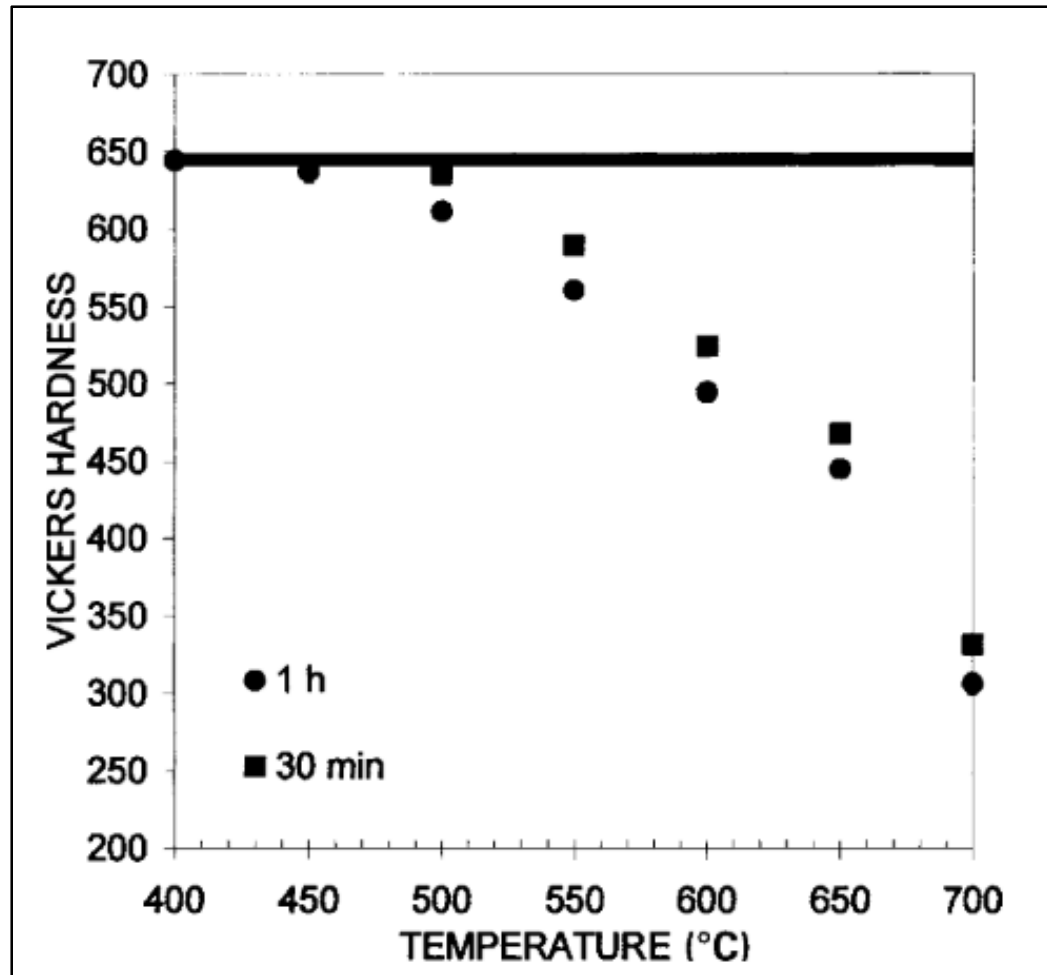
Figure 1-17 Hardness vs. tempering temperature of nanostructured bainitic steel
Taken from Caballero F.G et al. (2015, p. 279-284)

1.4.4 Current areas of application of nanostructured CFB

Because nanostructured CFB steel possesses good hardenability, large size parts can be produced. Commercial products of nanostructured steel with an excellent combination of strength (2.5 GPa), ductility, toughness, and fatigue resistance. Examples of commercial products of nanostructured CFB steel are illustrated in Figure 1-18a and 1-18b. Furthermore, this strong steel is used for the development of very strong armor. In armor application, the ballistic strength could reach 10 GPa during ballistic when steel is strained at a very high rate (e.g., 10^7 s^{-1}), where the results showed that the bainitic steel with 12 mm thickness resists the

penetration of projectile, as shown in Figure 1-18c. This ballistic performance exceeds that of titanium armor and approaches that of alumina. (H. K. D. H. Bhadeshia, 2013).
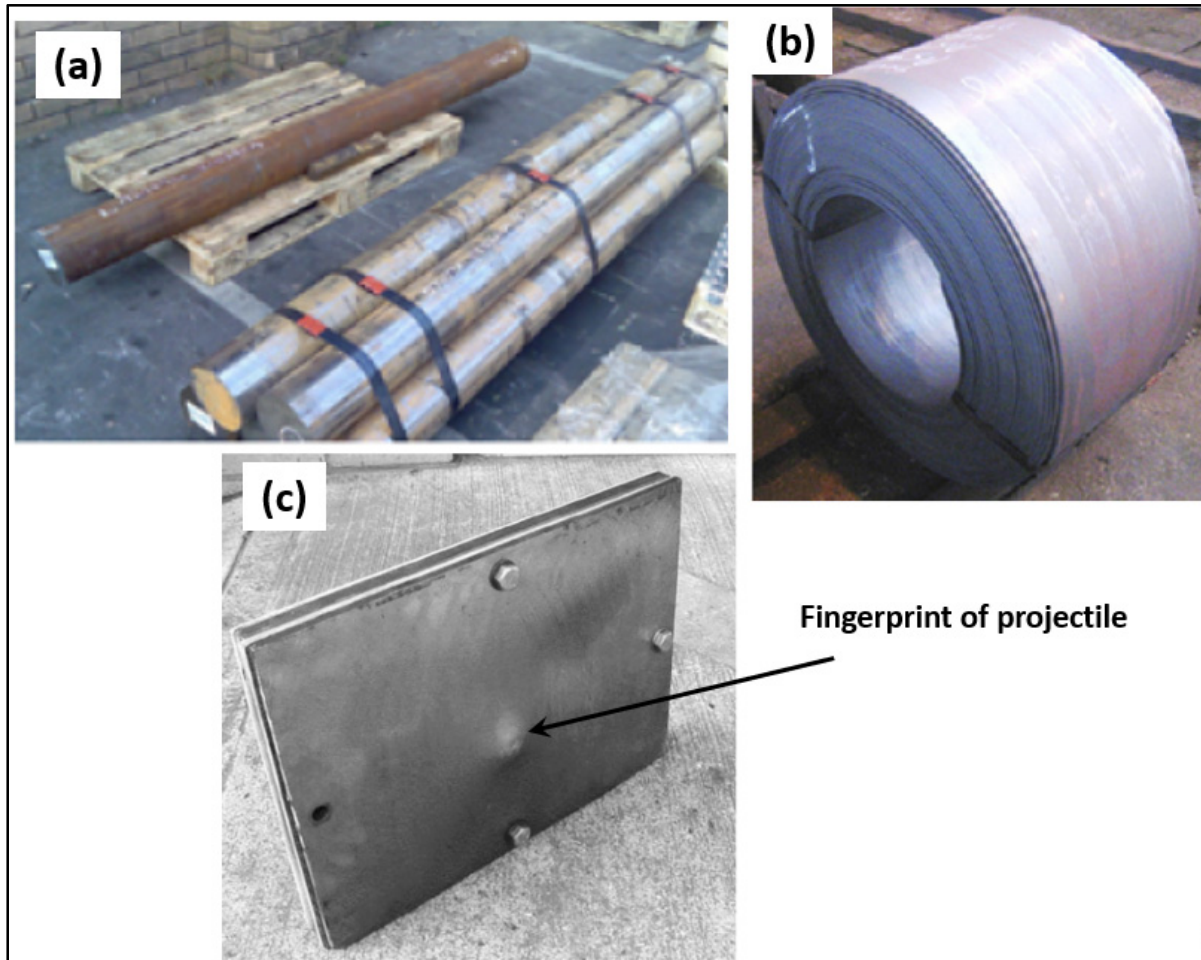
Figure 1-18 Large commercial components of nanostructured CFB steel (a) and (b); high-C-Si steel after the ballistic test (c)
Taken from Igwemezie (2014, p.148); H. K. D. H. Bhadeshia (2013, p. 405-410)

1.4.5   Restrictions on the use of high-C nanostructured CFB steel

Despite those mentioned above excellent mechanical properties of nanostructured bainite, such microstructure is only produced in high carbon steel. High carbon steel is difficult to weld because of the formation of untempered brittle martensite in the coarse-grained heat-affected

zones of the steel. The martensite fractures easily, leading to an evident deterioration in the weld integrity, therefore limiting the number of applications where this microstructure is industrially implemented.

Besides the poor weldability, the kinetics of high-C bainite transformation is very slow, and the transformation needs a longer time to complete compared with medium or low -C steel. The transformation of high-carbon steels can take days to complete at temperatures of 125–325 °C (H. K. D. H. Bhadeshia, 2009; C. Garcia-Mateo, Caballero, Sourmail, Smanio, & de Andres, 2014). This is a disadvantage in relation to the economy of rapid production rate; hence there is a need to find a way to accelerate the transformation kinetics. A study has been conducted to examine the effect of Co and/or Al on the transformation kinetics, and the reaction rate has been found to increase dramatically where the driving force for the transformation of austenite to ferrite ($\Delta G^{\gamma \to \alpha}$) increases, as shown in Figure 1-19a. Moreover, the transformation time significantly decreased by the addition of Co and Al at a concentration of less than 2 wt.% (H. K. D. H. Bhadeshia, 2009), as seen in Figure 1-19b. However, these alloying elements make steel more expensive and may influence its use in the industry. Another approach was to refine the prior austenite grain size (PAGS), which leads to an increase in the nucleation sites due to the increase in the grain boundary area. Refinement can be achieved by adding some alloying elements, such as vanadium (V), which controls the austenite grain size (H. K. D. H. Bhadeshia, 2009), or by changing the heat-treatment parameters, such as austenitizing temperature and holding time (C. Garcia-Mateo et al., 2003), as shown in   Figure 1-20.

However, other studies showed that large PAGS unhindered the growth of the bainitic sheaves and then the bainitic transformation is prompted (F. Hu et al., 2014). Hasan et al. (Hasan, Kumar, Chakrabarti, & Singh, 2020) reported that an enhancement in transformation rate was observed initially, while at the later stage of the transformation, it is reduced due to a slow reduction in the autocatalytic factor.

Accordingly, as a result of the obstacles mentioned above related to the higher-carbon nanostructured bainitic steel, the need to use a steel with a medium or low carbon content is key to ensure the comprehensive utilization of nanostructured CFB steel in several industrial sectors.
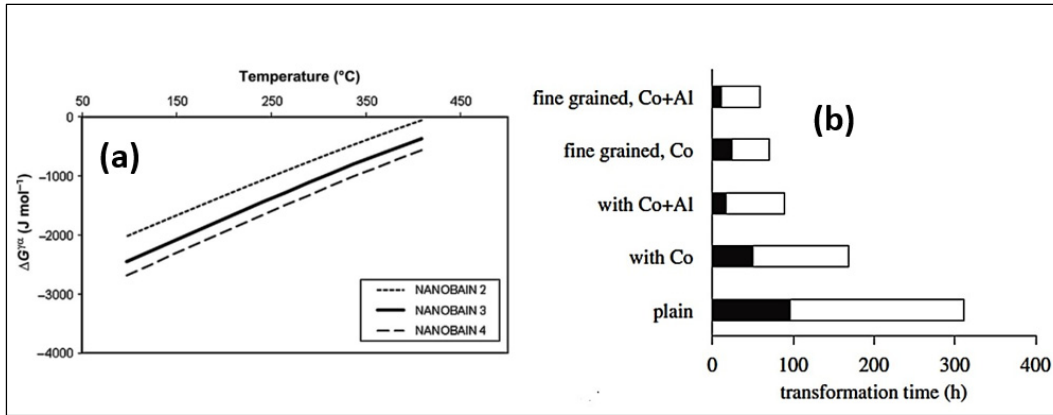
Figure 1-19 Effects of Co (NANOBAIN 3) and Co+Al (NANOBAIN 4) on the free-energy change $\Delta G^{\gamma \to \alpha}$ (a). Time was taken for starting (white bar) and completing (black bar) the transformation of bainite at 200 °C (b)
Taken from C. GARCIA-MATEO (2003, p. 1822); H. K. D. H. Bhadeshia (2009.p 12)
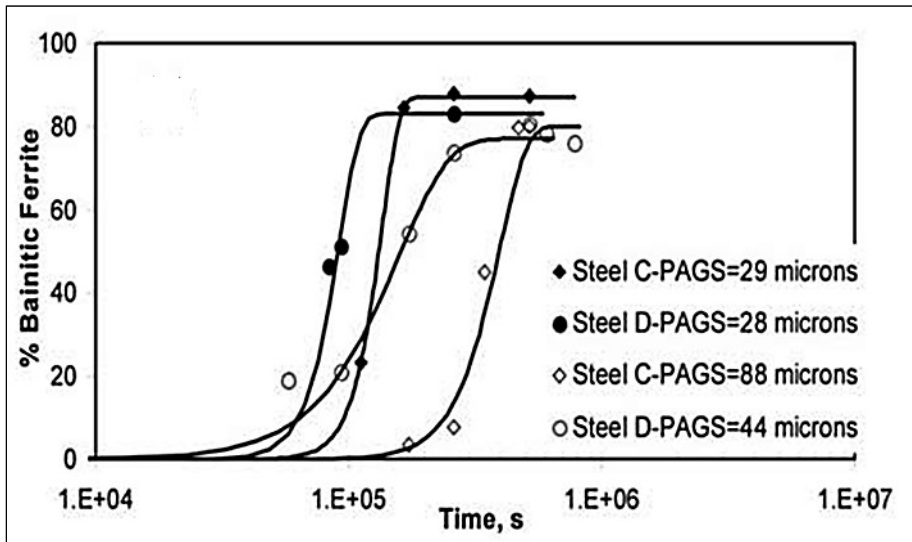
Figure 1-20 Effect of PAGS on the bainitic transformation rate
Taken from C. Garcia-Mateo et al. (2003, p. 1824)

1.5   Nanostructured CFB in medium and low carbon steels

The fundamental parameter to produce a nano-scale bainitic structure is to perform the isothermal transformation at low transformation temperature, 200-350 ºC (C. Garcia-Mateo, Paul, Georg, Somani, Mahesh C., Porter, David A., Bracke, Lieven, Latz, Andreas, Garcia De Andres, Carlos, Caballero, Francisca G., 2017), making it possible if the steel contains a carbon content of ~1 *wt.%*. Garcia-Mateo et al. (C. Garcia-Mateo, Paul, Georg, Somani, Mahesh C., Porter, David A., Bracke, Lieven, Latz, Andreas, Garcia De Andres, Carlos, Caballero, Francisca G., 2017) gathered, discussed, and classified the possible ways to obtained nanostructured bainitic steel according to four different approaches as following:

1.5.1   Modification of steel's chemical composition:

Various approaches have been taken to obtain nanostructured bainitic steels with lower carbon content. Yang and Bhadeshia (Yang & Bhadeshia, 2008) reported that producing nanostructured bainite in low carbon steel by adding large concentrations of substitutional solutes, such as nickel, to reduce B_S and M_S. The results were not encouraging because of two major drawbacks: 1) coarsening of the microstructure occurs due to the coalescence of fine bainite laths (Keehan, Karlsson, & Andrén, 2006; Pak, Bhadeshia, Karlsson, & Keehan, 2008); 2) the temperature gap between the B_S and M_S disappears (Yang & Bhadeshia, 2008), as shown in Figure 1-21 for the case of Ni additions.

Similar to the trial mentioned above, Soliman et al. used two systems of alloying elements in low and medium carbon steels. In low-C steel, the thickness of α_b plates were 150 nm by adding 3.44 and 1.85 wt.% of Mn and Ni, respectively (Soliman, Mostafa, El-Sabbagh, & Palkowski, 2010). Whereas the thickens was ≤ 120 nm when Co and Al were added to medium-C steel (Soliman & Palkowski, 2007). Wang et al. (Wang, Zhang, & Wang, 2013) and Long et al. (Long, Kang, Lv, & Zhang, 2014) reported that the thickness of α_b was in the range of 100-150 nm besides a very thins retained austenite (γ_{Rf} <100 nm) in Fe-0.35C-1.5Si-1.5Mn-0.8Al-1.15Cr-0.4Mo steel after either double isothermal transformation at 320-

275 °C, or continuous transformation between 320-275 °C. Keep in mind, adding such alloying elements, i.e., Mn, Ni, Al, and Co, could raise the cost of the required steel, hence it makes this steel uncompetitive to other steels that have similar mechanical properties.
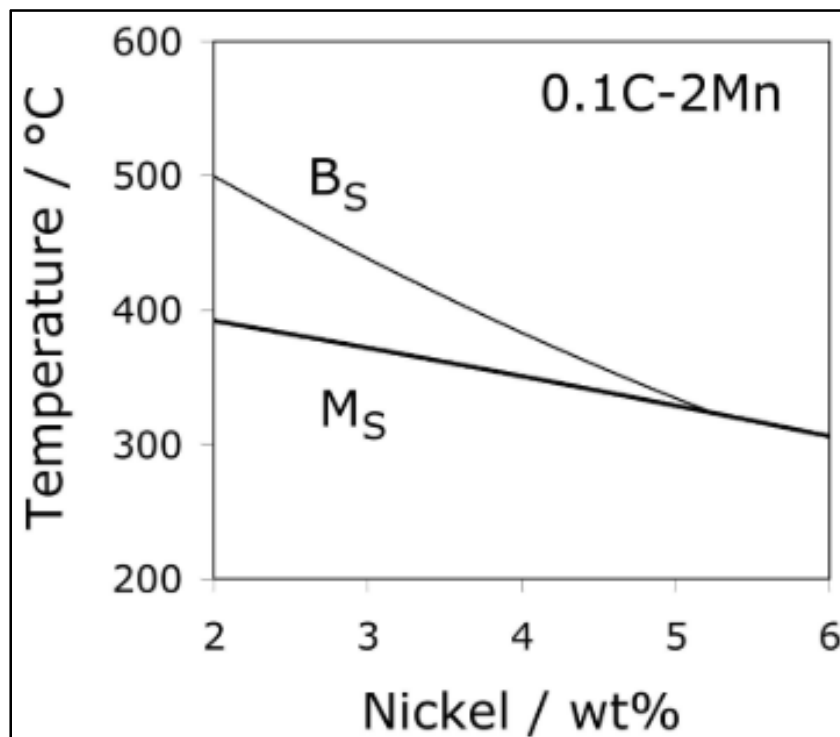
Figure 1-21 Calculated bainite and martensite–start temperatures for steel contains 0.1C and 2Mn in wt.%, as a function of nickel concentration
Taken from Yang & Bhadeshia (2008, p336)

1.5.2   Alteration of bainitic transformation routs

The bainite transformation, either isothermal or continues was adapted in order to force the α_b to form in thin plates. Two possible ways can be implemented. Using multiple bainite transformation stages to increase the carbon content in γ_R each stage, and at the end, a low-temperature transformation can be enhanced. Wang et al. (Wang et al., 2013) decreased the average bainite plate thickness to about 110 nm for steel with 0.30C-1.46Si-1.97Mn-1.50Ni-0.30Cr-0.96Cu-0.25Mo wt.% by using three isothermal transformation temperatures in

sequence (300, 250, and 200 °C) with different holding time. Another possible approach is to increase the bainite nucleation sites and to enhance the transformation via quenching below the M_S followed by bainitic transformation, similar to a quenching and partitioning treatment (Q&P). In this context, Li et al (Q. Li, Huang, & Huang, 2016) applied quenching and dynamic partitioning (Q-DP) process to produce a very fine microstructure consists of martensite, bainite and film-like retained austenite in medium-C steel. Similarly, Zhao et al. (L. Zhao, Qian, Meng, Zhou, & Zhang, 2016) decreased the plate thickness from 245 to 203 nm by quenched low carbon steel (0.13 wt.%) below M_S followed by bainitic transformation at 355 °C. The author reported equivalent reduction in thickness (185 to 141 nm) in 0.26 wt.% C steel at 320 °C bainite transformation.

Even though in the aforementioned heat treatments, the authors could reduce remarkably the bainitic ferrite plates, but the presence of athermal (fresh) martensite formed prior to bainite transformation can have a detrimental effect on the performance of the steel. Moreover, in the multi step transformation, the process can take more than 48 hrs to be completed.

1.5.3 Control of prior austenite grain size (PAGS)

Various researchers stated that smaller PAGS increases the amount of the obstacles that encounter the martensitic growth; as a result, the M_S decreases that gives the ability to make the bainitic transformation at a lower temperature (García-Junceda, Capdevila, Caballero, & de Andrés, 2008; Hanamura, Torizuka, Tamura, Enokida, & Takechi, 2013; H. Yang & Bhadeshia, 2009). The effect of reducing PAG on the bainite transformation can be assigned to two main aspects: i) enhancing the transformation kinetics by introducing a vast area of grain boundaries, i.e., high nucleation sites; 2) higher nucleation sites could increase the volume fraction of bainite per austinite grain; consequently, the growth of a plate of bainite can be stopped by another one (impingement effect)—likewise, Hu et al. (F. Hu et al., 2014) investigated the effect of PAGS on bainite morphology in super bainite with high carbon content. The author found that finer α_b sheaves was obtained in smaller PAGS compared to bigger PAGS. In medium carbon steel, Dong et al. (Dong, Hou, Zhou, Zhang, & Wu, 2018)

noticed that the thickness of bainitic ferrite was inversely proportional to the increase in PAGS, where the smallest thickness was 45 nm when the PAGS was 33 µm, while it was 70 nm for 82 µm PAGS.

On the other hand, contradictory results were also reported that reducing the PAGS could negatively impact obtaining a very fine bainitic microstructure. Singh et al. (K. Singh, Kumar, & Singh, 2018) showed that a larger PAGS resulted in thicker bainitic sheaves and a higher fraction of γ_{Rb}. The author attributed that to lateral growth of bainitic ferrite plates when the longitudinal growth was impeded at the austenite grain boundary. Interestingly, Jiang et al. (Jiang, Liu, Sun, Guo, & Liu, 2016) noted that although the bainitic transformation was accelerated by reducing the PAGS from 53 to 3 µm in high-C bainitic steel, the nanostructured morphology of α_b could only obtained when the PAGS was in 18 µm. However, larger (53 µm) or smaller (3 µm) PAGS, the bainitic plates were not in the nano-scale criteria. Therefore, the effect of PAGS on the final scale of the bainitic ferrite plates is debatable.

1.5.4 Modifying austenite state prior to bainite transformation (Ausforming)

Ausforming is the thermomechanical treatment where a deformation can be applied prior to phase transformation. High-temperature ausforming involves the deformation of steel in the austenite/ferrite (γ/α) or austenite (γ) regions, i.e., at a temperature greater than Ac$_1$, as shown in   Figure 1-22, and it is well reported that it enhances the kinetics of reconstructive phase transformation such as ferrite and pearlite, (H. Hu, Zurob, Xu, Embury, & Purdy, 2015; Khlestov, Konopleva, & McQueen, 1998). In displacive transformation (martensite and bainite), the ausforming process is implemented below the recrystallization temperature (T$_{NR}$) and above M_S, followed by either bainite or martensite transformation. Commonly, but not exclusively, this deformation occurs in the bay between the ferrite and bainite curves of the time-temperature-transformation (TTT) diagram, i.e., when austenite is in the metastable form, as see   Figure 1-22. Deformation can strengthen the microstructure by piling up the dislocations and dislocation substructures introduced in austenite grains (Tsuji & Maki, 2009). Therefore, the austenite yield strength increases (σ_γ). Accordingly, both, bainite and

martensite transformation can be delayed or even suppressed if a specific deformation is applied in austenite prior to the transformation, defined as critical strain. The reason lying beneath is the mechanical stabilization of the parent austenite due to the applied strain (Maalekian, Kozeschnik, Chatterjee, & Bhadeshia, 2013; H.-S. W. S. Chatterjee, J. R. Yang & H. K. D. H. Bhadeshia, 2013). Mechanical stabilization occurs when the stress that drives the transformation (i.e., the motion of the γ/α interface) equals the stresses opposing its motion, as expressed in equation (1-5) (Maalekian et al., 2013). Experimental results proved that the M_S can be reduced via the mechanical stabilization of austenite (Maalekian et al., 2013; Seo et al., 2015; M. Zhang, Wang, Wang, Yang, & Zhang, 2013).

$$\Delta G^{\gamma \to \alpha} = \frac{\mu b \rho^{0.5}}{8\pi(1-v)},$$ (1-5)

$\Delta G^{\gamma \to \alpha}$ is the driving force for the γ to α transformation, μ is the shear modulus, b is the Burgers vector, ρ is the dislocation density, and υ is the Poisson's ratio.
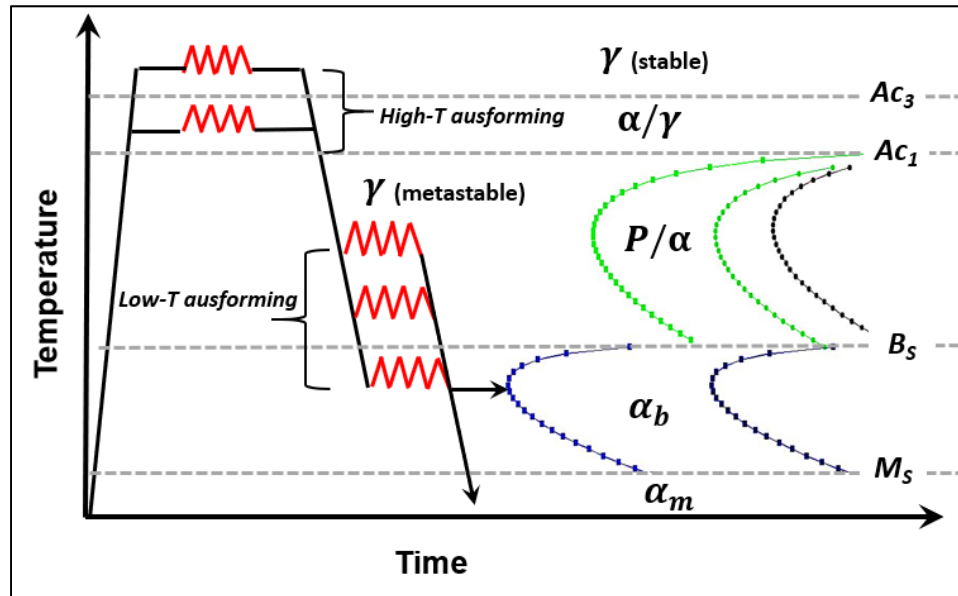
Figure 1-22 Different ausforming processes according to the deformation temperature (γ, α, p, and α_b, α_m represent austenite, ferrite, pearlite, bainite, and martensite, respectively)

The effect of ausforming on the bainite transformation can be classified into these three groups, which will be discussed in detail in the following section:

1.5.4.1   Transformation kinetics

The effect of ausforming on the kinetics of bainite transformation has been extensively studied; however, a clear image of the operating mechanisms cannot be depicted: On one hand, several reports have claimed that the deformation effect depends on ausforming parameters, such as percent and temperature of applied deformation. Schastlivtsev et al. (Schastlivtsev et al., 2013) demonstrated that the ausforming of low-carbon alloy steel at 920 °C could prompt the completion of the bainite reaction due to an increase in the nucleation sites originates from the deformed parent phase. Likewise, Golchin et al. (Golchin, Avishan, & Yazdani, 2016) indicated that a small deformation (10%) accelerates the bainitic transformation and increases the volume fraction of retained austenite. Hu et al. (H. Hu et al., 2015) demonstrated that bainite transformation could be enhanced by a slight deformation at 300 °C followed by isothermal treatment at 300 °C, whereas neither ausforming at higher temperature nor large deformation can promote the bainitic reaction, as illustrated in Figure 1-23. Similarly, He et al. (B. B. He, Xu, & Huang, 2015) investigated the effect of ausforming parameters on bainite transformation in low-carbon boron steel. The author highlighted that ausforming at 500-600 °C with 15-20% plastic deformation shortens the incubation time, accelerates the reaction rate, and increases the volume fraction of the transformed bainite, whereas large deformation at a high temperature slowed down bainite transformation kinetics. A similar conclusion was also stated by Gong et al. (Gong et al., 2013; Gong, Tomota, Koo, & Adachi, 2010).

On the other hand, other researchers claimed that deformation hindered the bainite transformation, Shipway et al. (Shipway & Bhadeshia, 1995b) reported that the transformation was delayed as a result of the accumulated of dislocations which hinder the motion of the transformation interface in the deformed austenite. Larn et al.(Larn & Yang, 2000) showed in Figure 1-24 that the overall transformation kinetics became slower, and the amount of transformed bainite decreased when a deformation was applied at 800 ºC with different

deformation amount (10, 20, 40%) compared to the non-deformed sample in two Fe-Mn-Si-C steel with different carbon content, steel A and steel B with 0.059 and 0.12 wt.%, respectively, and treated isothermally at 480 °C.
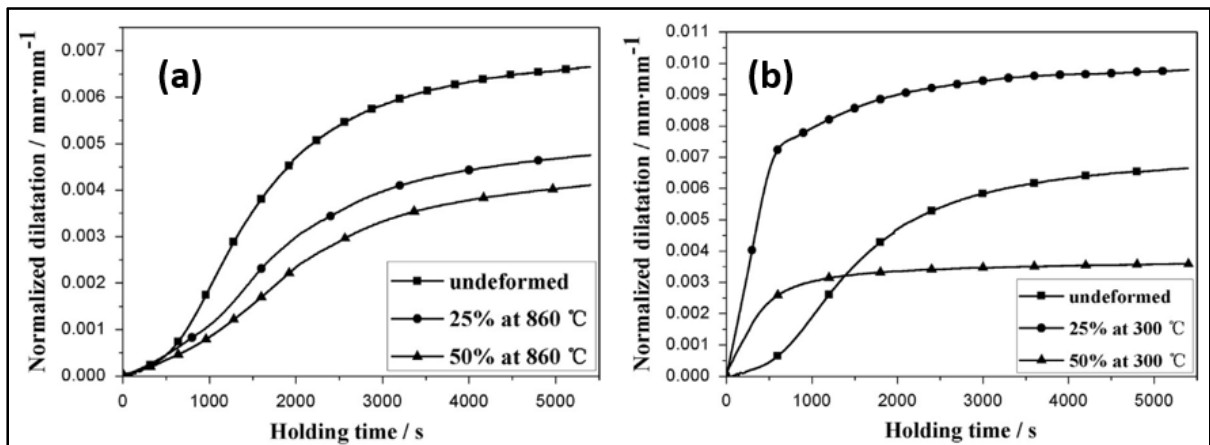
Figure 1-23 Dilatation behavior of bainite transformation for (a) ausformed 860 °C and (b) ausformed at 300 °C
Taken from H. Hu et al. (2015, p. 3)
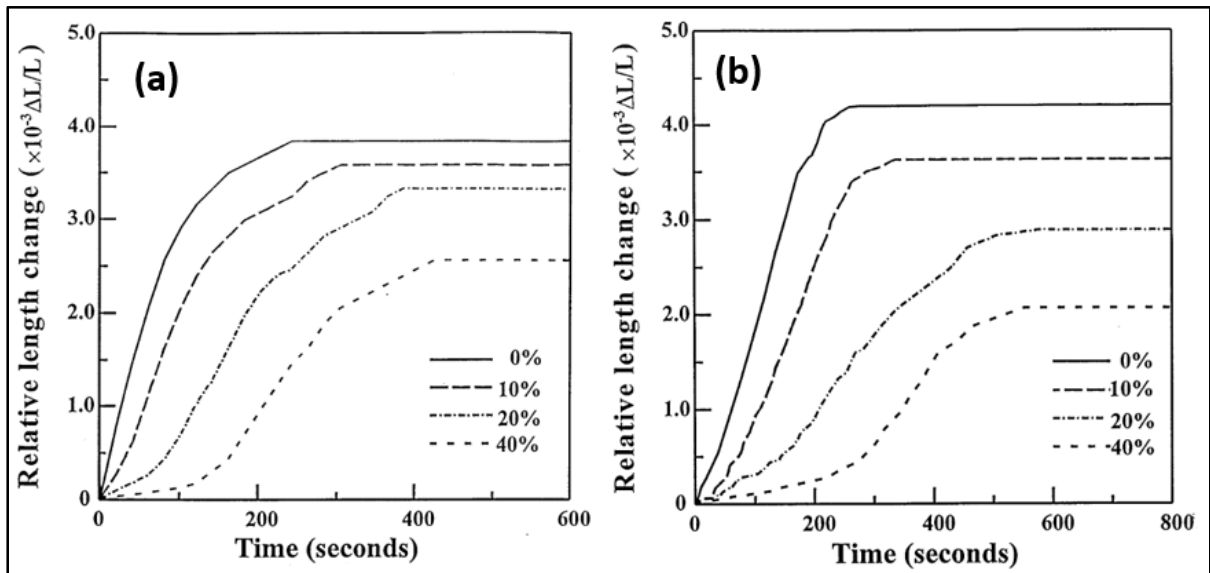
Figure 1-24 Dilatometric curves for samples isothermally treated at 480°C with and without prior deformation (the amount of prior deformation indicated). (a) steel A, (b) steel B
Taken from Larn & Yang (2000, p. 280)

In addition to the reports mentioned earlier, there is still another possibility in which the transformation can be accelerated at early stages followed by retardation. The increase of nucleation sites due to deformation can enhance the early stages of transformation, and then, as the transformation progresses, and more bainite forms, i.e. higher dislocation density is introduced in the microstructure, the advancing transformation encounter more obstacles that make it sluggish (Freiwillig, Kudrman, & Chráska, 1976; S. B. Singh & Bhadeshia, 1996). Shixin et al. (Shixin XU, 2018) stated that low pre-deformation temperature (300 °C) could accelerate bainite transformation at the whole isothermal region, while high pre-deformation temperature (850 °C) accelerated bainite transformation at the initial stage and hindered bainite transformation at a later stage.

1.5.4.2   Microstructure morphology (size of α_b and γ_r)

Here, the idea is to force the bainite plates to form in slender morphology by strengthening the austenite prior to transformation; then, growth of bainitic plates is hindered from being thicker. In this context, Zhang et al. (M. Zhang et al., 2013) reported that a nanoscale CFB microstructure was produced in medium-carbon Si-Al-rich alloy steels by ausforming at 300 to 600 °C with 50% plastic deformation. The thickness α_b was 128 nm in pure isothermal condition and it reduced to 48 nm after ausforming and subsequent isothermal transformation at 250 °C. In another study done by the same author (M. Zhang, Wang, Zheng, Zhang, & Wang, 2014b), he revealed that ausforming by 30% deformation at low temperatures (300-600 °C), followed by isothermal transformation at 235 °C–250 °C, nanostructured bainite with lath thickness considerably less than 100 nm was formed with a hardness of 592–655 HV. Chen et al. (Chen et al., 2020) investigated the effect of the combination of ausforming (deformation with a strain of 0.2) and isothermal transformation at 300 °C on the refinement bainite morphology in Fe-0.43C-1.90Si-2.83Mn-0.57Al-0.06Cu (wt.%) steel. The results showed that the bainitic ferrite plate thickness decreased to about 80%, from 724 nm to 151 nm. The SEM micrographs in Figure 1-25 showed the change in bainitic ferrite plate thickness after ausforming at 300 °C with 20% plastic compressive deformation.
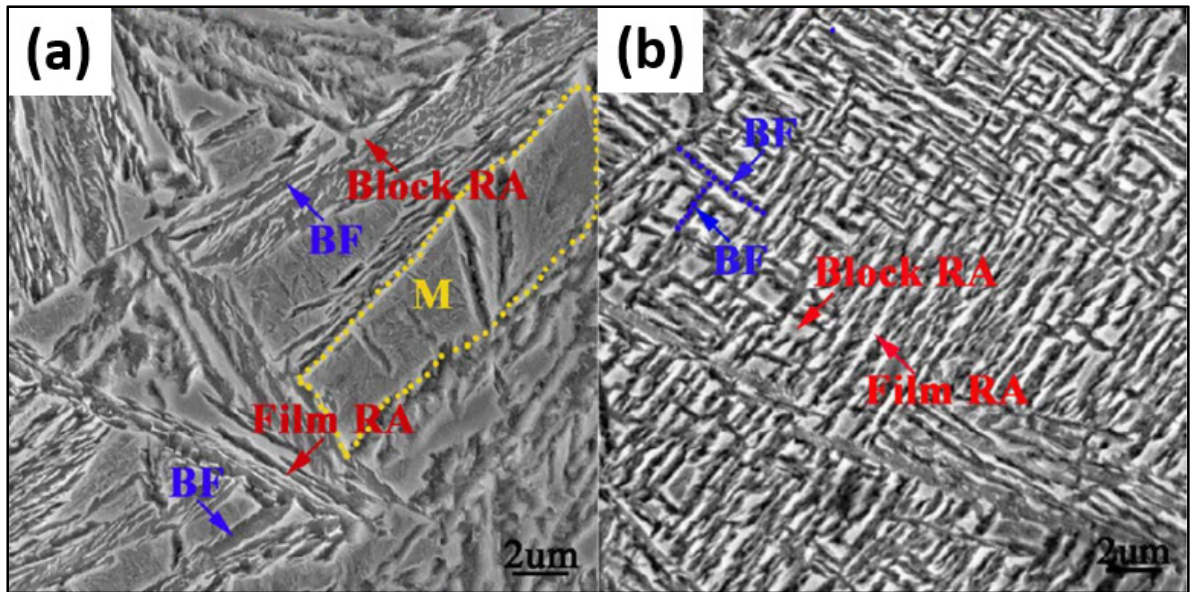
Figure 1-25 SEM micrographs for bainitic ferrite morphology for medium C steel after isothermal transformation ay 300 °C (a) non-ausformed (b) ausformed at 300 °C
Taken from Chen et al. (2020, p. 2009)

Other studies reported that there was a threshold limit for ausforming to refine the bainite plates; otherwise, thickening occurs. Hu et al. (H. Hu, Xu, Dai, Tian, & Chen, 2019) investigated the effect of deformation temperature on α_b plate thickness in medium-C-Si rich steel and concluded that the non-ausformed plate thickness, 375 nm, was decreased to about 150 nm and 300 nm when the ausforming was applied at 300 and 350 °C, respectively. In contrast, ausforming at higher temperature coarsen bainite plates compared with the non-ausformed case. Eres-Castellanos et al. (Eres-Castellanos, Morales-Rivas, Latz, Caballero, & Garcia-Mateo, 2018) also observed similar trend in SCM40 bainitic steel.

However, Shixin et al. (Shixin XU, 2018) showed that ausforming increases the thickness of bainite plates with decreasing pre-deformation temperature in medium carbon steel (Fe-0.43C-1.52Si-2.41Mn-1.43Cr-0.26Mo-1.33Co-0.64Al). The thickness of plates was 180, 100, and < 100 nm at ausforming temperatures of 300, 850 °C, and undeformed, respectively. As shown in Figure 1-26, the smallest thickness was obtained when ausforming applied at 850 °C.

42
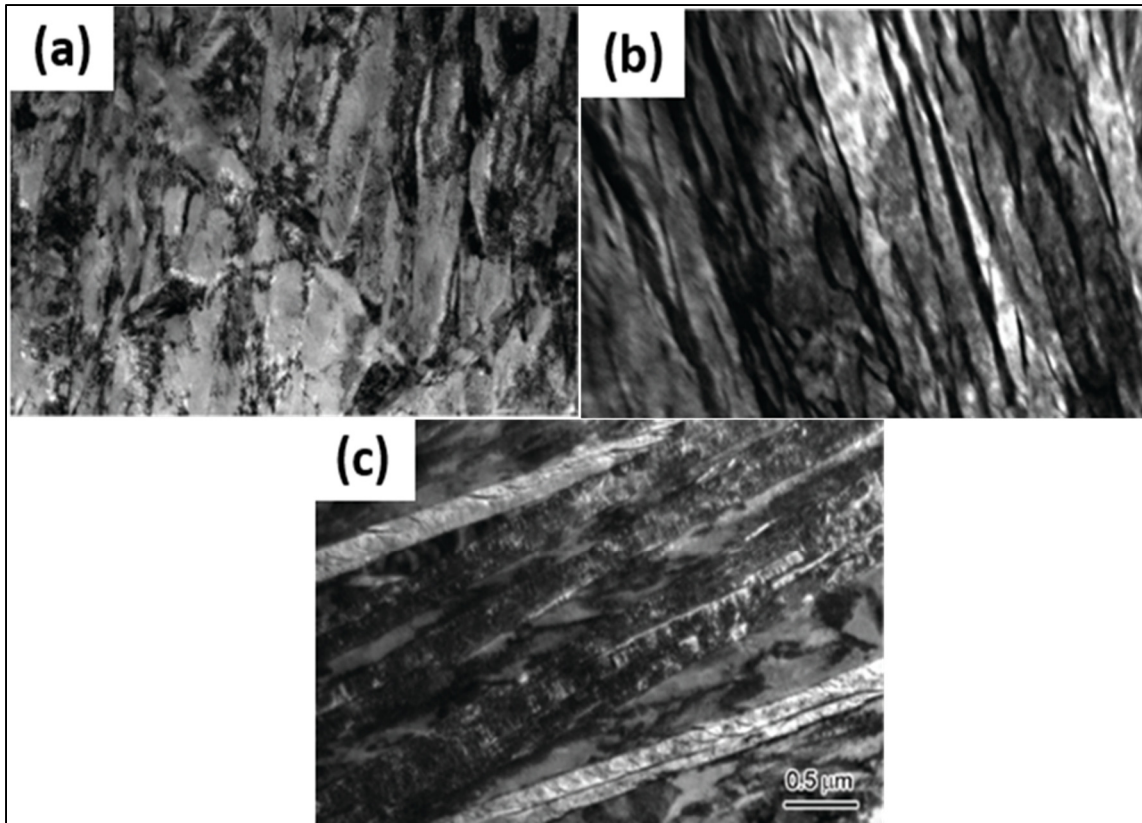
Figure 1-26 TEM images of sample under different pre-deformation processes (a) 300
°C (b) 850 °C (c) nondeformed
Adapted from Shixin XU et al. (2018, p. 1118)

Accordingly, the effect of ausforming on the bainitic ferrite plates is still inconclusive. The present research attempts to understand the influence of the ausforming process on refining the bainite morphology into a nanoscale using different deformation routes.

1.5.4.3   Stability of retained austenite

In this section, we are talking about the stability of retained austenite (γ_R) during the final stage of CFB transformation, i.e., during cooling down to ambient temperature. As already mentioned above, two types of γ_R are existent within the CFB matrix: film-like (γ_{Rf}) and blocky-shape (γ_{Rb}) retained austenite. However, introducing another factor, such as

deformation, can have a different effect. Hu et al. (H.-j. Hu, Xu, Wang, Zhou, & Xue, 2015) studied the effect of ausforming on the stability of retained austenite in C-Mn-Si bainitic steel. He demonstrated that the size of block-shape retained austenite decreased and the overall amount of γ_R i.e., $\gamma_{Rf} + \gamma_{Rb}$ increased due to martensite transformation resistance during cooling to room temperature (mechanical stabilization phenomenon). In another research (H. Hu et al., 2015) the author reported that 30% deformation before bainitic transformation increases the stability of retained austenite, while 50% leads to martensite transformation during the final stage of transformation (less stable). Zhang et al. (M. Zhang et al., 2013; M. Zhang et al., 2014b), reported that stability of γ_r was higher in deformed samples at 600 and 300 ℃ than its values in undeformed sample in medium-carbon Si–Al-rich steel.

There is no doubt that the role of retained austenite is a topic of paramount concern. However, changes in the initial fraction of retained austenite and its stability cannot be easily made without altering other factors, such as ausforming parameters and bainitic transformation conditions. Thus, in order to clarify it, mechanisms and factors affecting the martensitic transformation or austenite stability need to be well investigated.

1.5.4.4 Microstructural anisotropy and variant selection

Ausforming can increase the probability of specific variants to form since the energy that is needed to transform from austenite to that crystallographic variant is lower than for others. When only several of the variants have grown from each prior austenite grain, it is said that there is variant selection. Therefore, during bainite transformation, the ausformed bainitic plates' growth will be in limited spatial directions in each austenite grain because of variant selection existence, instead of a random manner as in undeformed conditions, resulting in the microstructural alignment and transformation texture, i.e., microstructure anisotropy. Since such anisotropy can result in a variation of mechanical properties, variant selection due to ausforming must be considered (Gong et al., 2010; Miyamoto, Iwata, Takayama, & Furuhara, 2013; Shirzadi et al., 2009; J. Zhao et al., 2017).

Variant selection is more likely to occur at lower ausforming temperatures than at high temperatures. In the former case, the existence of planar dislocation assists the $\gamma \rightarrow \alpha_b$ transformation due to low stacking fault energy of austenite at low temperature, while in the latter case (high temperature), the high stacking fault energy leads to the presence of curved and tangled dislocations, which minimize the existence of variant selection (Chen et al., 2020; Gong et al., 2013; B. B. He et al., 2015). Guo et al. (H. Guo, Feng, Zhao, Li, & Chai, 2020) reported that the impact toughness of medium-carbon bainitic steel could negatively be affected by strong variant selection due to ausforming at low temperature (300 °C). The author attributed that to the unfavourable suppressing crack propagation when the number of bainite variants reduced in each austenite grain. In contrast, Zhang et al. (M. Zhang et al., 2014b) stated that variant selection could prompt the increase of the γ_{Rf} rather than the γ_{Rb}.

It is approved that the toughness of steel can be enhanced by increasing the fraction of γ_{Rf} (Avishan, Yazdani, & Hossein Nedjad, 2012; H. K. D. H. Bhadeshia & Edmonds, 1983). Using electron backscattering diffraction (EBSD) with inverse pole figure (IPF) technique is helpful to reveal the presence of different levels of texturing due to variant selection. Liu et al. (M. Liu et al., 2019) studied the effect of elastic and plastic strain on the orientation of bainite plates and showed that variant selection occurred in both conditions; however, it was stronger in samples deformed plastically and the bainite plates oriented along a specific direction and the orientation is much more anisotropic and transformation texture with strong peaks observed in both elastically and plastically samples, as shown in the orientation imaging maps and IPF in Figure 1-27 a-c and Figure 1-27 d-f, respectively. Similarly, Eres-Castellanos et al. (Eres-Castellanos et al., 2018) showed the relationship between bainitic ferrite (α_b) and parent austenite in in medium C-high-Si steel followed Nishiyama–Wassermann (N-W) orientation after isothermal transformation at 300 °C, where twelve different crystallographic variants can form from the parent austenite. In the samples non-ausformed and ausformed at 520 °C conditions, all α_b variants existed, while low- temperature ausforming (400 and 300 °C) the variants decreased, as observed in Figure 1-28 a-d, and lead to strong texture, as shown in pole figures in Figure 1-28 e-h.
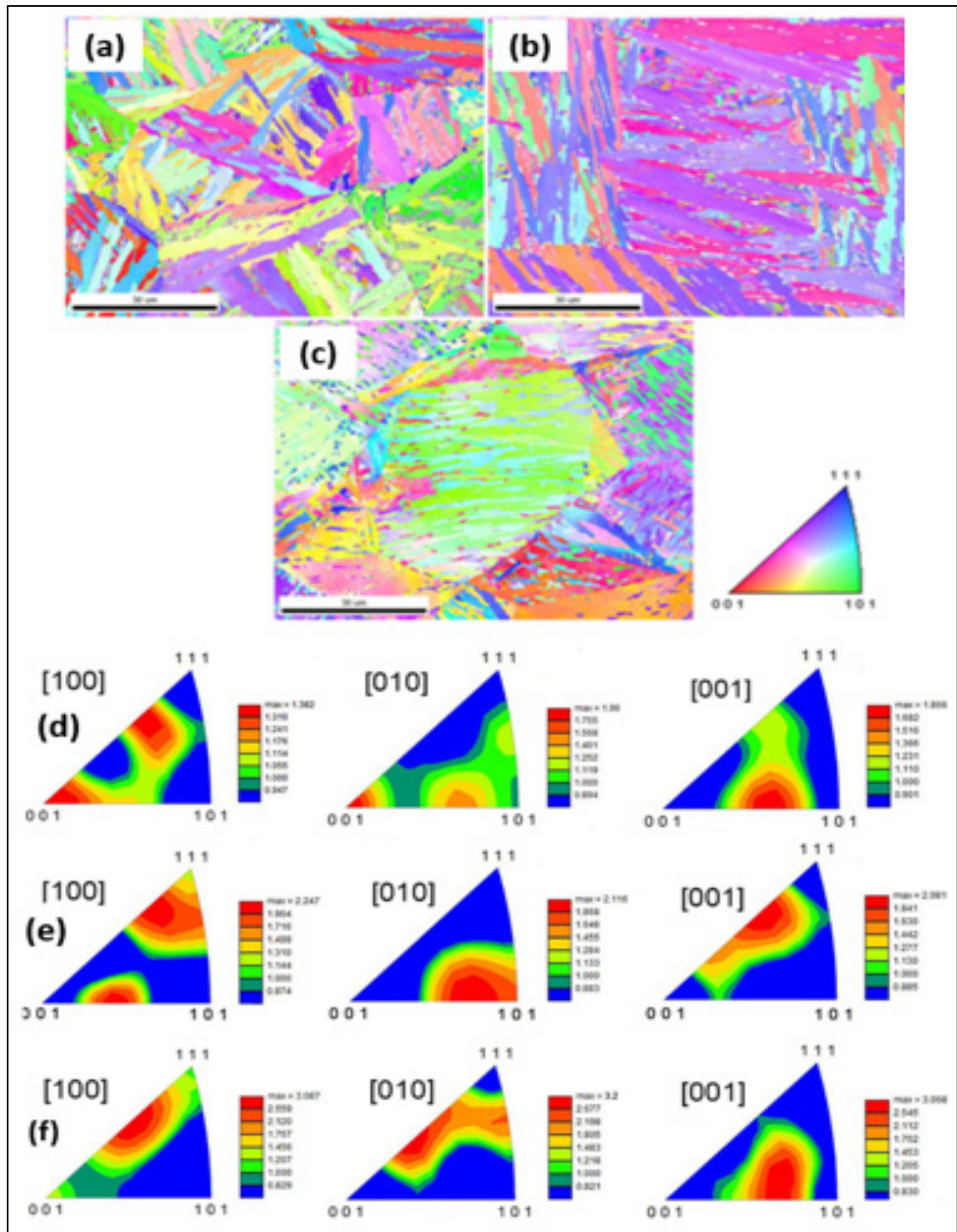
Figure 1-27 Orientation imaging maps and IPF of bainite in the samples with different stresses: (a, d) without stress; (b, e) compressive elastic stress; (c, f) plastic compressive stress
Taken from M. Liu et al. (2019, p. 162-163)
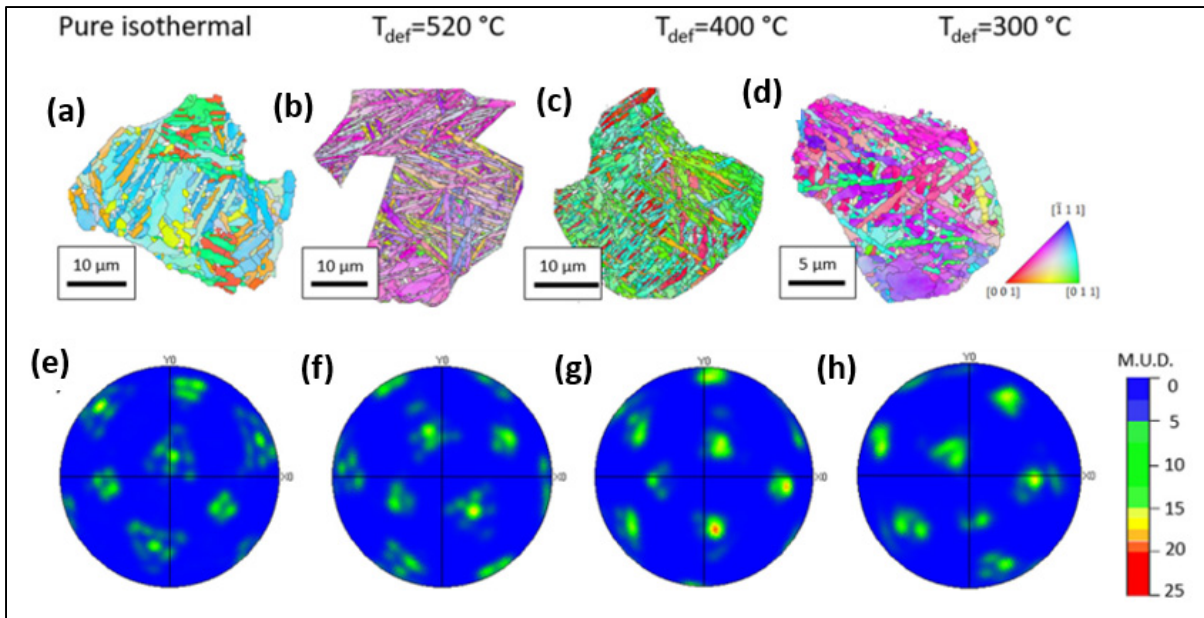
Figure 1-28 IPF maps of bainitic ferrite in single-parent austenite (upper images) and correspondent pole figures (lower images) for different conditions, (a-e) pure isothermal; (b-f) ausforming at 520 °C; (c-g) ausforming at 400 °C; (d-h) ausforming at 300 °C. T_{def} stands for deformation temperature
Taken from Eres-Castellanos et al. (2018, p. 378)

Furthermore, Eres-Castellanos et al. (Eres-Castellanos et al., 2018) revealed that the anisotropy of bainite transformation could be generated by ausforming process, and its degree can be controlled via competition between the transformation undercooling ($\Delta G^{\gamma \rightarrow \alpha}$) and the ability to promote certain crystallographic variants. From an experimental perspective, the anisotropy behavior due to variant selection can be detected by dilatation behavior during bainitic transformation. If the bainitic transformation undergoes an anisotropic behavior, a negative dilatometric signal (contraction) will be seen, and the degree of negativity can be considered as an indication of anisotropy level, i.e., non-uniform dilatation behavior (Chen et al., 2020; Eres-Castellanos et al., 2018; J. He et al., 2018). Eres-Castellanos et al. (Eres-Castellanos et al., 2021) showed that the anisotropic behavior of bainitic transformation due to prior deformation depends not only on the ausforming parameters but also on the steel chemical composition, which control of the selected the transformation temperature. Figure 1-29 illustrates the dilatometric response of three different bainitic steel after ausformed at different temperatures followed by isothermal transformation. The low C steel (02C2Si) shows only an

expansion signal in all conditions Figure 1-29(a), while the largest gap between the positive and negative dilatation (antitropy) was in steel with higher Si content (04C3Si) ausformed at a low temperature (LT ausforming), Figure 1-29(c).

Transformation plasticity strain (TP) due to the anisotropy and variant selection can also be distinguished during ausformed bainite transformation, which could occasionally complicate understanding the relation of dilatation behavior and the microstructural changes. The mechanisms underlying the evolution of TP strain during ausformed bainite transformation with respect to the dilatation behavior and its link with the microstructural are far from being understood.
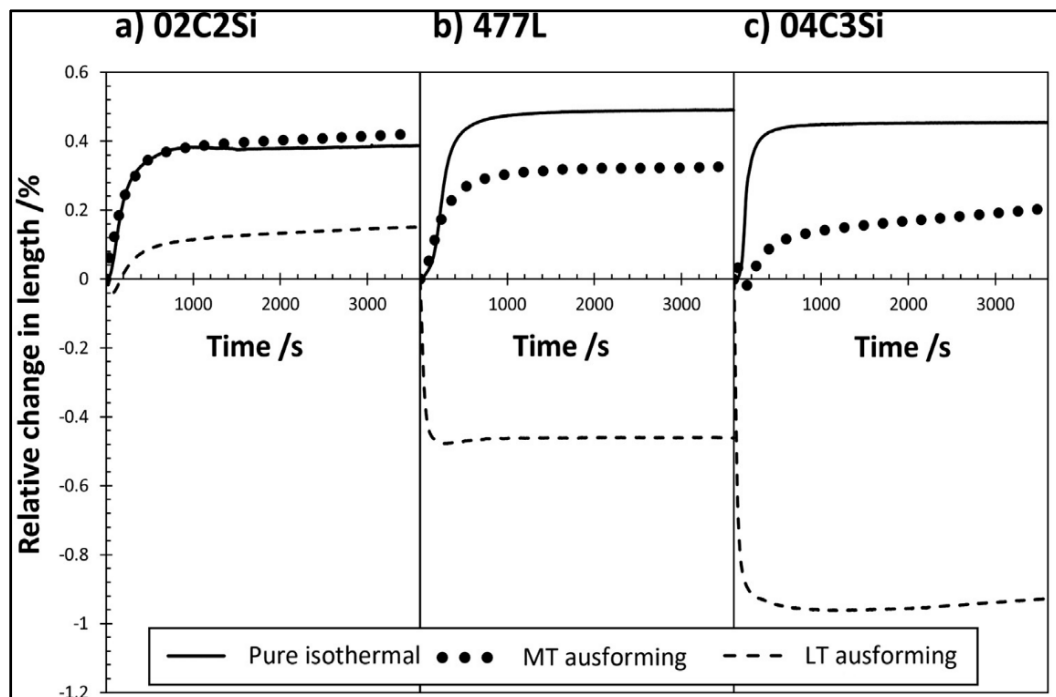
Figure 1-29 Relative change in length during bainite transformation for the steels (a) 02C2Si; (b) 477 L and (c) 04C3Si. MT and LT stand for medium and low temperature, respectively
Taken from Eres-Castellanos et al. (2021, p. 10)

1.5.4.5   Tempering resistance

As reported in section 1.2.3, high carbon CFB steel possesses very acceptable resistance to tempering softening up to 500 °C. In medium carbon steels, there are limited studies that have dealt with the effect of tempering. Like nanostructured bainite obtained in high C steel, it is reported that film-like retained austenite is more prone to decompose during tempering than blocky-shape due to its higher carbon content (Klein et al., 2019; A. Podder, Lonardelli, Molinari, & Bhadeshia, 2011). Sourmail et al. (Sourmail et al., 2021) investigated the effect of tempering at a temperature ranging from 450 -700 °C on low carbon steel having 0.2 wt.% vanadium(V), and the other is free of V. The results showed that both steels exhibited decomposition of γ_R in two ways: 1) $\gamma_R \rightarrow \alpha_m$ during cooling from tampering temperatures to room temperature; 2) $\gamma_R \rightarrow \alpha_b$ or pearlite during tempering holding time. In vanadium steel, the softening due to tempering could only be seen at 700 °C for 30 minutes, while in steel free of vanadium, softening has occurred at 550 °C regardless of the holding time. The softening was considered as a decrease in hardness, as shown in Figure 1-30. Similarly, Podder et al. (Saha Podder & Bhadeshia, 2010) found that the retained austenite decomposed into different stages
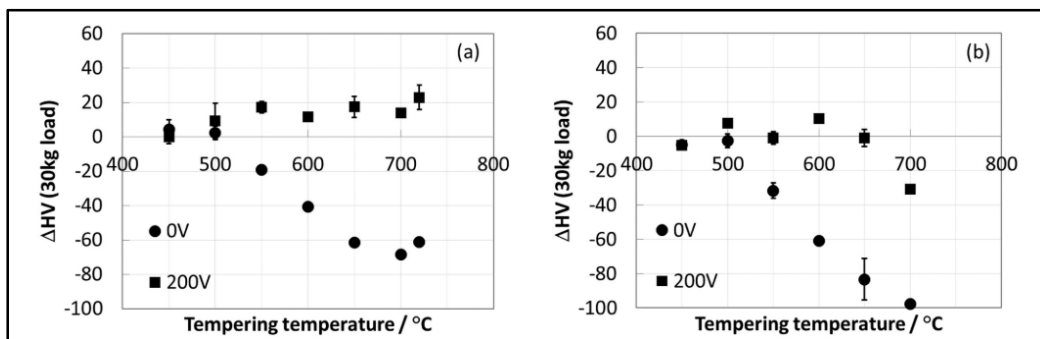
Figure 1-30 Evolution in hardness during different tempering temperatures in the two steels. (a) steel free of vanadium and (b) steel containing 0.2wt.% V
Taken from Sourmail et al. (2021, p. 3)

Dilatometry measurements can be used to trace the microstructural changes during or after tempering treatment. Gao et al. (Gao, Zhang, Gui, Tan, & Bai, 2015) studied the effect of

tempering temperatures on medium carbon CFB steel and correlated the metallurgical reactions that occurred during isothermal tempering at different temperatures to the relative length change ($\Delta L/L_o$) as follows:

- At 280 and 400 °C, decrease in $\Delta L/L_o$ due to martensite recovery and carbide formation, such as cementite and epsilon carbide, as shown in Figure 1-31a and 1-31b.

- At 450 °C, a sharp decrease in $\Delta L/L_o$ at the beginning of tempering holding time as a result of the fast recovery of martensite, and after 30 min., a slight decomposition of austenite lead to an expansion which slowed down the rate of dilatation reduction (Figure 1-31c).

- At 500 °C an increase in $\Delta L/L_o$ was observed due to the fast decomposition of retained austenite, as seen in Figure 1-31d.
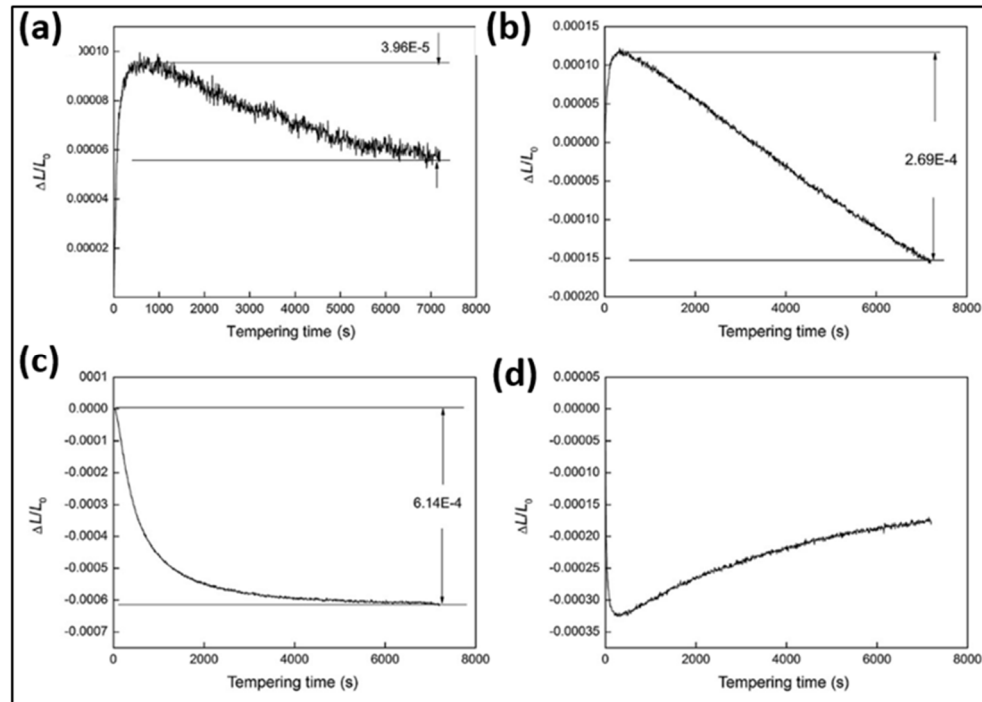
Figure 1-31 The relationship between $\Delta L/L_o$ and tempering holding time at:
(a) 280 °C, (b) 400 °C, (c) 450 °C, (d) 500 °C
Taken from Gao et al. (2015, p. 202)

It is worth noting, to the best of the author's knowledge, that all the research on the relationship between tempering and nanostructured CFB was done on the nanostructured bainite that obtained without any prior ausforming. Therefore, the influence of tempering on ausformed bainitic matrix has not been addressed yet.

1.6 Challenges and Objectives

The literature review provided detailed studies on the consequence of the main factors that alter carbide-free bainite, CFB, microstructure towards nanostructured morphology to enhance its mechanical properties. The microstructure of CFB mainly consists of bainitic ferrite plates and retained austenite in different morphologies. Steel's chemical composition, heat treatment, and thermomechanical process, i.e., ausforming, prior bainite transformation, are the main parameters that can be modified to achieve the desired microstructure of CFB.

The present study aims to determine the thermomechanical parameters controlling the microstructural changes of carbide-free bainite in medium carbon steel and provide a systematic approach to better understate how CFB morphology responded to plastic strain.

As discussed in the literature review, the enhancement of bainitic steel's ductility, specifically in CFB, is mainly dependent on retained austenite stability. No accurate description has been realized about the relationship between the stability of retained austenite and deformation prior to bainite transformation. In this context, the first objective in this work is to investigate the effect of ausforming with different deformation amounts on retained austenite stability. By employing dilatometric signals analysis, XRD, and SEM examinations, a model based on quantitative measurements will be presented explaining how the combination of the ausforming and bainite transformation temperature plays a role in changing retained austenite decomposition.

Deforming supercooled austenite (metastable) at different temperatures and its correlation to the microstructural changes in CFB morphology is reported in many studies; however, the

impact of ausforming temperature on the refinement of bainitic ferrite plates needs to be investigated. Furthermore, the link of these changes to transformation plasticity (TP) changes due to the anisotropy of the bainitic ferrite alignment is not discussed in the literature. Accordingly, the second objective is to address the interconnection between TP strains and morphological change in CFB microstructure using axial and radial strains measured by two different devices simultaneously. Hence, by means of electron backscatter diffraction (EBSD), different kinds of grains will be defined based on crystallography, and their level of texture will be interpreted based on TP strain evolution.

In the third objective, the approach is to study the influence of the tempering parameters on CFB steel's microstructure. Although several authors have studied this topic specifically for high-C nanostructure CFB steels, the current literature has dealt only with CFB microstructure obtained through pure isothermal transformation. However, it has not yet been investigated how CFB steel produced after the ausforming process responds to tempering treatment. Therefore, two different CFB morphologies will be generated via undeformed and deformed supercooled austenite. Non-isothermal and isothermal tempering treatments will be reviewed by tracking dilatometry changes during tempering and examine the microstructural changes using X-ray diffraction, XRD, and metallographic observation, and some new findings will be presented.

CHAPTER 2

MATERIAL AND EXPERIMENTAL METHODS

2.1 Material selection

Medium carbon steel with a particular composition was chosen to explain the effects of ausforming on bainite transformation. The selected steel which is the focus of this research was Ovako 477L (EN 40SiCrMnMo7-6-6), with the chemical composition shown in Table 2-1. Steel must contain other elements to meet unique requirements, namely, silicon (Si) to suppress the precipitation of carbides during isothermal transformation (H. K. D. H. Bhadeshia, 2015); manganese and chromium (Mn and Cr) for hardenability are crucial for avoiding equilibrium transformation to occur, and molybdenum (Mo) to prevent temper embrittlement due to the segregation of phosphors (P) at grain boundaries (A. S. M. International Handbook, 1991; J. I. Kim, 2014). The steel composition was selected to optimally create the desired microstructure of a CFB bainite matrix with some retained austenite.

Table 2-1 Chemical composition of the examined steel

Element	C	Mn	Si	Cr	Mo	P	S	Fe
wt.%	0.40	1.50	1.70	1.50	0.40	0.03	0.02	bal.

2.2 As-received microstructure

Different samples of as-received steel were examined to evaluate the homogeneity of the microstructure (Figure 2-1a). The steel microstructure comprises spherical carbides within a ferrite matrix; it is called a spheroidized microstructure with an average hardness of 18 HRC. This microstructure is desirable when machinability is required. X-ray diffraction (XRD) line scan in Figure 2-1b (small peaks) confirms the presence of carbides within the microstructure.
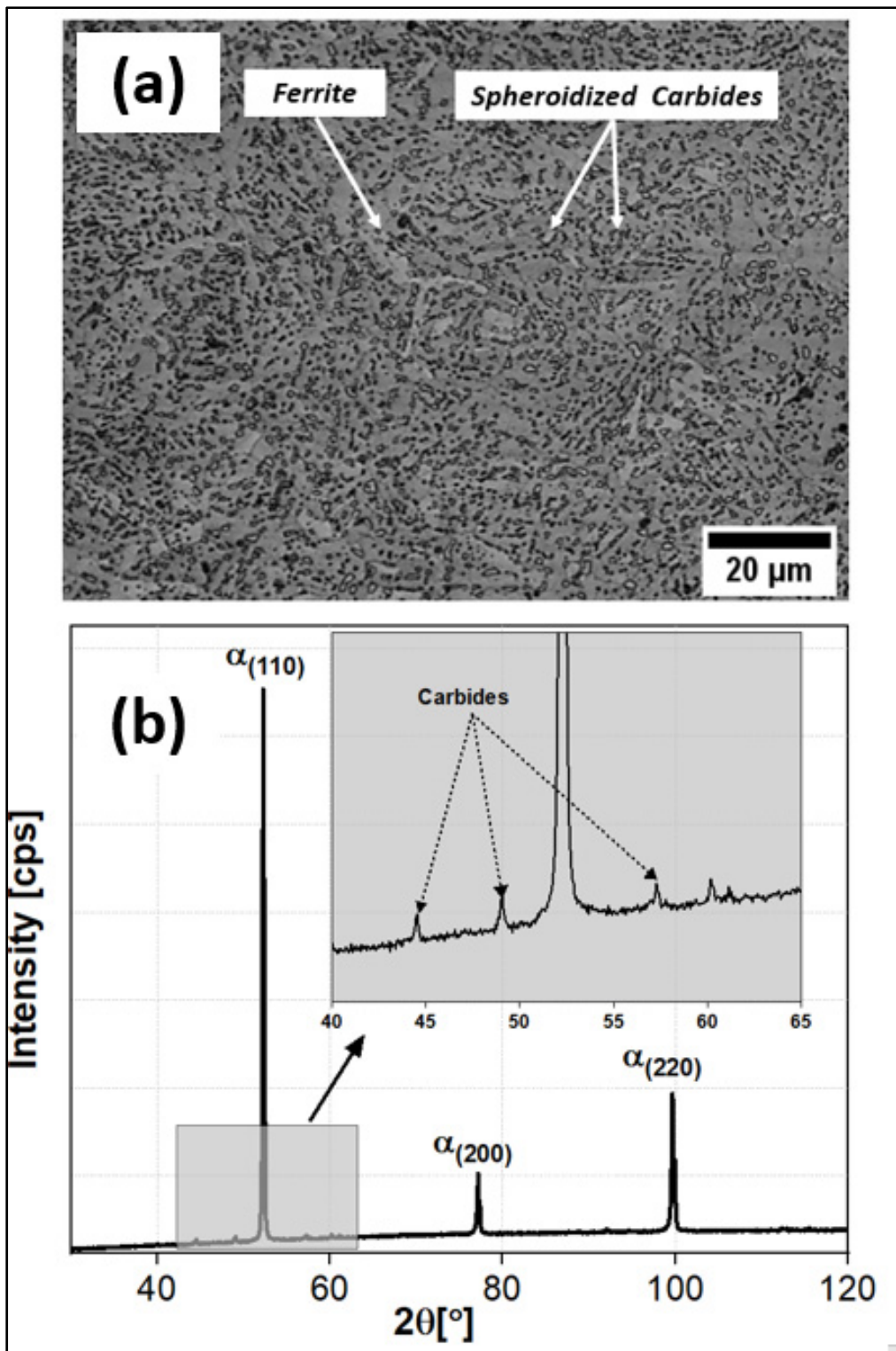
Figure 2-1 (a) Optical micrograph of the as-received microstructure for 477L steel; (b) XRD profile of as received 477L steel

2.3 Heat treatment

In heat-treatment operations, several variables are involved in determining suitable thermomechanical processing parameters, which can be categorized into two groups: Fixed parameters and variable parameters. The former is applied to all experimental regimes, while the latter is subject to change depending on the research requirements being examined. In the austenitization step (i.e., temperature and holding time), heating and cooling rates are among the fixed parameters in all experimental procedures. Isothermal temperature, percentage, deformation temperature, tempering temperature, and time are changed according to the research requirements. The experimental work was designed to obtain information regarding the microstructure and bainite transformation kinetics by changing the variable parameters as reported in Table 2-2

2.4 Thermal dilatometer

A DIL-805A/D (A: quenching; D: deformation) dilatometer was used in this research, with an achievable resolution of ~0.01μm/0.05°C. Figure 2-2 shows the dilatometry equipment used in this project, where the specimen dilatation is measured as a function of temperature and time in the absence of a reference specimen. Two modes can be used in the dilatometer: quenching and deformation. The difference between the two modes is discussed in the following sub-sections. The electrically conductive sample is heated by induction via a water-cooled copper induction heating coil to generate a high-frequency current. According to the heat-treatment process, inert gas quenching (helium or argon) is applied through an internal copper coil to cool the specimens. To control the specimen temperature, a type-k thermocouple is spot-welded on the specimen surface. The thermal dilatation signals caused by the expansion or contraction of the specimens during heating, cooling, and phase transformation are measured by the pushrods. The pushrods, which also hold the specimen, are either composed of fused silica (it is preferred because of its low thermal expansion coefficient) or alumina (Al_2O_3).

Table 2-2 Fixed and changeable parameters for different experimental stages

I. Austenitization step		
Parameter	**Value**	**Unit**
Heating rate	10	°C/s
Austenitizing temperature	980	°C
Austenitizing holding time	300	S
Cooling rate	20	°C/s

II. Isothermal Bainitic transformation step					
Parameter	**Value**				**Unit**
Isothermal temperature	325	350	375	400	°C
Isothermal holding time	1800				S
Cooling rate to RT	20				°C/s

III. Ausforming step				
Parameter	**Value**			**Unit**
Deformation temperature	600	400	325	°C
Deformation rate	1			mm/s
Deformation amount	10	20	30	40	%
Cooling rate to isothermal temperature	20			°C/s

IV. Non-isothermal tempering step		
Parameter	**Value**	**Unit**
Heating rate	1	°C/s
Tempering temperature	600	°C
Tempering holding time	3	S
Cooling rate to RT	20	°C/s

V. Isothermal tempering step		
Parameter	**Value**	**Unit**
Heating rate	10	°C/s
Tempering temperature	400	500	°C
Tempering holding time	3600		S
Cooling rate to RT	20		°C/s

Two measuring systems can be used in dilatometry: a linear variable differential transformer (LVDT) and an optical module (laser interferometer). The former measures the relative change in length of the sample (RCL) by using the pushrods, and the latter permits the contactless measurement of the relative change in diameter (RCD, i.e., radial expansion, of the specimen, where a laser beam focuses on the diagonal center of the specimen. Figure 2-3 shows the difference between the measuring systems. Notably, the entire system is insensitive to mechanical vibration. The measuring systems and specimen are kept isolated from each other by dividing a metal wall. Hence, the LVDT and laser interferometer are not affected by heat radiation or heat conduction from the specimen.

Figure 2-2 BAHR DIL805 high-resolution dilatometer
Taken from BEN FREDJ Emna (2019)
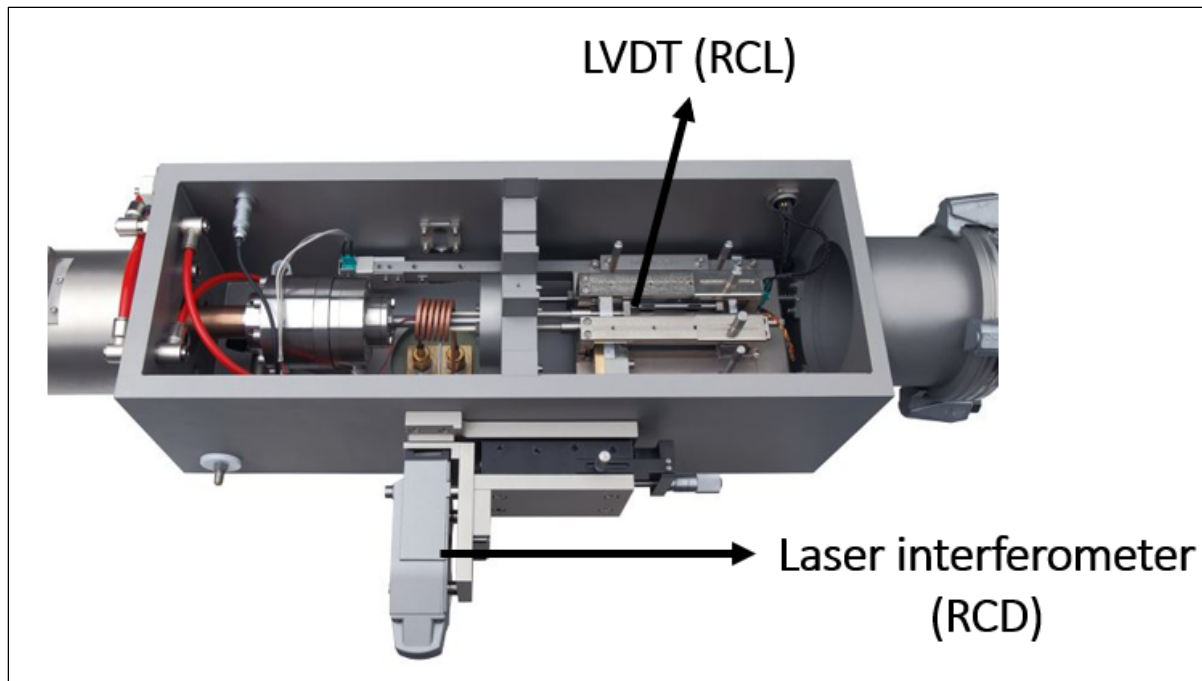
Figure 2-3 Position of the LVDT and laser interferometer devices used for dilatometry measurements
Taken from TA instrument website
(https://www.tainstruments.com/products/dilatometers/)

2.4.1 Quenching module

In the quenching unit shown in Figure 2-4a, the sample is held by two pushrods (1 and 2, respectively). Dilatation during the heat-treatment process is recorded either by pushrod 2, which is attached at the right of the specimen and conveys the progress of the expansion correlated to a reference pushrod (i.e., pushrod 3) or by a contactless device (laser interferometer), which records the radial expansion. Notably, the dilation (RCL and RCR) can be simultaneously recorded by the two devices mentioned above.

2.4.2 Deformation module

In the deformation mode (Figure 2-4b), the specimen is held by two punches (1 and 2, respectively), comprising alumina (Al_2O_3), quartz (SiO), or silicon nitride (SiN_4). The selection

of the punch type depends on the thermomechanical parameters. SiN$_4$ can be used for deformation at a wide range of temperatures and deformation amounts. RCL and RCD dilatations can be transmitted to the system either by pushrods or a laser interferometer, respectively. A hydraulic unit can apply a compressive load (elastic or plastic) up to 20 KN. Uniaxial stress and strain are recorded during the entire loading step via the pushrods.
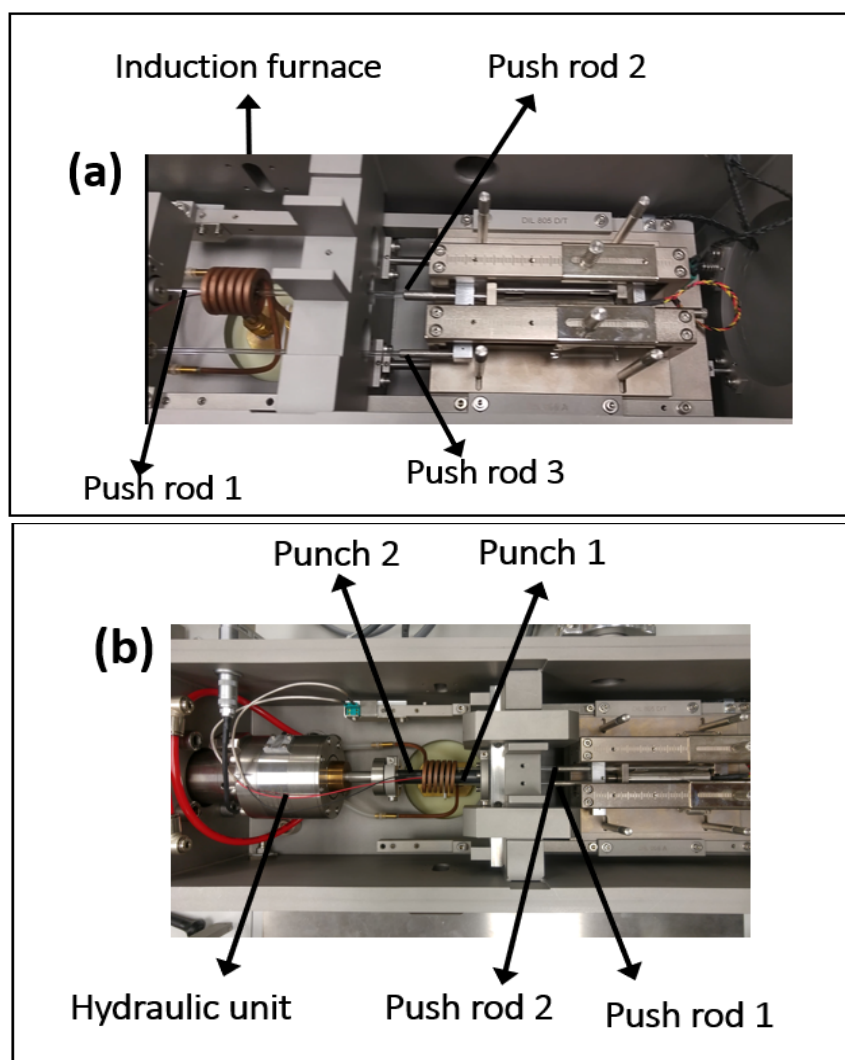
Figure 2-4 Dilatometry quenching module (a), and Deformation module (b)
Taken from TA instrument website
(https://www.tainstruments.com/products/dilatometers/)

2.4.3   The geometry of the dilatometer specimen

The samples are cut to final dimensions from the as-received steel using a precision wire-cut machine. The shape and dimensions of the specimen are shown in Figure 2-5 and Table 2-3.
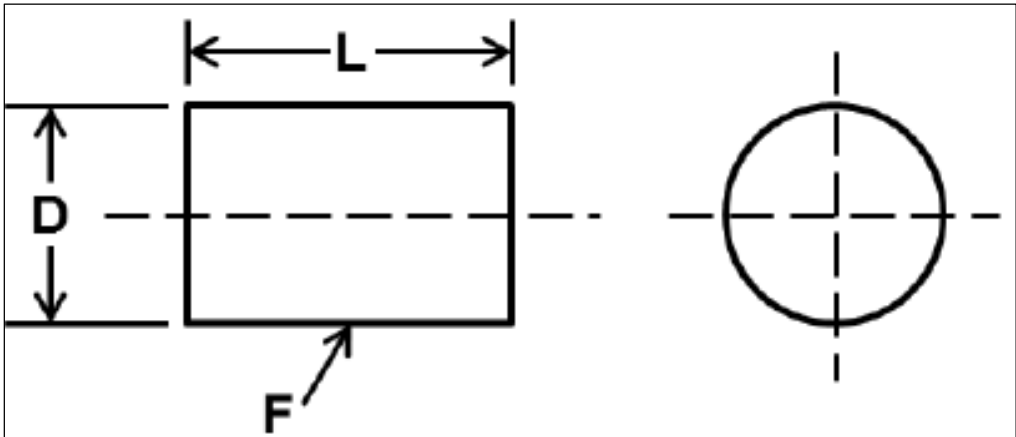
Figure 2-5 Shape of the dilatometer test sample

Table 2-3 Dimensions of the dilatometer test sample

Dimensions	Quenching	Deformation
	mm	mm
D-Diameter	4.0 ± 0.05	5.0 ± 0.05
L-Length	10.0 ± 0.05	10.0 ± 0.05
F-surface finish (Ra)	0.6 μm	0.6 μm
Perpendicular	$\pm 0.5°$	$\pm 0.5°$

CHAPTER 3

THE ROLE OF AUSFORMING IN THE STABILITY OF RETAINED AUSTENITE IN A MEDIUM-C CARBIDE-FREE BAINITIC STEEL

M. Zorgani[1], C. Garcia-Mateo[2], M. Jahazi[1]

[1] Department of Mechanical Engineering, École de Technologie Supérieure,
1100 Notre-Dame West, Montreal, Quebec, Canada H3C 1K3
[2] National Center for Metallurgical Research (CENIM-CSIC),
Avda. Gregorio del Amo 8, Madrid 28040, Spain

Abstract

In this work, the influence of thermomechanical treatments, consisting of a combination of ausforming followed by isothermal holding and cooling to room temperature, on the stability of retained austenite of a carbide-free medium carbon-high silicon steel was investigated. The amount of retained austenite and its transformation to martensite for a range of ausforming treatments was determined by means of X-ray diffraction, dilatometry signal analysis, and metallographic investigation. Different amounts of deformations were applied at 600 ºC in the austenite region prior to fast cooling into the bainitic transformation region. Four isothermal temperatures (325, 350, 375, and 400 ºC) with a holding time of 1800 s were selected to estimate the extent of the stability of the retained austenite after the completion of the bainitic transformation. The results show that the deformation-free austenite was more stable for the

samples isothermally treated at temperatures between 325 and 350 ºC. However, the decomposition of retained austenite to martensite during cooling to room temperature increased for isothermal holding temperatures above 350 ºC. It was found that the stability of retained austenite was a function of the temperature and percent deformation, and the critical temperature and percent deformations were determined. It was also found that ausforming enhanced the formation of blocky-shaped retained austenite for isothermal holdings above 350 ºC, resulting in a decrease in retained austenite stability. The results were analyzed in terms of the influence of thermomechanical conditions on bainitic transformation and its impact on the transformation of retained austenite to martensite.

Keywords: Ausforming; Retained austenite stability; Carbide-Free Bainite; Martensite; Dilatometer signal

3.1   Introduction

Nanostructured carbide-free bainite (CFB) in high-carbon (~ 1.0 wt. %) silicon-rich steel has a superior combination of strength, toughness, and ductility due to its composite-like microstructure (H. K. D. H. Bhadeshia, 2009; F. G. Caballero & Bhadeshia, 2004). The excellent combination of these properties comes from the unique microstructure, which consists of thin bainitic ferrite plates, which give the strength, and the stable metastable retained austenite that enhances the toughness and ductility through the transformation induced plasticity phenomenon (TRIP effect) (C. Garcia-Mateo & F. Caballero, 2005; Spanos, Fang, & Aaronson, 1990). Therefore, it is essential that the CFB steel microstructure contains only bainitic ferrite and retained austenite without the presence of martensite before being introduced into industrial applications. However, the steel's poor weldability, caused by its high carbon content, limits its use in many industrial sectors. On the other hand, it is difficult to obtain a very fine bainitic microstructure in low or medium carbon steels since the martensite start temperature is relatively high. One of the alternative ways of obtaining such fine morphology is to work- harden the unstable austenite before the bainitic transformation, using ausforming process (Cornide et al., 2013; S. B. Singh & Bhadeshia, 1998).

There are two types of retained austenite morphologies in CFB. The first one is film-like and located between the bainite plates. These films become stable due to carbon enrichment from the bainitic plates. The other one is the low-carbon blocky-shaped retained austenite located between the bainite sheaves. The stability of the retained austenite could be quantified by estimating the amount of transformed martensite from the decomposition of the remaining austenite at the end of the bainitic transformation (Edmonds, 1983). The formation of untempered martensite is of critical importance as it could act as crack initiation sites (Grajcar et al., 2018; A. S. Podder, 2011; Xie et al., 2014). It has been reported that the stability of the retained austenite is affected by its carbon content, morphology, and size (S. Lee et al., 2011; Luo et al., 2011; X.C. Xiong, 2013). On the other hand, the bainitic transformation temperature and the deformed state of supercooled austenite can also alter the above factors and therefore influence the retained austenite stability (Chiou et al., 2001; Leijie Zhao, 2019).

In pure isothermal bainitic transformation (deformation-free austenite), the probability of the decomposition of retained austenite to martensite is more significant when the bainitic transformation takes place at higher temperatures (Miihkinen & Edmonds, 2013). Specifically, it has been reported that the stability of blocky-shape retained austenite was higher when the isothermal temperatures were below 400 °C, but that transformation to fresh martensite occurred above 400 °C (Grajcar et al., 2018). Several authors (Klein et al., 2019; Tian et al., 2019a; H. D. Wu et al., 2017) have reported that the amount of retained austenite that could be stabilized, at the end of isothermal holding, depends on the degree of carbon enrichment during the bainitic reaction. Therefore, the higher the carbon enrichment, the more stable it would be the retained austenite (Mingxing Zhou, 2015; Varshney, Sangal, Kundu, & Mondal, 2016). Another research in low C-Mn steel (Y.X. Zhoua, 2018) reported that an increase in the bainitic isothermal temperature, from 330 to 390 °C, enhanced the stability of retained austenite and increased its amount at the end of the bainitic transformation. The authors associated the higher stability of retained austenite at higher bainitic transformation temperatures to higher diffusion of C and Mn. Hence, the bainitic isothermal temperature appears to have a substantial effect on the stability of blocky shape retained austenite and therefore needs further investigation. It has been reported that the deformation of austenite prior to the bainitic transformation, results

in a reduction in the retained austenite block size and an increase in its volume fraction after the isothermal transformation (J. Zhao et al., 2017; L. Zhao, Qian, Liu, et al., 2016). Hu et al. (H. Hu, Xu, Wang, & Zhou, 2017) studied the effects of strain and ausforming temperature on the stability of retained austenite and found a direct relationship between the stability of the retained austenite and the applied plastic strain when the deformation temperature was above 300 ℃. However, they reported that when the plastic strain reached 0.3, and the ausforming temperature was 300 ℃, the correlation was inversed. Seung-Woo et al. (Seo et al., 2015), reported that ausforming of medium carbon steel at 600 ℃, decreased the martensite start temperature, M_S, and stabilized the austenite during cooling to ambient temperatures and associated it with the effect of carbon diffusion on the stability of retained austenite.

Besides the effect of carbon diffusion, the stability of retained austenite has been analyzed in terms of mechanical stabilization through the introduction of a large number of dislocations into the microstructure when ausforming temperature is reduced (H. K. D. H. Bhadeshia, 2015; H. Hu et al., 2017; Maalekian et al., 2013). Therefore, increasing the number of defects, such as dislocations, is expected to retard martensitic and/or bainitic transformations(Maalekian et al., 2013). Bhadeshia et al. (H. K. D. H. Bhadeshia, 2015) reported that plastic deformation of austenite prior to its transformation, ausforming, hinders the growth of martensite or bainite and causes a reduction in the fraction of transformation in spite of an increased number density of nucleation sites.

However, in most of the above studies, little information is provided on the quantitative relationship between the stability of retained austenite due to the thermal and/or mechanical stabilization. Furthermore, whether the bainite transformation took place with or without the ausforming step, the stability of the retained austenite (i.e., its decomposition to martensite) has not been quantified. Such information will be of great value for a better understanding of the contribution of ausforming to the stability of retained austenite in the final microstructure of CFB steels. The selection of suitable conditions for ausforming and bainitic transformation is crucial for obtaining the optimal amount and stability of the retained austenite that minimizes the amount of untempered martensite in the final stage of the bainitic transformation. The

present research has been defined in this context and aims to systematically quantify the thermal and mechanical stability of retained austenite, obtained through ausforming followed by isothermal treatments of a carbide free medium-C high-Si steel, during cooling to room temperature.

3.2 Experimental procedure and material

A rod of 300 mm diameter of a commercial-grade medium-carbon steel Ovako 477L, with the nominal chemical composition of Fe-0.4C-1.7Si-1.5Mn-1.5Cr-0.4Mo (wt. %), was selected for this study. In order to reduce some of the experimental tests, the theoretical continuous cooling transformation (CCT) diagram was calculated using JMatPro® simulation software (Sente Software Ltd, Version 9.0).

Dilatometry tests were carried out using the DIL 805A/D-TA high-resolution dilatometer. The linear dilatation during the tests was recorded using a Linear Variable Differential Transducer (LVDT) attached to fused silica pushrods with a resolution of $\Delta L/ °C = 0.05 \mu m/0.05 °C$ (Instruments, 2013). The temperature was monitored using type S thermocouples welded at the center of the sample. For pure isothermal treatments (non-ausformed), the quenching module of the dilatometer was used with cylindrical samples 10 mm in length and 4 mm in diameter. The thermomechanical treatments (TMT) were performed using the deformation module of the dilatometer for which cylindrical samples 5 mm in diameter and 10 mm in length were used. For deformation tests, Molybdenum discs with a thickness of 1 mm were welded on both sides of the specimens to reduce the friction between the sample's cross-sectional surface and the deformation anvils (SiN). All the samples were prepared using wire-based Electro Discharge Machining (EDM) along the rolling direction of the as-received bar.

Four different treatment routes (A, B, C, and D) were applied, as shown in Figure 3-1a, and 4b. In route (A) (non-ausformed, Figure 3-1a), the samples were cooled with a cooling rate of 20 °C/s from the austenitization temperature to the isothermal treatment temperature, ranging
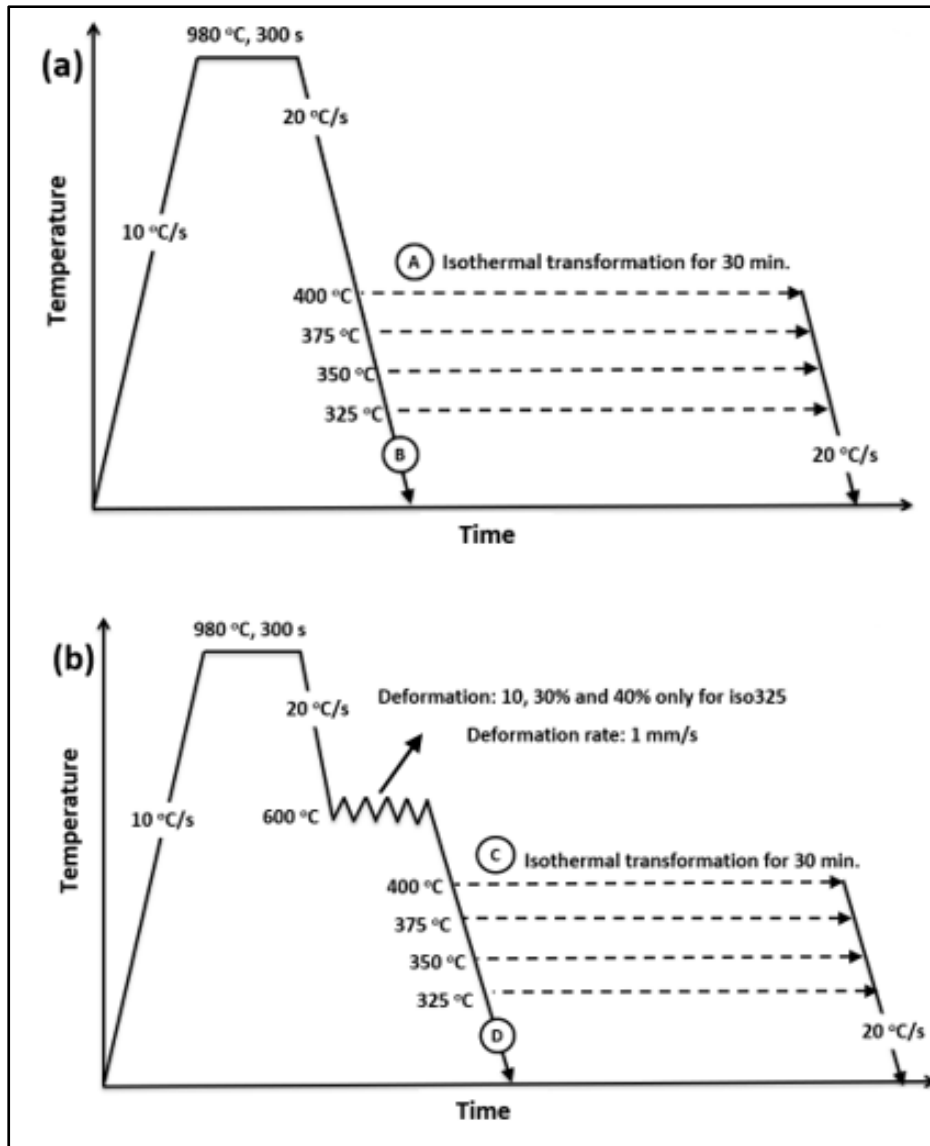
Figure 3-1Scheme of the performed tests and their corresponding conditions, (a) non-ausformed condition, (b) ausformed condition with different percent deformation

from 400 to 325 °C. They were then further cooled to room temperature at a cooling rate of 20 °C/s. Samples produced through route (A) are considered as a reference for comparison purposes with ausformed samples. In route (C) (ausformed, Figure 3-1b), the samples were first deformed at 600 °C, before applying the isothermal heat treatment under the same

conditions as those in route (A). Routes (B) and (D) were used to measure the M_S of the non-ausformed, route (B), and ausformed samples with different percent deformations, route (D). Microstructural examinations were conducted in the longitudinal-central section of the samples using standard metallography techniques. Sample preparation included grinding and polishing up to 1μm diamond paste, followed by a cycle of etching (% Nital for 10 s) and polishing to remove the deformed layer that formed during the grinding process (Eres-Castellanos et al., 2018).

Confocal laser microscopy (Olympus-LEXT4100) and field emission scanning electron microscopy (Hitachi SU-8230, FE-SEM) were used for microstructural characterizations. The volume fraction of retained austenite ($V_{γR}$) and its carbon content ($C_{γR}$) after isothermal transformation were determined by X-ray diffraction (XRD) using a X'PERT PANalytical diffractometer with Co Kα radiation. The operational conditions consisted of an acceleration voltage of 45 kV, a 2θ scan range from 30 to 120°, and a step size of 0.05°.

Retained austenite volume fraction determination, $V_{γR}$, was made based on a direct comparison method (Jatczak, 1980) and consisted in first determining its lattice parameter ($α_γ$), in ($\mathring{A}$), from the diffractograms according to equation (3-1). Then, using the average integrated intensities of ferrite ($I_α$) and austenite ($I_γ$) peaks, $V_{γR}$, and $C_{γR}$, were calculated in (wt. %) as per equations (3-2) and (3-3), respectively.

$$α_γ = \frac{λ\sqrt{h^2 + k^2 + l^2}}{2\sin θ} \tag{3-1}$$

$$V_{γR} = \frac{1.4 I_γ}{I_α + 1.4 I_γ} \tag{3-2}$$

$$C_{γR} = \frac{α_γ - 3.547}{0.046} \tag{3-3}$$

In the above equations, λ, (hkl), and θ is the wavelength of the radiation, the three Miller indices of a plane, and the Bragg angle, respectively.

As already mentioned, the stability of retained austenite is defined as its ability to resist decomposition to bainite during isothermal transformation or to martensite during cooling to room temperature. However, in this study, only the later phenomenon will be investigated. Therefore, it is of critical importance to accurately determine the amount of martensite formed ($V_{\alpha m}$) from the austenite during cooling to room temperature after the isothermal holding. To this end, two different methods were used: The first method was based on the change in the slope of dilatometry signals, as described in (Navarro-López, Sietsma, & Santofimia, 2015). In this method, the net relative change in length (RCL) at room temperature is compared with the net RCL of martensitic transformation, which is considered as a reference for non-ausformed (Q-00) and ausformed (Q-10, Q-30, and Q-40) samples. The reference dilatation is then correlated to the amount of transformed martensite determined by XRD (i.e., $V_{\alpha m} = 100 - V_{\gamma R \, (XRD)}$). For example, the net dilatation, $\Delta(\Delta L/L_o)$, corresponding to 92% martensite for the non-ausformed condition (Q-00), is about 0.97%. The amount of martensite, formed during cooling after the isothermal treatment, is calculated by comparing the recorded net RCL with that of the reference net RCL. The results thus obtained, will be designated as $V_{\alpha m \, (dil)}$, where the subscript (dil) refers to dilatometry-based results. It must be noted that all dilatometry tests were repeated three times, and the presented RCL values are the average of the three tests.

The second method is based on microstructural identification of blocky-shape retained austenite from the martensite within the martensite/austenite (M/A) islands, as described in references (Mingxing Zhou, 2015; Navarro-López, Hidalgo, Sietsma, & Santofimia, 2018; A. S. Podder, 2011; Saha Podder & Bhadeshia, 2010). For each test condition, at least four SEM micrographs at a 4000 magnification were used, and for accuracy, the area fraction measurement was repeated five times for each image. The volume fraction of transformed martensite, $V_{\alpha m \, (SEM)}$, was then determined by calculating the area fraction occupied with martensite in the micrographs using the image analysis software, MIP4 (Asia, February, 2018). The method consisted of, first, determine the fraction of M/A constituent in SEM images.

Then, the darkest/featured region within them (martensitic phase) was subtracted, and finally, the volume percentage of the martensite was determined.

The Vickers microhardness was measured using a 1kg load, and a dwell time of 15 s. The hardness values reported were taken at various locations around the center of the sample and sufficiently apart from each other to avoid interaction effects. The mean value and standard deviation of hardness measurements were obtained by statistical analysis using five hardness readings.

For simplification, the sample designation is as follows: the first three digits of the sample designation code (xxx-xx) represent isothermal temperature, while the second two digits after the dash represent the amount of deformation at 600 $^\circ$C. For example, 325-30 corresponds to the sample with 30% plastic deformation, followed by isothermal treatment at 325 $^\circ$C, whereas 325-00 indicates isothermal treatment at 325 °C with no deformation. For quenching samples, Q-00 represents the quenching treatment without deformation, and Q-10, Q-30, and Q-40 are quenching treatments after the sample was deformed with 10, 30, and 40 % plastic deformation at 600 $^\circ$C.

3.3 Results and discussions

3.3.1 Selection of thermomechanical treatment conditions

The critical transformation temperatures Ac_1 and Ac_3 were found experimentally, as illustrated in Figure 3-2a, using heat treatment parameters shown in Figure 3-1a (route (B)), to be 840 and 930 $^\circ$C, respectively. As shown in the same Figure 3-2a, a cooling rate of 20 $^\circ$C/s is sufficient to activate martensitic transformation avoiding any other previous transformation. The martensite start temperature, M_S, was determined to be 310±5 $^\circ$C using the tangent method (H.-S. Yang & Bhadeshia, 2013).

Based on the above results, isothermal transformation treatments at 325, 350, 375, and 400 ºC were selected to study the bainitic transformation during isothermal holding. Furthermore, an isothermal time of 1800 s was selected in all conditions to ensure the end of the bainitic transformation in agreement with experiments previously reported in the literature (Eres-Castellanos et al., 2018; M. Liu et al., 2019; Santajuana et al., 2019).

The first set of calculations using JMatPro® software (Sente Software Ltd, Version 9.0) showed that the bay between the ferrite/pearlite and the bainite regions is located in the temperature interval of 500 to 600 ºC and also that the critical cooling rate is 1ºC/s (Figure 3-2b). Such temperature would be ideal to plastically deform austenite prior to bainitic transformation, as no other transformation would be expected to interfere. In order to ensure the validity of the calculations, selected isothermal dilatometry tests at 500, 600, and 700 ºC, using the same conditions as those previously described, have been performed. As expected from the calculations and the dilatometric curve is shown in Figure 3-2c, reveal the absence of any relative change in length, thereby confirming that no phase transformation occurred at 500 and 600 ºC after 1800 s dwell time. Furthermore, the microstructure examination of the samples reported in Figure 3-2d showed that only martensite was present at room temperature. In contrast, at 700 ºC, a ferrite-pearlite transformation started after about 700 s, which was also confirmed by metallographic analysis reported in Figure 3-2d, where a mixture of pearlitic and martensitic phases was identified. Therefore 600 ºC was selected as the ausforming temperature, where deformations between 10 and 30%, at a deformation rate of 1 mm/s, were applied. As will be described later, some experiments were conducted with a 40% deformation to validate the interpretations and the proposed mechanisms for the interpretation of the results. A summary of all test conditions is presented in Figure 3-1a and 3-1b.
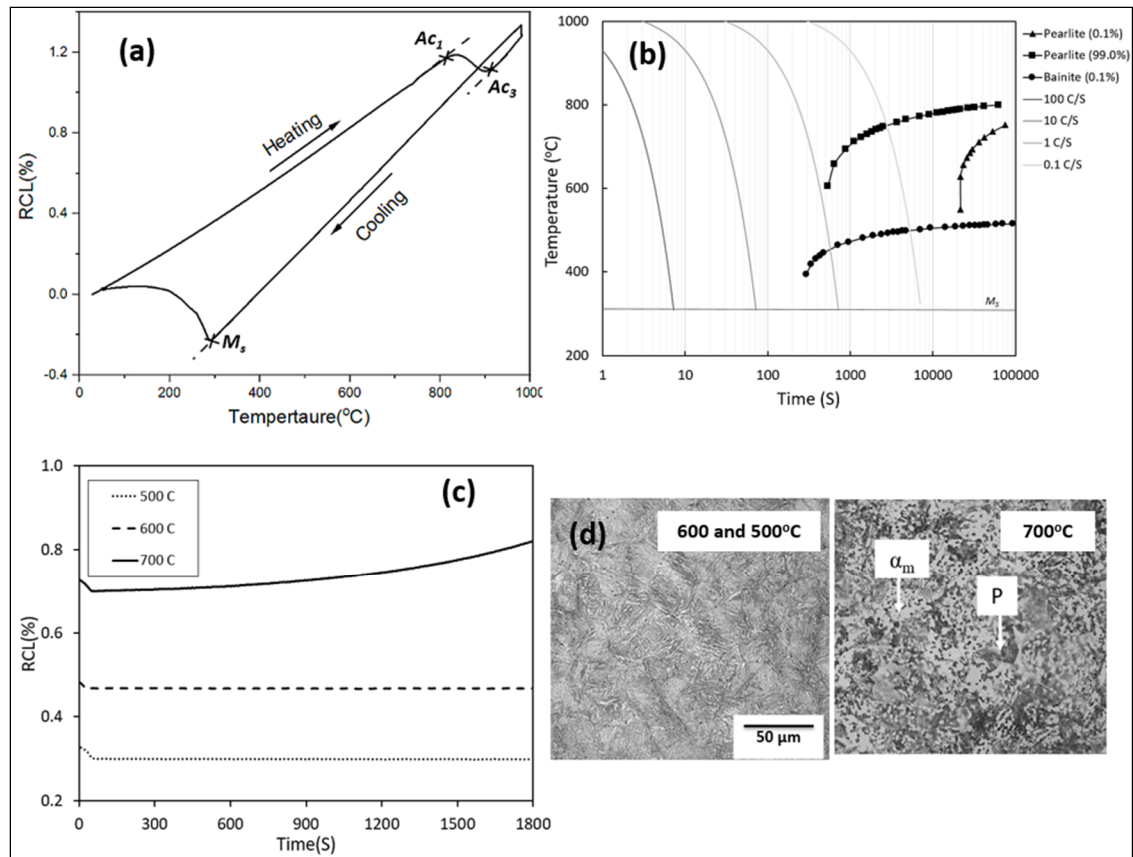
Figure 3-2 The dilatation versus temperature during the entire thermal simulation (a), CCT diagram for 477L steel constructed by JMat-pro program (b), dilatation – time curves for 500, 600 and 700 °C isothermal treatments (c), optical micrographs for 500, 600, and 700 °C sample (d)

3.3.2 Stability of retained austenite of non-ausformed samples (reference condition)

3.3.2.1 Dilatometry analysis

Figure 3-3 illustrates the dilatometry signals (RCL) for isothermally treated samples at 325, 350, 375, and 400 °C, and the quenched condition. Note that in the case of the isothermal treatments, any change in length is directly related to the formation of bainitic ferrite. As already mentioned, the selected isothermal holding time, 1800 s, was sufficiently long to allow for the bainite transformation to finish, as shown in the inserted curve in Figure 3-3 corresponding to the isothermal transformation at 325 °C and 400 °C, i.e., the slowest and

fastest of transformations. It is clear that the increment of dilatation values is negligible after about 1500 and that the curve has reached its steady-state (plateau) at that time, no more transformation. In the same inset of Figure 3-3, the dilatation rate (first derivative curve), related to the transformation rate, is almost zero at 1500 s, further confirming that no more bainitic transformation could be observed after 1500 s. It must be noted that the increase in the RCL with the decrease in isothermal transformation temperature is in agreement with other results that the amount of bainitic ferrite, $V_{\alpha b}$, is higher when the transformation temperature is lower (H. K. D. H. Bhadeshia, 2015; Koo, Xu, Tomota, & Suzuki, 2009).

The obtained results on isothermal transformation at 325 and 350 ºC (325-00 and 350-00), as shown in Figure 3-3, also confirm that no martensitic transformation is occurring on cooling to room temperature, meaning that austenite present in the microstructure is sufficiently enriched in C to be stable, M_S less than room temperature. However, as the C enrichment in austenite decreases, by increasing the isothermal bainitic transformation temperature at 375 and 400 ºC, it is clear that austenite transforms to martensite (H. K. D. H. Bhadeshia, 2015). The first deviation in the dilatometric signal during cooling to room temperature represents the M_S of C-enriched retained austenite due to bainite transformation, as shown in Figure 3-3. The results in Table 3-1 showed that the M_S decreased by about 50% (150 ºC) and 27% (225 ºC) for 375-00 and 400-00 samples, respectively, compared with the quenched condition (310 ºC). As already explained, the deviation of the dilatation curve can be considered as an indicator of the extent of decomposition of retained austenite to martensite (Suh, Oh, Han, & Kim, 2007; L. Zhao, Qian, Lihe, Zhou, Qian, Li, Dongdong, Wang, Tongliang, Jia, Zhigeng, Zhang, Fucheng, Meng, Jiangying, 2019; Zhi, Zhao, He, Yang, & Qi, 2016). Note that the change in slope occurs more gradually as compared to that of the quenched sample, Figure 3-3, and this is due to the more heterogeneous C distribution in the remaining austenite after bainitic transformation, with block-shaped and thin films of retained austenite having very different C contents (Grajcar et al., 2018; B. Liu, Li, Lu, Jia, & Jin, 2019; Y.X. Zhoua, 2018).

In the as quench condition, a fraction of 92% of martensite was measured, see Table 1, which corresponds to a net difference in RCL of about 0.97±1%, using the method described in the

previous section, the fraction of martensite, $V_{\alpha m\,(dil)}$, was calculated for all conditions, and the results are reported in Table 3-1. Specifically, the amount of austenite transformed to martensite was almost twice when the temperature increased from 375 to 400 °C.
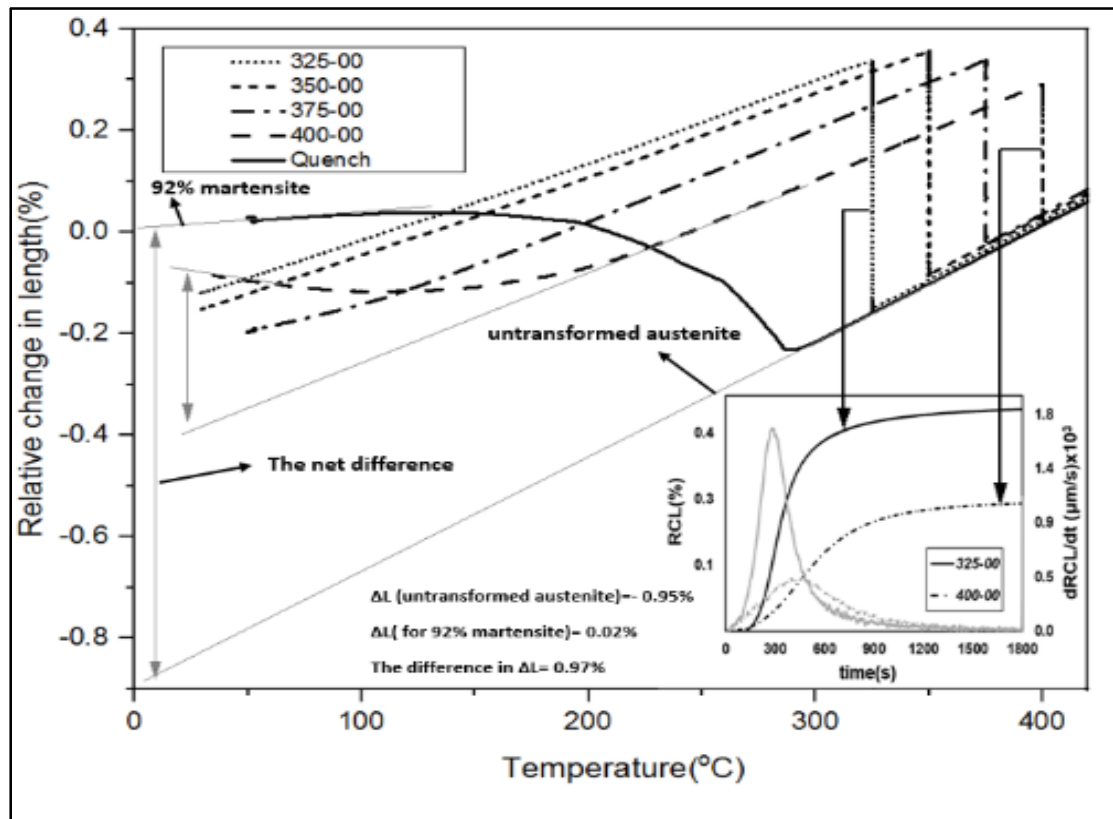
Figure 3-3 Relative change in length vs. temperature during the quenching to room temperature for different non-ausformed treatments, and image in bottom right is a relative change in length and transformation rate vs. time for the lowest (325 °C) and the highest (400 °C) isothermal temperatures

3.3.2.2   XRD analysis

The XRD diffractograms for the non-ausformed samples are reported in Figure 3-4a, where the presence of ferrite phases (α_b and α_m) (α-110), (α-200), (α-211), and austenite (γ-111), (γ-200), (γ-220) planes with no cementite peaks after bainitic transformation are revealed. These findings further confirm the dilatometric results on the phase transformation process at

different isothermal holding temperatures. The corresponding fractions of the different phases and austenite carbon content ($C_{\gamma R}$) were also calculated and are given in Table 3-1 Volume fraction of different phases for non-ausformed and ausformed samples in (%): $V\alpha m_{(dil)}$ for martensite based on dilatometry, $V\alpha m_{(XRD)}$ (=100-VγR), from XRD, $V\gamma R$ retained austenite calculated by XRD, $V\alpha b$ (=100-VγR- $V\alpha m_{(dil)}$) bainitic ferrite; the carbon content of retained austenite, $C\gamma R$, in (*wt.%*) from XRD for, and the *MS* in (°C) for comparison purposes. The results indicate that, as expected, the fraction of bainitic ferrite decreases (i.e., smaller RCL in Figure 3-3) as transformation temperature increases; however, it appears that increasing the isothermal transformation by 25 °C (from 325 to 350 °C), had a limited effect on the variation of the bainite volume fractions. For instance, the variation in $V\alpha b$ was less than 2.5%, leading to about 10% variation in $V_{\gamma R}$ as reported in Table 3-1. The obtained results suggest that martensitic transformation after isothermal transformation at 350 °C, and probably 325 °C, could not be detected by the dilatometry technique. As for the 375 and 400 °C transformation temperatures, there is an apparent decrease in the amount of transformed bainite, once the calculated amount of martensite, $V_{\alpha m(dil)}$, is considered. For example, the variation in $V\alpha b$ was about 45% between 325-00 and 400-00 samples, while the variation in $V_{\gamma R}$ was about 25% for the same conditions due to its decomposition during cooling to room temperature as seen in Figure 3-3.

During the bainitic transformation, austenite receives C from the surrounding C saturated bainitic ferrite, and it is expected that the level of C enrichment, $C_{\gamma R}$, increases with the amount of bainitic ferrite (H. K. D. H. Bhadeshia, 1989; Harshad K. D. H. Bhadeshia, 2005). Although the results reported in Table 3-1 seems to go in that direction, it must be considered that such results were obtained at room temperature, where part of that austenite has transformed to martensite. Therefore, the actual level of C enrichment must be lower than the one obtained from XRD results reported in Table 3-1. In other words, the higher the amount of martensite, the lower would be the actual value of $C_{\gamma R}$ as compared to the one given in Table 3-1. For instance, using the lever rule, it was found that for the 400 °C testing condition, $C_{\gamma R}$ could be as low as 0.4-0.5 wt.% for martensite containing 0.2-0.3 wt.% of C.
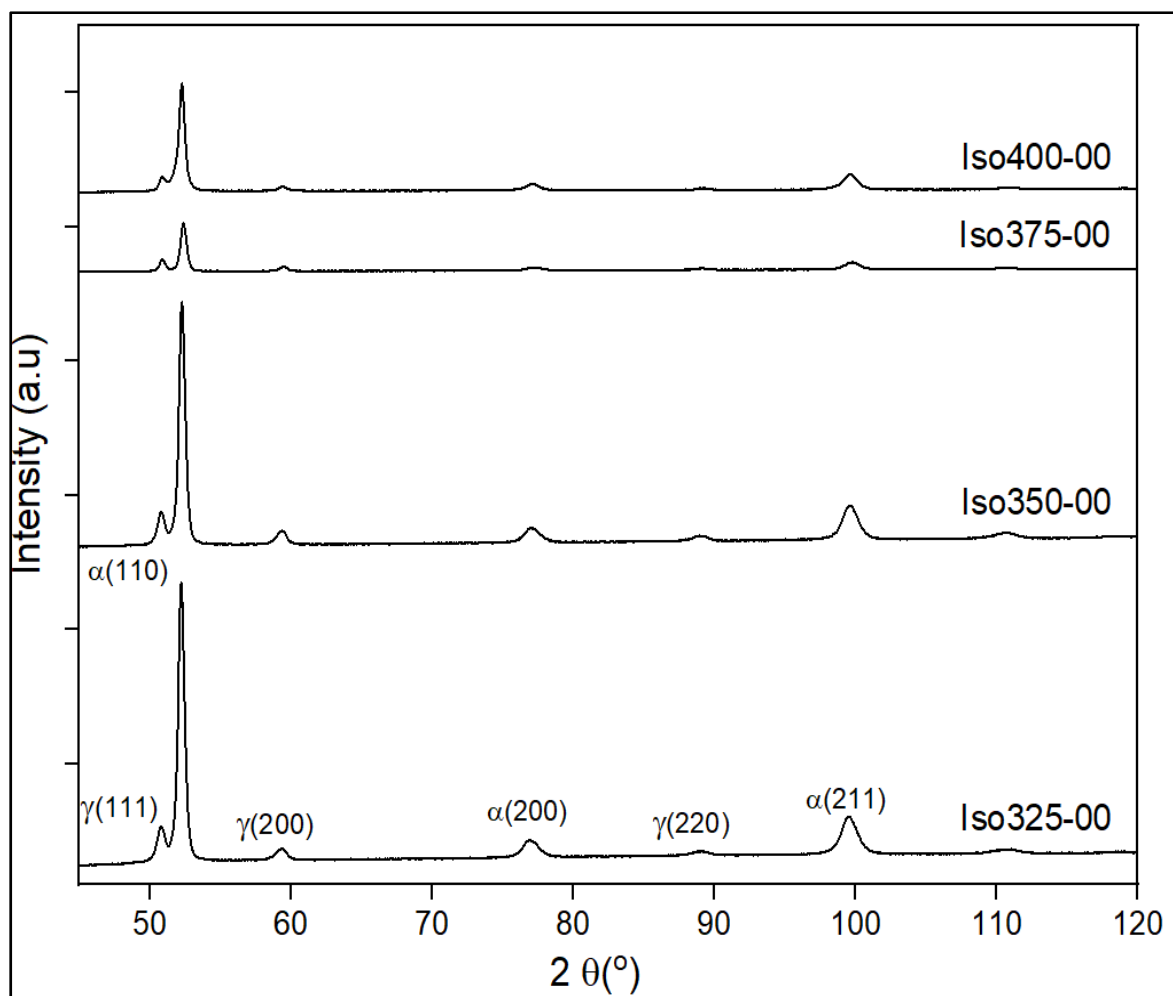
Figure 3-4 XRD diffraction spectrum of non-ausformed samples

Table 3-1 Volume fraction of different phases for non-ausformed and ausformed samples in (%): $V\alpha_{m\,(dil)}$ for martensite based on dilatometry, $V\alpha_{m\,(XRD)}$ (=100-$V_{\gamma R}$), from XRD, $V_{\gamma R}$ retained austenite calculated by XRD, $V\alpha_b$ (=100-$V_{\gamma R}$- $V\alpha_{m\,(dil)}$) bainitic ferrite; the carbon content of retained austenite, $C_{\gamma R}$, in (wt.%) from XRD for, and the M_S in (°C)

TMT condition	Sample Code	$V\alpha_{m(Dil.)}$	$V\alpha_{m(XRD)}$	$V_{\gamma R}$	$V\alpha_b$	$C_{\gamma R}$	M_S
Non-ausformed+Quenching	Q-00	--	92±2	8±2	--	--	310±5
Non-ausforming+Austempering	325-00	0	--	14±2	86±2	1.22±0.21	< RT
	350-00	0	--	16±3	84±3	1.23±0.22	< RT
	375-00	16±4	--	14±3	70±3	0.98±0.11	150±3
	400-00	29±4	--	18±2	53±2	0.85±0.13	225±4
Ausforming+Quenching	Q-10	--	89±3	11±3	--	--	310±2
	Q-30	--	90±2	10±2	--	--	310±2
	Q-40	--	86±2	14±2	--	--	300±2
Ausforming+Austempering	325-10	0	--	19±2	81±2	1.18±0.20	< RT
	325-30	0	--	23±5	77±5	1.16±0.25	< RT
	325-40	0	--	27±2	73±2	1.17±0.15	< RT
	350-10	8±3	--	19±3	73±3	1.05±0.30	180±2
	350-30	11±5	--	18±5	71±5	0.95±0.20	275±3
	375-10	17±6	--	17±6	66±6	0.93±0.11	250±2
	375-30	20±4	--	16±4	64±4	0.90±0.10	260±3
	400-10	34±4	--	19±4	47±4	0.88±0.20	290±2
	400-30	37±4	--	18±4	45±4	0.82±0.16	300±4

3.3.2.3   Microstructural and microhardness analysis

SEM images of the non-ausformed samples at different temperatures are shown in Figure 3-5(a-d). At the lowest temperatures, 325 and 350 °C, the microstructure consists of plate-like

bainite, retained austenite (in the form of films (γ_{Rf}) and blocks (γ_{Rb})), and some dispersed martensite in the form of M/A constituents (Figure 3-5a and 3-5b). As the transformation temperature increases, the bainitic ferrite morphology evolves from plate-like towards granular, and blocky shape austenite increase in number and size in detriment of the thin films, which are almost inexistent at 400 °C as seen in Figure 3-5d.

Microstructural observations revealed that the decomposition of retained austenite to martensite always occurred within the blocky-shape retained austenite, including M/A islands, rather than the film-like ones, which has also been reported by Zhao et al. (L. Zhao, Qian, Lihe, Zhou, Qian, Li, Dongdong, Wang, Tongliang, Jia, Zhigeng, Zhang, Fucheng, Meng, Jiangying, 2019). Thus, it is vital to understand the relationship between the size changes of the M/A constituents as a function of isothermal temperature and deformation. Table 3-2 summarizes the average size of the M/A constituents as well as the volume fraction of the martensitic phase obtained based on an electron microscopy examination of the samples for all testing conditions. The microhardness measurements are also reported for all conditions for comparison and validation purposes of the microstructural evaluations. It must be noted that the amount of $V\alpha_m$ (SEM) reported in Table 3-2, was estimated based on the observed variations in the contrasts between martensite and blocky-shaped austenite in the M/A constituent, as shown in Figure 3-5e and in agreement with similar studies reported in the literature (Mingxing Zhou, 2015; A. S. Podder, 2011; Saha Podder & Bhadeshia, 2010).

Metallographic examination revealed a small fraction (< 5%) of *transformed martensite*, $\alpha_{m(SEM)}$ for lower isothermal temperatures of 325 and 350 °C. However, it must be noted that such a presence was not detected in the dilatometry tests shown in Figure 3-3, probably due to its small percentage. In contrast, the dilatometric observations and XRD results of the tests at 375 and 400 °C revealed that the fraction of transformed martensite increased to about 15 and then 25%, respectively, with the increase in the test temperature from 375 °C to 400 °C. These findings further reinforce the argument that retained austenite after the bainitic transformation is not sufficiently stable at these temperatures. It is also worth noticing the good agreement between the volume fraction of martensite calculated by dilatometry, $V\alpha_{m\,(dil)}$, in Table 1, and

the one by microstructure examination, $V\alpha_m$ (SEM), in Table 3-2.

The evolution of microhardness, shown in Table 3-2, reveals that for the undeformed samples, it decreases from 325 to 350 ℃ but starts to increase again when the test temperature increases to 375 and 400 ℃. As reported in Table 3-2 and Figure 3-5a, a small increase in bainitic ferrite fraction and finer microstructural features are observed in the 325-00 sample compared to the 350-00. It has been reported that the final strength of the microstructure in CFB steels is susceptible to the bainitic ferrite plate thickness (C. Garcia-Mateo et al., 2003); therefore, the observed hardness drop between 325 and 350 ℃ could be related to such microstructural changes. In contrast, the presence of increasing amounts of martensite (as reported in Table 3-2 and Figure 3-5c and 3-5d) is probably at the root cause for the observed hardness increase at higher isothermal holding temperatures.

3.3.3 Stability of retained austenite of ausformed samples

3.3.3.1 Deformation behavior of supercooled austenite

Figure 3-6 shows the flow curves of the supercooled austenite obtained during compressive deformation at 600 ℃ (10, 30, and 40%) prior to bainitic transformation. As can be seen, a continuous work hardening is observed for al deformation levels. The absence of any softening in the stress-strain curve indicates that very little or no dynamic recrystallization has taken place under any of the tested experimental conditions. Therefore, only an increase in the dislocations density as a result of the applied plastic deformation has modified the microstructure.

Utilizing the Bergström model (Zhao-Dong Li 2010), it is possible to estimate the variation in dislocation density (ρ) of for medium carbon steels (Bergström, 1970) as a function of the applied true strain (ε) (Bodin, Sietsma, & van der Zwaag, 2001) as:

$$\rho = \frac{U[1 - exp(-\Omega\varepsilon)]}{\Omega} \tag{3-4}$$

$$\Omega = k\{Z\}^m \tag{3-5}$$

$$Z = \dot{\varepsilon}exp\left(\frac{Q}{RT}\right) \tag{3-6}$$

In the above equations, U refers to the immobilization parameter, and its value is 1.55×10^{15} m^{-2}, and Ω stands for remobilization parameter (Bodin et al., 2001) and equal to 4×10^3 according to Eq. (5), k is a constant with a value taken equal to 180, and m is the exponent for the Zener-Holloman parameter taken equal to -0.1 for austenite in medium carbon steel (Z.-D. Li, Yang, Zhang, & Liu, 2010). The strain rate was equal to 0.1 s^{-1} in the present study, and the activation energy for remobilization, Q, was taken equal to 270 KJ.mol^{-1} as reported by (Z.-D. Li et al., 2010)for medium carbon steel. Finally, R represents the gas constant (8.31 J.mol^{-1}. K^{-1}), and T the deformation temperature (600 ºC).

Using the above equations and constant values, the dislocation densities were calculated for each condition. It can be seen that the dislocation density increased by one order of magnitude when the deformation increased from 10 to 40%. These findings are in agreement with those of Seo et al. (Seo et al., 2015) who reported that, in medium carbon steel, the dislocation density increased from about $8\times10^{+15}$ to about $2\times10^{+16}$ m^{-2} when the percent deformation of austenite increased 10% to 50% at 600 ºC.
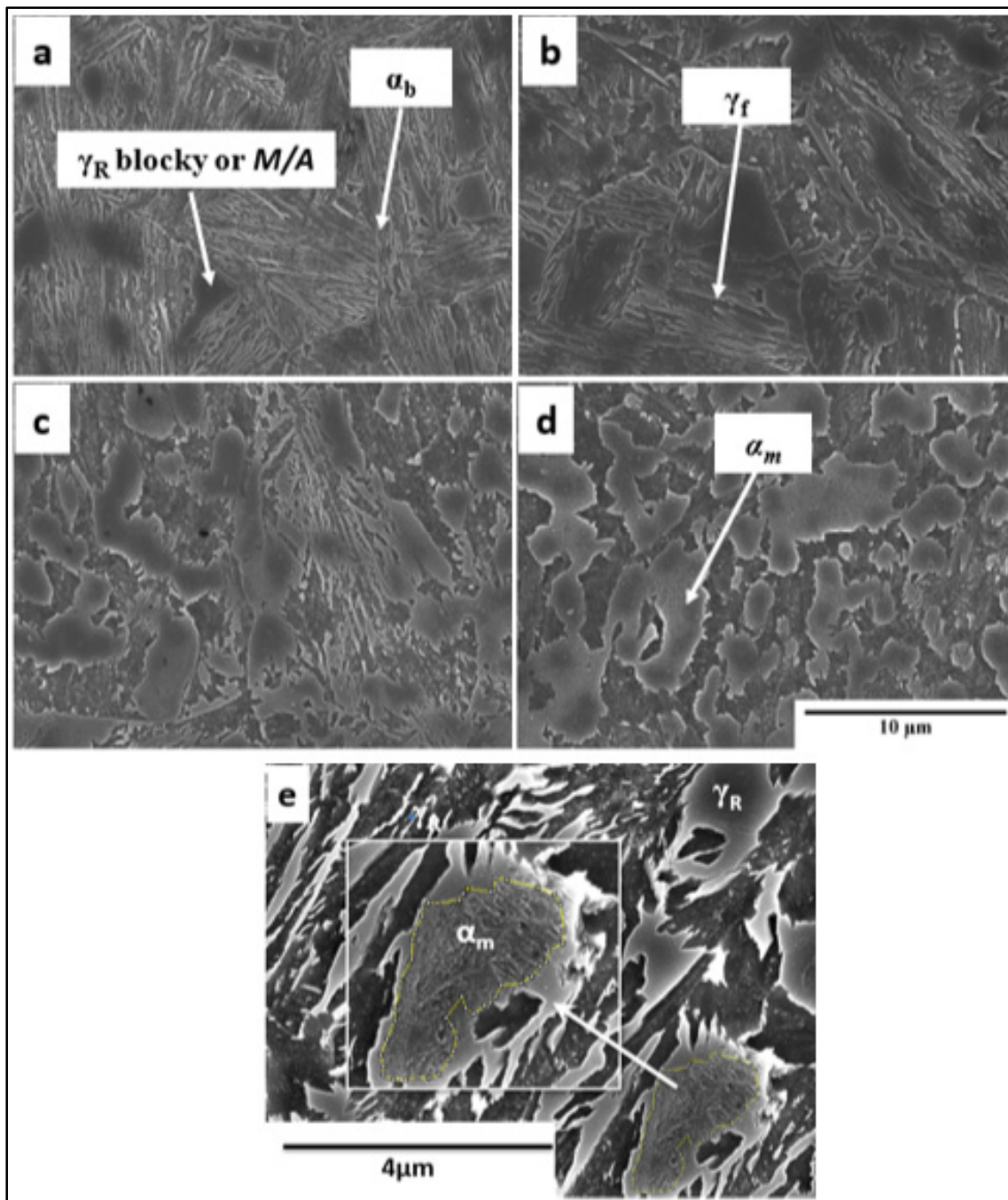
Figure 3-5 SEM micrographs showing a microstructure obtained for the non-ausformed specimens, (a) 325-00, (b) 350-00, (c) 375-00, 400-00, and (e) the contrast between martensite (manually marked by yellow) and retained austenite in M/A constitute. α_b stands for bainitic ferrite, α_m martensite, γ_{Rf} and γ_{Rb} film and block of retained austenite, respectively

Table 3-2 Size of M/A constitutes, and volume fraction of the martensite phase, $V\alpha_m$ (SEM), in (%) based on SEM examination and microhardness of non-ausformed and ausformed samples

TMT condition	Sample Code	M/A(µm)	$V\alpha_m$ (SEM)	HV$_1$
Non-ausforming+Austempering	325-00	1.9±0.1	2±0.5	435±9
	350-00	2.1±0.3	4±1.0	408±11
	375-00	3.2±0.5	13±4.0	415±17
	400-00	3.8±0.6	26±3.0	525±18
Ausforming+Austempering	325-10	1.7±0.25	2±1	439±6
	325-30	0.8±0.10	2±1	435±6
	325-40	0.8±0.30	3±2	445±5
	350-10	1.9±0.30	10±2	420±13
	350-30	1.4±0.25	12±3	436±12
	375-10	3.4±0.60	17±2	485±17
	375-30	3.6±0.50	21±6	495±17
	400-10	4.3±0.60	33±4	533±16
	400-30	4.5±0.60	35±5	565±20

3.3.3.2   Dilatometry analysis

In order to calculate the fraction of martensite formed after the isothermal transformation, $V\alpha_m$ (dil), in ausformed samples, a series of experiments were carried out where the samples were quenched immediately after the deformation at 600 ºC, rout (D) in Figure 3-1b.

Figure 3-7a show the dilatometric curves on cooling to room temperature after deformation was applied as in route (D) in Figure 3-1b.

The martensitic transformation is occurring in the three tested conditions. While the M_S after 10 and 30% deformation is nearly the same (~310 °C), like that of the no-deformed samples, the results also reveal that the M_S decreases to about 300 °C after 40% of plastic deformation.
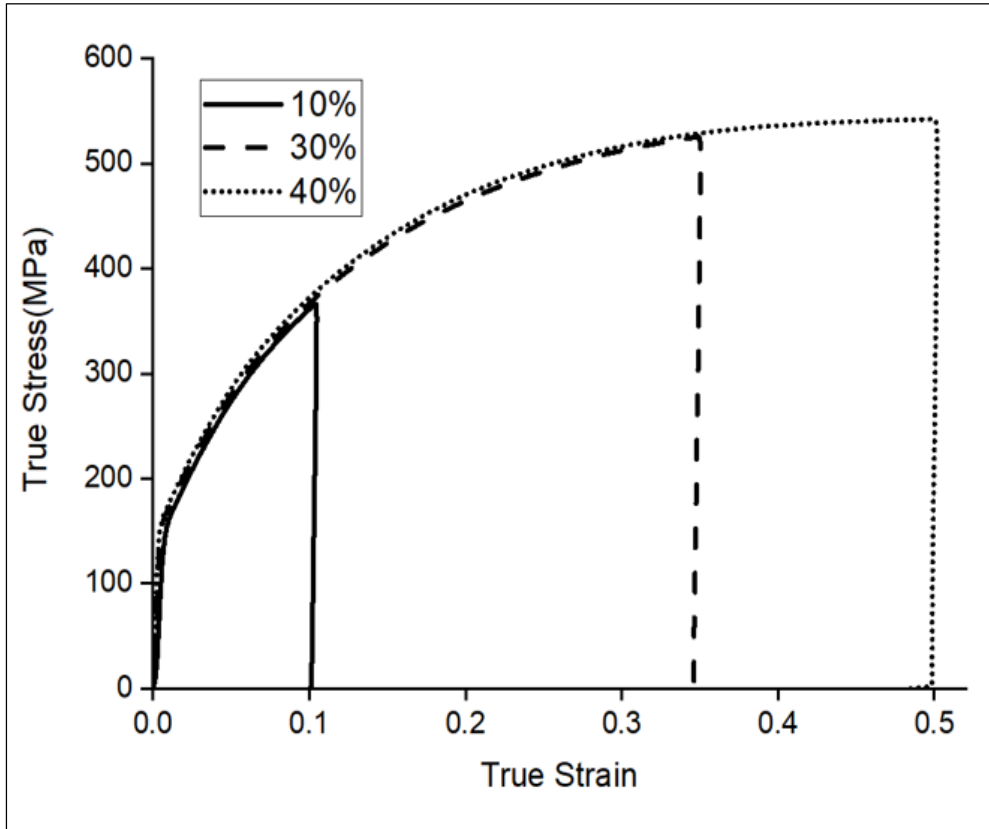
Figure 3-6 Flow curves during ausforming at 600 °C for 10, 30 and 40 % deformation

This slight decrease in the M_S can be rationalized by the significant increase in dislocation density at 40% deformation that would hinder the martensitic transformation through mechanical stabilization and move it to lower temperatures, as also reported by other authors (C. Garcia-Mateo, Caballero, Chao, Capdevila, & Garcia de Andres, 2009; Nikravesh, Naderi, & Akbari, 2012; M. Zhang, Wang, Zheng, Zhang, & Wang, 2014a; M. Zhang et al., 2014b). Furthermore, the bainite transformation during cooling from ausforming temperature to isothermal temperature could not be avoided, especially for 30 and 40 % deformation, as

indicated by arrows in Figure 3-7a. This bainitic transformation might be so small that it could be challenging to be observed by microstructural examinations. Note that deforming austenite is known to displace the entire CCT and TTT diagrams towards shorter times, explaining the appearance of bainite on cooling (Gong et al., 2013; H. Hu et al., 2015; J. Zhao et al., 2017).
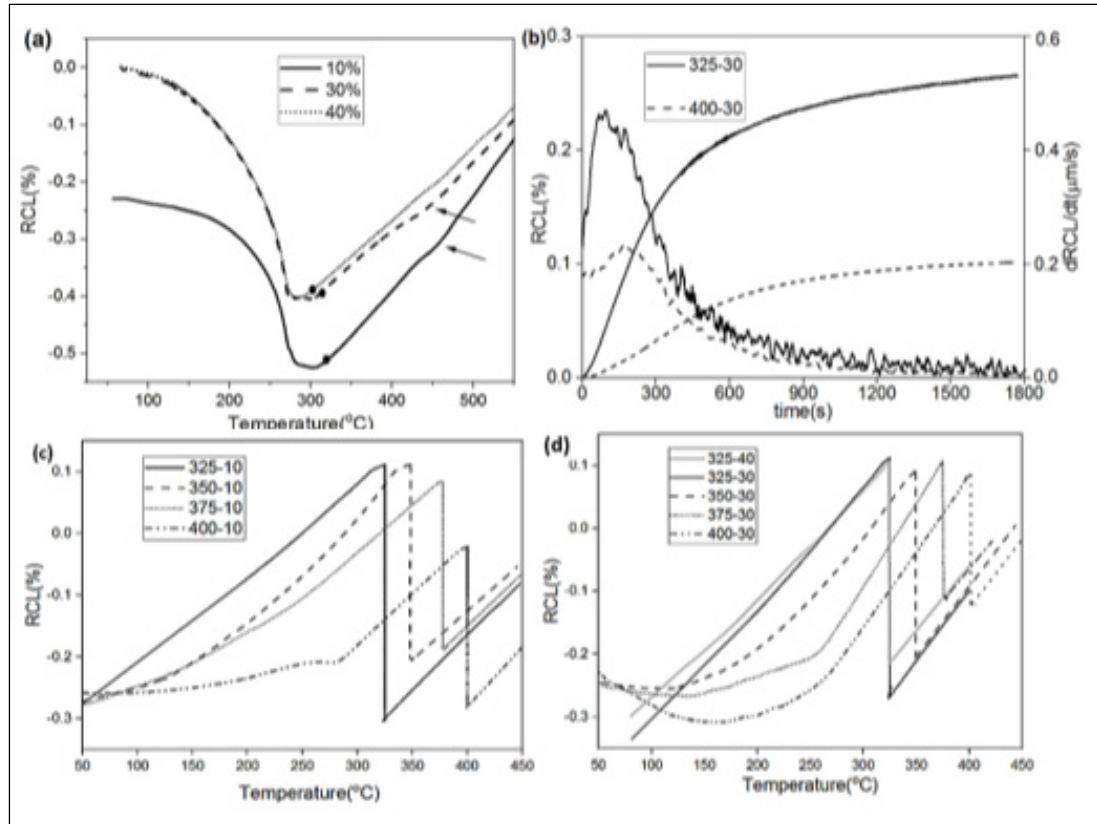
Figure 3-7 Relative change in length vs. temperature during the quenching to room temperature for ausformed samples (a), the transformation kinetic as function of temperature (325 and 400 °C) and deformation amount (30%) (b), the dilatation behavior during cooling to room temperature after ausforming at 600 °C and isothermal treatment at different temperatures for 10% deformation (c), for 30 and 40%. (Black dots indicate the M_S in a) (d)

An example of the sigmoidal curves during bainitic transformation at 325 and 400 °C after 30% deformation is shown in Figure 3-7b. The curves show a similar trend to that of non-ausformed treatments, i.e., the bainitic transformation appears to be completed during the isothermal holding with the RCL reaching a steady-state and the transformation rate reaching

almost zero after approximately 1500 s. Moreover, the curves in Figure 3-3 and Figure 3-7c and 3-7d, show that ausforming leads to a decrease in the volume fraction of bainite compared with the non-deformed treatments, especially for higher isothermal temperature (400 °C).

It has been reported that as the plastic deformation of austenite increases, so does the dislocation density at the interface between austenite and bainitic ferrite. The increased dislocation density increases the resistance to the growth of the bainitic ferrite plates and could hinder and even stop displacive transformation (H.-S. W. S. Chatterjee, J. R. Yang & H. K. D. H. Bhadeshia, 2013; Shipway & Bhadeshia, 2013). This resistance becomes more and more significant as the austenite becomes stronger with increased C enrichment resulting in the stabilization of the austenite phase (Yoozbashi, Yazdani, & Wang, 2011). It must be noted that, as reported by (Eres-Castellanos et al., 2018; Gong et al., 2013; M. Liu et al., 2019) in addition to mechanical stabilization, preferred ordination due to deformation could also affect the dilatometric signal and produce a similar effect as that of mechanical stabilization. However, the contribution from deformation textures should be minor in the present study as the influence of strain on crystallographic orientation is limited when the supercooled austenite deformed above the bainite start temperature can be considered isotropic (Eres-Castellanos et al., 2018; Fan, Zhao, Li, Guo, & He, 2017). Therefore, the dilatation curves can be considered as representative of the bainite transformation.

Figure 3-7c and 3-7d reveal the dilatometric behavior of the microstructure on cooling to room temperature after isothermal treatment, rout (C) in Figure 3-1b. While the sample treated at 325 °C remains unchanged throughout all deformation stages (10 and 30%). However, at 350 °C and higher temperatures, there is a noticeable change in slope linearity even at 10% deformation. The corresponding martensite volume fractions were calculated as already described, and the results thus obtained are presented in Table 3-2. Together with results in Table 3-1, it can be said that at 325 °C, the deformation has a minimal effect on the decomposition of retained austenite to martensite as well as on bainitic transformation. However, as the isothermal temperature is increased to 350 °C and above (Figure 3-7c), the stability of the retained austenite significantly decreased by introducing even a small amount of deformation. The above changes could be related to the steep decrease in the fraction of the

bainitic phase compared to 325 °C. Moreover, the M_S of retained austenite that decomposed to martensite increased with deformation amount probably because the retained austenite has less and less carbon when percent deformation increases. For example, as reported in Table 3-1, the M_S for sample isothermally treated at 350 °C, increased from a temperature below the room temperature for non-ausformed condition, as seen in Figure 3-3 and Table 3-1, to about 180 °C and 275 °C for 10 and 30% deformation as shown in Figure 3-7c and 3-7d, respectively. For higher isothermal temperatures (375 and 400 °C), the difference in M_S between 10 and 30 % deformation conditions was around 5%.

The above results revealed that retained austenite has higher stability at 325 °C. In order to validate this finding, a new test with a higher deformation level had to be conducted. To this end, various tests were run, and it was found that the maximum achievable deformation at 600 °C in the dilatometer for the investigated alloy was 40%. The results are reported in Figure 3-7d (light gray line), where a very slight change in the slope of the dilatation curve can be seen. This minor change can be considered negligible, and therefore, it can be said that the retained austenite is very stable at 325 °C.

3.3.3.3 XRD analysis

The XRD patterns of the 30% deformed samples for the lowest and highest isothermal treatments (325 and 400 °C) are shown in Figure 3-8. The XRD spectrum confirms, within the limits of XRD resolution, the absence of any strain induced precipitation and the strong inhibiting role of Si on carbide precipitation (Tian et al., 2019b). Furthermore, the austenite peak (200) in Figure 3-8 (enlarged image) shows that there was a slight displacement of the diffraction angle (2θ) to the right. This could be an indication of a significant reduction in $C_{\gamma R}$ concentration for 400-30 samples as a result of the substantial delay in the bainitic transformation, due to the higher deformation and isothermal holding temperature. Zhao et al. (L. Zhao, Qian, Lihe, Zhou, Qian, Li, Dongdong, Wang, Tongliang, Jia, Zhigeng, Zhang, Fucheng, Meng, Jiangying, 2019) reported a similar phenomenon in ausformed low-C bainitic steel.

Analysis of the XRD results reported in Table 3-1, showed that after 10% deformation at 325 ºC the bainitic transformation is very slightly affected by the possible mechanical stabilization of austenite with only a reduction of 4% in the amount of bainite. Nevertheless, after a 40% deformation, the amount of bainite is reduced by more than 10%. At higher isothermal holding temperatures, the stabilization of austenite against bainitic transformation is more visible, although no significant differences are found between the 10 and 30% deformation cases. It must also be noted that, as reported in Table 3-1, lower degrees of transformation results in higher amounts of martensite.

At higher bainite transformation temperatures, the variation in retained austenite fractions for the ausformed and non-ausformed was minimal, as shown in Table 3-1. This finding implies that the decomposition of the retained austenite into martensite increased by increasing the amount of deformation, making the volume fraction of retained austenite almost equal for all deformation levels. In contrast, the retained austenite was stabilized for the samples treated at 325 ºC, and its volume fraction increased from 14% for the non-ausformed sample to about 23% when the 30% deformation was applied. At 350 ºC, there was no evidence that martensite formed during cooling to room temperature for non-ausformed treatment, as shown in the dilatation curve (Figure 3-3). However, the decomposition of retained austenite was initiated (Figure 3-7c), with the percentage of martensite increasing when the amount of deformation reached 10%, as also presented in Table 3-1.

3.3.3.4 Microstructural and microhardness observations

SEM micrographs in Figure 3-9 reveal the effect of deformation on the retained austenite and martensite evolution after the bainitic transformation has been completed. The presence of blocky-shaped retained austenite along with martensite as well as globular bainite increased with increased deformation and isothermal holding temperatures. The combination of higher isothermal temperature and even a small of deformation, as seen in samples 375-10 and 400-10 (Figure 3-9), increased the size of the M/A constituents compared with non-deformed samples, 375-00 and 400-00, as shown in Figure 3-5c and 3-5d. The latter contains lower

carbon, due to the smaller amount of bainitic transformation, compared with lower isothermal temperatures with a large deformation amount (samples 325-30 and 350-30).

The measurements of the size of the M/A constituents were reported in Table 3-2. It can be seen that the size of M/A constituents increases with the increase in the percent deformation in the case of the 375 and 400 °C isothermal treatments. Whereas, it decreases with increasing the deformation amount for the samples isothermally hold at temperatures lower than 375 °C. The M/A size became finer and reduced by about 50% (~0.8 μm) at 325 °C when the percent deformation increased from 10 to 30%. Thus, based on the above results, as the size of the M/A islands becomes larger, more and more martensite is formed during cooling to room temperature.
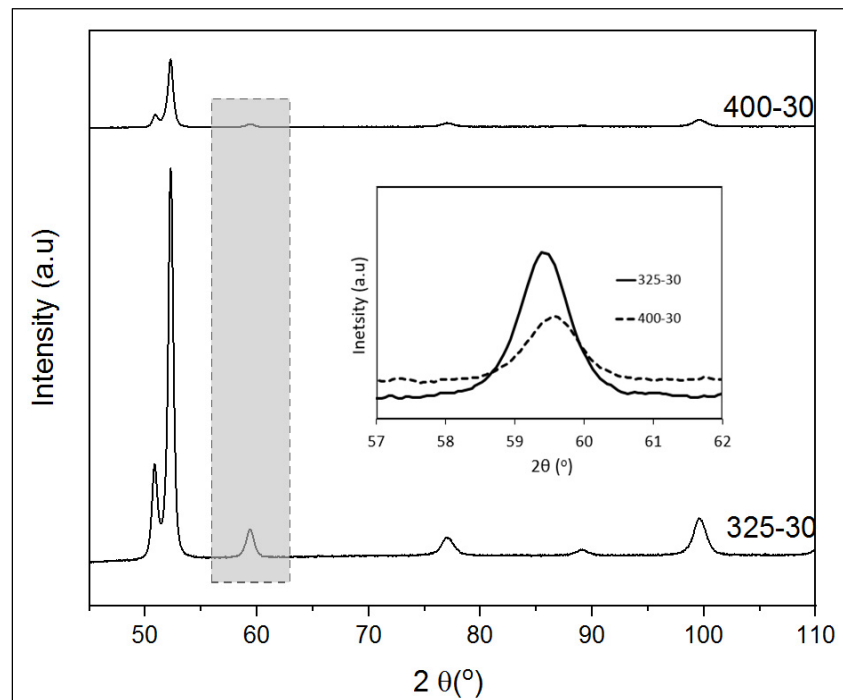
Figure 3-8 XRD diffractogram of ausformed samples 30% deformation, and the inserted image is magnified γ (200) spectra for 325-30 and 400-30 samples

The evolution of the microhardness of the ausformed samples is also reported in Table 3-2. It can be seen that independently of the testing temperature, the hardness increases with percent deformation though the increase in hardness became more evident when the bainitic transformation temperature increased. For instance, at 325 °C, the hardness was almost constant for the samples 325-10 and 325-30 (less than 1% difference) owing to the limited effect of deformation on the bainite volume fraction for both samples. However, for treatment at 350 °C, the hardness continuously increased from 420 to about 436 HV for samples 350-10 and 350-30, respectively. The increase in hardness is probably related to the increase of transformed martensite from 10 to 12% for samples 350-10 and 350-30, respectively, as well as the higher dislocation density for 30% deformation, as discussed earlier. The combination of higher isothermal temperature and the percentage deformation led to a cessation in the bainitic transformation and resulted in a higher amount of martensite, thus leading to a significant increase in hardness (above 500 HV), as measured in samples 375-30 and 400-30. Furthermore, it must be noted that the error ranges of hardness measurements were more significant for the highly deformed samples (30 and 40%) and higher isothermal temperatures (375 and 400 °C), probably due to the presence of martensite islands that are non-uniformly distributed in the samples, resulting in a less homogeneous microstructure.

Based on the obtained results, the test condition corresponding to 10% ausforming followed by isothermal treatment at 350 °C appears to be a threshold, below and above which the effect of deformation on the stability of retained austenite is different. To further validate this finding, the difference in bainite volume fraction transformed at different isothermal temperatures for ausformed (10% deformation) and non-ausformed samples was calculated, and it was found that the most substantial difference was observed in sample 350-10, as shown in Figure 3-10. This could explain why the effect of deformation on retained austenite stability was also more noticeable in 350-10 samples.

In summary, the mechanism of the effect of deformation on the stability of retained austenite could be classified into three stages, as schematically illustrated in Figure 3-11. At the isothermal temperature of 325 °C (Figure 3-11a), the deformation effect is minimal and could

be neglected. This can be explained by the presence of higher bainitic volume fractions. This is due to the high driving force at low transformation temperatures, which overcome the resistance of the bainitic sheave growth because of the introduction of either small (10%) or large (40%) deformation.

At 375 and 400 $^{\circ}$C temperatures, as seen in Figure 3-11b, the reductions in retained austenite stability was directly proportional to the amount of deformation. However, it is difficult to accurately quantify the effect of strain on retained austenite stability compared with non-deformed ones, due to the presence of the martensite phase, even for non-ausformed samples submitted to pure isothermal transformation.

At 350 $^{\circ}$C, as shown in Figure 3-11c, the results showed that the retained austenite was stable for non-ausformed isothermal treatment, and the amount of transformed martensite was negligible. However, this stability was reduced, and the amount of martensite increased substantially, after 10% deformation. Specifically, in this case, the bainite volume fraction and $C\gamma_R$ increased to above 14 and 15%, respectively. Under these conditions, dislocation resistance to the growth of bainitic sheaves overcome the bainite nucleation rate, as also reported in (H. Hu et al., 2015). As a result, the large islands of retained austenite contained less carbon, which transformed to martensite at a higher M_S and distributed among the bainite sheaves.
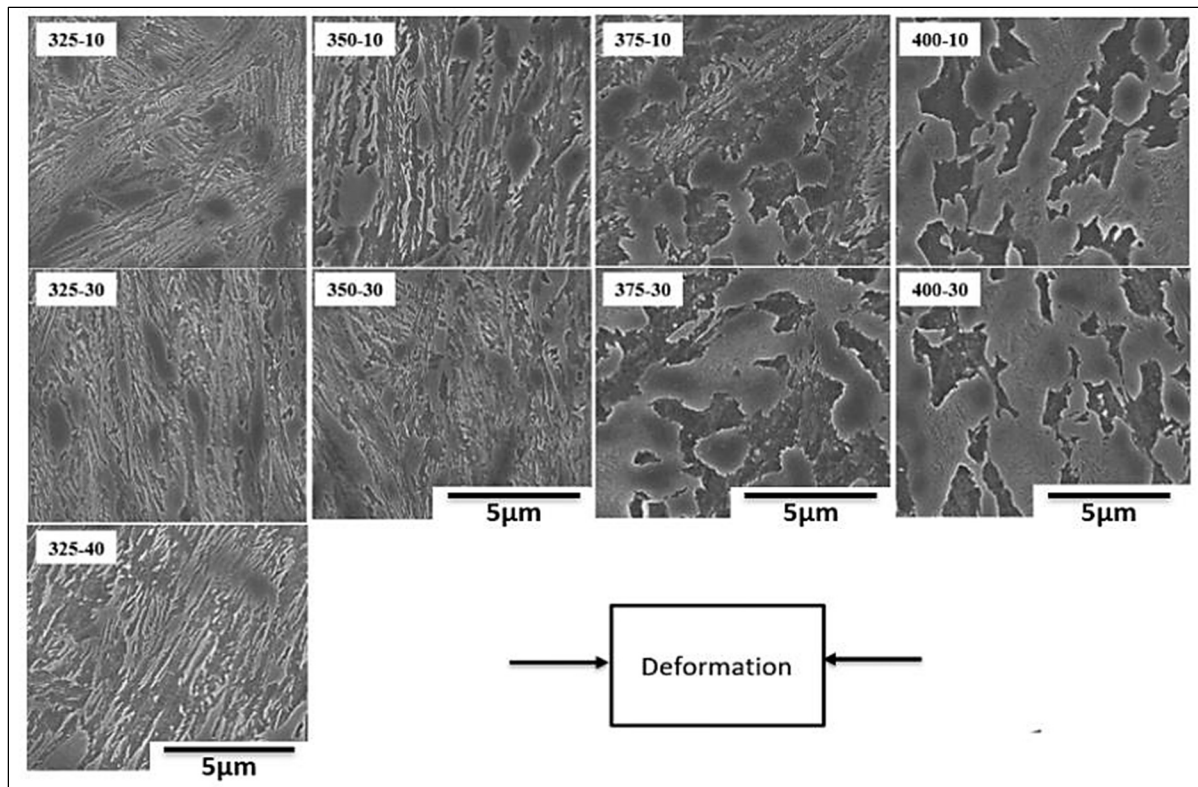
Figure 3-9 SEM images of ausformed samples at 600oC with different deformation amounts followed by bainitic transformation at different isothermal temperatures
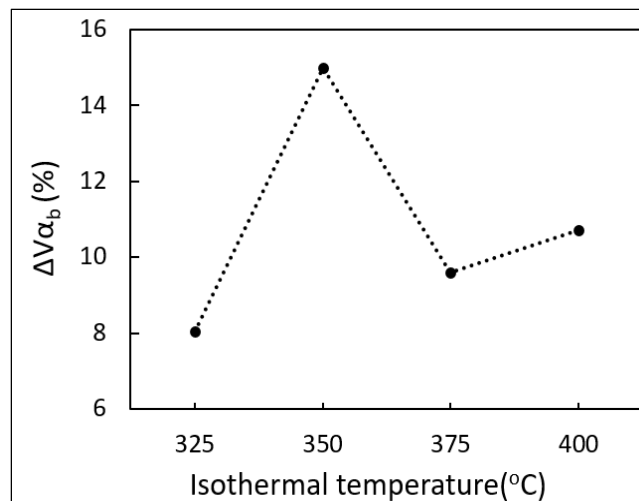
Figure 3-10 Difference in bainite volume fractions between non-ausformed and 10% ausformed samples for different bainite transformation temperatures
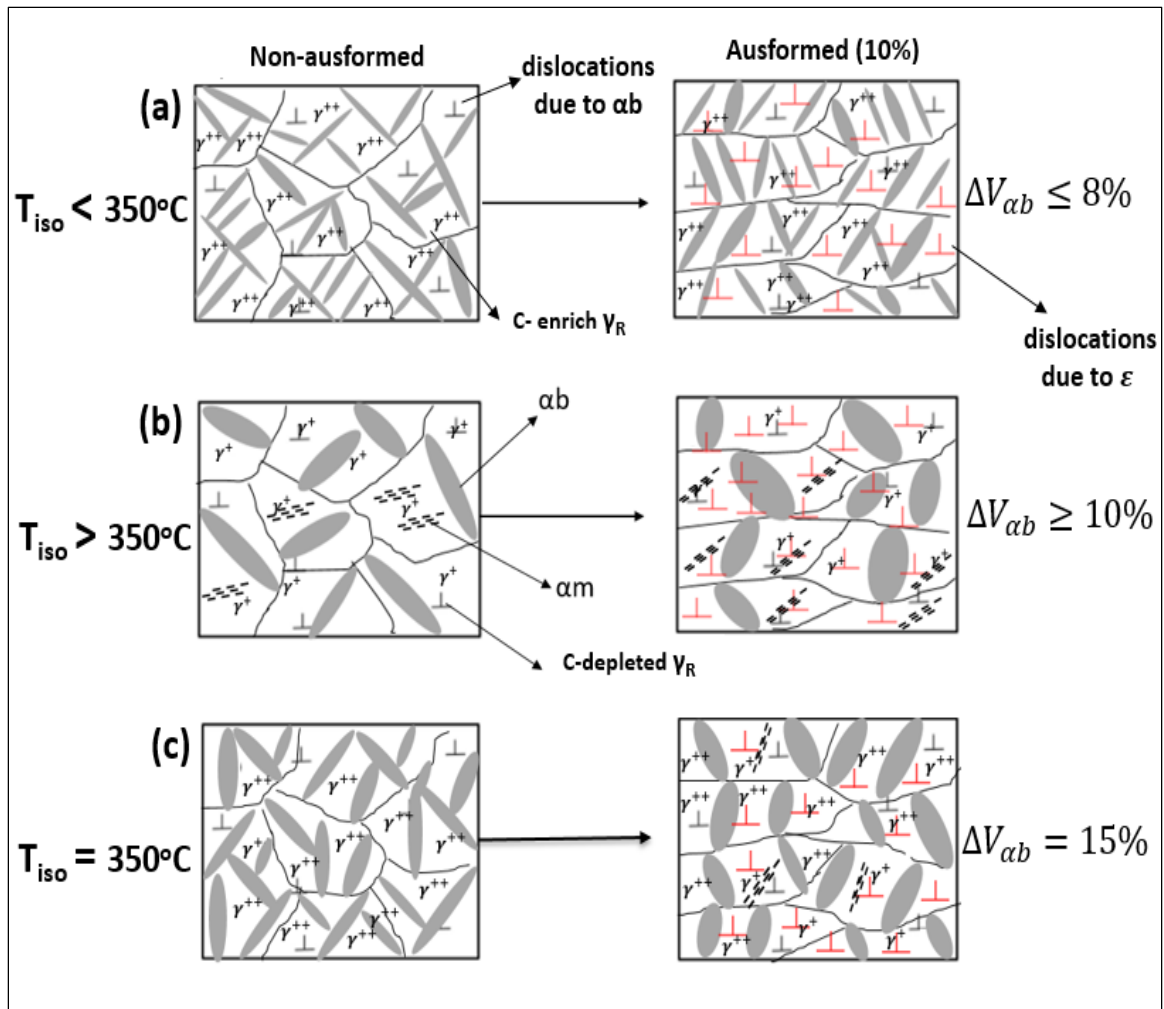
Figure 3-11 Schematic graph of the effect of deformation on the stability of retained austenite, (a) below 350 ºC, (b) above 350 ºC, (c) at 350 ºC

3.4 Conclusions

In the present study, the effect of ausforming on the stability of retained austenite and its decomposition to martensite after the completion of isothermal holding treatment in medium C-Si steel was investigated. The following conclusions can be drawn from this study:

- The amount of transformed bainite is a critical parameter controlling the decomposition of retained austenite to martensite during cooling to room temperature.

- In pure isothermal treatments (non-ausformed), the isothermal holding temperature of 350 °C can be considered as the threshold temperature for retained austenite stability. At 350 °C and below, the retained austenite is very stable, and above it, the retained austenite is unstable.

- For ausformed samples, the decomposition of retained austenite to martensite can be altered via a small deformation amount (10%) at and above the threshold temperature (i.e., 350 °C). Whereas, at a lower temperature, the retained austenite is very stable, regardless of percent deformation.

- Above 350 °C, ausforming enhances the formation of blocky-shaped retained austenite that contains lower carbon content than the film-like retained austenite morphology, resulting in increased martensitic transformation during cooling to room temperature.

- At lower isothermal transformation temperatures (325 and 350 °C), the blocks were thinner with increased percent deformation.

EFFECTS OF AUSFORMING TEMPERATURE ON CARBIDE-FREE BAINITE
TRANSFORMATION AND ITS CORRELATION TO THE TRANSFORMATION
PLASTICITY STRAIN IN A MEDIUM C- SI-RICH STEEL

M. Zorgani[1], C. Garcia-Mateo[2], M. Jahazi[1]

[1] Department of Mechanical Engineering, École de Technologie Supérieure,
1100 Notre-Dame West, Montreal, Quebec, Canada H3C 1K3
[2] National Center for Metallurgical Research (CENIM-CSIC),
Avda. Gregorio del Amo 8, Madrid 28040, Spain

Abstract

Ausforming treatments at different temperatures were applied to a medium C-Si rich carbide-free bainitic steel, and the role of transformation plasticity on the evolution of the microstructure is discussed. Three ausforming temperatures were selected prior to isothermal bainite transformation at 325 ºC. Deformation was applied above the bainite start temperature, B_S, (600 ºC), below B_S (400 ºC), and at the isothermal transformation temperature (325 ºC). A combination of high-resolution dilatometry, XRD, SEM, and EBSD was used to investigate phase changes, microstructure evolution, and variant selections for the different ausforming conditions. The results indicated that the transformation rate was enhanced for all deformation conditions compared with the pure isothermal condition. Ausforming above B_S did not modify the morphology of the carbide free microstructure, while ausforming below B_S led to an asymmetrical morphology in the specimen. The alignment of the bainite plates can be at a

random or a specific angle, depending on the supercooled austenite condition prior to the bainitic transformation. The thickness of the bainitic ferrite plates was refined to about 100 nm for the ausforming cycle at 325 ºC resulting in a hardness of values of 540 HV. Transformation plasticity strains increased with increasing bainite transformation and were more intense with increasing microstructure alignment at the two lower ausforming temperatures. Texture studies revealed that both pure isothermal and ausforming at temperatures above B_S resulted in an almost random texture, while a strong texture was obtained when ausforming below B_S, a which was attributed to variant selection.

Keywords: Ausforming; Carbide-Free Bainite; Transformation plasticity; microstructure alignment

4.1   Introduction

Deforming metastable austenite followed by bainite transformation, also termed ausforming, is an alternative way to modify carbide-free-bainite (CFB) morphology to a nanostructure in medium and low carbon steels. The pre-straining is usually applied in the bay between the ferrite/pearlite and bainite curves of the time-temperature-transformation (TTT) diagram, or it can be done at lower temperatures, between the bainite start temperature (B_S) and martensite start temperature (M_S). The nanostructured bainitic microstructure has been produced in medium-carbon Si-rich alloy steels by applying deformation in the 600-300 ºC temperature interval, followed by an isothermal transformation at a temperature close to M_S (Eres-Castellanos et al., 2018; Fan et al., 2017; H. Hu et al., 2017; M. Zhang et al., 2013; M. Zhang et al., 2014b; J. Zhao et al., 2017; L. Zhao, Qian, Lihe, Zhou, Qian, Li, Dongdong, Wang, Tongliang, Jia, Zhigeng, Zhang, Fucheng, Meng, Jiangying, 2019). In addition to altering the morphology, ausforming can enhance the transformation kinetics and, in some cases, the amount of transformed bainite (B. B. He et al., 2015). The incubation and transformation times are shortened as the pre-deformation temperature is reduced (H. Hu et al., 2019; H. Hu et al., 2015).

Displacive transformations, such as martensite and bainite, are always associated with a shape deformation that encompasses a significant shear component (s≈0.26) and small dilatation strain (δ≈0.03) as a result of the invariant plane strain (IPS) (H. K. D. H. Bhadeshia, 2002; Garcia-Mateo & Caballero, 2014). Due to the IPS, the volume change is always assumed to be isotropic when the bainitic reaction occurs without influences of other factors (e.g., external superimposed stress and/or deformation before transformation) (H. K. D. H. Bhadeshia, David, Vitek, & Reed, 2013; H.-G. Lambers, 2011; M. Liu et al., 2019). The transformed bainite commonly has a Kurdjumov-Sachs, K-S, orientation relationship with the parent austenite, where 24 variants could be grown in one austenite grain (Han & Suh, 2003; Morales-Rivas et al., 2018; B. B. Wu, Wang, X. L., Wang, Z. Q., Zhao, J. X., Jin, Y. H., Wang, C. S., Shang, C. J., Misra, R. D. K., 2018). However, when the bainite plates grow in a specific/preferred orientation, the transformation is considered anisotropic, and therefore the volume change could not be assumed identical in all directions. The anisotropy in volume change during bainite transformation could be described in terms of transformation plasticity (TP) or, in other words, the strain associated with the anisotropic bainitic transformation. It has been reported that an increase in nucleation and growth of bainite subunits intensified the TP strains (H. K. D. H. Bhadeshia et al., 2013; Grostabussiat, Taleb, Jullien, & Sidoroff, 2001; Han & Suh, 2003; M. Liu et al., 2019), and therefore, TP strain could be used to quantify the influence of process parameters on the level of anisotropy in bainitic transformation.

Magee (Magee, 1966) and Greenwood-Johnson (Greenwood, Johnson, & Rotherham, 1997) proposed models describing the evolution of TP strains. The former explained that the increase in TP strains could be due to an alignment in the martensite or bainite variants in specific directions and angles. The author referred that to the additional mechanical driving force due to the applied stresses that promote specific variants to grow faster than others during bainitic and martensitic transformation. Greenwood-Johnson linked the evolution of the TP strains to the volumetric difference between the austenite and the bainite or martensite phases due to the micro deformations that occur in the weaker phase, i.e., austenite (Lambers, Canadinc, & Maier, 2012; M. Zhou, Xu, Hu, Yuan, & Tian, 2018). Han et al. and Liu et al. (Han & Suh, 2003; Z. Liu, Yao, & Liu, 2013) in their work provided supporting evidence that in the case of

low carbon steels, the evolution of TP strain followed the Greenwood-Johnson model while Rees et al. and Uslu et al. (Rees & Shipway, 1997; Uslu, Canadinc, Lambers, Tschumak, & Maier, 2011) reported that in medium carbon steels the evolution of TP strain was according to the Megge model. Note that in the studies mentioned above, the bainitic transformation took place under the influence of applied stress.

Recently Liu et al. (M. Liu et al., 2019) investigated the effect of plastic stress applied during bainite transformation at different temperatures on the evolution of TP strains in a CFB steel with medium C content. The authors concluded that the development of the TP strain was compatible with the Magee mechanism. Their results showed that the TP strain slightly increased when the stress was *below* the yield strength of the parent phase (i.e., austenite), while the TP increased remarkably if the applied stress was *above* austenite yield stress (i.e., austenite was plastically deformed). In contrast, Zhou et al. reported a strong variant selection (i.e., high TP values) in the microstructure when the applied stress was *below* austenite yield strength (M. Zhou, Xu, Wang, & Yuan, 2016). Furthermore, the impact of the pre-deformation temperature prior to the bainitic reaction was not investigated in the above studies.

Lambers et al. (H.-G. Lambers, 2011) reported that TP strains altered and increased with applied external stresses, whether below or above the austenite yield stress, during bainitic transformation in a low-alloy 51CrV4 steel. The authors found that changes in the TP strain evolution were initiated during the pre-straining stage of the supercooled austenite prior to transformation. The changes in the TP strain reached a steady state when the deformation level reached about 3% for all conditions. Such changes were associated with the crystallographic texture in the deformed austenite and the invariant-plane strain shape accompanying the displacive growth (H. K. D. H. Bhadeshia et al., 2013). The authors also found that the enhancement of the bainite transformation, due to the plastic pre-deformations, generated more residual stresses in the supercooled austenite and increased the TP strains. In another study conducted on the same steel (H.-G. Lambers, 2010), the author found that the TP strain was reduced when a 4% pre-strain temperature increased by 100 ºC, from 400 ºC to 500 ºC. Note that in these studies, the pre-deformation amount was only 6.5% at 1050 ºC and 3% at 340 ºC, which are quite low values to be able to determine a clear and quantifiable trend.

The present work is defined in this context and has for objective to investigate the effect of the compressive plastic deformation temperature on the CFB transformation in terms of microstructural and kinetic behavior and their relation to the evolution of TP strains during the bainitic transformation in medium-carbon CFB steel. The temperatures and deformation levels were selected to allow for quantification of the impact of TP strain and a clear distinction of the role of variant selection in the transformation process.

4.2   Material and experimental procedure

A medium C-high Si steel was used in this study, and its nominal chemical composition is shown in Table 4-1. The presence of Mn and Cr enhances the steel hardenability and makes it suitable to perform the ausforming process, and Mo also can increase the hardenability and prevent temper embrittlement (Francisca García Caballero, 2006). Silicon (Si) is typically added to suppress cementite precipitation during the bainitic reaction (H. K. D. H. Bhadeshia, 1989).

Table 4-1 Chemical composition of the steel studied in wt. %

C	Si	Mn	Cr	Mo	Fe
0.4	1.7	1.5	1.5	0.4	Balance

The thermal and thermomechanical treatments, with and without deformation, were performed in a high-resolution deformation dilatometer (DIL805A/D-TA) using a particular module for thermomechanical treatments. For this purpose, cylindrical specimens 10 mm in length and 5 mm in diameter were used for both pure isothermal and ausforming tests. Molybdenum discs were spot welded on specimen sides to reduce the friction between the specimen and the silicon nitride (Si_3N_4) stamps during the deformation step and ensure a uniform distribution of temperature along with the specimen during the thermomechanical process. For controlling the temperature cycle, a type-K thermocouple was welded in the middle of the specimen, where the variation along the specimen length was ±5 °C. Figure 4-1a and 4-1b are the schematic descriptions of the dilatometry used in this study.

The thermal and thermomechanical cycles are schematically illustrated in Figure 4-1c, and further details on the selection of the conditions can be found in ref. (Zorgani, Garcia-Mateo, & Jahazi, 2020). Specimens were heated at 10 °Cs^{-1} to a temperature of 980 °C, where they were held for 5 min under vacuum. They were then cooled at 20 °Cs^{-1} to the three selected deformation temperatures, where a 20% deformation at a deformation rate of 1mms^{-1} was applied. Considering that bainite and martensite start temperatures (B_S and M_S) of the steel were determined to be 470±10 and 310±5 °C, respectively, and the bay between ferrite/pearlite and bainite (F/P-B) delimited between 500-600 ºC (Zorgani et al., 2020).

Deformation temperatures (T_{def}) prior to isothermal transformation at 325 °C (T_{Iso}) were selected as follows: i) $T_{def} > B_S$ at 600 °C; ii) $B_S > T_{def} > T_{Iso}$ at 400 ºC; and iii) $T_{def} = T_{Iso}$ at 325 °C. The deformation step was selected to be less than 10 s to avoid possible bainite transformation during the deformation process (Zorgani et al., 2020). The deformed samples were cooled down to T_{Iso} = 325 °C at a cooling rate of 20 °C/s and then held for 30 min to allow the bainitic transformation to finish. For comparison purposes, a pure isothermal test at 325 ºC (with no previous deformation) was also carried out under the same conditions as the ausformed specimens. It must be noted that no other phase transformations were detected by dilatometry prior to deformation or during cooling to the isothermal transformation stage, indicating that the microstructure is fully austenitic in all cases prior to the bainitic transformation. Moreover, no martensitic transformation was detected on cooling to room temperature after isothermal holding time.

In order to accurately determine the bainitic transformation's kinetics, diametrical and longitudinal dilatations were recorded to calculate the Relative Change in Volume (RCV) of each specimen. The Relative Change in Length (RCL) was recorded using a Linear Variable Differential Transducer (LVDT), while the Relative Change in Diameter (RCD) was measured using a laser scanning system that automatically locates itself at the specimen's mid-length regardless of deformation. It should be noted that the RCL and RCD dilatometric signals were recorded simultaneously during bainitic transformation. The amount of expansion obtained from the dilatometer, whether longitudinal or diametrical, was normalized by dividing the

instantaneous dilatation of the specimen length or diameter before the transformation. As anticipated, for consistency, all the treatments were performed on the specific *deformation* module of the DIL 805 dilatometer, where a minimal load of the order of 4 MPa is applied to hold the specimen.
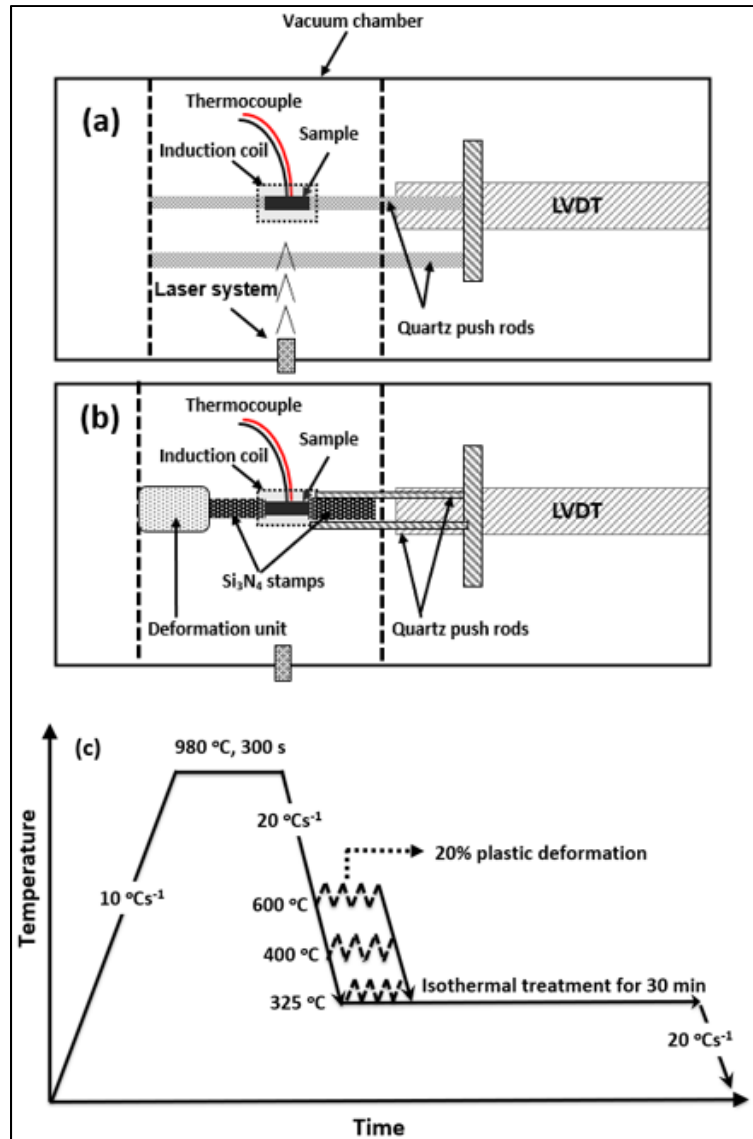
Figure 4-1 Dilatometry set up for two used modules (a) quenching; (b) deformation, (c) pure isothermal and ausforming experimental procedures

Microstructural characterization was carried out on both longitudinal (L) and transverse (T) sections of the tested specimens using optical and Scanning Electron Microscopy (SEM). Specimens for SEM investigations were prepared according to standard metallography procedures. After the final polishing step was completed, a cycle of etching (3 % Nital for 5 s) and polishing with 1μm cloth was implemented to remove the deformed layer formed during the grinding process, ending with an etching step for SEM examination.

Measurements of the bainite plate thickness were done in the longitudinal ($t_{L\alpha b}$) and transverse ($t_{T\alpha b}$) sections by using the linear intercept (l_i) method in a direction normal to the plate length. Four SEM frame images were taken for each specimen to determine the bainite plates thickness, with 50 measurements for each frame (total of 200 measurements for each condition), and a stereological correction factor ($t_{\alpha b}=2\ (l_i)\ /\pi$) was applied (S. B. Singh & Bhadeshia, 1998) to obtain the actual plate thickness. Electron backscattered diffraction (EBSD) analysis was conducted using a Bruker e-Flash HR EBSD detector mounted on a Field Emission SU8230 Hitachi SEM. The orientation data were analyzed using the non-commercial orientation imaging software ATEX. (B. Beausir, 2017). The EBSD specimens were prepared in the same way as SEM imaging specimens plus a final preparation step with a colloidal silica solution to clean the specimens and remove any deformed sub-layer from the studied surface. The volume fraction of the blocky-shape retained austenite (RA_{block}) was estimated using the EBSD phase-detection method. The RA_{block} larger than 100 nm was considered as blocky-shape retained austenite; otherwise, the remainder was considered film-like austenite (RA_{film}). Two maps with an area of 800 μm^2 with a step size of 50 nm were used to obtain the average amount of RA_{block}.

The total amount of retained austenite ($RA_T = RA_{block} + RA_{film}$) was measured using X-ray diffractometer (X'PERT PANalytical) with Co Kα radiation by means of the direct comparison method (Jatczak, 1980). All XRD specimens were prepared using a method similar to that used for metallographic assessment. The acceleration voltage was 45 kV with a scan range of 2θ from 40 to 120º, with a step size of 0.05°. Four integrated intensities were used to reduce the influence of crystallographic texture, as reported in previous studies (E975-13, 2013; Jatczak,

1980). For austenite, (111), (200), (220), and (311) peaks; and for ferrite (110), (200), (211), and (220) peaks were examined. Two specimens were tested for each condition for repeatability purposes.

Hardness measurements were conducted using a Vickers hardness tester with a 10-kilogram force (kgf) and a dwell time of 15 s. The 10 Kgf load was chosen to reduce the load-sensitive effect due to expected fine features. The reported hardness values on each section of the specimen corresponding to an average of three indentations.

4.3   Results and discussion

4.3.1   Dilatation behavior during bainitic transformation

Figure 4-2 shows the RCL and RCD behavior during the isothermal transformation at 325 °C for the pure isothermal (Iso) and ausformed conditions at the three deformation temperatures, at 600 °C (Def_600), 400 °C (Def_400), and 325 °C (Def_325). As shown in Figure 4-2a, the dilatation behavior in the non-ausformed (Iso) sample is very similar in both RCL and RCD directions and largely overlaps each other, suggesting a random growth of the bainite plates in a different direction. Such growth has been called isotropic by some authors (Ming-xing Zhou, 2015; Mingxing Zhou, 2015). Nearly similar behavior is observed for the Def_600 sample with a slight difference between RCL and RCD singles (Figure 4-2b), revealing that high-temperature ausforming results in an isotropic development of bainitic plates like those in Iso condition.

In contrast, for the low deformation conditions (< BS), the dilatation diverged into two opposite directions. Specifically, while a contraction was observed in the RCL signal for Def_400 and Def_325 specimens, RCD curves showed an expansion (Figure 4-2c and 4-2d). The above-observed anisotropy in the dilatometric behavior could be analyzed in terms of preferred orientation of bainite plates and a stronger or weaker variant selection which assist their growth as will be discussed further in the manuscript [36, 37] The observed significant increase in the

RCD and $\frac{dRCD}{dt}$ of the low-temperature deformed specimens could be related to the increase in the number of nucleation sites for bainite as a result of deformation. Hu et al. (H. Hu et al., 2015), Shipway et al. (Shipway & Bhadeshia, 2013), and Gong et al. (Gong et al., 2013) reported that defects such as dislocations, twins, and grain boundaries generated by deformation prior to transformation act as bainite nucleation sites. Specifically, Gong et al. (Gong et al., 2013), using a 3D-SEM technique, reported that pre-existence bainitic ferrite plat acted as nucleation site for secondary bainite plate in case of ausforming, thereby enhancing the bainite transformation, especially at the beginning of the transformation.

As shown in Figure 4-2a (blue lines), slight variations are present in the RCL and RCD signals for the pure isothermal test. In order to validate whether this variation was material or equipment related, a validation test was conducted for the pure isothermal condition by utilizing the *quench module* of the dilatometer (i.e., the slight pressure that is applied on the specimen when the *deformation module* is used was eliminated). Figure 4-2a (orange lines) shows that the RCL curve coincided with the RCD curve, indicating that the slight variations were due to the small load to hold the specimen. This experiment also revealed that the shape of the RCD curves was almost identical for both modules; Therefore, and for the sake of higher accuracy, the analysis of the data will be based on the evolution of the RCD values.

The RCD signals in Figure 4-2 indicate that the incubation time was shortened when the ausforming was conducted at 600 °C (Def_600) compared with the pure isothermal condition, although the maximum RCD dilatation was almost equal in both situations. However, the incubation time was barely seen for the low-temperature ausforming conditions (Def_400 and Def_325). Specifically, compared to the Iso specimen, radial expansion (RCD) increased by about 60 and 70 % in Def_400 and Def_325 specimens.

By means of the derivate of the RCD ($\frac{dRCD}{dt}$), the kinetics of the bainitic transformation can be depicted in more detail. The values above each peak in Figure 4-3 represent the relevant time intervals for reaching the maximum transformation rate for each condition. As shown in Figure 4-3, when transformation starts almost immediately at the isothermal temperature, and the vast

majority of the transformation occurs in a very short time, Def_400 and Def_325 in Figure 4-2 and Figure 4-3, the $\frac{dRCD}{dt}$ peaks are high and narrow. On the other hand, if transformation requires an incubation time to start and then progressively occurs during a longer span of time, the resulting dRCD/dt peaks are shorter and broader, as in Iso and Def_600 conditions.
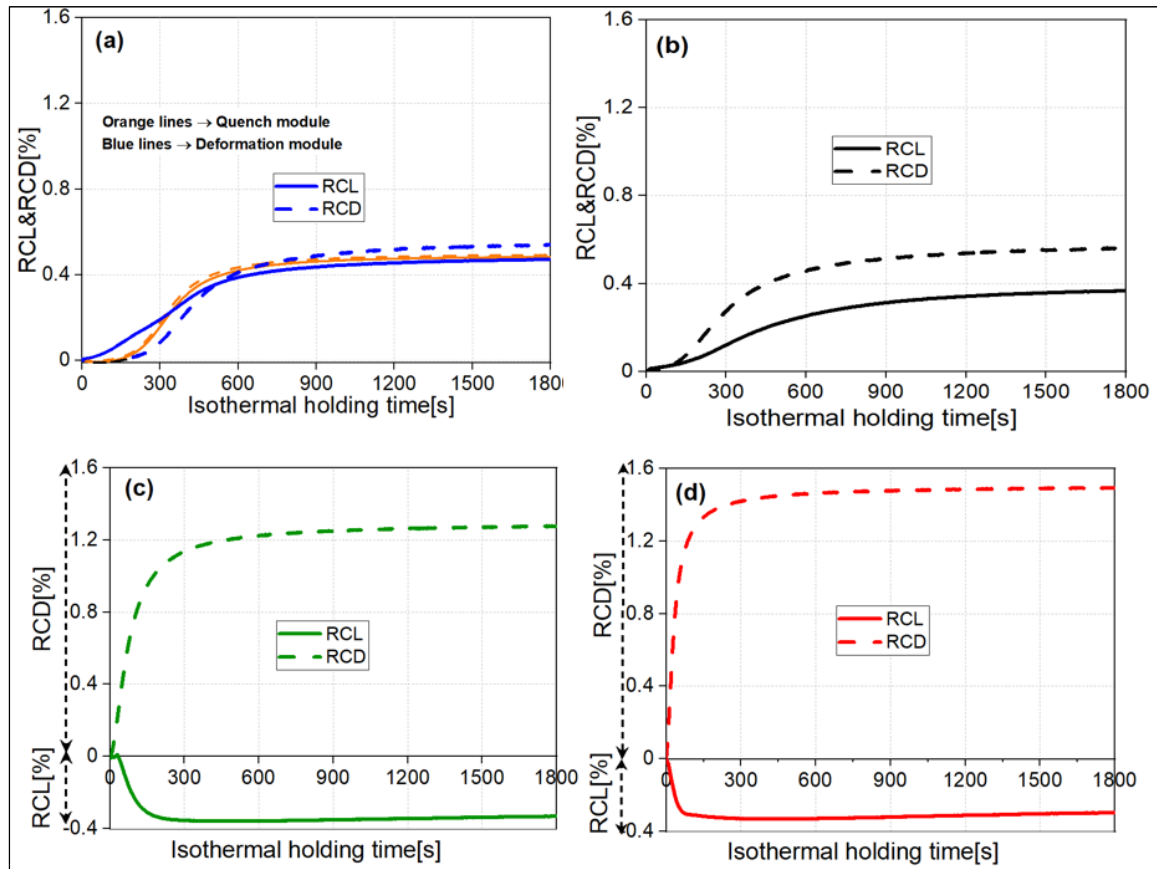
Figure 4-2 RCL and RCD. versus transformation time for all experimental conditions: (a) Iso, (b, c, and d) Def_600, Def_400, and Def_325, respectively (The solid and dashed lines stand for RCL and RCD)

.
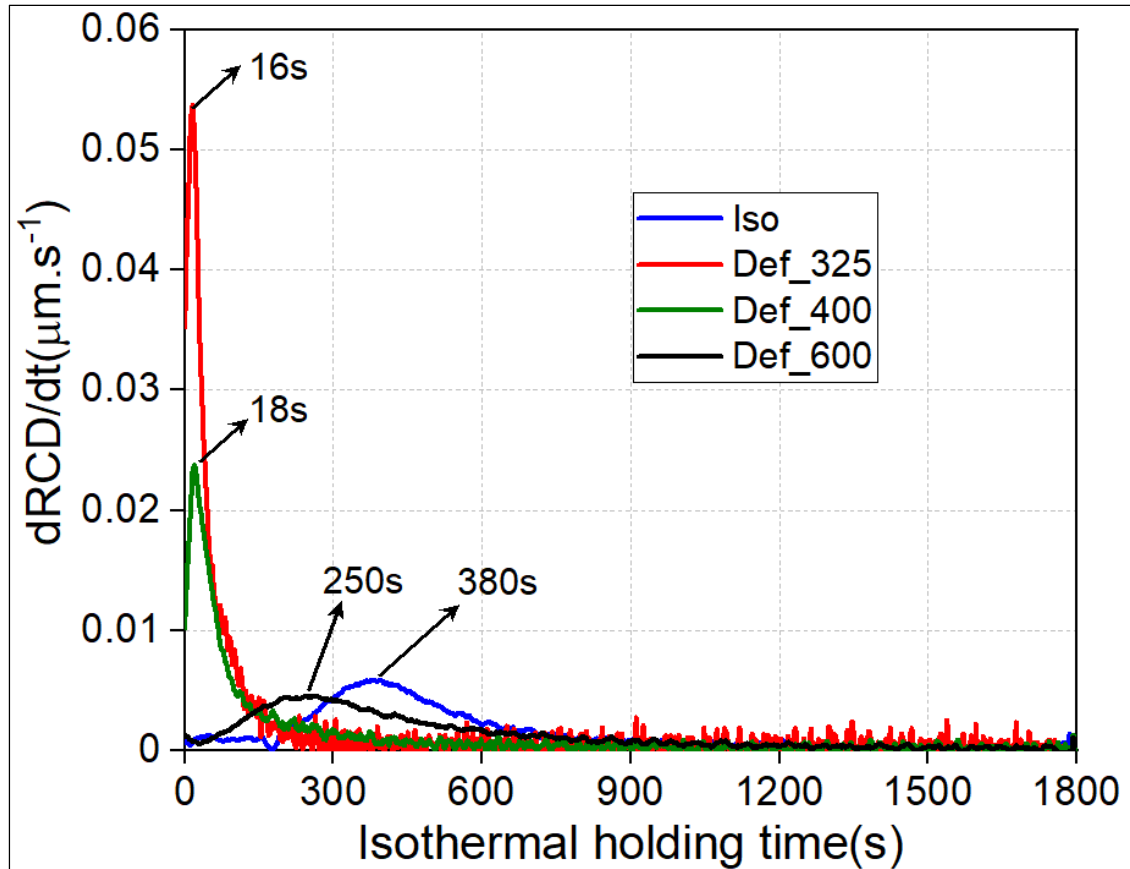
Figure 4-3 Transformation rate for pure isothermal and ausformed conditions:
Iso is the non-ausformed condition, Def-600, Def-400, and Def_325 are
ausforming at 600, 400, and 325 °C, respectively

4.3.2 Microstructural analysis

The SEM micrographs in Figure 4-4 depict the changes occurring as a consequence of the applied deformation in longitudinal (L) and transverse (T) sections. Typically, regardless of the test condition, the microstructures consisted of a bainitic matrix (α_b) with plate-like morphology with retained austenite in the form of blocks (RA_{block}) and film (RA_{film}), as illustrated in Figure 4-4a-L. Note that, considering the composition of the investigated steel, SEM examination of the microstructure did not reveal any presence of cementite particles.

As anticipated by the dilatometry results, both Iso and Def_600 microstructures in Figure 4-4 and 4-4b are comparable in both sections. It is clear then that deformation at 600 °C did not introduce relevant or detectable changes in the resulting microstructure compared to the pure isothermal specimen. The quantitative measurements reported in Table 4-2 show that the variation in the average bainite plate thickness (tα_b) is the same in both L and T sections. Furthermore, the differences in tα_b between Iso and Def_600 conditions are within the measurement error margins. Eres-Castellanos et al. (Eres-Castellanos et al., 2018) and Hu et al. (H. Hu et al., 2019; H. Hu et al., 2015) reported similar observations when the ausforming step was applied at a temperature above B_S in medium C -Si-rich alloyed steels.

The effect of the ausforming on the CFB microstructure is more noticeable at 400 °C, as revealed by Figure 4-4c and 4-4d. The SEM images show a refinement of the microstructure and a very evident alignment of the bainitic ferrite plates with a specific angle to the deformation direction, as compared with the Iso and Def_600 conditions. The refinement of the microstructure being more pronounced with decreasing deformation temperature, as reported in Table 4-2.

Figure 4-5 shows the flow stress curves for the three deformation temperatures. The yield strength (σ_{ys}) of deformed austenite at 325 °C, using the 0.2% offset criterion, is about 695 MPa. This value drops to 600 and 450 MPa for Def_400 and Def_600 specimens, respectively. A comparison between the results of Table 4-2 and Figure 4-5 confirms that the higher is the strength of austenite, the thinner will be the bainitic ferrite plates; however, for an accurate analysis, the contribution from other factors, such as transformation kinetics and the carbon content of austenite, must also be taken into account (Eres-Castellanos et al., 2021). Finally, as shown in Table 4-2, the largest values of bainite plate thickness were measured on the non-ausformed samples isothermally treated at 325 °C (Iso) is about one third of the one ausformed at 325 °C; thereby, confirming the influence of applied stress on bainite plat thickness.

Table 4-2 Thickness of the bainite ferritic plate in the longitudinal ($t\alpha_b$–L) and transverse ($t\alpha_b$ –T) sections; and the average thickness ($t\alpha_b$) in nm

Condition	$t\alpha_b$–L (±8)	$t\alpha_b$–T (±7)	$t\alpha_b$
Def_325	94	111	103
Def_400	140	125	133
Def_600	170	178	174
Iso	164	168	166

A systematic analysis of the bainitic ferrite growth angle to the deformation direction was performed to understand the observed alignment in the SEM micrographs. The alignment of the bainitic ferrite plate to a specific angle with respect to the deformation axis, Def_400, and Def_325 cases in Figure 4-4c and 4-4d were studied in further details. The statistical distribution of the alignment angle with respect to the deformation axis is reported in Figure 4-6. For comparison purposes, the same data with respect to the vertical axis was also measured for the non-ausformed specimen are shown in the same figure. It is worth noting that angle measurements were made only for the plates with an angle from zero to 90º with respect to the deformation or vertical direction. In the pure isothermal (Iso) and Def_600 specimens, as illustrated in Figure 4-6 and 6-6b, the distribution was almost symmetrical within three main groups (10-19º, 50-59º, and 70-79º) with slight differences in pure isothermal condition. This finding indicates that the growth of the bainite plates for pure isothermal and Def_600 is isotropic while it is anisotropic under the other investigated conditions.
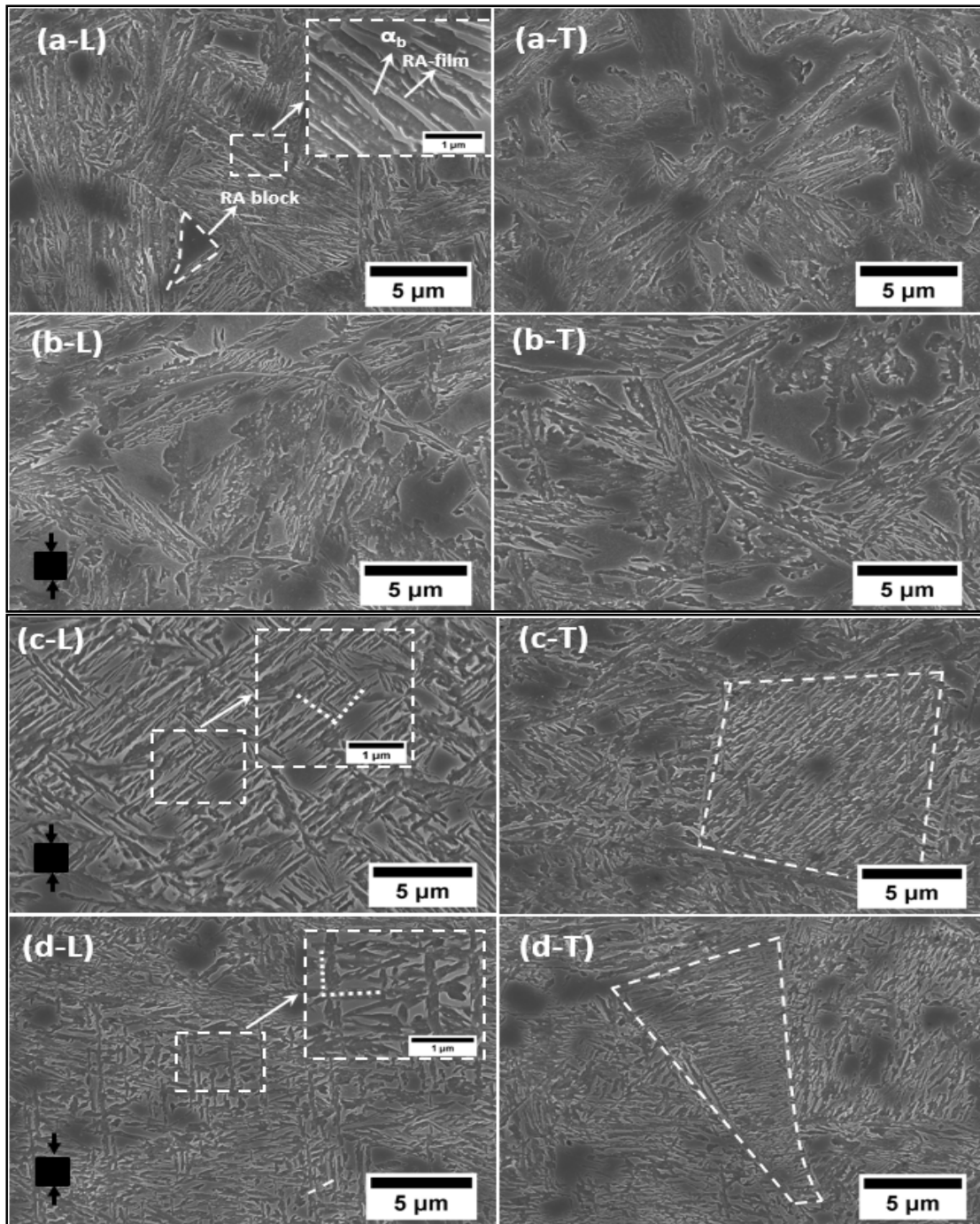
Figure 4-4 SEM micrographs for all experimental conditions, (a) pure isothermal, Iso; (b, c, and d) ausforming at 600 (Def_600), 400 (Def_400), and 325 °C (Def_325), respectively. L stands for the longitudinal section and T for the transverse section. RA-block, RA-film, and α$_b$ are block-like, film-like retained austenite and bainitic ferrite, respectively
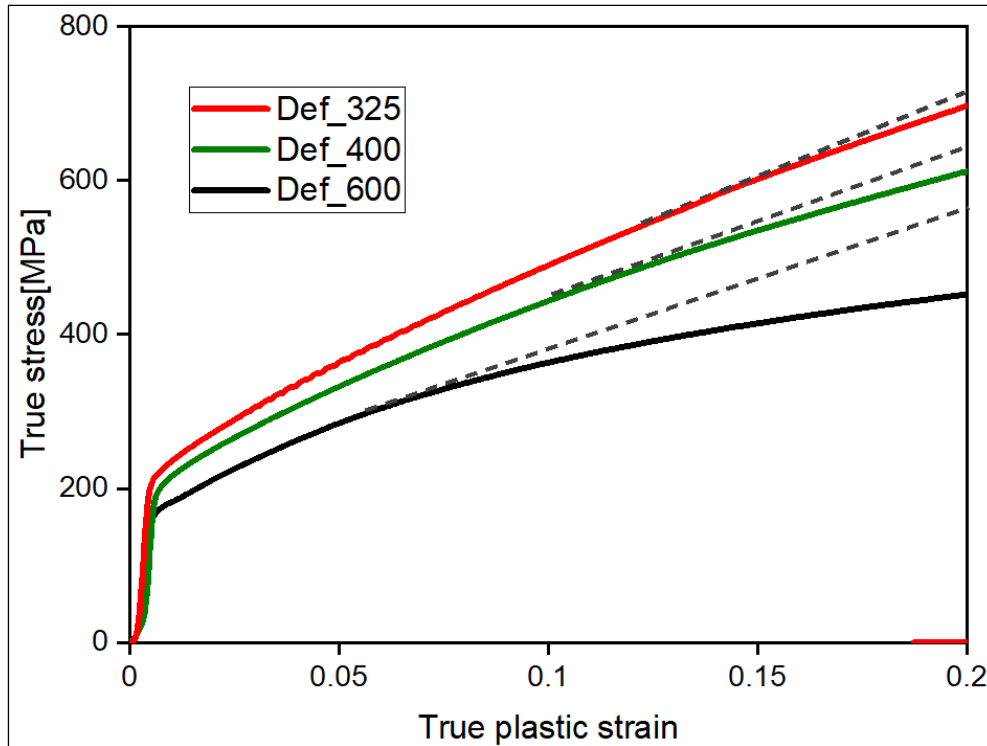
Figure 4-5 True stress vs. true plastic strain for ausforming conditions at 325, 400, and 600 ºC. The dashed lines were plotted to illustrate the change in the slope of the curve with increased strain

However, for low-temperature ausforming conditions (Def_400 and Def_325), the angle distribution was significantly different. In the Def_400 condition (Figure 4-4c-L), most of the bainite plates aligned with an angle of 40-60º to the deformation direction axis with few austenite grains having < 10º>80º alignment angles, as shown in Figure 4-6c. The above findings are in good agreement with those of Eres-Castellanos et al. (Eres-Castellanos et al., 2018), who reported an alignment angle in the range of 45º in medium CFB steel. While Zhou et al. (M. Zhou et al., 2016) found that the angles were at an extent of 65-90º when applied stress was below austenite yodel strength during bainite transformation in medium C–Mn–Si alloy steel. In contrast, in the Def_325 specimen (Figure 4-4d-L), the bainitic ferrite plates were mostly aligned parallel (i.e., zero degree) or with an angle of about 80-90º to the deformation direction; and only a few grains were aligned in the range of 40-60º (Figure 4-6d). Such differences could be related to the variant selection in specific austenite grains, which promote the formation of bainite plates in particular directions when deforming at lower

temperatures (Eres-Castellanos et al., 2018; H. Hu et al., 2015; L. Zhao, Qian, Lihe, Zhou, Qian, Li, Dongdong, Wang, Tongliang, Jia, Zhigeng, Zhang, Fucheng, Meng, Jiangying, 2019). The above findings suggest that a preferential growth with an alignment at a specific angle of the bainitic plates occurs when ausforming below the B_S temperature. This preferential alignment is probably the main reason for the observed contraction in the longitudinal direction (RCL) and the expansion (RCD) during bainitic transformation in Figure 4-2c and 4-2d (Eres-Castellanos et al., 2018; García Mateo, 2020).
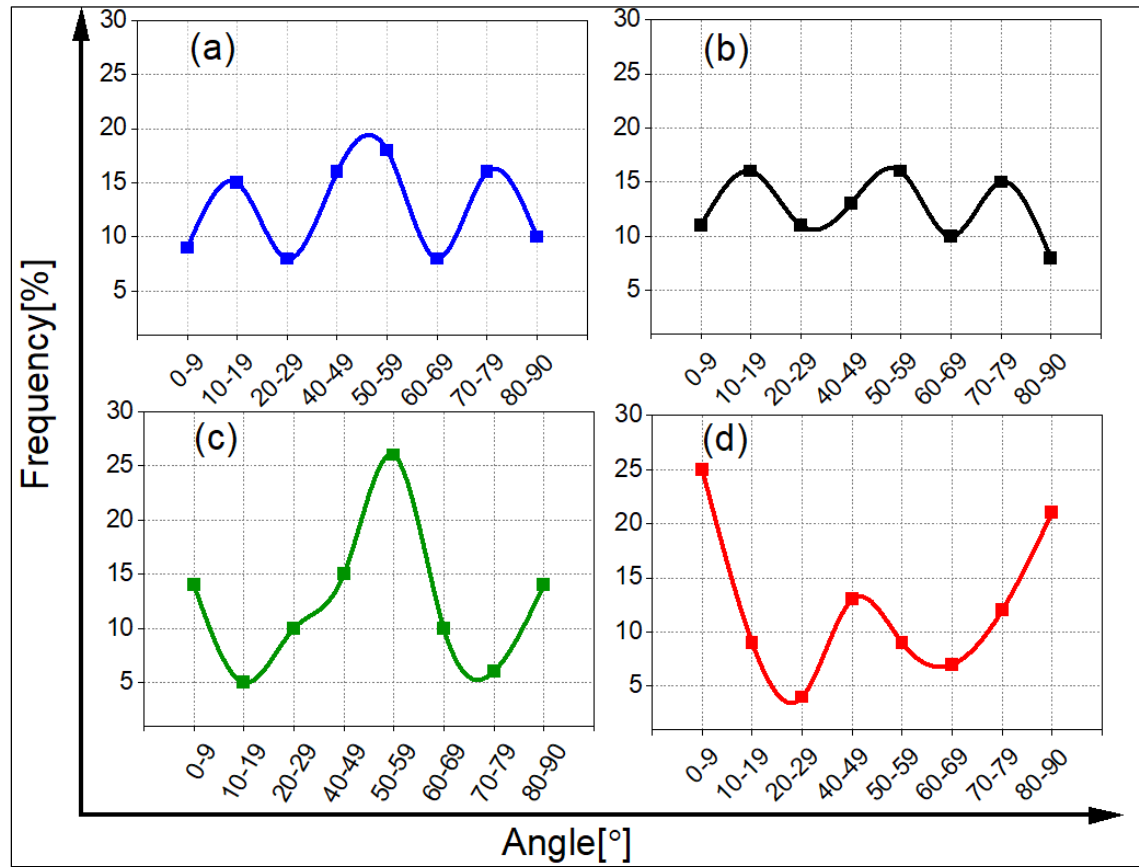
Figure 4-6 Angle distribution of bainitic ferrite plates in some austenite grains with the vertical axis for pure isothermal condition as in (a); or the deformation direction as in (b) Def_600, (c) Def_400, and (d) Def_325 conditions (the inserted images indicates the direction of bainite plate growth to the vertical axis)

4.3.3   Fractions of microstructural constituents

XRD investigation results, reported in Table 4-3, further confirm the microstructural characterization and dilatometric findings that ferrite (bainitic ferrite) and austenite, RA_T are the main phases present in the material. For instance, the results reported in Table 4-3 show that the amount of bainite (α_b) for Iso and Def_600 samples is almost identical, 0.86-0.85, while it decreases as the ausforming temperature process decreases to 400 °C and then to 325 °C. The above findings could be interpreted in terms of the increase in dislocation density. In fact, although plastic deformation increases the density of bainite nucleation sites, it also increases the dislocation density through the so-called mechanical stabilization phenomenon (C. Zhi, 2016; J.R.Yang, 1996; Maalekian et al., 2013; Min et al., 2016; H.-S. W. S. Chatterjee, J. R. Yang and H. K. D. H. Bhadeshia, 2006; Schicchi & Hunkel, 2016; Tsuzaki, Fukasaku, Tomota, & Maki, 1991). The generated dislocations hinder the movement of the glissile interfaces that must occur in order for the bainite plates to grow. As the ausforming temperatures decrease, more and more dislocations are created, and the austenite becomes stronger (see Figure 4-5), resulting in a significant slowdown of the bainitic transformation.

4.3.4   Evolution of the retained austenite

In order to determine the effect of ausforming on the RA, the EBSD phase maps of RA_{block} were analyzed for the different testing conditions, as shown in Figure 4-7. The results reveal that, with the pure isothermal case, Figure 4-7a, the size of the RA_{block} is reduced with decreasing ausforming temperature (Figure 4-7b-d). Further analysis could be made by comparing the ratio of blocky austenite regions to the total retained austenite, $\left[\frac{RA_{block}}{RA_T}\right]$, as reported in Table 4-3. The amount of blocky austenite decreases by almost 20% despite the increase in the fraction of retained austenite with decreasing temperature. This finding indicates that larger regions of untransformed austenite are partitioned (i.e., geometrically divided) by the formation of oriented bainitic ferrite plates during the Def_400 and Def_325 treatment. A desirable secondary effect of this blocky subdivision is that it enhances the presence of RA_{film}, which is thermally and mechanically more stable, improving the ductility

and toughness response of the microstructure (Chen et al., 2020; B. Liu et al., 2019; J. Z. Zhao, Fucheng; Lv, Bo; Yang, Zhinan; Chen, Chen; Long, Xiaoyan; Zhao, Xiaojie; Chu, Chunhe, 2019).

Hardness measurement results, also reported in Table 4-3, further confirm the positive impact of the refinement of both bainitic ferrite plates and retained austenite as well as austenite work hardening in increasing the hardness levels with decreasing ausforming temperatures.
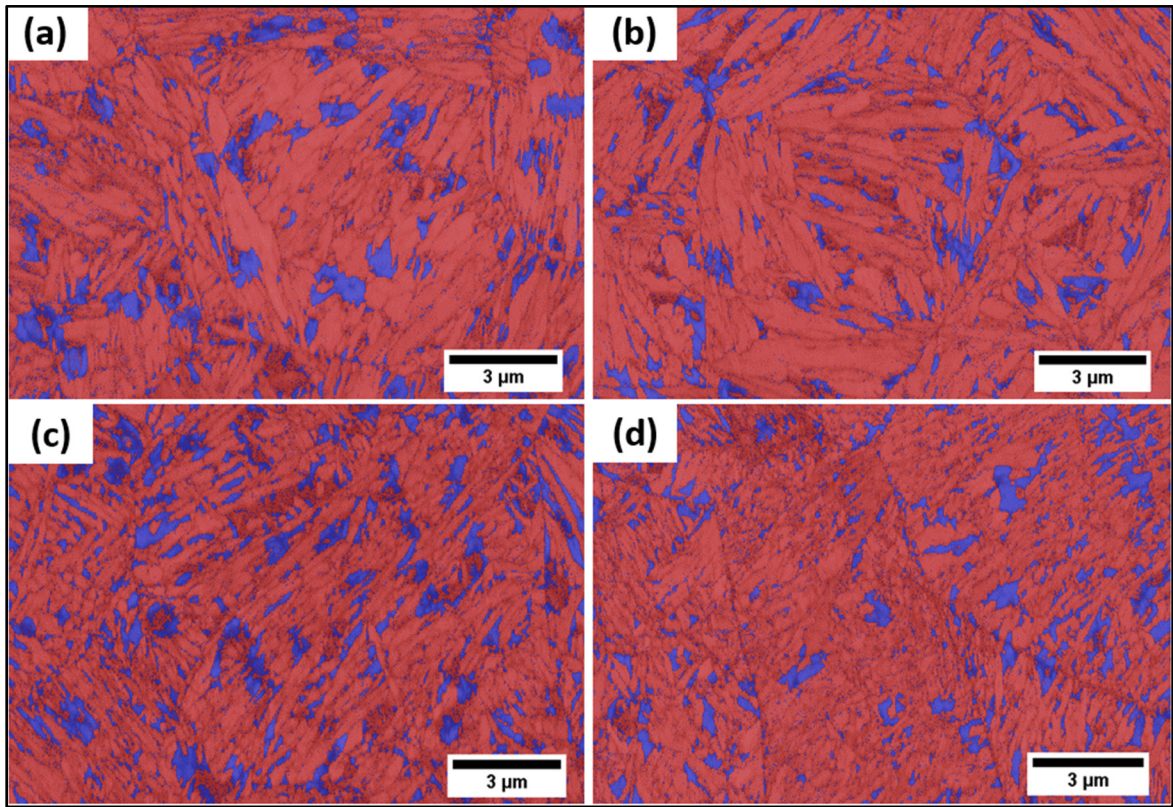
Figure 4-7 EBSD. phase map of RA$_{block}$ for different conditions; (a) non-ausformed, (b) ausformed at 600 ºC, (c) ausformed at 400 ºC, and (d) ausformed at 325 ºC; blue and red are RA and bainitic ferrite phases, respectively. (Standard deviation is ±0.6%).

Table 4-3 Volume fractions of the total retained austenite (RA$_T$) measured by XRD, blocky-shape (RA$_{block}$) estimated using EBSD and its corresponding percentage to the RA$_T$; and bainitic ferrite (α_b); hardness measurements. (note: all the measurement was done on the L section)

Condition	RA$_T$ (±0.03)	RA$_{block}$ (±0.03)	$\%\left[\dfrac{RA_{block}}{RA_T}\right]$	α_b (±0.03)	HV$_{10}$ (±9)
Iso	0.13	0.11	84	0.87	435
Def_600	0.14	0.12	83	0.86	440
Def_400	0.21	0.15	68	0.79	490
Def_325	0.24	0.16	65	0.76	540

4.3.5   Evolution of RCV

It is generally accepted that a higher volume change, RCV, associated with bainitic transformation should be expected when more bainitic ferrite is formed. The RCV value intrinsically depends on the volume of the unit cell of the different phases and their corresponding fractions (Holzweissig, Canadinc, & Maier, 2012; H.-j. Hu et al., 2015; H. Hu et al., 2019; Ming-xing Zhou, 2015; L. Zhao, Qian, Lihe, Zhou, Qian, Li, Dongdong, Wang, Tongliang, Jia, Zhigeng, Zhang, Fucheng, Meng, Jiangying, 2019; M.-x. Zhou, Xu, Wang, Xue, & Hu, 2015; M. Zhou et al., 2016).

Such volume change can be calculated using the RCL and RCD signals in accordance with the approach proposed in the literature (Holzweissig, Uslu, Lambers, Canadinc, & Maier, 2013; Matsuzaki, Bhadeshia, & Harada, 1994; Shipway & Bhadeshia, 1995a):

$$RCV = \frac{\Delta V}{V_{iso}} = (1 + RCL)(1 + RCD)^2 - 1 \tag{4-1}$$

Where ΔV is the volume change of the specimen, and V_{iso} is the volume of the specimen at the isothermal temperature.

However, as shown in Figure 4-8a, where RCV evolution is depicted for the different testing conditions, it is clear that the original premise, higher ferrite fraction leads to higher RCV value, does not occur, see Figure 4-8b. Therefore, another factor must be considered to explain the observed behavior as described in the next section.
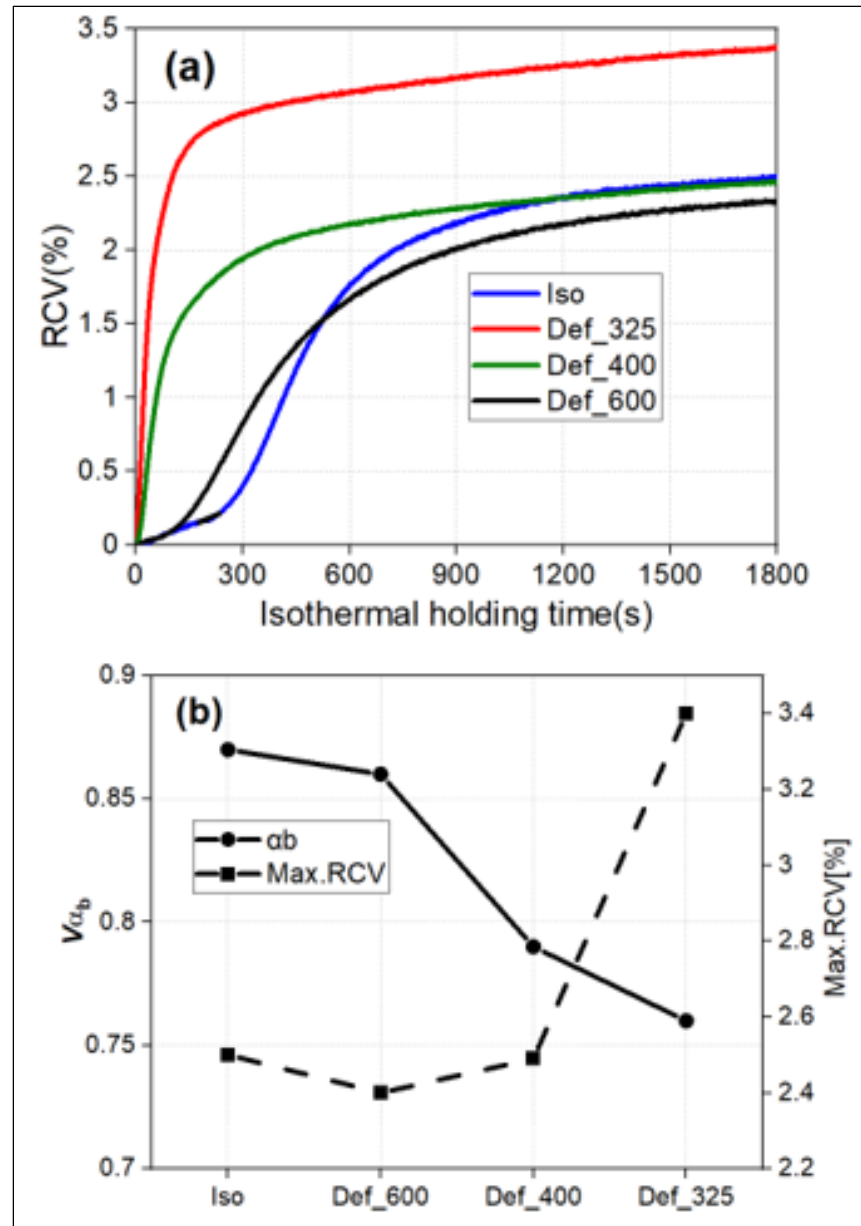
Figure 4-8 RCV for all tested conditions (a); and volume fraction of α_b vs. the maximum RCV values (b)

4.3.6   Evolution of transformation plasticity strains (TP)

As described in the introduction of this manuscript, there is still another important factor that must be considered before a proper interpretation of the RCV curves is done, i.e., transformation plasticity associated with the bainitic transformation.

The development of the TP strains is related to the changes in volume strain during any displacive transformation, such as bainite, and it can be calculated according to the following expression (H. K. D. H. Bhadeshia et al., 2013; Rees & Shipway, 1997; M. Zhou et al., 2016):

$$\overline{TP} = \frac{1}{2}(RCL - 2RCD + 0.33RCV) \qquad\qquad (4\text{-}2)$$

Where $\overline{TP}$ is the mean values of the transformation plasticity strains in the longitudinal and transverse directions.

The evolution of TP strain as a function of the ausforming temperature is illustrated in Figure 4-9a. The increment of the TP strains reaches a steady-state toward the end of the isothermal transformation holding time. This indicates that TP strains decrease as the bainite transformation diminishes. This finding agrees with those reported by Liu (M. Liu et al., 2019), who also reported a reduction of the TP strains with the holding time in a medium carbon CFB steel.

TP strains could be divided into two categories according to their intensities: the first group, Iso, and Def_600 conditions, the TP strains were minimal indicating that the TP strains in the longitudinal and transverse directions nearly cancel out each other. Although the TP curve for specimen deformed at 600 °C, started to deviate slightly at about 100 s towards the negative sign, it eventually reverts to zero. The slight increase in TP strain could be related to the preferably oriented bainite plates in some austenite grains due to the deformation, which reduces the deformation effect and allows other variants to grow randomly, such that in the no-deformed condition. The obtained results are in good agreement with the growth distribution

angle of bainite plates reported in Figure 4-6 and the dilatation in Figure 4-2. Bhadeshia et al. and Matsuzaki et al. (H. K. D. H. Bhadeshia et al., 2013; Matsuzaki et al., 1994) found that when higher stresses are applied during bainite transformation in low carbon steel, the negative transverse strain evolved towards the positive sign as the transformation progressed further. The authors inferred that some variants grow favourably with the stress and others do not. When the number of variants that align or favorably grow in the direction of the applied stress is small, then the microstructure is called isotropic in regard to the variants.

In the second group, Def_400 and Def_325 conditions, the TP strains were more significant and deviated from zero toward higher negative values (see Figure 4-9). The TP strain developed in the Def_325 specimen was slightly higher than the one in the Def_400 specimen. Furthermore, as reported in Figure 4-6d, many bainitic plates were aligned at an angle of 0 or 90 degrees with the deformation axis. This behavior could be explained in terms of a strong variant selection that occurred for some bainite plates in specific austenite grains when the ausforming took place at lower temperatures and supports the arguments in favour of the effect of deformation on variant selection during the growth of bainitic plates. (Gong et al., 2013; J. He, Zhao, Zhi, & Fan, 2015; J. G. He, Zhao, Yao, Zhi, & Zhao, 2015). Thus, variant selection could be another factor contributing to a higher radial dilatation signal at the expense of axial dilatation, as demonstrated in the results reported in Figure 4-2.

Furthermore, the TP strains in the Def_325 specimen started to increase at around 600 s and became closer to the TP strain in the Def_400 specimen at the end of the isothermal holding. This can be attributed to the larger driving force for transformation gained under these conditions that overcome the anisotropic growth in bainite plates when the ausforming process is applied at lower temperatures before bainite transformation (Eres-Castellanos et al., 2018). The relationship between the volume fraction of transformed bainite and the highest value of the TP strain is represented in Figure 4-9b. The TP strain response to the progress of the bainite transformation is changing according to the ausforming states, i.e., first or second group. The TP amplified remarkably during the bainite transformation following ausforming below B_S

(second group), while in the first group (Iso and Def_600), the increase in TP strain was nearly constant (almost zero) regardless of the amount of transformed bainite.
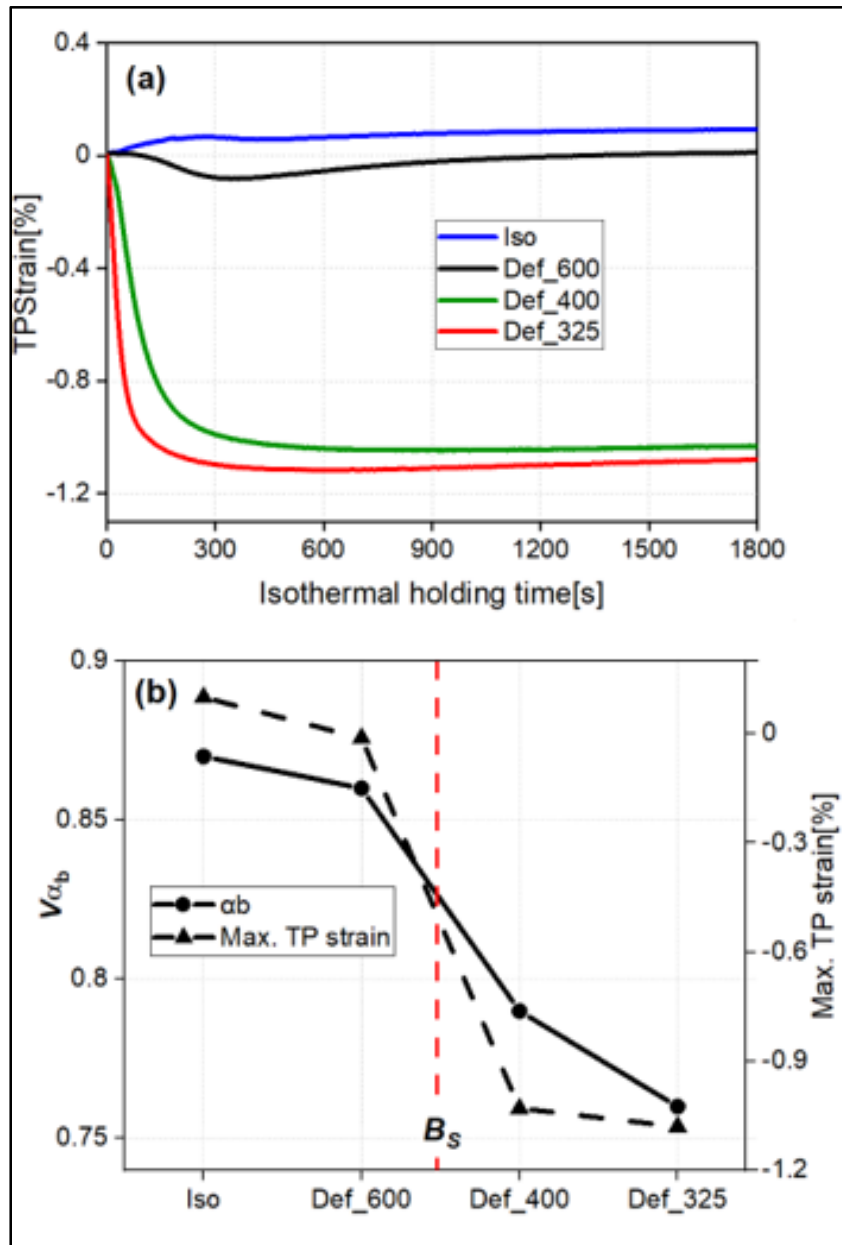
Figure 4-9 Evolution of TP strains during bainite transformation holding time (a); volume fraction of α_b vs. and the maximum TP strain in all tested conditions (b). The dashed red line shows an imaginary limit between ausforming above and below the B_S temperature

In order to confirm the above results, the orientation of bainite was analyzed by the EBSD technique. The maps were taken at low magnifications to cover a large area (about 1600 μm2) with a step size of 100 nm for texture analyses (Figure 4-10). The loading direction is shown in each image. In this figure, the elongated colored shape represents a bainitic block that aggregates of subunits (or plates) of ferrite of the same variant or two variants misoriented by a small angle (<15º) (Rivas, 2016). The morphology and number of variants did not differ much between the pure isothermal specimen and the high temperature (600 ºC) ausformed one, where many variants were formed and randomly aligned in one austenite grain (i.e., black dashed lines in Figure 10). Moreover, the variations in the orientation map with respect to the (001) direction between the longitudinal section (Figure 4-10a-T and 4-10b-T) are minor for both conditions.

The results also agree well with the evolution of the TP strain, as reported in Figure 4-9. However, for the lower ausforming temperature conditions, there were few preferably oriented variants formed in each deformed austenite, as can be seen in Figure 4-10d-L and 4-10d-T. The above results are in agreement with those reported by Liu and Lambers, who also found that the number of bainitic ferrite variants decreased with compressive elastic and plastic stresses applied during bainite transformation and resulted in a strong variant selection (H.-G. Lambers, 2011; M. Liu et al., 2019). Furthermore, Figure 4-10c-L and 4-10d-L show that the variant orientation within the L sections is entirely different from the one in the T sections (Figure 4-10c-T and 4-10d-T). This difference could be linked to the presence of a strong texture under these conditions. The above findings are also consistent with the results reported in Figure 4-6, where it can be seen that the bainite plates in Iso and Def_600 specimens are distributed almost uniformly at three different angles around the vertical axis. In contrast, in the Def_400 and Def_325 specimens, the distribution of the angles was non-symmetrical. The influence of plastic deformation and superimposed stress on bainitic transformation was also reported by Liu et al. (M. Liu et al., 2019) and Lambers et al. (Lambers et al., 2012)], who found that limited bainite variants formed in the austenite and were aligned at a specific direction when a plastic deformation was applied prior to the bainite transformation.

Figure 4-12a-d illustrate the Pole Figures (PF) for the investigated conditions, where it can be seen that the T section always has the highest level of texture for all testing conditions.

Figure 4-12 shows the relationship between the texture intensity and the ausforming state. Interestingly, the texture level in the specimen ausformed at 400 °C, especially in the L section, is higher than the one in the specimen deformed at 325 °C for the same section. This behavior was also seen in the TP strains evolution, as reported in Figure 4-9. This could be related to the higher amount of bainite transformed when the deformation takes place at the transformation temperature (Eres-Castellanos et al., 2018). The lower transformation rate can also explain the decrease in texture intensity in specimens ausformed at 600 °C compared with the pure isothermal specimen.
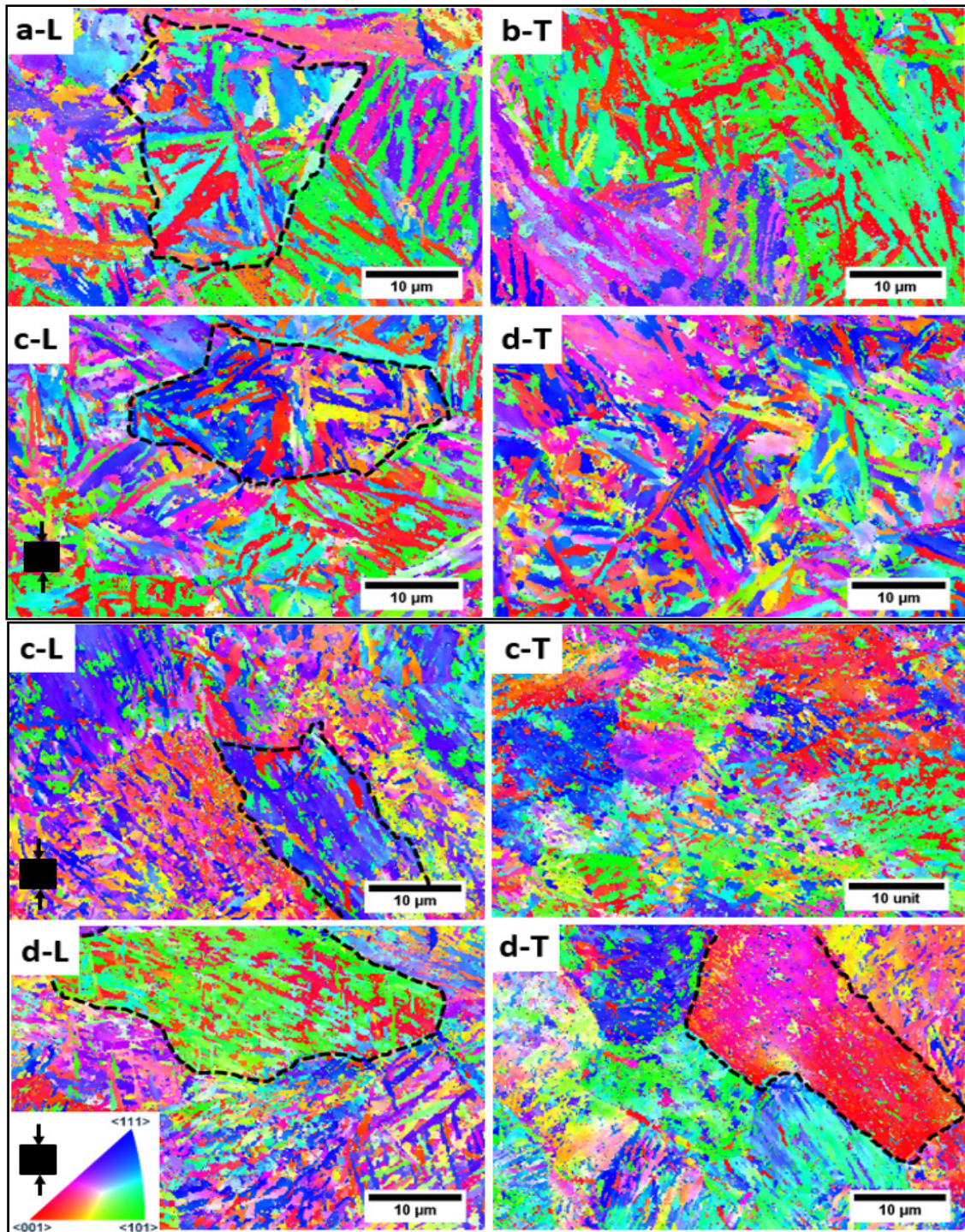
Figure 4-10 Orientation imaging maps in (001) α_b direction in the specimens with different conditions: (a) non-ausformed; (b) ausformed at 600 ºC; (c) ausformed at 400 ºC; (d) ausformed at 325 ºC, L and T are longitudinal and transverse respectively (black dashed lines are PAGB)
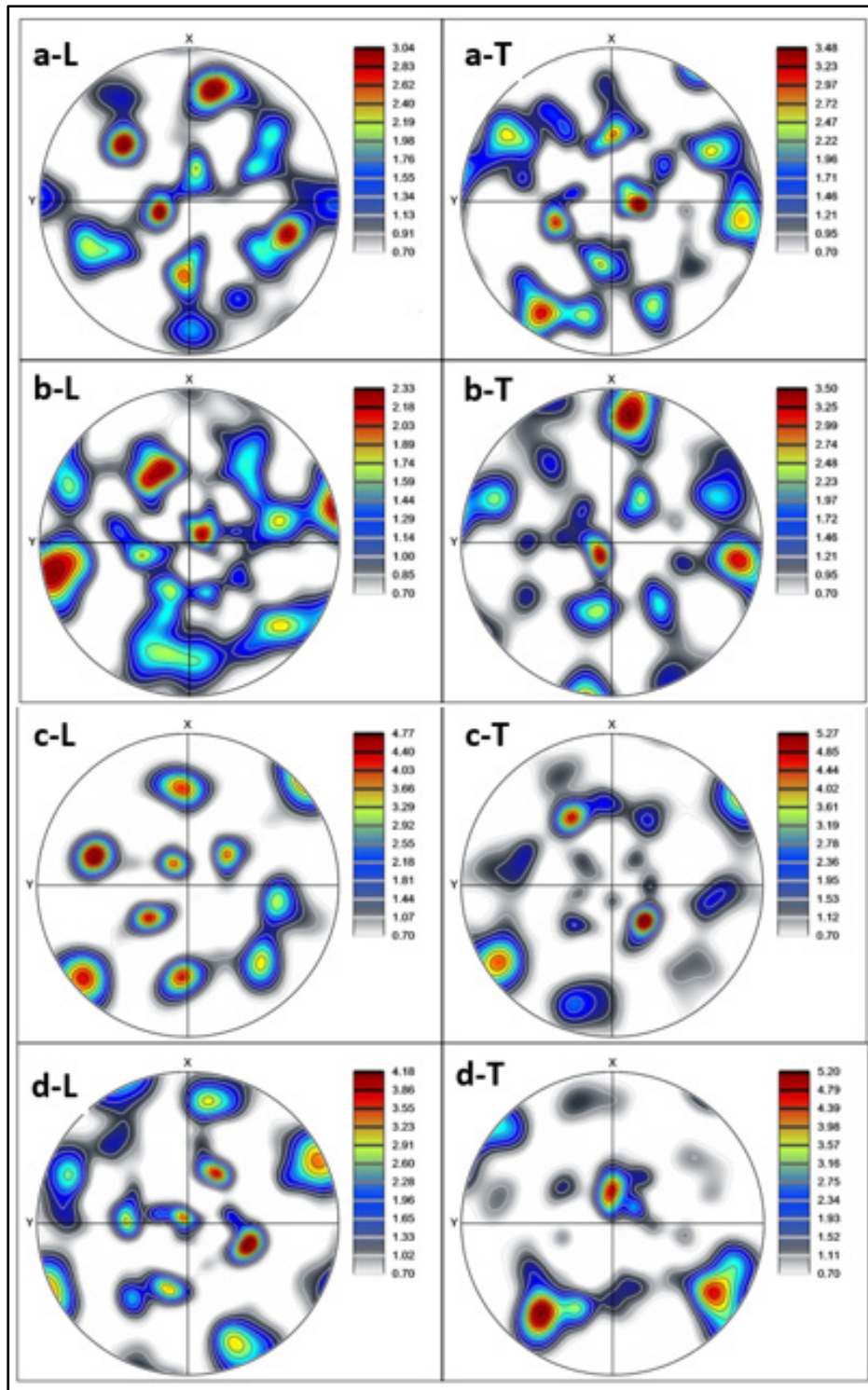
Figure 4-11 PFs of bainitic ferrite phase treated with different conditions:
(a) non-ausformed; (b) ausformed at 600 ºC; (c) ausformed at 400 ºC; (d)
ausformed at 325 ºC, L and T are longitudinal and transverse, respectively
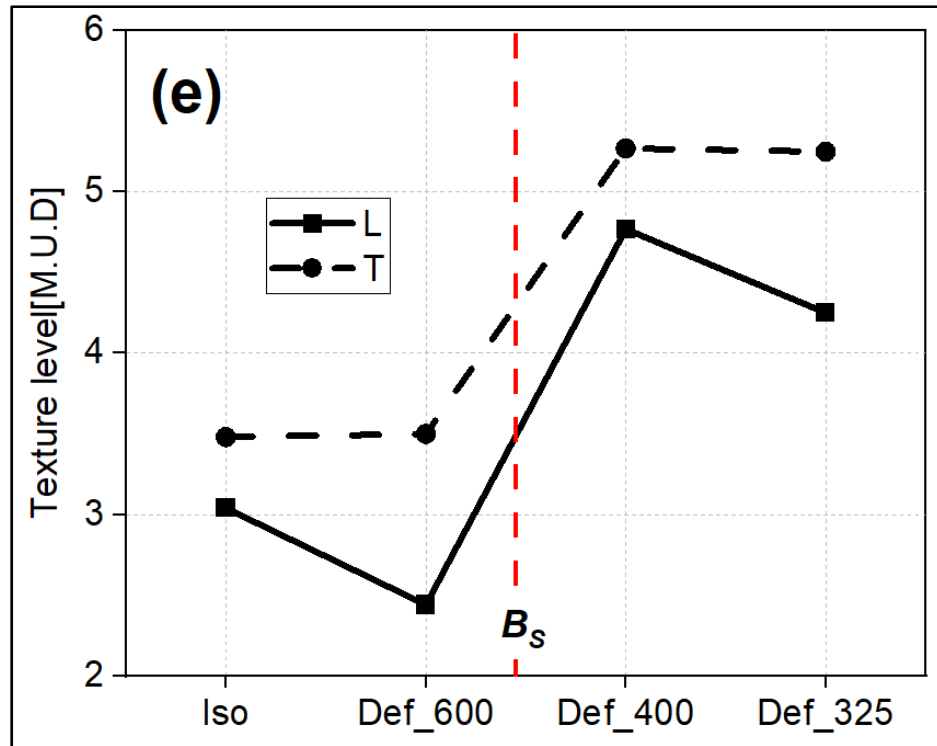
Figure 4-12 The difference in texture level of all conditions for longitudinal (L) and transverse (T) sections. The dashed red line shows an imaginary limit between ausforming above and below the B_S temperature

4.4   Conclusion

The influence of different ausforming temperatures in altering the morphology of a CFB microstructure and its relationship to the transformation plasticity strains (TP) was studied in a medium carbon- high Si steel. The findings can be summarized as follows:

- The effect of ausforming above B_S temperature was negligible on the bainitic ferrite plate thickness and its morphology, compared to pure isothermal condition.
- Low-temperature ausforming (325 or 400 °C) prior to bainite transformation leads to an anisotropic microstructure accompanied by a remarkable refinement of the bainitic ferrite plates to reach a nanoscale level (~100 nm).

- Volume strain cannot be considered an indication of austenite's boost to bainite transformation when the deformation occurred below B_S temperature.

- Bainite plates were aligned randomly in the case of pure isothermal and ausforming at 600 °C. In comparison, an alignment at a specific angle, 45°, and 0-90° was the characteristic of the specimen ausformed at 400 and 325 °C, respectively.

- TP strains were amplified during bainitic transformation when the ausforming was below B_S (400 and 325 °C) and resulted from the alignment and strong texturing of CFB microstructure.

CHAPTER 5

MICROSTRUCTURAL EVOLUTION DURING TEMPERING OF AN
AUSFORMED CARBIDE-FREE NANO-BAINITIC STEEL

M. Zorgani[1], C. Garcia-Mateo[2], M. Jahazi[1]

[1] Department of Mechanical Engineering, École de Technologie Supérieure,
1100 Notre-Dame West, Montreal, Quebec, Canada H3C 1K3
[2] National Center for Metallurgical Research (CENIM-CSIC),
Avda. Gregorio del Amo 8, Madrid 28040, Spain

Abstract

The influence of isothermal tempering on two different bainitic ferrite microstructures obtained via pure isothermal transformation or ausforming followed by the isothermal transformation of supercooled austenite was studied in a medium C-Si rich bainitic steel. A high-resolution deformation dilatometer was used to ausform the samples at 325 ºC, followed by tempering treatments at 400 and 500 ºC. To understand the dilatometric behavior and mechanisms of bainitic ferrite decomposition, extensive microstructural characterization using scanning electron microscopy, X-ray diffraction, and microhardness measurements were conducted. The two bainitic microstructures showed a limited response of the tempering up to 400 ºC. The softening due to tempering at 400 ºC was negligible. Tempering at 500 ºC led to a remarkable contraction in dilatometric signal in an ausformed sample, while a pure isothermal sample showed a limited change in relative length. The main mechanism governing microstructural

124

changes during tempering at 500 ºC was determined to be the decomposition of as-ausformed highly dislocated bainitic ferrite plates and/or film-like retained austenite into cementite and ferrite as a result of enhanced carbon diffusion. While tempering at 400 ºC did not result in changes in the size of the bainitic plates, the higher tempering temperature of 500 ºC led to a thickening of the bainitic ferrite plates for both testing conditions. However, the thickening was restricted in the ausformed bainite, which was related to the pinning effect of very small cementite precipitates, which moderate the tempering effects on hardness reduction. All tempering conditions had a limited impact on retained austenite stability above room temperature.

Keywords: Dilatometry; Ausforming; Isothermal tempering; Cementite precipitation; Pip diffusion

5.1 Introduction

The exceptional mechanical properties of advanced high-strength steels (AHSS) are desirable because of their combined high strength, ductility, and toughness required in many applications. Nanostructured carbide-free bainitic (CFB) steels belong to the AHSS family characterized by nanometer scale (≤ 100 nm) bainitic ferrite providing the superior strength (2500 MPa) and film-like and blocky-shaped retained austenite enhancing the steel's ductility and toughness (H. K. D. H. Bhadeshia, 2004; F. G. Caballero et al., 2002; F. G. Caballero, 2001). The film-like morphology located between the bainitic ferrite plates holds a higher carbon content than the blocky shape retained austenite. The properties mentioned above are obtained thanks to high carbon and silicon contents that allow the formation of nano-scale bainite transformation at low temperatures (200–300 °C) without the risk of carbide precipitation (Harshad K. D. H. Bhadeshia, 2005; H. K. D. H. Bhadeshia, 2006; F. G. Caballero & Bhadeshia, 2004).

However, high carbon content is a major disadvantage when it comes to using these steels in applications where thermal cycling operations such as welding are applied. Therefore, it is imperative to reduce the bainitic steel carbon content to a level that overcomes the

disadvantages of high carbon content and retaining the benefits gained from the superior nano-scale microstructure. Although the bainite transformation occurs at higher temperatures in medium carbon steels, due to the higher martensite start temperature (M_S), ausforming prior to transformation can produce acceptable nanostructured constituents. However, tempering operations, commonly conducted in industry after cold working, welding, or hot-dip galvanizing, could alter the microstructure and thus negatively affect the higher performances obtained from the nano bainitic structure

There are no reports available in the literature on the influence of tempering on the CFB steel's microstructure produced from ausformed austenite. The limited published literature focuses on conventional tempering of CFB steels where the impact of a deformed austenite state on the evolution of bainite characteristics, retained austenite and carbides evolution is not reported.

The essential microstructural changes that could take place during tempering of a CFB steel could be summarized as follows (Ruiz-Jimenez et al., 2020):

- Decomposition of film-like (γ_{Rf}) into very fine cementite particles.

- Fine cementite precipitation within blocky retained austenite (γ_{Rb}) while the C-depleted austenite can transform to fresh martensite on cooling to room temperature.

- In the later stages of tempering, the same C-depleted austenite decomposes into a mixture of ferrite and cementite, while from supersaturated bainitic ferrite (α_b) precipitation of cementite occurs, changing its lattice from body-centred tetragonal (BCT) to its body-centred cubic (BCC) equilibrium state. This transformation could also lead to a remarkable reduction in the dislocation density generated during bainitic transformation.

- Possible partition of the excess carbon present in the bainitic ferrite into retained austenite during the tempering process.

The scenarios mentioned above have been reported in various studies either as a single event or sequentially. For instance, Santajuana et al. (M. A. Santajuana et al., 2018) reported no change in the microstructure when two high-C-nanostructured bainite steel with carbon contents of 0.7 wt.% and 1 wt.% were tempered in the temperature range of 200–400 °C. In contrast, when the tempering temperature interval was increased to 450 –500 °C a decrease in the retained austenite amount was observed, which was related to carbide precipitation. However, when tempering was done in the 550 - 600 °C interval, significant changes were observed in the microstructure, illustrated by the decomposition of the retained austenite and bainitic ferrite blocks into mixtures of ferrite and cementite. Peet et al. (Mathew J. Peet et al., 2017) studied the effect of tempering temperature on the microstructure of a high-carbon nanostructured CFB steel. They found that nano-size cementite precipitates were formed after tempering at 400 °C and 500 °C for 30 min, which prevented the coarsening of bainitic ferrite plates. Ruiz-Jimenez et al. (Ruiz-Jimenez et al., 2020) noted that tempering at 450 °C did not produce noticeable microstructural changes in 0.6 wt.% C carbide-free bainitic steel and the overall hardness remained unchanged.

In contrast, tempering at 500 to 550 °C resulted in the formation of cementite precipitates, from both film-like and blocky shape retained austenite, which led to a decrease in the carbon content of the retained austenite. Thus, carbon-depleted retained austenite transformed to fresh martensite during cooling to room temperature. The above two factors enhanced the increase of the hardness. Tempering in the 550-650 °C interval produced a remarkable decrease in hardness associated with a larger decomposition of retained austenite, dislocation recovery and coarsening of bainitic ferrite plates. Podder and Bhadeshia (Saha Podder & Bhadeshia, 2010) found that a two-stage microstructure evolution occurred during tempering at 450 °C for 0.5–5 h of a medium carbon bainitic steel. In the early stage, cementite precipitated from the pre-existing martensite (tempered martensite). Then, an extended tempering time of 5 hours led to the decomposition of retained austenite into a mixture of ferrite and carbides. Klein et al. (Klein et al., 2019) observed a contraction in the dilatometric signal during heating of a CFB steel in the 250–350 °C interval. They related their findings to the decomposition of film-like retained austenite.

On the other hand, when the reheating temperature was higher (480-570 °C), an expansion in the specimen was observed, which was related to the decomposition of blocky-shaped retained austenite. Furthermore, Kang et al. (Kang, Zhang, Yang, Lv, & Wu, 2017), in a study on the tempering of a medium carbon bainitic steel reported that, tempering at 340 °C resulted in optimal mechanical properties of the investigated steel. In contrast, when the tempering temperature was increased to 450 °C, the bainitic ferrite plates became thicker, and the amount of retained austenite reduced because of the decomposition of the film-like retained austenite to carbides.

The objective of the present work is to investigate the microstructure evolution of an ausformed CFB steel during tempering and determine the contribution of the mechanisms that affect such evolution. Such information is of critical importance in designing heat treatment processes for the broader application of CFB steels.

5.2   Materials and Methods

The steel used in this study was medium carbon-Si rich with the following nominal chemical composition: Fe-0.4C-1.5Mn-1.7Si-1.5Cr-0.4Mo (wt.%). It was received in a spheroidized annealed state in the form of 36 mm rolled bars. Cylindrical samples were cut using wire electrical discharge machining into 4 x 10 mm^3 and 5 x 10 mm^3 dimensions for dilatometry experiments. The first size was used for the heat treatment with no deformation applied, while the second was used for the ausforming treatments. The samples were austenitized at 980 °C (T_γ) for 5 min with a heating rate of 10 °C/s and then quenched to 325 °C for isothermal bainite transformation. They were then cooled to room temperatures. These samples are identified as pure isothermal bainitic transformation (P-bainite) in the rest of the manuscript. For the ausforming process, a 20% compressive plastic strain (ε) with a strain rate of 0.1 s^{-1} was applied prior to isothermal bainite transformation and identified as ausformed bainite (A-bainite) condition.

In order to establish the tempering conditions, a non-isothermal tempering (NIT) was performed right after bainitic transformation, as shown in Figure 5-1a. The temperature of NIT was selected based on published data in the literature, where CFB steel has good resistance to tempering under 450 °C and full decomposition in the range of 550-650 °C (Klein et al., 2019; M. A. Santajuana et al., 2018; Ståhlkrantz et al., 2020). In NIT tests, the samples were heated to 600 °C with a relatively slow heating rate of 1 °C/s and immediately (~3 seconds) cooled to the ambient temperature.

Isothermal tempering (IT) treatments were selected based on the results obtained from the NIT cycle and applied on both P-bainite and A-bainite conditions (Figure 5-1b). In the IT tests, the samples were heated up to two different temperatures (400 and 500 °C) with a heating rate of 10 °C/s. The samples were held at the tempering temperature for 60 min and then cooled to ambient temperature. The cooling rate was 20 °C/s in all cases.

The thermal cycles illustrated in Figure 5-1 were conducted using a high-resolution dilatometer (BAHR DIL805 A/D) equipped with quenching and deformation units. The sample was supported by two fused quartz silica during conventional dilatometry tests, i.e., no deformation step before bainite transformation. For the ausforming experiments, silicon nitride punches were used to support the sample, and disk shape molybdenum foils were welded on both ends of the samples to minimize friction. The temperature was controlled using a type K thermocouple welded on the mid-length of the sample. Induction heating coils were used for heating, and argon gas was used for cooling. The dilatation strain during the tests was recorded using a linear variable differential transducer (LVDT). It must be noted that to ensure accurate and comparable measurements, both tempering treatments—NIT and IT—were performed using the quench module of the dilatometer equipped with quartz pushrods. The whole system operated under 5×10^{-4} mbar vacuum conditions during the heating and holding times to avoid oxidation and decarburization of the samples.

After the dilatometry tests, specimens were prepared for light optical microscopy (3D laser Olympus LEXT OLS4100) and field-emission gun scanning electron microscopy (Hitachi

SU8230) observations according to standard metallographic procedures. They were cut in the centre, perpendicular to their length; mechanically ground with SiC paper up to 1200 grit; polished with a diamond paste; and then etched in 3% Nital. The thickness of bainitic ferrite plates was measured using the method described in (Zorgani et al., 2020).

Vickers microhardness measurements were conducted using an automatic tester with a load of 1 kgf for 15 s. On average, 10 indents were produced on the polished surface of the specimen for hardness evaluation.
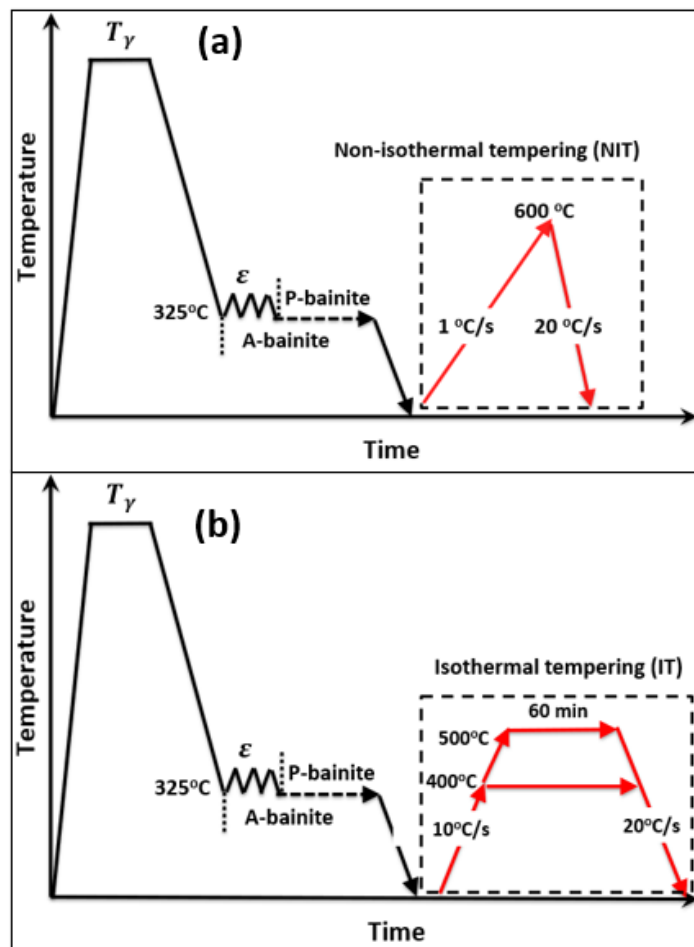
Figure 5-1 Schematic representation of different heat treatments used for this study; (a) non-isothermal tempering, and (b) isothermal tempering. P-bainite and A-bainite are pure isothermal bainite transformation, ausforming prior to isothermal bainitic transformation, respectively

X-ray diffraction (XRD) analysis was performed on a X'Pert3 MRD PANalytical machine with Rietveld refinement using X'pert Highscore Plus program for constituent phase quantification. XRD patterns were obtained using Co-Kα radiation, consisting of an acceleration voltage of 45 kV, a 2θ scan range of 40°–120°, with a step size of 0.05°. An additional specific scan range of 40°–80°, with a narrow step size of 0.01°, was employed to enhance the detection of the expected low-volume fractions of carbide diffractions during tempering. The volume fraction of the retained austenite (γ_R) was determined using the Jatczak model, as described in (Jatczak, 1980) and according to equation (5-1) This model was used when the microstructure consisted only of two phases, that is, retained austenite and bainite; otherwise, SEM and XRD techniques were used to calculate phase fractions:

$$\gamma_R = \frac{1/n \sum_1^n I_\gamma / R_\gamma}{\left[1/n \sum_1^n I_\gamma / R_\gamma\right] + \left[1/n \sum_1^n I_\alpha / R_\alpha\right]},$$

(5-1)

In the above equation, n is the number of examined peaks; I_γ and I_α are the integrated intensity of the face-centred cubic (FCC) and body-centred cubic or tetragonal (BCC/BCT) diffraction peaks, respectively, and R is the material scattering factor. The carbon content in retained austenite ($X_{\gamma R}$) and bainitic ferrite (X_α) were calculated using lattice parameter values obtained from XRD analysis, assuming that only carbon diffuses during bainitic transformation; the bainitic ferrite, α_b lattice was considered BCT instead of BCC (Cohen, 1969; Lobodyuk, Meshkov, & Pereloma, 2018; Ridley, 1969; Tanaka, Maruyama, Nakamura, & Wilkinson, 2020; M. X. Zhang & Kelly, 1998):

$$a_{\gamma R} = 0.36003 + 0.0044 X_{\gamma R},$$

(5-2)

$$a_{\alpha b} = 0.28664 + 0.00116 X_{\alpha b,}$$

(5-3)

$$c_{\alpha b} = 0.36003 + 0.0044 X_{\alpha b},$$

(5-4)

$$\frac{a_{\alpha b}}{c_{\alpha b}} = 1 + 0.046 X_{\alpha b}, \tag{5-5}$$

$X_{\gamma R}$ and $X_{\alpha b}$ are the weight percentage of carbon in retained austenite and bainite; a_γ is the lattice parameter in nanometer (nm) calculated from the peak positions of (111), (200), and (220); and a_α and c_α are the lattice parameters in nm of (110), (200), and (211) of bainitic ferrite peaks.

5.3 Results and Discussion

5.3.1 Initial microstructure prior to tempering treatments

The resultant microstructures after P-bainite and A-bainite processes are shown in Figure 5-2a and 5-2b. For both conditions, it consisted of bainitic ferrite (α_b), thin films (γ_{Rf}) and coarse blocks (γ_{Rb}) retained austenite, and with the absence of any carbides. SEM observations also revealed that the microstructure obtained via the P-bainite route is coarser than the A-bainite condition. Using image analysis, the thickness distribution of the bainitic plates were calculated for each condition, and the results are reported in Figure 5-2c and 5-2d. The results show that for P-bainite that about 70% of the plates were within the size range of 150–250 nm, with an average of 170 nm.

In contrast, finer bainitic plates formed when ausforming was followed by isothermal bainitic transformation (A-bainite). More than 75% of bainite plates were sized less than 150 nm in thickness, with an average in the nano-scale range, ~102 nm, as seen in Figure 5-2b. Furthermore, the dilatometry results in Figure 5-3a show that, after the completion of bainite transformation, the retained austenite within the matrix in both non-ausformed (P-bainite) and ausformed (A-bainite) states was stabilized, and no martensite transformation was observed in the final stage of cooling to ambient temperature.

The XRD pattern in Figure 5-3b shows that only BCT (α_b) and FCC (γ_R) were present. The intensity of the austenite peaks, especially $\gamma_{(111)}$ and $\gamma_{(200)}$, were higher in the A-bainite

sample than they were in the P-bainite sample, which means that the amount of γ_r was higher in the former case. This could be related to the mechanical stabilization of austenite as a result of deformation against bainitic transformation (Eres-Castellanos et al., 2021; H. Hu et al., 2017; H.-S. W. S. Chatterjee, J. R. Yang & H. K. D. H. Bhadeshia, 2013; Shipway & Bhadeshia, 2013). Furthermore, as shown in Figure 5-3b, no carbide peaks are present in the XRD diagram, which further confirms the SEM microstructural observations and is probably related to the higher percentage of Si in the studied steel (1.7 wt.%) that helped suppress carbide formation during bainite transformation (H. K. D. H. Bhadeshia, 2009; C. Garcia-Mateo, Caballero, Sourmail, Smanio, & García de Andrés, 2014; Yang & Bhadeshia, 2008).

It is also interesting to note that austenite peaks show a slight shifting toward lower diffraction angles (2θ) for the P-bainite compared to that of the A-bainite treatment. This shift is related to the increase of austenite lattice parameter due to carbon partition from bainitic ferrite into retained austenite, i.e., a higher amount of transformed bainite (Kopp, Bernthaler, Schmid, Ketzer-Raichle, & Schneider, 2017; Rementeria, Garcia-Mateo, & Caballero, 2018; L. Zhao, Qian, Lihe, Zhou, Qian, Li, Dongdong, Wang, Tongliang, Jia, Zhigeng, Zhang, Fucheng, Meng, Jiangying, 2019). The calculated austenite carbon content in P-bainite and A-bainite treatments was 1.21 and 0.88 wt.%, respectively.
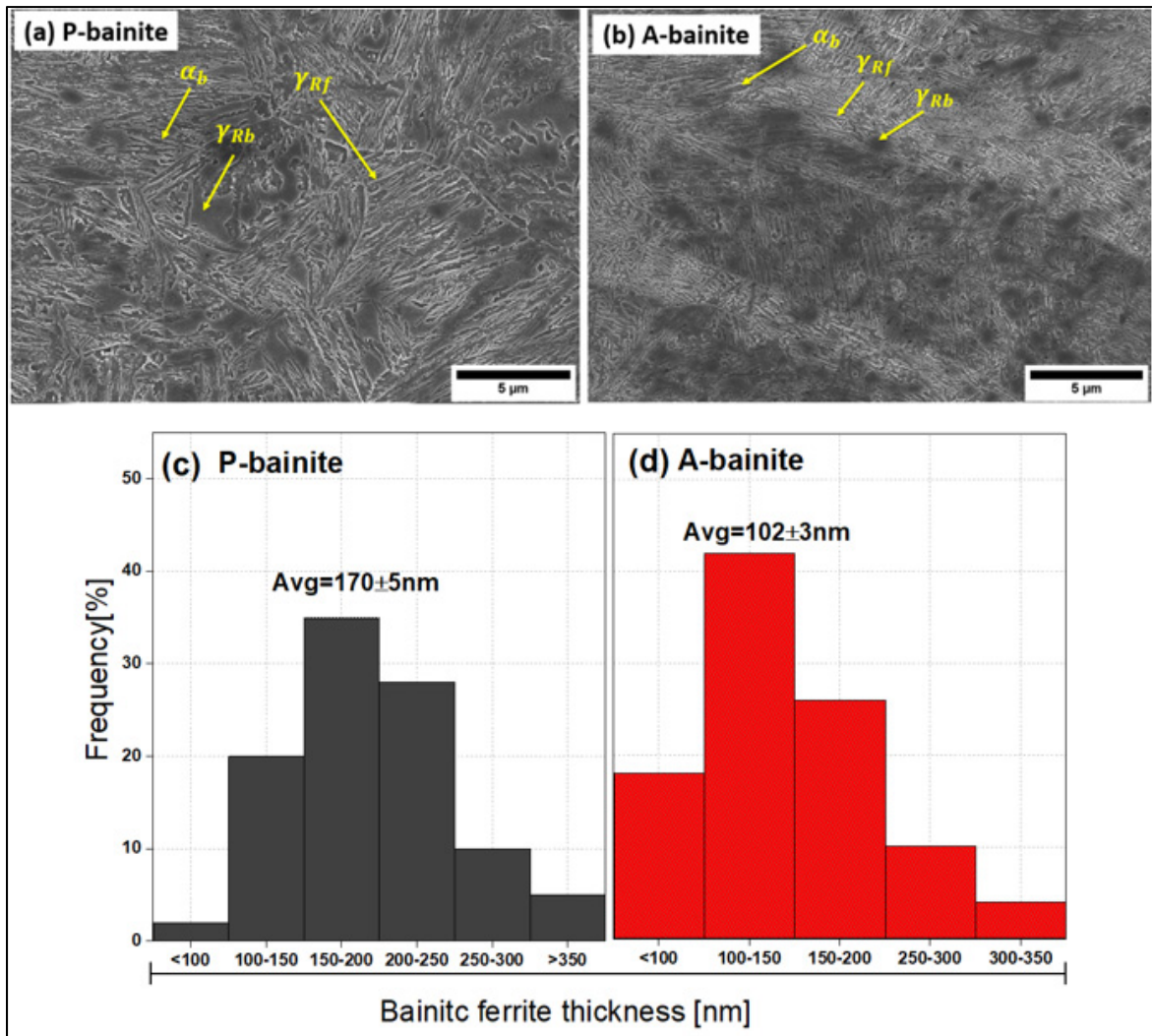
Figure 5-2 Initial microstructure after: (a) pure bainite isothermal, P-bainite (b) ausforming prior isothermal transformation, A-bainite; distribution of bainitic ferrite plate thickness: (c) P-bainite and (d) A-bainite
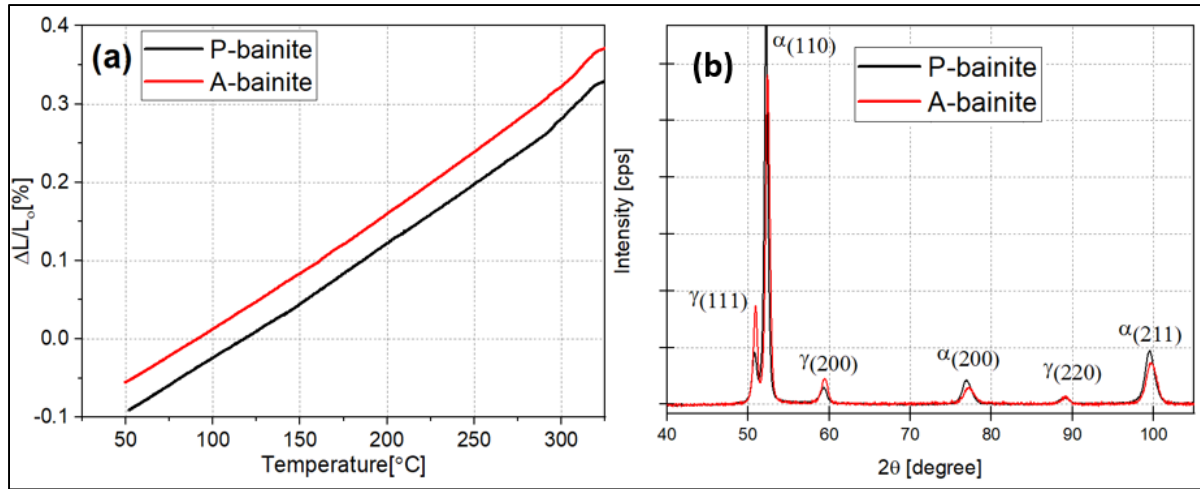
Figure 5-3 (a) dilatometric behavior during cooling to the ambient temperature for P-bainite and A-bainite conditions, (b) XRD patterns for P-bainite and A-bainite samples

5.3.2   Design of tempering treatment

In order to study the response of nanostructured CFB to the isothermal tempering treatment, preliminary experiments were carried out where both P-bainite and A-bainite microstructures were subjected to continuous heating up to 600 °C, NIT in Figure 1 and the dilatation behavior was analyzed. The results, reported in Figure 5-4a, show that for both samples, the slope of the dilatation signal ($\Delta l / L_o$) was unchanged until about 400 °C. In the case of the P-bainite sample, a contraction was observed at around 500 °C, while deviation from linearity gradually starts right after 400°C and a second and more prominent contraction occurred at approximately 500 °C occurred in the A-bainite, the decrease in $\Delta l / L_o$ in both conditions continued until the end of the heating cycle, i.e., at 600 °C.

Similarly, the derivative curves, $[d(\Delta l / L_o)/dt]$, in Figure 5-4b, show that no change in dilatation behavior was observed during heating from room temperature until about 500 and 400 °C in P-bainite and A-bainite samples, respectively. In both samples, the maximum drop in the derivative curve was observed at around 535 °C; however, the reduction was more significant for the A-bainite condition than for the P-bainite condition. Specifically, the

decrease in $[d(\Delta l/L_o)/dt]$ started gradually at about 400 °C until reaching its minimum value at 535 °C, while for the P-bainite condition, the drop started at around 500 °C.

Hence, in order to better understand the differences in dilatometric behaviors of A-bainite and P-bainite samples between 400 and 500 °C, isothermal tempering (IT) treatments were performed at both temperatures for both microstructures, P-bainite and A-bainite.
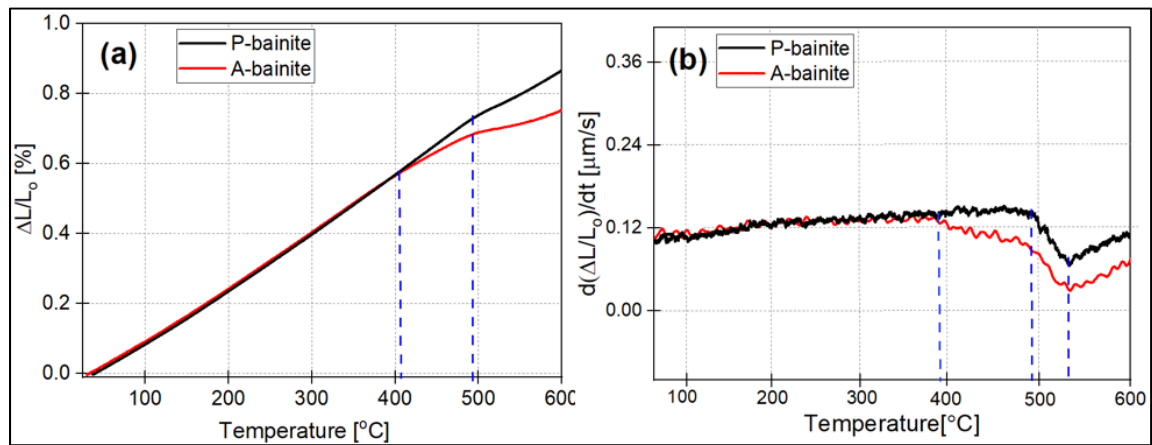
Figure 5-4 NIT dilatometric signals during heating and cooling for bainitic samples produced by P-bainite and A-bainite

5.4 Isothermal tempering (IT) at 400 and 500 ºC

5.4.1 Dilatometry response during tempering treatment

According to the NIT results, IT processes at 400 and 500 °C for 1 hour were chosen for further study. Figure 5-5 shows the dilatation behavior during heating and isothermal tempering at 400 and 500 °C for the P-bainite and A-bainite conditions. The $\Delta L/L_o$ of the P-bainite sample was unchanged during the tempering holding time at 400 °C, as shown in Figure 5-5a. However, in the A-bainite sample, the change in the dilatation curve gradually decreased until it reached a relatively steady state at about 1500 s, with a maximum decrease in $\Delta L/L_o = 0.044\%$ until the end of the tempering holding time. (see Figure 5-5a). It must be noted that the relative

change in length with time remained constant during heating from room temperature to 500 °C in the P-bainite sample, while in the A-bainite case, a decrease in the slope of the curve (i.e., a contraction) started to appear at around 400 °C and was further accentuated until the target temperature of 500 °C. This change in slope (contraction in the dilatometry curve) has been related to the start of the cementite precipitation (Hunkel, 2020; Mola, 2016). Klein et al. (Klein et al., 2019) reported that during heating of a Carbide-Free Bainitic Steel, decomposition of highly C-enriched retained austenite (film-like) led to a sample contraction. In contrast, decomposition of lower C-enrich retained austenite (blocky-shape) resulted in an expansion in the dilatometric behavior.

During the isothermal step, both conditions—P-bainite and A-bainite —exhibited a continued decrease in $\Delta L/L_o$ as the tempering time was increased, as reported in Figure 5-5b. The contraction in the ausformed sample, A-bainite, was about 65% higher than in the P-bainite sample. Furthermore, a nearly steady-state was reached for the P-bainite sample after about 2500 s of tempering, whereas the reduction in $\Delta L/L_o$ continued for the A-bainite samples, demonstrating that more time is needed to complete the tempering reactions at 500 °C for the ausformed samples (S. H. Talebi, Jahazi, & Melkonyan, 2018). It is also worth noting that the contraction in signal started at the later stages of the heating process and continued during the holding time, as reported in the inset image in Figure 5-5b. This finding confirms that the microstructural changes began before reaching 500 °C.

In general, the maximum reductions in $\Delta L/L_o$ for P-bainite tempered at 500 °C, and A-bainite tempered at 400 °C were nearly identical (0.046 and 0.050, respectively). Such reductions could be related either to the formation of cementite and ferrite from the supersaturated bainitic ferrite plates or the decomposition of retained austenite. Ruiz-Jimenez et al. (Ruiz-Jimenez et al., 2020) studied the relation between relative change in length and microstructural changes during tempering using experimental and theoretical approaches and concluded that the contraction of $\Delta L/L_o$ is characteristic of the precipitation of cementite due to the decomposition of film-like retained austenite and tetragonal bainitic ferrite. The authors also observed cementite precipitates formed within the blocks of retained austenite (γ_{Rb}) following

the decomposition of γ_{Rf} and as a result and observed formation of martensite in the dilatometric signal during cooling to room temperature.

In the present study, no changes were observed in the dilatation slope ($\Delta L/L_o$), when cooling from 400 C for the P-bainite or 500 °C for the A-bainite tempering temperatures to ambient temperature, as reported in Figure 5-6a and 5-6b. Thus, it can be said that the chemical composition of γ_R, specifically the carbon content ($C_{\gamma R}$), was high enough to prevent the formation of fresh martensite during cooling to room temperature after the end of the tempering holding time, i.e., the stability of γ_R against any other transformation was not affected.
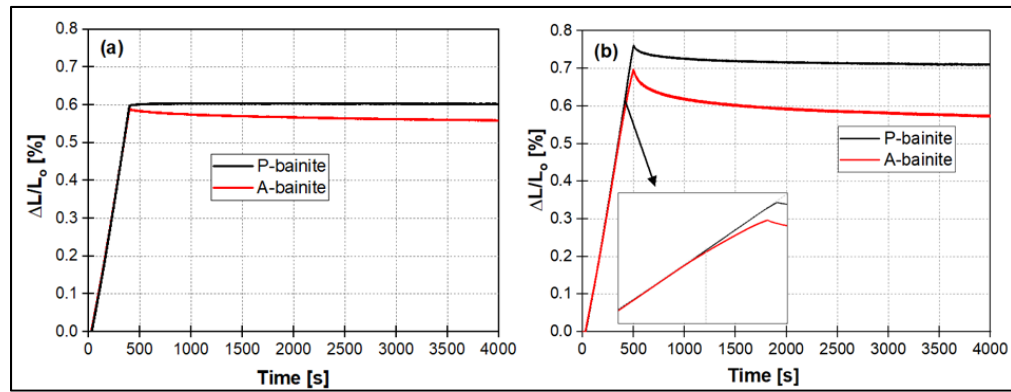
Figure 5-5 Relative change in length during tempering for 1 hour for P-bainite and A-bainite conditions (a) 400 °C and (b) 500 °C
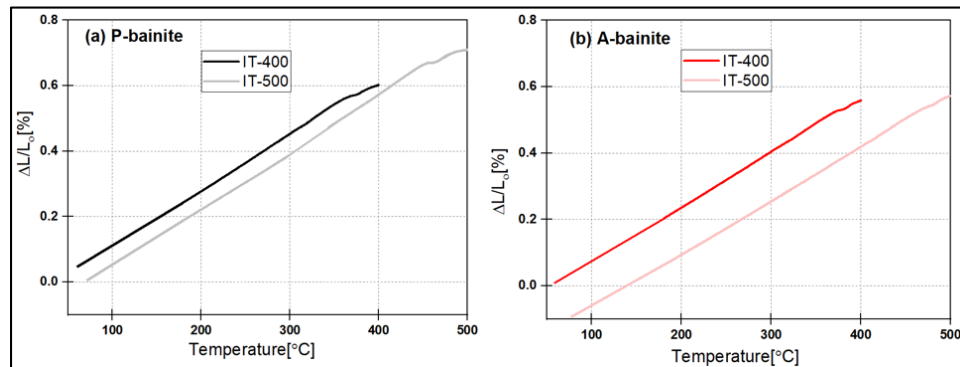
Figure 5-6 Dilatometric signals during cooling to ambient temperature after completion of the isothermal tempering (IT) process at 400 °C and 500 °C: (a) P-bainite and (b) A-bainite

5.4.2   Microstructural and hardness response after isothermal tempering treatments at 400 and 500 °C

Microstructure analysis of P-bainite and A-bainite samples tempered at 400 °C (IT-400), as reported in Figure 5-7b and 5-7b, revealed very similar features to those from the initial P-bainite and A-bainite *prior* to tempering, as reported in Figure 5-2a and 5-2b. Although the dilatometry results in Figure 5-5a showed a slight contraction in the A-bainite sample during isothermal tempering at 400 °C, the microscopic examination showed that microstructure remained stable and no sign of decomposition occurred (see Figure 5-7b). Specifically, extensive SEM examination did not reveal any indication of retained austenite decomposition or cementite precipitates. Although it is possible that a very small amount of nanometric size cementite precipitates might have been formed, but not revealed even by a FE-SEM. The only notable difference that was observed between the microstructures of the two conditions was a slight decrease (<6%) in the thickness of bainitic ferrite plates, 185 nm and 108 nm for P-bainite and A-bainite after tempering at 400 °C; while they were 175 and 100 nm before tempering, respectively (see Figure 5-2).

However, the microstructure of P-bainite and A-bainite —showed a noticeable variation after isothermal tempering at 500 °C (IT-500), as can be clearly seen by comparing Figure 5-8a and 5-8b with the initial microstructure in Figure 5-2a and 5-2b. The P-bainite and A-bainite samples underwent 20 and 13% thickening in α_b plate thickness, as reported in Figure 5-8c and 5-8d, respectively. Furthermore, thickness distribution measurements indicated that the 150–250 nm thickness range was dominant in the P-bainite sample, whereas in the A-bainite sample, a wide range of plate thickness was observed (<100 up to 300 nm), as illustrated in Figure 5-8d. The asymmetrical distribution of the plates in the A-bainite condition is due to an inconsistent thickening mechanism in the A-bainite sample. The inhomogeneity of the strain distribution during ausforming prior to bainite transformation could have an impact on the growth of the bainite ferrite (Eres-Castellanos, 2018; Fan et al., 2017; Seo et al., 2015). Although microstructure characterization was made in the central region of the samples to minimize the deformation inhomogeneity effect, the inconsistent response of austenite grains

to deformation is inevitable. It was also possible to reveal very small cementite precipitates (~ 8±2 nm) along the bainite/austenite grain boundaries, as indicated in the inset of Figure 5-8b and the higher magnification image of Figure 5-9.
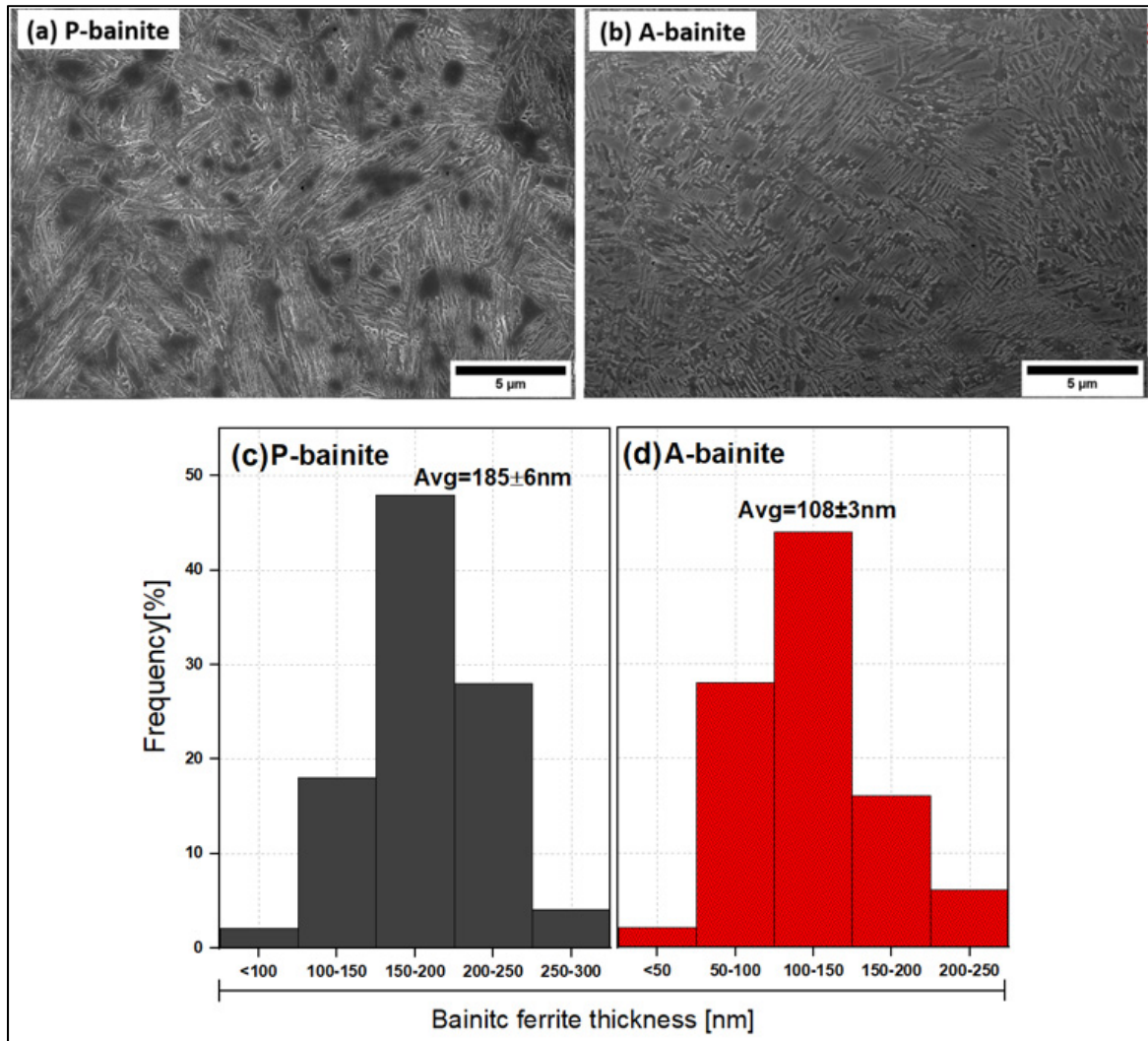
Figure 5-7 Microstructure and distribution of bainitic ferrite plate thickness after IT at 400 °C: (a and c) for P-bainite; (b and d) for A-bainite
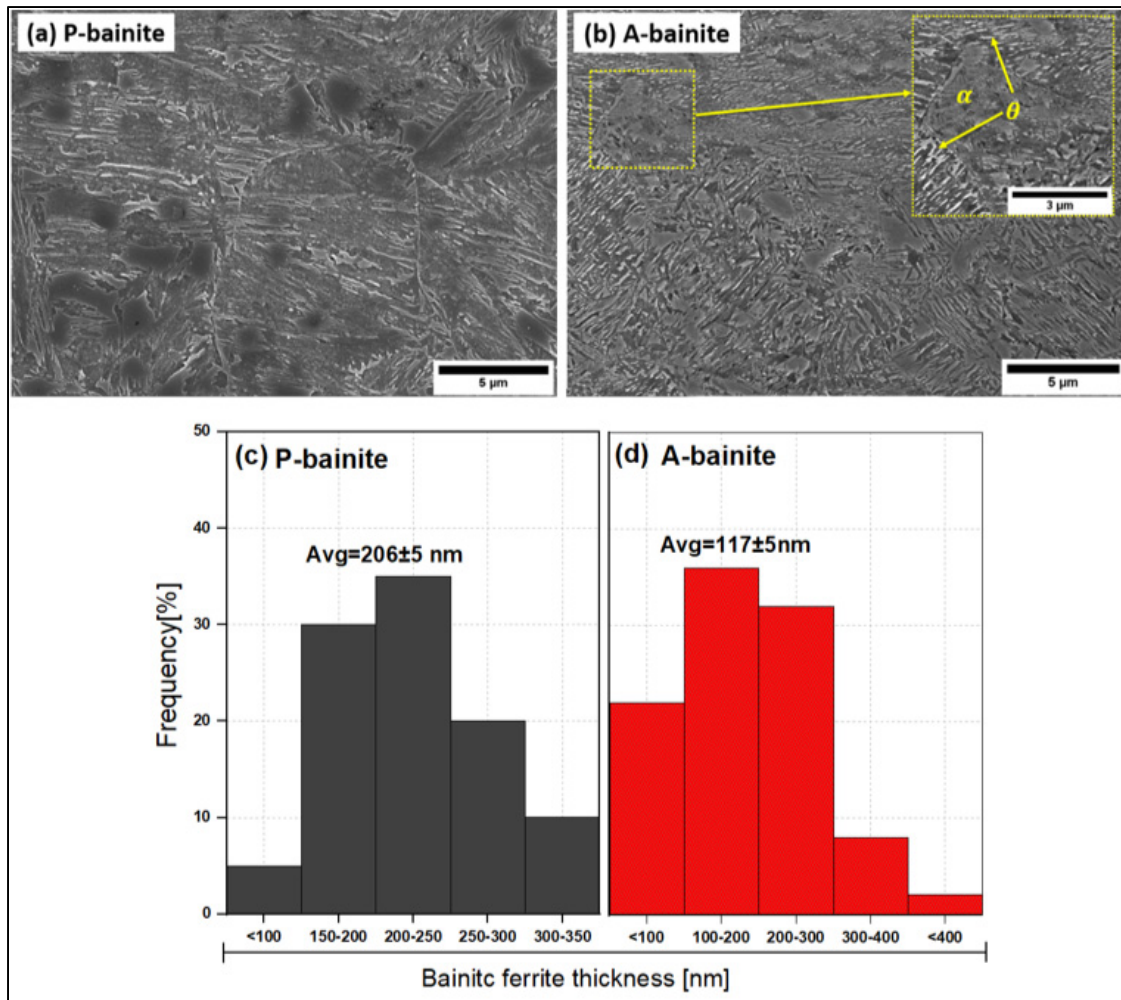
Figure 5-8 Microstructure and distribution of bainitic ferrite plate thickness after IT at 500 °C (a and c) for P-bainite, (b and d) for A-bainite. θ and α stand for cementite and ferrite, respectively

The higher magnification SEM image in Figure 5-9 clearly shows that the cementite precipitates decorated the α_b/γ_R austenite interfaces, as indicated by the white arrows. In addition, ferrite grains could also be distinguished, as designated by yellow arrows in Figure 5-9. The fraction of these particles was estimated using 10 images from different sample sections at high SEM magnification. The measured volume fraction was determined to be about 6%. The above value should be seen as a tool to evaluate the effect of tempering on microstructural change rather than an *absolute* determination of the volume fraction of cementite particles. The decomposition of retained austenite and bainitic ferrite during

tempering are possible governing mechanisms that lead to the formation of the observed cementite in the microstructure of the investigated steel (M.J. Peet, 2010; S. Talebi, Ghasemi-Nanesa, Jahazi, & Melkonyan, 2017). The coarse blocks of retained austenite, γ_{Rb} , are characterized by smooth surfaces with no features present within the grain. Such blocky retained austenite did not transform to martensite during cooling to room temperature at the end of the tempering process (Saha Podder & Bhadeshia, 2010; Zorgani et al., 2020). An illustrative example is highlighted with a dashed white line in Figure 5-9. The above findings are in agreement with the dilatometry results reported in Figure 5-6.

In addition, precipitation of small carbides at the α_b/γ_R interface is probably the main factor that prevented the significant thickening of some of the bainite plates in the A-bainite sample. This effect is particularly well illustrated for the samples tempered at 500 ºC, as reported in Figure 5-8d. The delay in thickening of bainitic ferrite plates due to the pinning effect of carbides has also been observed by Peet et al. and Garcia-Mateo et al. (C. Garcia-Mateo et al., 2013; M.J. Peet, 2010). However, in the present study, the precipitation of these cementite particles took place in an irregular manner around the bainitic plates due to the uneven distribution of strain during the ausforming step, as mentioned above.

The hardness evolution in Table 5-1 shows that a slight decrease in hardness can be noticed in both P-bainite and A-bainite samples after tempering at 400 °C ($< 5\%$). After tempering at 500 ºC, the hardness drop was also modest in the P-bainite condition (reduction by about 7%), similar to what happened in the IT-400 case. However, the reduction was more noticeable in the A-bainite sample, about 15%, as shown in Table 5-1. Although an increase in hardness was expected due to the presence of such nano-sized precipitates (Jia et al., 2017), the transition of superstrated bainite ferrite (BCT) to the equilibrium BCC state, i.e., a less deformed structure, has resulted in an overall decrease in hardness (Smokvina Hanza, Smoljan, Štic, & Hajdek, 2021). Furthermore, an additional effect that results from carbon diffusion from the BCT structure and the formation of cementite precipitates at the α_b/γ_R is their role in delaying the thickening of bainite plates. F.G. Caballero et al. (F. G. Caballero & Bhadeshia, 2004) reported

that the formation of the very fine cementite particles at the α_b/γ_R interface, which prevent the coarsening of the bainitic ferrite plates at higher tempering temperatures.
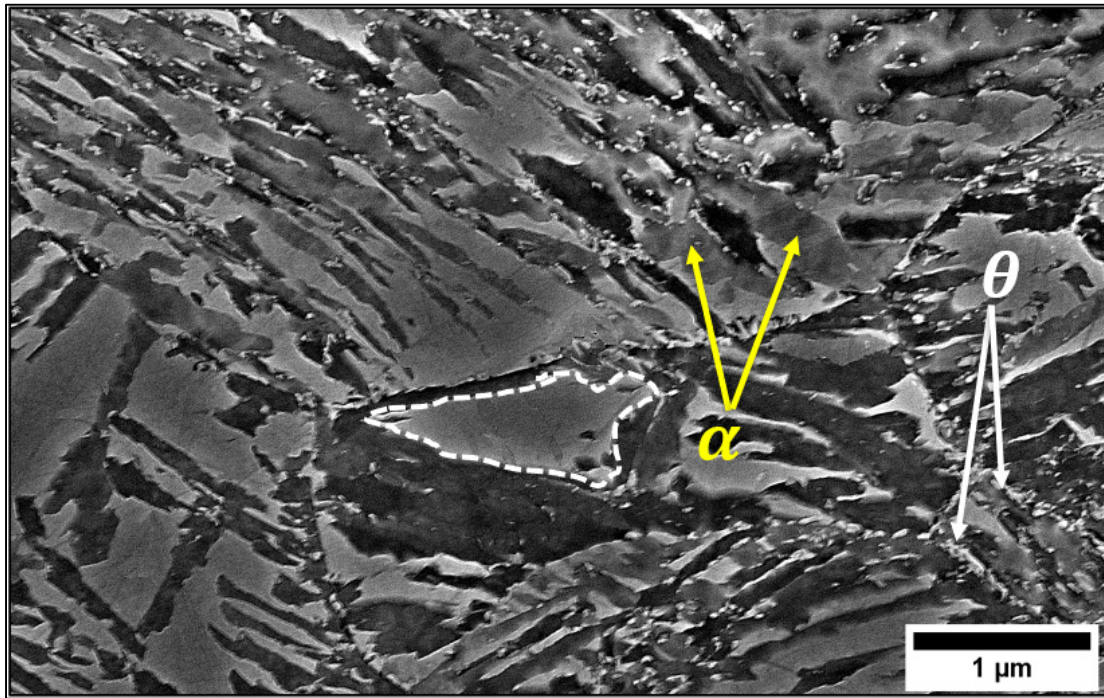
Figure 5-9 Higher SEM magnification of A-bainite sample tempered at 500 °C for 3600 s; θ and α stand for cementite and ferrite, respectively.

Table 5-1 Estimated bainitic ferrite plate thickness (α_b) and microhardness (HV1)

Condition	Thickness of α_b(nm)	HV$_1$
P-bainite	170±5	442±3
P-bainite -IT-400	185±6	434±5
P-bainite -IT-500	206±5	414±4
A-bainite	102±2	547±8
A-bainite -IT-400	108±4	522±8
A-bainite -IT-500	117±5	469±9

5.4.2.1 X-ray diffraction analysis

The XRD scan for P-bainite and A-bainite samples after isothermal tempering at 400 °C (IT-400) and 500 °C (IT-500) are shown in Figure 5-10b and 5-10f. In the P-bainite sample, no cementite peak appeared after IT-400 or IT-500 conditions (Figure 5-10b and 5-10c). The retained austenite peaks in the IT-400 case were almost identical to those in the initial condition (i.e., P-bainite). The normalized $\gamma_{R(111)}$ peaks in Figure 5-10a and 5-10b show that the amount of γ_R did not change after tempering at 400 °C. A similar tendency was observed for the IT-500 conditions shown in Figure 5-10c. Although a slight decrease can be observed in $\gamma_{R(200)}$ peaks for IT-400 and IT-500, the measurement of γ_R, as reported in Table 5-2, shows that the amount of γ_R after IT-400 or IT-500 is almost the same (difference of less than 5%) as that of the conditions before tempering. It must be noted that no indication of carbide precipitation could be found by either SEM or XRD examinations.

The XRD results of tempering at 400 °C do not reveal any significant effect on the A-bainite sample (Figure 5-10e and Table 5-2), where it can be seen that the change in retained austenite fraction before and after tempering was negligible ($< 3\%$). It must be noted that the formation of the small cementite precipitates could be undetectable using the XRD technique because its resolution limit is in the range of 1–3 wt.% (A. Podder et al., 2011). In contrast, when the A-bainite sample was tempered at 500 °C for 3600 s (IT-500), some cementite (θ) peaks appeared at the diffraction angle range of $48 < 2\theta > 44$ and $58 < 2\theta > 54$ (Figure 5-10f). Furthermore, the intensities of FCC (γ_R) peaks were decreased, while those of the BCT/BCC, which could include both bainite and ferrite ($\alpha_b + \alpha$), were increased compared with the original peaks (i.e., the isothermal transformation condition prior to tempering; see peaks $\gamma_{R(111)}$ and $\alpha_{(110)}$ in Figure 5-10d and 5-10f). It is evident that the austenite peaks ($\gamma_{R(200)}$ peak) moved to smaller 2θ values compared with the initial peaks before tempering. This could be attributed to an increase in lattice size as a result of redistribution of carbon that is rejected from α_b (Rementeria et al., 2018). Comparable observations were made by Santajuana et al. and Talebi et al. (M. A. Santajuana et al., 2018; S. Talebi et al., 2017) when high-carbon nano-bainitic steel was tempered at 600 °C for 1h and medium-carbon bainitic steel was tempered via NIT

up to 600 °C, respectively. However, Podder et al. (Saha Podder & Bhadeshia, 2010) reported that cementite peaks were present at angles between 41.5° and 42.5° after tempering a CFB steel at 450 °C for 2 and 5 h, respectively. The results obtained in the present investigation, reported in Table 5-2 that the amount of γ_R was reduced by 15% after tempering at 500 °C compared with its original amount in the as-initial state (P-bainite and A-bainite).

Based on the above XRD observations, the cementite precipitations in the A-bainite sample can possibly be the result of two reactions, namely, $\alpha_b \rightarrow \alpha + \theta$ or $\gamma_R \rightarrow \alpha + \theta$. However, the contractions observed in dilatometry curves reported in section 3.3.1 indicate that only film-like retained austenite, which is present in small quantities within the CFB microstructure, has been decomposed. It must be noted that when blocky shape retained austenite is decomposed, an expansion is observed in the dilatometry curve, as also reported by (Francisca G. Caballero, 2005; Ruiz-Jimenez et al., 2020; S. Talebi et al., 2017; S. H. Talebi et al., 2018). Such transformations are all fundamentally dependent on carbon diffusion through the microstructure. The calculated carbon content in the remaining austenite ($X_{\gamma R}$) and bainitic ferrite ($X_{\alpha b}$), based on lattice parameter measurements in equations (5-2 to 5-5) and reported in Table 5-2, shows that the $X_{\gamma R}$ obtained through P-bainite is higher by about 38 % compared to the one after ausforming at 325 °C (A-bainite). This is probably related to a higher amount of transformed bainite during isothermal bainite transformation in this case. However, a comparison between the results obtained for P-bainite and A-bainite conditions shows that $X_{\gamma R}$ is not significantly affected by tempering with the maximum difference in carbon content being below 6%, except for A-bainite when tempered at 500 °C, where the variation in austenite's carbon content reaches about 12% (0.88 to 0.78 wt.%).

Accordingly, the state of γ_R must be unchanged in all other conditions, which explains why γ_R stayed stable above room temperature during cool down to room temperature after completion of the tempering holding time; that is, the martensite start temperature of γ_R ($M_{S-\gamma R}$) should be below room temperature, as also reported in Figure 5-6.

In the present work, the $M_{S-\gamma R}$ of the retained austenite was estimated according to the mathematical model used for bainitic steel (5-6) reported in Ref (Young & Bhadeshia, 1995).

$$M_{S-\gamma R}(°C) = M_S^°(°C) - 564 \left(X_{\gamma R} - \overline{X} \right)(wt.\%),\tag{5-6}$$

$M_S^°$ is the martensite start temperature measured by dilatometry in the previous study (Zorgani et al., 2020), and $\overline{X}$ is the average carbon content of the studied steel Table 5-2. shows that the $M_{S-\gamma R}$ for all A-bainite samples is in the range of 40–100 °C. This finding is not consistent with the experimental dilatometric results, in which no martensitic transformation was observed above room temperature. Therefore, it could be said that another factor played a role in moving the martensitic transformation to below room temperature levels.

Higher dislocation densities produced as a result of the ausforming process before the isothermal bainitic reformation step resulting in the modification of lattice parameters could be a possible mechanism to explain the above findings. As reported by Chatterjee, Yi, and Garcia-Mateo (Chatterjee, Wang, Yang, & Bhadeshia, 2013; C. Garcia-Mateo et al., 2009; Yi, Lee, & Bhadeshia, 2011), displacive transformations, such as austenite–martensite transformations, can also be hindered by high dislocation densities, that is, mechanical stabilization of austenite. The carbon content in α_b ($X_{\alpha b}$) of the P-bainite sample did not change during isothermal treatment at 400 °C, while it decreased from 0.18 to 0.15 wt.% after IT at 500 °C. The reduction in bainite carbon content could be attributed to a smaller transformation of α_{b-BCT} to α_{b-BCC} and cementite precipitation when holding at 500 °C. Interestingly, the trend was different in the A-bainite samples, where the variation in $X_{\alpha b}$ reached a maximum of 80% in the IT-500 condition (see Table 5-2). The remarkable reduction in $X_{\alpha b}$ could be correlated with changes in the tetragonality of supersaturated bainitic ferrite toward an equilibrium BCC state ($X_{\alpha b}$= 0.03%). Bhadeshia et al. (H.K.D.H.Bhadeshia, 1989) reported that the decomposition sequence of a microstructure containing superstrated upper bainite and enriched carbon austenite consists of : $\alpha_{b-supersturted} + \gamma_R \rightarrow \alpha_{b-unsaturated} + \alpha + \theta$. The authors related the higher reduction in carbon concentration to the acceleration of carbon diffusion from carbon-rich regions, such as α_{b-BCT}, to from cementite when higher tempering temperatures (e.g., 500 °C) are used. However, if temperature was the root cause of

such behavior, similar trend must have been observed for the P-bainite condition. Thus, the acceleration in carbon diffusivity must be due to another factor.
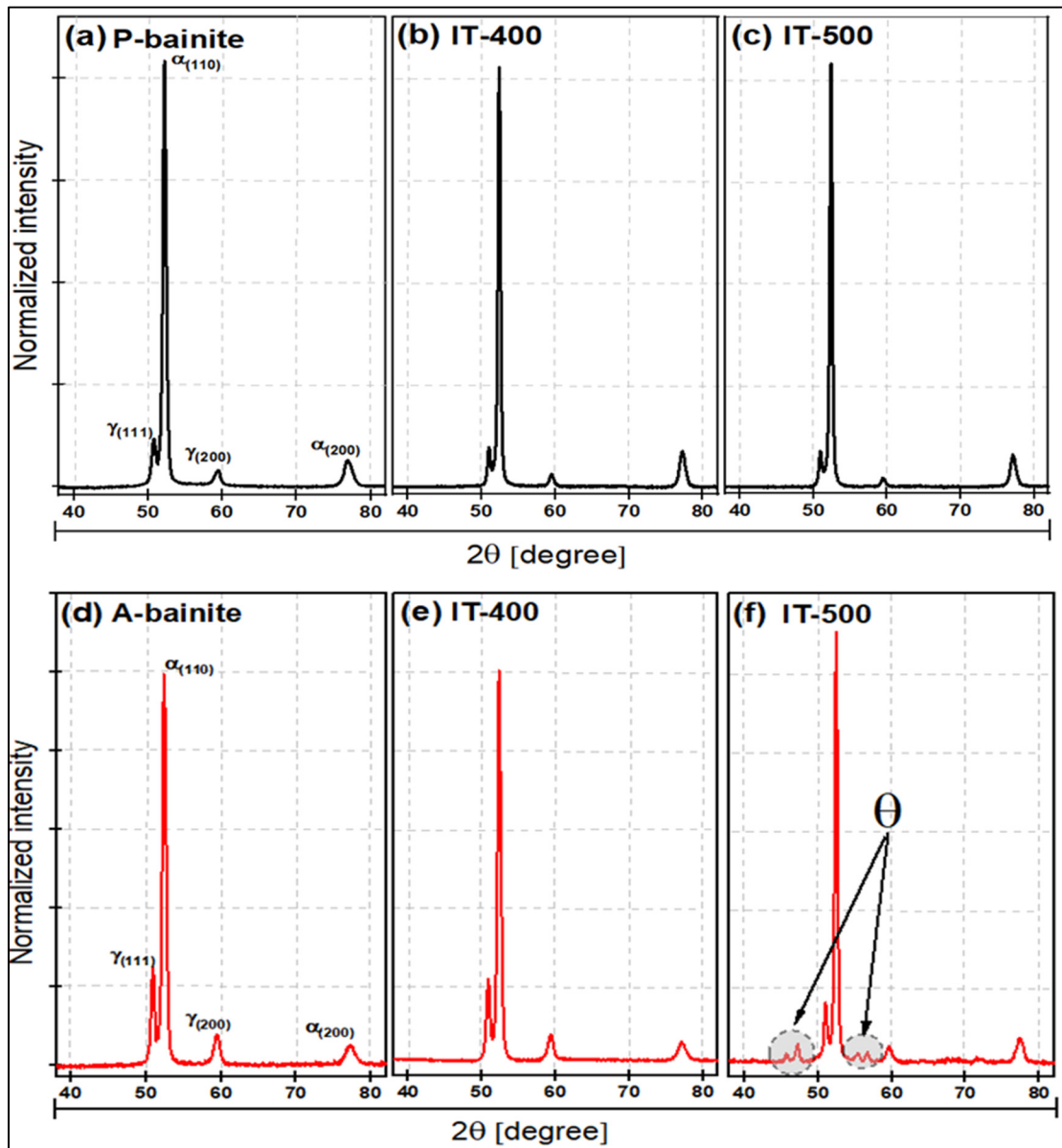
Figure 5-10 XRD patterns of the as-tempered condition: (a, b, c) for P-bainite sample and (d, e, f) for A-bainite. NIT, IT-400, and IT-500 are non-isothermal tempering at 600 °C, isothermal tempering at 400 °C, and isothermal tempering at 500 °C, respectively

Table 5-2 Volume fractions of FCC (γR), BCC (αb and α) obtained from XRD, and cementite (θ) measured by SEM, where $\gamma_R + \alpha_b + \theta = 100$; retained austenite ($X_{\gamma R}$) and bainitic ferrite ($X_\alpha$) carbon content calculated by XRD technique; $M_{S-\gamma R}$ for retained austenite at room temperature. The error values of phases content and carbon contents are ±2 % and ±0.2 wt.%, respectively.

Condition	γ_{RXRD} %	θ_{SEM} %	$(\alpha_b + \alpha)_{XRD}$ %	$X_{\gamma R}$ wt.%	$X_{\alpha b}$ wt.%	$M_{S-\gamma R}$ °C
P-bainite	13.0	---	87.0	1.21	0.18	-146
P-bainite -IT-400	12.6	---	87.4	1.20	0.18	-141
P-bainite -IT-00	12.1	---	88.2	1.14	0.15	-113
A-bainite	24.2	---	75.8	0.88	0.19	39
A-bainite -IT-400	23.5	---	75.5	0.86	0.17	51
A-bainite -IT-500	20.8	6.3	72.9	0.78	0.08	95

5.5   Evolution of dislocation density during tempering

In order to quantify the contribution of different operating mechanisms on the evolution of the A-bainite at 500 °C, the evolution of dislocation density needs to be considered. It has been reported that the formation of cementite (θ) occurs via a paraequilibrium mechanism, where only the C diffuses, and there is no redistribution of other elements atoms, such as Fe, Cr, and Mn, between the phases (H. K. D. H. Bhadeshia, 2015; C. C. Garcia-Mateo, F.G., 2016). Thus, carbon diffusion plays a significant role in enhancing the $\gamma_{\alpha b} \rightarrow \alpha + \theta$ reaction during either heating to the tempering temperature or isothermal holding time (N. F. Kennon & Burgess, 1978; M.J. Peet, 2010). Consequently, any factor promoting carbon diffusivity will have a major influence in accelerating the decomposition process.

Carbon atoms tend to diffuse to octahedral or tetragonal lattice sites in the vicinity of dislocations to reduce their chemical potential because of the attraction forces between carbon atoms and the stress fields of the dislocations (Leiva, Morales, Villar-Cociña, Donis, & de S. Bott, 2010; Nechaev, 2017; Shima et al., 2002; Ståhlkrantz et al., 2020). On the other hand, pipe diffusion of interstitial atoms (carbon), which occurs through dislocation loops, is much

higher (1000 times) than lattice diffusion (Mimkes, 1979), and there is a proportional relationship between dislocation density and pipe diffusion phenomenon ($D_p \propto \rho$) (Mehrer, 1989; MORRISON, 1970). Therefore, carbon diffusion is higher in a microstructure with higher dislocation density. Consequently, estimation of dislocation density could be used as indirect evidence of carbon diffusion behavior.

In the present work, the Williamson–Hall method was used for determining dislocation density evolution based on the full width at half maximum (FWHM) of the diffraction peaks (A. S. Podder, 2011; Williamson & Hall, 1953; Williamson & Smallman, 1956). To this end, a linear fitting was applied to plot peak broadening (ΔK) as a function of the diffraction vector (K) using equations (5-7) and (5-8), respectively; the microstrain, ε, was determined as the slop of the fitted curve as in equation (5-9) (A. S. Podder, 2011; Ståhlkrantz et al., 2020):

$$\Delta K = \frac{cos\theta}{\lambda}\Delta(2\theta), 5 \tag{5-7}$$

$$K = \frac{2sin\theta}{\lambda}, \tag{5-8}$$

$$\Delta K = \alpha + \varepsilon K, \tag{5-9}$$

Where λ is the X-ray wavelength, θ is the Bragg angle in radians, and α is the inverse of the crystallite size. Then, the dislocation density (ρ) was calculated according to equation (5-10) (HajyAkbary, Sietsma, Böttger, & Santofimia, 2015; A. S. Podder, 2011; Ståhlkrantz et al., 2020):

$$\rho = \frac{k}{F} \cdot \frac{\varepsilon^2}{b^2} \tag{5-10}$$

Where k is a constant set to 14.4 for a BCC lattice, F is the interaction factor among dislocations ($F = 1$) (A. S. Podder, 2011; Ståhlkrantz et al., 2020), and b is the Burgers vector of the dislocation (2.47×10^{-10} m).

The results reported in Figure 5-11 Dislocation densities calculated from the XRD data as a function of microstructure condition show that the decrease in the dislocation density is directly proportional to the increase of tempering temperature. The dislocation density declined by about 10% in the P-bainite sample tempered at 400 and 20% when tempered at 500 ºC. However, the difference increased to about 25 and 40% in A-bainite samples tempered at 400 and 500 ºC, respectively. The larger difference could be related to the higher recovery of dislocation, which could have occurred under these conditions. However, it must be noted that the dislocation density in the ausformed microstructure for all tested conditions was always higher than that for pure isothermal treatments.

The dislocation present in the microstructure has two primary sources: i) displacive transformation, which is present under both isothermal and ausformed conditions; and ii) deformation at 325 °C (only applicable for A-bainite condition). The dislocations produced in the latter process are in a much higher number than those in the former, as reported in Figure 5-11. The diffusivity of interstitial elements, such as carbon, can be enhanced quickly at a higher temperature; thus, it can be assumed that the carbon atoms diffused more rapidly in the A-bainite sample tempered at 500 ºC than they did at 400 ºC. Combining the above two factors in enhancing carbon diffusion correlates well with the evolution of the carbon content in supersaturated bainite shown in Table 5-2.
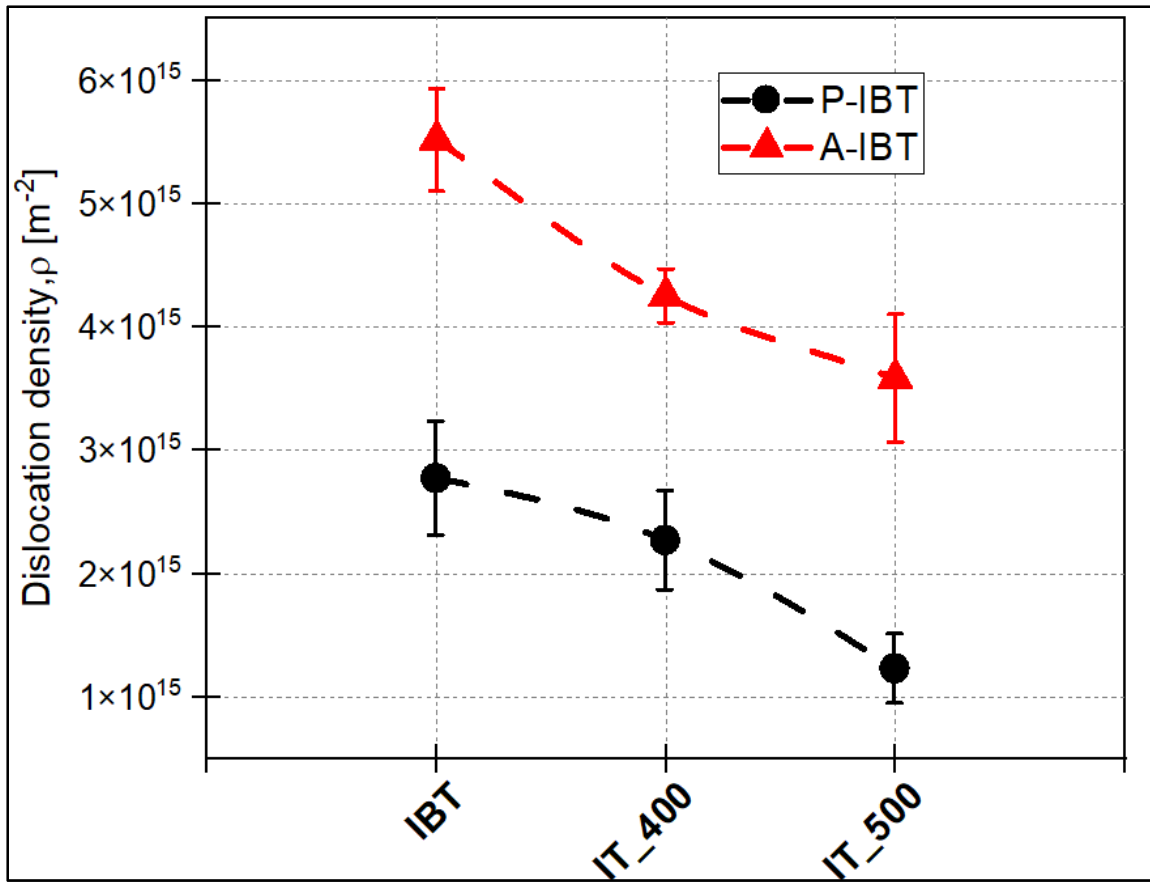
Figure 5-11 Dislocation densities calculated from the XRD data as a function of microstructure condition

5.6　Conclusion

The dilatometric behavior of ausformed and non-ausformed carbide-free nano-bainitic steel during isothermal tempering at 400 and 500 °C and its relation to the microstructural response were investigated. The following main conclusions can be summarized as follows:

- Even though a slight dilatometric contraction was observed during tempering at 500 and 400 °C for P-bainite and A-bainite, respectively, the SEM and XRD results showed that both conditions, bainitic ferrite and retained austenite, did not decompose, and hardness was found to be almost similar to its pre-tempering condition.

- Ausforming prior to bainite transformation resulted in significant microstructural changes that occurred after isothermal tempering at 500 °C.

- The formation of nano-size cementite precipitates along with the formation of BCC bainitic ferrite was identified as the main mechanism responsible for the observed changes in microstructure and hardness.

- The thickening of bainitic ferrite plates was hindered by the nano-sized cementite particles formed at the bainite/austenite interface.

- The amount of retained austenite and its carbon content did not change significantly for all tempering conditions except when the ausformed bainite sample was tempered at 500 ºC.

- The dislocation density was consistently higher in ausformed bainite samples than non-ausformed, enhancing the carbon diffusivity via the pipe diffusion process.

GLOBAL DISCUSSION

Nanostructured carbide free bainitic (CFB) microstructures consists in an interwoven mixture of extremely thin plates of bainitic ferrite plates and thin films of C-enriched retained austenite, known as sheaves of bainite. Retained austenite is also found, with a blocky morphology, trapped between the sheaves. The typical precipitation of cementite that accompanies bainitic transformation can be hindered and even stopped by the addition of Si in suffice quantities (> 1.5 wt.%) to the chemical composition of the steel.

Nowadays ausforming, or plastic deformation of austenite previous to its transformation either to bainite or martensite, is being insensibly explored as a way to obtain nanostructured carbide free bainitic (CFB) microstructures in medium carbon steels.

In any case, ausformed or not, given the negative effect that martensite has on the toughness and ductility of the room temperature microstructure, it is paramount to control the thermal and mechanical stability of austenite remaining after bainitic transformation, avoiding or minimising its transformation to martensite on cooling to RT (thermal stability) or induced by plasticity (TRIP effect) when on service (mechanical stability).

In the case of no-ausformed processes, there is suffice evidence pointing out that stability of retained austenite is mainly affected by its chemical composition, morphology/size, surrounding matrix and dislocation density.

What is still not clear in the specialised bibliography is how those parameters are affected when austenite is plastically deformed previous to bainitic transformation, i.e., ausforming.

Therefore, in the present project, the effect of ausforming and bainite transformation temperature on the stability of retained austenite was evaluated using, among other, high-resolution dilatometry and quantitative metallography. Ausforming was applied at 600 ºC prior to isothermal bainite transformation at different temperatures. The results showed that, regardless of the selected route (ausforming or pure isothermal) retained austenite was stable at room temperature when bainite transformation took place close to the martensite start

temperature (M_S), 325 ℃. This was related to the austenite high C enrichment as a consequence of the high amount of transformed bainite.

However, when isothermal temperature was increased to 350 °C, the mechanical stability of retained austenite increased remarkably by applying a 10% compressive deformation. However, a certain amount of martensite was detected on cooling to room temperature, denoting a decrease in the thermal stability of austenite, due to lower C in solid solution.

Although the results showed that a mixture of bainitic ferrite and retained austenite, with no presence of martensite, was obtained by ausforming followed by bainite transformation at 325 °C, the obtained microstructure was not in the desired nano-scale level.

Considering that the final plate thickness of bainitic ferrite is mainly controlled by three main factors: 1) the strength of the austenite from which it forms; 2) the transformation temperature, and 3) the dislocation network introduced during the displacive transformation; experiments were designed to evaluate how ausforming parameters, deformation amount and temperature, will affect the final scale of the microstructure.

Therefore, ausforming was applied at different temperatures, 600, 400, and 325 ℃ with a 20 % compressive deformation, prior to bainite transformation at 325 ℃.

The study revealed that, ausforming at 600 °C did not introduce significant changes to the scale of the microstructure, as compared to that of the pure isothermal. But, as ausforming temperature decreased from 600 to 325 °C, the bainitic ferrite plates became 50% thinner as compared to that of the pure isothermal treatment, reaching values as low as 100 nm. In addition to such refinement, low temperature ausforming also led to an alignment of the bainitic ferrite plates to specific angles of 45° and 90°, relative to the compression direction, as the ausforming temperature decreased to 400 and 325 °C, respectively. The anisotropy in the bainitic transformation was thoroughly characterized and it was concluded that the bainitic plate alignments and the generation of texture were both consequence of crystallographic variant selection resulting from the low temperature ausforming process.

Furthermore, both, longitudinal and diametric strains were recorded simultaneously during the bainitic transformation in the dilatometer, revealing that strong plasticity strains were

responsible for the anisotropy in the transformation when preceded by ausforming at low temperatures.

Finally, taking into account the possibility of future industrial application, it was necessary to evaluate the effect that typical operations to which these microstructures could be subjected, such as welding, galvanizing and coating, have on the stability of the developed microstructures. In order to do so, a study of the tempering resistance of ausformed (deformed at 325 ºC with 20% compressive plastic stress) nanostructured bainite (isothermally transformed at 325 °C) was performed.

The tempering temperatures, 400 and 500 ºC, were selected on the basis of the results that revealed major microstructural changes took place in the 400- 535 °C interval. A detailed analysis of the dilatometric curves during the tempering treatment in combination with microstructural characterization of the final microstructure by means of SEM and XRD allowed to concluded that, i) at tempering temperature as high as 400 ºC ausformed and no ausformed bainite remained stable and no major microstructural changes could be detected except for a discrete increase in bainitic ferrite plate thickness, ii) when tempering temperature is increased to 500 °C further increase in plate thickness alongside with the formation of cementite particles and the concomitant decrease of the C content in the bainitic ferrite took place in ausformed bainite. It was rationalized that for both tempering temperatures, the dislocation density, was the main rate controlling parameter. As carbon diffusivity is enhanced through pipe diffusion when the dislocation density is high, precipitation of C from supersaturated bainitic ferrite in the form of cementite precipitates in the ferrite/austenite interface refrain the plate thickening while at the same time allows for a faster transition from a tetragonal to a body centered structure.

CONCLUSION

Based on the global discussion the following conclusions can be drawn from the thesis:

- The main factor contributing to retained austenite's stability was bainitic isothermal temperature regardless of percent deformation.

- Bainitic transformation above M_S and below 350 °C was the threshold temperature above which the retained austenite within the CFB matrix decomposed dramatically to martensite as percent deformation increased.

- CFB microstructure obtained at 325 °C had the highest retained austenite thermal stability among other bainite transformation temperatures.

- Ausforming at 600 °C had a limited effect on microstructural changes and TP strains and comparable with the pure isothermal condition.

- An alignment in bainitic ferrite plates was observed when a compressive plastic deformation was applied below B_S. The TP strain intensified with severe alignment in the microstructure when the ausforming was applied at the isotehrmal transformation tempertaure (325 °C).

- Nanostructured morphology with ~100 nm bainiitc ferrite plates thickness was obtained and the hardness reached a level similar to that of a martensitic state (~550 HV).

- CFB microstructure obtained by pure isothermal treatment had a higher tempering resistance at 400 and 500 °C than the ausformed CFB microstructure

- Nanostructured CFB produced via ausforming followed by isothermal transformation underwent cementite precipitation, after isothermal tempering at 500 °C.

- The thickening of the bainitic ferrite plates was hindered by the nano-sized cementite particles formed at the bainite/austenite interface which reduced the tempering softening.

- The dislocation density was always higher in ausformed bainite samples than non-ausformed, enhancing the carbon diffusivity via the pipe diffusion process.

RECOMMENDATIONS

The following areas would be beneficial to support or supplement the work conducted in this thesis by further developing the understanding of how the ausforming and isothermal transformation may alter the CFB microstructures and the mechanical properties in *medium C-Si rich steels.*

- In the present study a laboratory-size samples, i.e., dilatometry samples, were used for the pure isothermal and ausforming thermomechanical treatments. It is recommended to carry out an investigation on industrial-size samples to study the effect of sample size on the evolution of nanostructured CFB microstructure.

- It was concluded in this study that microstructural anisotropy occurred when a nanostructured CFB obtained via low-temperature ausforming. Therefore, studying the effect of this anisotropy on the mechanical properties, and specifically on the fracture mechanisms can be useful in gaining a better understanding of the mechanical properties/microstructure relationship.

- Further characterization of the steels using techniques such as transmission electron microscopy (TEM). The XRD data showed a small volume fraction of carbides in the microstructure after tempering process (too small to quantify using the analytical methods), so using more advanced techniques may better reveal the microstructural constituents and further explain carbide formation in the bainite.

- In the present study, the prior austenite grain size (PAGS) was fixed in all thermomechanical treatments. It is suggested to investigate the relation between PAGS and ausforming parameters to obtain optimal mechanical/microstructure properties.

LIST OF BIBLIOGRAPHICAL REFERENCES

A. S. M. International Handbook, C. (1991). *ASM handbook. Volume 4, Volume 4*. [Materials Park, Ohio]: ASM International.

Ashby, M. F., & Jones, D. R. H. (1998). Engineering Materials 2 An Introduction to Microstructures, Processing and Design. In M. F. Ashby & D. R. H. Jones (Eds.), *Engineering Materials 2 (Fourth Edition)* (pp. xvii-xx). Boston: Butterworth-Heinemann.

Asia, N. P. (February, 2018). MIP (Metallographical Image Processing), http://metsofts.com/.

Avishan, B., Yazdani, S., & Hossein Nedjad, S. (2012). Toughness variations in nanostructured bainitic steels. *Materials Science and Engineering: A, 548*, 106-111. doi:10.1016/j.msea.2012.03.098.

Azuma, M., Fujita, N., Takahashi, M., Senuma, T., Quidort, D., & Lung, T. (2005). Modelling Upper and Lower Bainite Trasformation in Steels. *Isij International, 45*(2), 221-228. doi:10.2355/isijinternational.45.221.

B. Beausir, J.-J. F. (2017). Analysis Tools for Electron and X-ray diffraction, ATEX - software. *Université de Lorraine Metz*. Retrieved from http://www.atex-software.eu/.

Bain, J., & Davenport, R. (1930). The Kinetics of Phase Changes in Metals. *Trans. AIME, 90*, 117.

Beladi, H., Adachi, Y., Timokhina, I., & Hodgson, P. (2009). Crystallographic analysis of nanobainitic steels. *Scripta Materialia, 60*(6), 455-458. doi:10.1016/j.scriptamat.2008.11.030.

Beladi, H., Timokhina, I. B., Hodgson, P. D., & Adachi, Y. (2012). Characterization of Nano-Structured Bainitic Steel. *International Journal of Modern Physics: Conference Series, 05*, 1-8. doi:10.1142/s2010194512001778.

Bergström, Y. (1970). A dislocation model for the stress-strain behaviour of polycrystalline α-Fe with special emphasis on the variation of the densities of mobile and immobile dislocations. *Materials Science and Engineering, 5*(4), 193-200. doi:10.1016/0025-5416(70)90081-9.

Bhadeshia, & Honeycombe. (2003). Steels: microstructure and properties *3rd addition*.

162

Bhadeshia, H. (2010). Phase transformations contributing to the properties of modern steels. *58*(No 2), 255-265. Retrieved from http://journals.pan.pl/Content/83072.

http://journals.pan.pl/dlibra/docmetadata?id=83072DOI - 10.2478/v10175-010-0024-4.

Bhadeshia, H. K. D. H. (1989). New bainitic steels by design. *The Minerals, Metals and Materials Society*.

Bhadeshia, H. K. D. H. (2001). *Bainite in steels: transformations, microstructure and properties* (2nd edition ed.): IOM Communications.

Bhadeshia, H. K. D. H. (2002). Bainite-in-Steels. *Materials Science & Metallurgy*.

Bhadeshia, H. K. D. H. (2004). Developments in martensitic and bainitic steels: role of the shape deformation. *Materials Science and Engineering: A, 378*(1-2), 34-39. doi:10.1016/j.msea.2003.10.328.

Bhadeshia, H. K. D. H. (2005). High Performance Bainitic Steels. *Materials Science Forum, 500-501*, 63-74. doi:10.4028/www.scientific.net/MSF.500-501.63.

Bhadeshia, H. K. D. H. (2006). Bainitic bulk-nanocrystalline steel. *The 3rd International Conference on Advanced Structural Steels, Gyeongju, Korean Institute for Metals*, pp.33–40.

Bhadeshia, H. K. D. H. (2009). Nanostructured bainite. *Proceedings of the Royal Society A: Mathematical, Physical and Engineering Sciences, 466*(2113), 3-18. doi:10.1098/rspa.2009.0407.

Bhadeshia, H. K. D. H. (2013). Bulk nanocrystalline steel. *Ironmaking & Steelmaking, 32*(5), 405-410. doi:10.1179/174328105x71308.

Bhadeshia, H. K. D. H. (2013). Data on Displacements caused by the Growth of Bainite in Steels.

Bhadeshia, H. K. D. H. (2015). BAINITE IN STEELS, THEORY AND PRACTICE. *Book, University of Cambridge and POSTECH, Third edition*.

Bhadeshia, H. K. D. H., David, S. A., Vitek, J. M., & Reed, R. W. (2013). Stress induced transformation to bainite in Fe–Cr–Mo–C pressure vessel steel. *Materials Science and Technology, 7*(8), 686-698. doi:10.1179/mst.1991.7.8.686.

Bhadeshia, H. K. D. H., & Edmonds, D. V. (1983). Bainite in silicon steels: new composition–property approach Part 2. *Metal Science, 17*(9), 420-425. doi:10.1179/030634583790420646.

Bodin, A., Sietsma, J., & van der Zwaag, S. (2001). Flow stress prediction during intercritical deformation of a low-carbon steel with a rule of mixtures and Fe-simulations. *Scripta Materialia, 45*(8), 875-882. doi:10.1016/s1359-6462(01)01050-8.

C. Zhi, A. Z., J. He & H. Yang. (2016). Effect of multi-step ausforming process on the microstructure evaluation of nanobainite steel.

Caballero, F. G. (2012). Carbide-free bainite in steels. In E. Pereloma & D. V. Edmonds (Eds.), *Phase Transformations in Steels* (Vol. 1, pp. 436-467): Woodhead Publishing.

Caballero, F. G. (2014). Microstructure Evolution in Steels. In R. B. Hetnarski (Ed.), *Encyclopedia of Thermal Stresses* (pp. 3056-3065). Dordrecht: Springer Netherlands.

Caballero, F. G., & Bhadeshia, H. K. D. H. (2004). Very strong bainite. *Current Opinion in Solid State and Materials Science, 8*(3-4), 251-257. doi:10.1016/j.cossms.2004.09.005.

Caballero, F. G., Bhadeshia, H. K. D. H., Mawella, K. J. A., Jones, D. G., & Brown, P. (2001). Design of novel high strength bainitic steels: Part 1. *Materials Science and Technology, 17*(5), 512-516. doi:10.1179/026708301101510348,

Caballero, F. G., Bhadeshia, H. K. D. H., Mawella, K. J. A., Jones, D. G., & Brown, P. (2002). Very strong low temperature bainite. *Materials Science and Technology, 18*(3), 279-284. doi:10.1179/026708301225000725,

Caballero, F. G., Bhadeshia, H. K. D. H., Mawella, K. J. A., Jones, D. G., & Brown, P. (2013). Very strong low temperature bainite. *Materials Science and Technology, 18*(3), 279-284. doi:10.1179/026708301225000725,

Caballero, F. G., Miller, M. K., & Garcia-Mateo, C. (2010). Carbon supersaturation of ferrite in a nanocrystalline bainitic steel. *Acta Materialia, 58*(7), 2338-2343. doi:10.1016/j.actamat.2009.12.020,

Chatterjee, S., Wang, H. S., Yang, J. R., & Bhadeshia, H. K. D. H. (2013). Mechanical stabilisation of austenite. *Materials Science and Technology, 22*(6), 641-644. doi:10.1179/174328406x86128,

164

Chen, G., Hu, H., Xu, G., Tian, J., Wan, X., & Wang, X. (2020). Optimizing Microstructure and Property by Ausforming in a Medium-carbon Bainitic Steel. *Isij International, 60*(9), 2007-2014. doi:10.2355/isijinternical.ISIJINT-2020-054,

Cheng, L., Brakman, C. M., Korevaar, B. M., & Mittemeijer, E. J. (1988). The tempering of iron- carbon martensite; dilatometric and calorimetric analysis. *Metallurgical Transactions A, 19*(10), 2415-2426. doi:10.1007/bf02645469,

Chiou, C. S., Yang, J. R., & Huang, C. Y. (2001). The effect of prior compressive deformation of austenite on toughness property in an ultra-low carbon bainitic steel. *Materials Chemistry and Physics, 69*(1-3), 113-124. doi:10.1016/s0254-0584(00)00379-5,

Cohen, R. C. R. a. M. (1969). Splat Quenching of Iron-Carbon Alloys. *Transactions of the metallurgical society of aim, 245*.

Cornide, J., Garcia-Mateo, C., Capdevila, C., & Caballero, F. G. (2013). An assessment of the contributing factors to the nanoscale structural refinement of advanced bainitic steels. *Journal of Alloys and Compounds, 577*, S43-S47. doi:10.1016/j.jallcom.2011.11.066,

Dong, B., Hou, T., Zhou, W., Zhang, G., & Wu, K. (2018). The Role of Retained Austenite and Its Carbon Concentration on Elongation of Low Temperature Bainitic Steels at Different Austenitising Temperature. *Metals, 8*(11), 931. doi:10.3390/met8110931,

E975-13, A. (2013). Standard Practice for X-Ray Determination of Retained Austenite in Steel with Near Random Crystallographic Orientation. *ASTM International, West Conshohocken, PA*. doi:10.1520/e0975-13.

Edmonds, H. K. D. H. B. a. D. V. (1983). Bainite in silicon steels: new composition-property approach. Part1. *The Minerals, Metals & Materials Society*.

Eres-Castellanos, A. (2018). Effect of ausforming on the bainitic transformation in medium carbon steels. *Thesis, Universidad Politécnica de Madrid Escuela Técnica Superior de Ingenieros de Caminos, Canales y Puertos*.

Eres-Castellanos, A., Hidalgo, J., Zorgani, M., Jahazi, M., Toda-Caraballo, I., Caballero, F. G., & Garcia-Mateo, C. (2021). Assessing the scale contributing factors of three carbide-free bainitic steels: A complementary theoretical and experimental approach. *Materials & Design, 197*, 109217. doi:10.1016/j.matdes.2020.109217.

Eres-Castellanos, A., Morales-Rivas, L., Latz, A., Caballero, F. G., & Garcia-Mateo, C. (2018). Effect of ausforming on the anisotropy of low temperature bainitic transformation. *Materials Characterization, 145*, 371-380. doi:10.1016/j.matchar.2018.08.062.

F. G. Caballero, H. K. D. H. B., K. J. A. Mawella, D. G. Jones and P. Brown. (2001). Design of novel high-strength bainitic steels. Part1.

Fan, H.-l., Zhao, A.-m., Li, Q.-c., Guo, H., & He, J.-g. (2017). Effects of ausforming strain on bainite transformation in nanostructured bainite steel. *International Journal of Minerals, Metallurgy, and Materials, 24*(3), 264-270. doi:10.1007/s12613-017-1404-7.

Fielding, L. C. D. (2013). The Bainite Controversy. *Materials Science and Technology, 29*(4), 383-399. doi:10.1179/1743284712y.0000000157.

Francisca G. Caballero, C. G.-M., Carlos García de Andrés. (2005). Dilatometric Study of Reaustenitisation of High Silicon Bainitic Steels: Decomposition of Retained Austenite. *Materials Transactions, 46*(3), 581-586. doi:10.2320/matertrans.46.581.

Francisca García Caballero, M. J. S., Carlos Capdevila, Carlos García-Mateo, Carlos García de Andrés. (2006). Design of Advanced Bainitic Steels by Optimisation of TTT Diagrams and T0 Curves. *Isij International, 46*, 1479-1488. doi:doi.org/10.2355/isijinternational.46.1479.

Freiwillig, R., Kudrman, J., & Chráska, P. (1976). Bainite transformation in deformed austenite. *Metallurgical Transactions A, 7*(8), 1091-1097. doi:10.1007/bf02656591.

Gao, G., Zhang, H., Gui, X., Tan, Z., & Bai, B. (2015). Tempering Behavior of Ductile 1700 MPa Mn–Si–Cr–C Steel Treated by Quenching and Partitioning Process Incorporating Bainite Formation. *Journal of Materials Science & Technology, 31*(2), 199-204. doi:10.1016/j.jmst.2014.07.010.

García-Junceda, A., Capdevila, C., Caballero, F. G., & de Andrés, C. G. (2008). Dependence of martensite start temperature on fine austenite grain size. *Scripta Materialia, 58*(2), 134-137. doi:10.1016/j.scriptamat.2007.09.017.

Garcia-Mateo, & Caballero, F. G. (2014). Advanced High Strength Bainitic Steels. 165-190. doi:10.1016/b978-0-08-096532-1.00114-x.

Garcia-Mateo, C., & Caballero, F. (2005). The Role of Retained Austenite on Tensile Properties of Steels with Bainitic Microstructures. *Materials Transactions, 46*. doi:10.2320/matertrans.46.1839.

Garcia-Mateo, C., Caballero, F., Sourmail, T., Smanio, V., & García de Andrés, C. (2014). Industrialised nanocrystalline bainitic steels. Design approach. *International Journal of Materials Research, 105*, 725-734. doi:10.3139/146.111090.

Garcia-Mateo, C., & Caballero, F. G. (2005). Ultra-high-strength Bainitic Steels. *Isij International, 45*(11), 1736-1740. doi:10.2355/isijinternational.45.1736.

Garcia-Mateo, C., Caballero, F. G., & Bhadeshia, H. K. D. H. (2003). Acceleration of Low-temperature Bainite. *Isij International, 43*(11), 1821-1825. doi:10.2355/isijinternational.43.1821

Garcia-Mateo, C., Caballero, F. G., Chao, J., Capdevila, C., & Garcia de Andres, C. (2009). Mechanical stability of retained austenite during plastic deformation of super high strength carbide free bainitic steels. *Journal of Materials Science, 44*(17), 4617-4624. doi:10.1007/s10853-009-3704-4.

Garcia-Mateo, C., Caballero, F. G., Sourmail, T., Kuntz, M., Cornide, J., Smanio, V., & Elvira, R. (2012). Tensile behaviour of a nanocrystalline bainitic steel containing 3wt% silicon. *Materials Science and Engineering: A, 549*, 185-192. doi:10.1016/j.msea.2012.04.031.

Garcia-Mateo, C., Caballero, F. G., Sourmail, T., Smanio, V., & de Andres, C. G. (2014). Industrialised nanocrystalline bainitic steels. Design approach. *International Journal of Materials Research, 105*(8), 725-734. doi:10.3139/146.111090.

Garcia-Mateo, C., Paul, Georg, Somani, Mahesh C., Porter, David A., Bracke, Lieven, Latz, Andreas, Garcia De Andres, Carlos, Caballero, Francisca G. (2017). Transferring Nanoscale Bainite Concept to Lower C Contents: A Perspective. *Metals, 7*(5), 159. Retrieved from https://www.mdpi.com/2075-4701/7/5/159.

Garcia-Mateo, C., Peet, M., Caballero, F. G., & Bhadeshia, H. K. D. H. (2013). Tempering of hard mixture of bainitic ferrite and austenite. *Materials Science and Technology, 20*(7), 814-818. doi:10.1179/026708304225017355.

Garcia-Mateo, C. C., F.G. (2016). Bainitic steels: Tempering. *In Encyclopedia of Iron, Steel, and Their Alloys; Taylor & Francis: Milton Park, Abingdon, UK*, 1–14.

García Mateo, C. E.-C., A.; García Caballero, Francisca; Lazt, Andreas; Schreiber, Sebastian; Ray, Arunim; Bracke, Lieven; Somani, Mahesh; Kaikkonen, Pentti; Pohjonen, Aarne; Porter, David A. (2020). Towards industrial applicability of (medium C) nanostructured bainitic steels (TIANOBAIN). *Final Technical Report - Part B*.

Golchin, S., Avishan, B., & Yazdani, S. (2016). Effect of 10% ausforming on impact toughness of nano bainite austempered at 300 °C. *Materials Science and Engineering: A, 656*, 94-101. doi:10.1016/j.msea.2016.01.025.

Gong, W., Tomota, Y., Adachi, Y., Paradowska, A. M., Kelleher, J. F., & Zhang, S. Y. (2013). Effects of ausforming temperature on bainite transformation, microstructure and variant selection in nanobainite steel. *Acta Materialia, 61*(11), 4142-4154. doi:10.1016/j.actamat.2013.03.041.

Gong, W., Tomota, Y., Koo, M. S., & Adachi, Y. (2010). Effect of ausforming on nanobainite steel. *Scripta Materialia, 63*(8), 819-822. doi:10.1016/j.scriptamat.2010.06.024.

Grajcar, A., Skrzypczyk, P., & Kozłowska, A. (2018). Effects of Temperature and Time of Isothermal Holding on Retained Austenite Stability in Medium-Mn Steels. *Applied Sciences, 8*(11). doi:10.3390/app8112156.

Granger, & Stewart. (1946). The Temperature Range of Martensite Formation. *Transactions of the AIME, 167*, 467-490.

Greenwood, G. W., Johnson, R. H., & Rotherham, L. (1997). The deformation of metals under small stresses during phase transformations. *Proceedings of the Royal Society of London. Series A. Mathematical and Physical Sciences, 283*(1394), 403-422. doi:10.1098/rspa.1965.0029.

Grostabussiat, S., Taleb, L., Jullien, J. F., & Sidoroff, F. (2001). Transformation induced plasticity in martensitic transformation of ferrous alloys. *Le Journal de Physique IV, 11*(PR4), Pr4-173-Pr174-180. doi:10.1051/jp4:2001422.

Guo, H., Feng, X., Zhao, A., Li, Q., & Chai, M. (2020). Effects of ausforming temperature on bainite transformation kinetics, microstructures and mechanical properties in ultra-fine bainitic steel. *Journal of Materials Research and Technology, 9*(2), 1593-1605. doi:10.1016/j.jmrt.2019.11.085.

Guo, Y., Yao, C., Feng, K., Li, Z., Chu, P. K., & Wu, Y. (2017). Effect of Isothermal Temperature on Growth Behavior of Nanostructured Bainite in Laser Cladded Coatings. *Materials (Basel, Switzerland), 10*(7), 800. doi:10.3390/ma10070800.

H.-G. Lambers, S. T., H.J. Maier, D. Canadinc. (2010). Pre-deformation–transformation plasticity relationship during martensitic transformation. *Materials Science and Engineering A 527*, 625–633.

H.-G. Lambers, S. T., H.J. Maier, D. Canadinc. (2011). Evolution of transformation plasticity during bainitic transformation. *Metallurgical and Materials Transactions A, 102*, 1152-1163.

H.K.D.H.Bhadeshia. (1989). Theoretical analysis of chnages in cemnetite composition during tempering of bainite. *Materials Science and Technology, 5*(2), 131-137.

HajyAkbary, F., Sietsma, J., Böttger, A. J., & Santofimia, M. J. (2015). An improved X-ray diffraction analysis method to characterize dislocation density in lath martensitic structures. *Materials Science and Engineering: A, 639*, 208-218. doi:10.1016/j.msea.2015.05.003.

Hala Salman Hasan, M. J. P., Marie-Noëlle Avettand Fénoël, H. K. D. H. Bhadeshia. (2014). Effect of tempering upon the tensile properties of a nanostructured bainitic steel. *Materials Science and Engineering*.

Han, H. N., & Suh, D.-W. (2003). A model for transformation plasticity during bainite transformation of steel under external stress. *Acta Materialia, 51*(16), 4907-4917. doi:10.1016/s1359-6454(03)00333-1.

Hanamura, T., Torizuka, S., Tamura, S., Enokida, S., & Takechi, H. (2013). Effect of Austenite Grain Size on Transformation Behavior, Microstructure and Mechanical Properties of 0.1C–5Mn Martensitic Steel. *Isij International, 53*(12), 2218-2225. doi:10.2355/isijinternational.53.2218.

Hasan, S. M., Kumar, S., Chakrabarti, D., & Singh, S. B. (2020). Effect of prior austenite grain size on the formation of carbide-free bainite in low-alloy steel. *Philosophical Magazine, 100*(18), 2320-2334. doi:10.1080/14786435.2020.1764653.

He, B. B., Xu, W., & Huang, M. X. (2015). Effect of ausforming temperature and strain on the bainitic transformation kinetics of a low carbon boron steel. *Philosophical Magazine, 95*(11), 1150-1163. doi:10.1080/14786435.2015.1025886.

He, J., Du, J., Zhang, W., Zhang, C., Yang, Z.-G., & Chen, H. (2018). Abnormal Anisotropic Dilatation During Bainitic Transformation of Ausformed Austenite. *Metallurgical and Materials Transactions A, 50*(2), 540-546. doi:10.1007/s11661-018-5038-9.

He, J., Zhao, A., Zhi, C., & Fan, H. (2015). Acceleration of nanobainite transformation by multi-step ausforming process. *Scripta Materialia, 107*, 71-74. doi:10.1016/j.scriptamat.2015.05.023.

He, J. G., Zhao, A. M., Yao, H., Zhi, C., & Zhao, F. Q. (2015). Effect of Ausforming Temperature on Bainite Transformation of High Carbon Low Alloy Steel. *Materials Science Forum, 817*, 454-459. doi:10.4028/www.scientific.net/MSF.817.454.

Hofer, C., Winkelhofer, F., Clemens, H., & Primig, S. (2016). Morphology change of retained austenite during austempering of carbide-free bainitic steel. *Materials Science and Engineering: A, 664*, 236-246. doi:10.1016/j.msea.2016.04.005.

Holzweissig, M. J., Canadinc, D., & Maier, H. J. (2012). In situ characterization of backstress effects on the austenite-to-bainite phase transformation. *Scripta Materialia, 67*(4), 368-371. doi:10.1016/j.scriptamat.2012.05.027.

Holzweissig, M. J., Uslu, M. C., Lambers, H. G., Canadinc, D., & Maier, H. J. (2013). A Comparative Analysis of Austenite-to-Martensite and Austenite-to-Bainite Phase Transformation Kinetics in Steels. *Materials Research Letters, 1*(3), 141-147. doi:10.1080/21663831.2013.798748.

Hossein Beladi, I. B. T., and Peter D. Hodgson (2012). CHARACTERIZATION OF NANO-STRUCTURED BAINITIC STEEL *2nd International Conference on Ultrafine Grained & Nanostructured Materials(UFGNSM) Vol. 5 (2012) 1–8.*

Hu, F., Hodgson, P. D., & Wu, K. M. (2014). Acceleration of the super bainite transformation through a coarse austenite grain size. *Materials Letters, 122*, 240-243. doi:10.1016/j.matlet.2014.02.051.

Hu, H.-j., Xu, G., Wang, L., Zhou, M.-x., & Xue, Z.-l. (2015). Effect of ausforming on the stability of retained austenite in a C-Mn-Si bainitic steel. *Metals and Materials International, 21*(5), 929-935. doi:10.1007/s12540-015-5156-5.

Hu, H., Xu, G., Dai, F., Tian, J., & Chen, G. (2019). Critical ausforming temperature to promote isothermal bainitic transformation in prior-deformed austenite. *Materials Science and Technology, 35*(4), 420-428. doi:10.1080/02670836.2019.1567663.

Hu, H., Xu, G., Wang, L., & Zhou, M. (2017). Effects of Strain and Deformation Temperature on Bainitic Transformation in a Fe-C-Mn-Si Alloy. *steel research international, 88*(3). doi:10.1002/srin.201600170.

Hu, H., Zurob, H. S., Xu, G., Embury, D., & Purdy, G. R. (2015). New insights to the effects of ausforming on the bainitic transformation. *Materials Science and Engineering: A, 626*, 34-40. doi:10.1016/j.msea.2014.12.043.

Huang, Y., Zhao, A.-m., He, J.-g., Wang, X.-p., Wang, Z.-g., & Qi, L. (2013). Microstructure, crystallography and nucleation mechanism of NANOBAIN steel. *International Journal of Minerals, Metallurgy, and Materials, 20*(12), 1155-1163. doi:10.1007/s12613-013-0849-6.

Hunkel, M., Dong, Juan, Epp, Jérémy, Kaiser, Daniel, Dietrich, Stefan, Schulze, V, Rajaei, Ali, Hallstedt, Bengt, Broeckmann, Christoph. (2020). Comparative Study of the Tempering Behavior of Different Martensitic Steels by Means of In-Situ Diffractometry and Dilatometry. *Materials, 13*, 5058. doi:10.3390/ma13225058.

Instruments, T. (2013). DIL 805A/D. Retrieved from http://www.tainstruments.com/wp-content/uploads/BROCH-DIL-2013-EN.pdf.

International, A. S. M., & Handbook, C. (1991). *ASM handbook. Volume 4, Volume 4*. [Materials Park, Ohio]: ASM International.

J. I. Kim, J. H. P., K. S. Park, J. H. Jang, D. W. Suh and H. K. D. H. Bhadeshia. (2014). Segregation of phosphorus to ferrite grain boundaries during transformation in Fe-P alloy. *International Journal of Materials Research, 105*.

J.R.Yang, C. Y. H., W.H. Hsieh, and C.S. Chiou. (1996). Mechanicla stablization of austenite against Bainitic reaction in Fe-Mn-Si-C Bainitic steel. *Mater. Trans. , JIM 37* 579–585.

Jatczak, C. F. (1980). Retained Austenite and Its Measurement by X-Ray Diffraction. *SAE Transactions, 89*, 1657-1676.

Jia, N., Shen, Y. F., Liang, J. W., Feng, X. W., Wang, H. B., & Misra, R. D. K. (2017). Nanoscale spheroidized cementite induced ultrahigh strength-ductility combination in innovatively processed ultrafine-grained low alloy medium-carbon steel. *Sci Rep, 7*(1), 2679. doi:10.1038/s41598-017-02920-9.

Jiang, T., Liu, H., Sun, J., Guo, S., & Liu, Y. (2016). Effect of austenite grain size on transformation of nanobainite and its mechanical properties. *Materials Science and Engineering: A, 666*, 207-213. doi:10.1016/j.msea.2016.04.041.

Kaneshita, T., Miyamoto, G., & Furuhara, T. (2017). Variant selection in grain boundary nucleation of bainite in Fe-2Mn-C alloys. *Acta Materialia, 127*, 368-378. doi:10.1016/j.actamat.2017.01.035.

Kang, J., Zhang, F. C., Yang, X. W., Lv, B., & Wu, K. M. (2017). Effect of tempering on the microstructure and mechanical properties of a medium carbon bainitic steel. *Materials Science and Engineering: A, 686*, 150-159. doi:10.1016/j.msea.2017.01.044.

Keehan, E., Karlsson, L., & Andrén, H. O. (2006). Influence of carbon, manganese and nickel on microstructure and properties of strong steel weld metals: Part 1 – Effect of nickel content. *Science and Technology of Welding and Joining, 11*(1), 1-8. doi:10.1179/174329306X77830.

Khlestov, V. M., Konopleva, E. V., & McQueen, H. J. (1998). Kinetics of austenite transformation during thermomechanical processes. *Canadian Metallurgical Quarterly, 37*(2), 75-89. doi:10.1179/cmq.1998.37.2.75.

Klein, T., Lukas, M., Haslberger, P., Friessnegger, B., Galler, M., & Ressel, G. (2019). Complementary Thermal Analysis Protocols for the Investigation of the Tempering Reactions of a Carbide-Free Bainitic Steel. *JOM, 71*(4), 1357-1365. doi:10.1007/s11837-019-03331-z.

Koo, M., Xu, P., Tomota, Y., & Suzuki, H. (2009). Bainitic transformation behavior studied by simultaneous neutron diffraction and dilatometric measurement. *Scripta Materialia, 61*(8), 797-800. doi:10.1016/j.scriptamat.2009.06.032.

Kopp, A., Bernthaler, T., Schmid, D., Ketzer-Raichle, G., & Schneider, G. (2017). In-situ Investigation of Bainite Formation with fast X-Ray Diffraction (iXRD). *HTM Journal of Heat Treatment and Materials, 72*(6), 355-364. doi:10.3139/105.110341.

Krauss, G. (2014). Quench and Tempered Martensitic Steels. In S. Hashmi, G. F. Batalha, C. J. Van Tyne, & B. Yilbas (Eds.), *Comprehensive Materials Processing* (pp. 363-378). Oxford: Elsevier.

Lambers, H. G., Canadinc, D., & Maier, H. J. (2012). Evolution of transformation plasticity in austenite-to-bainite phase transformation: A multi parameter problem. *Materials Science and Engineering: A, 541*, 73-80. doi:10.1016/j.msea.2012.02.004.

Larn, R. H., & Yang, J. R. (2000). The effect of compressive deformation of austenite on the bainitic ferrite transformation in Fe-Mn-Si-C steels. *Materials Science and Engineering: A, 278*(1-2), 278-291. doi:10.1016/s0921-5093(99)00597-3.

Lee, S.-J., & Van Tyne, C. J. (2011). A Kinetics Model for Martensite Transformation in Plain Carbon and Low-Alloyed Steels. *Metallurgical and Materials Transactions A, 43*(2), 422-427. doi:10.1007/s11661-011-0872-z.

Lee, S., Lee, S.-J., & De Cooman, B. C. (2011). Austenite stability of ultrafine-grained transformation-induced plasticity steel with Mn partitioning. *Scripta Materialia, 65*(3), 225-228. doi:10.1016/j.scriptamat.2011.04.010.

Leijie Zhao, L. Q., Qian Zhoua, Dongdong Li, Tongliang Wang, Zhigeng Jia, Fucheng Zhang, Jiangying Meng (2019). The combining effects of ausforming and below-Ms or above-Ms austempering on the transformation kinetics, microstructure and mechanical properties of low-carbon bainitic steel.

Leiva, J. A. V., Morales, E. V., Villar-Cociña, E., Donis, C. A., & de S. Bott, I. (2010). Kinetic parameters during the tempering of low-alloy steel through the non-isothermal dilatometry. *Journal of Materials Science, 45*(2), 418-428. doi:10.1007/s10853-009-3957-y.

Li, Q., Huang, X., & Huang, W. (2016). Microstructure and mechanical properties of a medium-carbon bainitic steel by a novel quenching and dynamic partitioning (Q-DP) process. *Materials Science and Engineering: A, 662*, 129-135. doi:10.1016/j.msea.2016.03.042.

Li, Z.-D., Yang, Z.-G., Zhang, C., & Liu, Z.-Q. (2010). Influence of austenite deformation on ferrite growth in a Fe–C–Mn alloy. *Materials Science and Engineering: A, 527*(16-17), 4406-4411. doi:10.1016/j.msea.2010.03.092.

Liu, B., Li, W., Lu, X., Jia, X., & Jin, X. (2019). The effect of retained austenite stability on impact-abrasion wear resistance in carbide-free bainitic steels. *Wear, 428-429*, 127-136. doi:10.1016/j.wear.2019.02.032.

Liu, M., Ma, Y., Xu, G., Cai, G., Zhou, M., & Zhang, X. (2019). Effects of Plastic Stress on Transformation Plasticity and Microstructure of a Carbide-Free Bainite Steel. *Metallography, Microstructure, and Analysis, 8*(2), 159-166. doi:10.1007/s13632-019-00527-2.

Liu, Z., Yao, K. F., & Liu, Z. (2013). Quantitative research on effects of stresses and strains on bainitic transformation kinetics and transformation plasticity. *Materials Science and Technology, 16*(6), 643-647. doi:10.1179/026708300101508216.

Lobodyuk, V. A., Meshkov, Y. Y., & Pereloma, E. V. (2018). On Tetragonality of the Martensite Crystal Lattice in Steels. *Metallurgical and Materials Transactions A, 50*(1), 97-103. doi:10.1007/s11661-018-4999-z.

Long, X. Y., Kang, J., Lv, B., & Zhang, F. C. (2014). Carbide-free bainite in medium carbon steel. *Materials & Design, 64*, 237-245. doi:10.1016/j.matdes.2014.07.055.

Luo, H., Shi, J., Wang, C., Cao, W., Sun, X., & Dong, H. (2011). Experimental and numerical analysis on formation of stable austenite during the intercritical annealing of 5Mn steel. *Acta Materialia, 59*(10), 4002-4014. doi:10.1016/j.actamat.2011.03.025.

Maalekian, M., Kozeschnik, E., Chatterjee, S., & Bhadeshia, H. K. D. H. (2013). Mechanical stabilisation of eutectoid steel. *Materials Science and Technology, 23*(5), 610-612. doi:10.1179/174328407x158686.

Maalekian, M., Lendinez, M. L., Kozeschnik, E., Brantner, H. P., & Cerjak, H. (2007). Effect of hot plastic deformation of austenite on the transformation characteristics of eutectoid carbon steel under fast heating and cooling conditions. *Materials Science and Engineering: A, 454-455*, 446-452. doi:10.1016/j.msea.2006.11.102.

Magee, C. L., Paxton, H.W. (1966). *Transformation Kinetics, Microplasticity and Aging of Martensite in Fe-31Ni*: Carnegie INST of Tech. Pittsburgh PA.

Maki, T. (2012). Morphology and substructure of martensite in steels. In E. Pereloma & D. V. Edmonds (Eds.), *Phase Transformations in Steels* (Vol. 2, pp. 34-58): Woodhead Publishing.

Matsuzaki, A., Bhadeshia, H. K. D. H., & Harada, H. (1994). Stress affected bainitic transformation in a Fe-C-Si-Mn alloy. *Acta Metallurgica et Materialia, 42*(4), 1081-1090. doi:10.1016/0956-7151(94)90125-2.

Mehrer, H. (1989). Diffusion in solids. *Wiley, 191–222.*

Miihkinen, V. T. T., & Edmonds, D. V. (2013). Tensile deformation of two experimental high-strength bainitic low-alloy steels containing silicon. *Materials Science and Technology, 3*(6), 432-440. doi:10.1179/mst.1987.3.6.432.

Mimkes, J. (1979). Calculations of Disloctaion Pipe Diffusion. *Journal de Physique Colloques, C6*, C6-181-C186-183. doi:10.1051/jphyscol:1979637.

Min, J., Hector, L. G., Zhang, L., Lin, J., Carsley, J. E., & Sun, L. (2016). Elevated-temperature mechanical stability and transformation behavior of retained austenite in a quenching and partitioning steel. *Materials Science and Engineering: A, 673*, 423-429. doi:10.1016/j.msea.2016.07.090.

Ming-xing Zhou, G. X., Li Wang, Zheng-Liang Xue, and Hai-Jiang Hu. (2015). Comprehensive Analysis of the Dilatation During Bainitic Transformation Under Stress.

174

Mingxing Zhou, G., Yulong Zhang, Zhengliang Xue. (2015). The effects of external compressive stress on the kinetic of flow temperature bainitic transformation and microstructure in a superbainite steel. *International Journal of Materials Research*.

Miyamoto, G., Iwata, N., Takayama, N., & Furuhara, T. (2013). Variant selection of lath martensite and bainite transformation in low carbon steel by ausforming. *Journal of Alloys and Compounds, 577*, S528-S532. doi:10.1016/j.jallcom.2011.12.111.

Mola, J. (2016). *Dilatometry Analysis of Cementite Precipitation in Medium Mn High Carbon Steels*.

Morales-Rivas, L., Archie, F., Zaefferer, S., Benito-Alfonso, M., Tsai, S.-P., Yang, J.-R., . . . Caballero, F. G. (2018). Crystallographic examination of the interaction between texture evolution, mechanically induced martensitic transformation and twinning in nanostructured bainite. *Journal of Alloys and Compounds, 752*, 505-519. doi:10.1016/j.jallcom.2018.04.189.

Morra, P. V., Böttger, A. J., & Mittemeijer, E. J. (2001). Decomposition of Iron-based Martensite. A kinetic analysis by means of differential scanning calorimetry and dilatometry. *Journal of Thermal Analysis and Calorimetry, 64*(3), 905-914. doi:10.1023/a:1011514727891.

MORRISON, C. T. L. a. H. M. (1970). Dislocation-enhanced diffusion in silver single crystals. *Canadian Journal of Physics, 48*, 1548.

N. F. Kennon, & Burgess, P. B. (1978). The second stage of tempering. *Metals Forum 1, 185–190*.

Nambu, S., Shibuta, N., Ojima, M., Inoue, J., Koseki, T., & Bhadeshia, H. K. D. H. (2013). In situ observations and crystallographic analysis of martensitic transformation in steel. *Acta Materialia, 61*(13), 4831-4839. doi:10.1016/j.actamat.2013.04.065.

Navarro-López, A., Hidalgo, J., Sietsma, J., & Santofimia, M. J. (2018). Influence of the prior athermal martensite on the mechanical response of advanced bainitic steel. *Materials Science and Engineering: A, 735*, 343-353. doi:10.1016/j.msea.2018.08.047.

Navarro-López, A., Sietsma, J., & Santofimia, M. J. (2015). Effect of Prior Athermal Martensite on the Isothermal Transformation Kinetics Below M s in a Low-C High-Si Steel. *Metallurgical and Materials Transactions A, 47*(3), 1028-1039. doi:10.1007/s11661-015-3285-6.

Nechaev, Y. S. (2017). On the Carbon Kinetics in Martensite, relevance to Nanosegregation at Dislocations and Grain Boundaries *Journal for the Basic Principles of Diffusion Theory, Experiment and Application*.

Nikravesh, M., Naderi, M., & Akbari, G. H. (2012). Influence of hot plastic deformation and cooling rate on martensite and bainite start temperatures in 22MnB5 steel. *Materials Science and Engineering: A, 540*, 24-29. doi:10.1016/j.msea.2012.01.018.

Pak, J. H., Bhadeshia, H. K. D. H., Karlsson, L., & Keehan, E. (2008). Coalesced bainite by isothermal transformation of reheated weld metal. *Science and Technology of Welding and Joining, 13*(7), 593-597. doi:10.1179/136217108X338926.

Park, H.-S., Seol, J.-B., Lim, N.-S., Kim, S.-I., & Park, C.-G. (2015). Study of the decomposition behavior of retained austenite and the partitioning of alloying elements during tempering in CMnSiAl TRIP steels. *Materials & Design, 82*, 173-180. doi:10.1016/j.matdes.2015.05.059.

Peet, M. J. (2010). Transformation and tempering of low–temperature bainite. *PhD Thesis, University of Cambridge*.

Peet, M. J., Babu, S. S., Miller, M. K., & Bhadeshia, H. K. D. H. (2017). Tempering of Low-Temperature Bainite. *Metallurgical and Materials Transactions A, 48*(7), 3410-3418. doi:10.1007/s11661-017-4086-x.

Podder, A., Lonardelli, I., Molinari, A., & Bhadeshia, H. (2011). Thermal stability of retained austenite in bainitic steel: an in situ study. *Royal Society of London Proceedings Series A, 467*, 3141–3156. doi:10.1098/rspa.2011.0212.

Podder, A. S. (2011). Tempering of a Mixture of Bainite and Retained Austenite. *Ph.D thesis, University of Cambridge, epartment of Materials Science and Metallurgy*.

Primig, S., & Leitner, H. (2011). Separation of overlapping retained austenite decomposition and cementite precipitation reactions during tempering of martensitic steel by means of thermal analysis. *Thermochimica Acta, 526*(1-2), 111-117. doi:10.1016/j.tca.2011.09.001

Radionov, A. A. (2019). Hardenability of Medium Carbon Cr-Mn-Mo Alloyed Steels. *Materials Science Forum Volume 946*, 341-345.

Rees, G. I., & Shipway, P. H. (1997). Modelling transformation plasticity during the growth of bainite under stress. *Materials Science and Engineering: A, 223*(1-2), 168-178. doi:10.1016/s0921-5093(96)10478-0.

Rementeria, R., Garcia-Mateo, C., & Caballero, F. G. (2018). New Insights into Carbon Distribution in Bainitic Ferrite. *HTM Journal of Heat Treatment and Materials, 73*(2), 68-79. doi:10.3139/105.110351.

Ridley, N. S., H.; Zwell. (1969). Lattice parameters of Fe-C austenite at room temperature. *Trans. Met. Soc. AIME, 245*, 1834–1836.

Rivas, L. M. (2016). Microstructure and mechanical response of nanostructured bainitic steels. *National Center for Metallurgical Research (CENIM-CSIC), Spain, PhD Thesis*.

Ruiz-Jimenez, V., Kuntz, M., Sourmail, T., Caballero, F. G., Jimenez, J. A., & Garcia-Mateo, C. (2020). Retained Austenite Destabilization during Tempering of Low-Temperature Bainite. *Applied Sciences, 10*(24), 8901. Retrieved from https://www.mdpi.com/2076-3417/10/24/8901.

S. Chatterjee, H.-S. W., J. R. Yang & H. K. D. H. Bhadeshia. (2013). Mechanical stabilisation of austenite. *Materials Science and Technology*.

S. Chatterjee, H.-S. W., J. R. Yang and H. K. D. H. Bhadeshia. (2006). Mechanical stabilisation of austenite. *Mater. Sci. Technol, 22*, 641–644.

Saha Podder, A., & Bhadeshia, H. K. D. H. (2010). Thermal stability of austenite retained in bainitic steels. *Materials Science and Engineering: A, 527*(7-8), 2121-2128. doi:10.1016/j.msea.2009.11.063.

Santajuana, Eres, C., Ruiz, J., Allain, Geandier, Caballero, & Garcia, M. (2019). Quantitative Assessment of the Time to End Bainitic Transformation. *Metals, 9*(9). doi:10.3390/met9090925.

Santajuana, M. A., Rementeria, R., Kuntz, M., Jimenez, J. A., Caballero, F. G., & Garcia-Mateo, C. (2018). Low-Temperature Bainite: A Thermal Stability Study. *Metallurgical and Materials Transactions A, 49*(6), 2026-2036. doi:10.1007/s11661-018-4595-2.

Schastlivtsev, V. M., Tabatchikova, T. I., Yakovleva, I. L., Klyueva, S. Y., Kruglova, A. A., Khlusova, E. I., & Orlov, V. V. (2013). Effect of austenite-decomposition temperature on bainite morphology and properties of low-carbon steel after thermomechanical treatment. *The Physics of Metals and Metallography, 114*(5), 419-429. doi:10.1134/s0031918x13050086.

Schicchi, D. S., & Hunkel, M. (2016). Transformation plasticity and kinetic during bainite transformation on a 22MnB5 steel grade. *Materialwissenschaft und Werkstofftechnik, 47*(8), 771-779. doi:10.1002/mawe.201600611.

Sente Software Ltd, U. (Version 9.0). JMarPro the Materials Property Simulation Package.

Seo, S. W., Jung, G. S., Lee, J. S., Bae, C. M., Bhadeshia, H. K. D. H., & Suh, D. W. (2015). Ausforming of medium carbon steel. *Materials Science and Technology, 31*(4), 436-442. doi:10.1179/1743284714Y.0000000574.

Sherif, M., Mateo, C. G., Sourmail, T., & Bhadeshia, H. K. D. H. (2004). Stability of Retained Austenite in TRIP–Assisted Steels. *Materials Science and Technology, 20* 319-322.

Shima, Y., Ishikawa, Y., Nitta, H., Yamazaki, Y., Mimura, K., Isshiki, M., & Iijima, Y. (2002). Self-Diffusion along Dislocations in Ultra High Purity Iron. *Materials Transactions, 43*, 173-177.

Shipway, P. H., & Bhadeshia, H. K. D. H. (1995a). The effect of small stresses on the kinetics of the bainite transformation. *Materials Science and Engineering: A, 201*(1-2), 143-149. doi:10.1016/0921-5093(95)09769-4.

Shipway, P. H., & Bhadeshia, H. K. D. H. (1995b). Mechanical stabilisation of bainite. *Materials Science and Technology, 11*(11), 1116-1128. doi:10.1179/mst.1995.11.11.1116.

Shipway, P. H., & Bhadeshia, H. K. D. H. (2013). Mechanical stabilisation of bainite. *Materials Science and Technology, 11*(11), 1116-1128. doi:10.1179/mst.1995.11.11.1116.

Shirzadi, A. A., Abreu, H., Pocock, L., Klobčuar, D., Withers, P. J., & Bhadeshia, H. K. D. H. (2009). Bainite orientation in plastically deformed austenite. *International Journal of Materials Research, 100*(1), 40-45. doi:10.3139/146.101789.

Shixin XU, W. Y., Shujia LI, Kun WANG, Qisong SUN. (2018). Effects of Pre-Deformation Temperature on Nanobainite Transformation Kinetics and Microstructure. *Acta Metall Sin, 54*(8), 1113-1121. doi:10.11900/0412.1961.2017.00506.

Singh, K., Kumar, A., & Singh, A. (2018). Effect of Prior Austenite Grain Size on the Morphology of Nano-Bainitic Steels. *Metallurgical and Materials Transactions A, 49*(4), 1348-1354. doi:10.1007/s11661-018-4492-8.

Singh, S. B., & Bhadeshia, H. K. D. H. (1996). Quantitative evidence for mechanical stabilization of bainite. *Materials Science and Technology, 12*(7), 610-612. doi:10.1179/mst.1996.12.7.610.

178

Singh, S. B., & Bhadeshia, H. K. D. H. (1998). Estimation of bainite plate-thickness in low-alloy steels. *Materials Science and Engineering: A, 245*(1), 72-79. doi:10.1016/s0921-5093(97)00701-6.

Smokvina Hanza, S., Smoljan, B., Štic, L., & Hajdek, K. (2021). Prediction of Microstructure Constituents' Hardness after the Isothermal Decomposition of Austenite. *Metals, 11*(2), 180. Retrieved from https://www.mdpi.com/2075-4701/11/2/180.

Soliman, M., Mostafa, H., El-Sabbagh, A. S., & Palkowski, H. (2010). Low temperature bainite in steel with 0.26wt% C. *Materials Science and Engineering: A, 527*(29-30), 7706-7713. doi:10.1016/j.msea.2010.08.037.

Soliman, M., & Palkowski, H. (2007). Ultra-fine Bainite Structure in Hypo-eutectoid Steels. *Isij International, 47*(12), 1703-1710. doi:10.2355/isijinternational.47.1703.

Sourmail, T., Otter, L., Collin, S., Billet, M., Philippot, A., Cristofari, F., & Secordel, P. (2021). Direct and indirect decomposition of retained austenite in continuously cooled bainitic steels: Influence of vanadium. *Materials Characterization, 173*, 110922. doi:10.1016/j.matchar.2021.110922.

Spanos, G., Fang, H. S., & Aaronson, H. I. (1990). A mechanism for the formation of lower bainite. *Metallurgical Transactions A, 21*(6), 1381-1390. doi:10.1007/bf02672558.

Spanos, G., Fang, H. S., Sarma, D. S., & Aaronson, H. I. (1990). Influence of carbon concentration and reaction temperature upon bainite morphology in Fe-C-2 Pct Mn alloys. *Metallurgical Transactions A, 21*(6), 1391-1411. doi:10.1007/bf02672559.

Ståhlkrantz, A., Hedström, P., Sarius, N., Sundberg, H.-Å., Kahl, S., Thuvander, M., & Borgenstam, A. (2020). Effect of Tempering on the Bainitic Microstructure Evolution Correlated with the Hardness in a Low-Alloy Medium-Carbon Steel. *Metallurgical and Materials Transactions A, 51*(12), 6470-6481. doi:10.1007/s11661-020-06030-6.

Suh, D.-W., Oh, C.-S., Han, H. N., & Kim, S.-J. (2007). Dilatometric analysis of austenite decomposition considering the effect of non-isotropic volume change. *Acta Materialia, 55*(8), 2659-2669. doi:10.1016/j.actamat.2006.12.007.

Swallow, E., & Bhadeshia, H. K. D. H. (2013). High resolution observations of displacements caused by bainitic transformation. *Materials Science and Technology, 12*(2), 121-125. doi:10.1179/mst.1996.12.2.121.

Takahashi, M., & Bhadeshia, H. K. D. H. (1991). A Model for the Microstructure of Some Advanced Bainitic Steels. *Materials Transactions, JIM, 32*(8), 689-696. doi:10.2320/matertrans1989.32.689.

Talebi, S., Ghasemi-Nanesa, H., Jahazi, M., & Melkonyan, H. (2017). In Situ Study of Phase Transformations during Non-Isothermal Tempering of Bainitic and Martensitic Microstructures. *Metals, 7*(9), 346. doi:10.3390/met7090346.

Talebi, S. H., Jahazi, M., & Melkonyan, H. (2018). Retained Austenite Decomposition and Carbide Precipitation during Isothermal Tempering of a Medium-Carbon Low-Alloy Bainitic Steel. *Materials (Basel, Switzerland), 11*(8), 1441. doi:10.3390/ma11081441.

Tanaka, T., Maruyama, N., Nakamura, N., & Wilkinson, A. J. (2020). Tetragonality of Fe-C martensite – a pattern matching electron backscatter diffraction analysis compared to X-ray diffraction. *Acta Materialia, 195*, 728-738. doi:10.1016/j.actamat.2020.06.017.

Tian, J., Xu, G., Jiang, Z., Wan, X., Hu, H., & Yuan, Q. (2019a). Transformation Behavior and Properties of Carbide-Free Bainite Steels with Different Si Contents. *steel research international, 90*(3). doi:10.1002/srin.201800474.

Tian, J., Xu, G., Jiang, Z., Wan, X., Hu, H., & Yuan, Q. (2019b). Transformation Behavior and Properties of Carbide-Free Bainite Steels with Different Si Contents. *steel research international, 90*(3), 1800474. doi:10.1002/srin.201800474.

Timokhina, I., Beladi, H., Xiong, X., & Hodgson, P. (2011). Effect of Composition and Processing Parameters on the Formation of Nano-Bainite in Advanced High Strength Steels. *Journal of Iron and Steel Research International, 18*, 238-241. Retrieved from <Go to ISI>://WOS:000292229000036.

Timokhina, I. B., Liss, K. D., Raabe, D., Rakha, K., Beladi, H., Xiong, X. Y., & Hodgson, P. D. (2016). Growth of bainitic ferrite and carbon partitioning during the early stages of bainite transformation in a 2 mass% silicon steel studied by in situ neutron diffraction, TEM and APT. *Journal of Applied Crystallography, 49*(2), 399-414. doi:10.1107/s1600576716000418.

Tsuji, N., & Maki, T. (2009). Enhanced structural refinement by combining phase transformation and plastic deformation in steels. *Scripta Materialia, 60*(12), 1044-1049. doi:10.1016/j.scriptamat.2009.02.028.

Tsuzaki, K., Fukasaku, S.-i., Tomota, Y., & Maki, T. (1991). Effect of Prior Deformation of Austenite on the γ→ε Martensitic Transformation in Fe–Mn Alloys. *Materials Transactions, JIM, 32*(3), 222-228. doi:10.2320/matertrans1989.32.222.

Uslu, M. C., Canadinc, D., Lambers, H. G., Tschumak, S., & Maier, H. J. (2011). Modeling the role of external stresses on the austenite-to-bainite phase transformation in 51CrV4 steel. *Modelling and Simulation in Materials Science and Engineering, 19*(4), 045007. doi:10.1088/0965-0393/19/4/045007.

V. Igwemezie, a. C. U. (2014). Development of nanostructured steel for engineering application. *Int. J. Nano and Biomaterials, 5*, 2/3.

van Bohemen, S. M. C. (2013). Bainite and martensite start temperature calculated with exponential carbon dependence. *Materials Science and Technology, 28*(4), 487-495. doi:10.1179/1743284711y.0000000097.

Varshney, A., Sangal, S., Kundu, S., & Mondal, K. (2016). Super strong and highly ductile low alloy multiphase steels consisting of bainite, ferrite and retained austenite. *Materials & Design, 95*, 75-88. doi:10.1016/j.matdes.2016.01.078.

Wang, Y. H., Zhang, F. C., & Wang, T. S. (2013). A novel bainitic steel comparable to maraging steel in mechanical properties. *Scripta Materialia, 68*(9), 763-766. doi:https://doi.org/10.1016/j.scriptamat.2012.12.031.

Williamson, G. K., & Hall, W. H. (1953). X-ray line broadening from filed aluminium and wolfram. *Acta Metallurgica, 1*(1), 22-31. doi:10.1016/0001-6160(53)90006-6.

Williamson, G. K., & Smallman, R. E. (1956). III. Dislocation densities in some annealed and cold-worked metals from measurements on the X-ray debye-scherrer spectrum. *Philosophical Magazine, 1*(1), 34-46. doi:10.1080/14786435608238074.

Wu, B. B., Wang, X. L., Wang, Z. Q., Zhao, J. X., Jin, Y. H., Wang, C. S., Shang, C. J., Misra, R. D. K. (2018). New insights from crystallography into the effect of refining prior austenite grain size on transformation phenomenon and consequent mechanical properties of ultra-high strength low alloy steel. *Materials Science and Engineering: A, 745*, 126-136. doi:10.1016/j.msea.2018.12.057.

Wu, H. D., Miyamoto, G., Yang, Z. G., Zhang, C., Chen, H., & Furuhara, T. (2017). Incomplete bainite transformation in Fe-Si-C alloys. *Acta Materialia, 133*, 1-9. doi:10.1016/j.actamat.2017.05.017.

X.C. Xiong, B. C., M.X. Huang, J.F. Wanga and L. Wang. (2013). The effect of morphology on the stability of retained austenite in a quenched and partitioned steel. *Scripta Materialia 6*.

Xie, Z. J., Ren, Y. Q., Zhou, W. H., Yang, J. R., Shang, C. J., & Misra, R. D. K. (2014). Stability of retained austenite in multi-phase microstructure during austempering and its effect on the ductility of a low carbon steel. *Materials Science and Engineering: A, 603*, 69-75. doi:10.1016/j.msea.2014.02.059.

Y.X. Zhoua, X. T. S., J.W. Lianga, Y.F. Shena,, R.D.K. Misrab. (2018). Innovative processing of obtaining nanostructured bainite with high strength - high ductility combination in low-carbon-medium-Mn steel: Process-structure-property relationship. *Materials Science & Engineering A*.

Yang, & Bhadeshia. (2008). Designing low carbon, low temperature bainite. *Materials Science and Technology, Vol. 24*, 335-342.

Yang, H.-S., & Bhadeshia, H. K. D. H. (2013). Uncertainties in dilatometric determination of martensite start temperature. *Materials Science and Technology, 23*(5), 556-560. doi:10.1179/174328407x176857.

Yang, H., & Bhadeshia, H. (2009). Austenite grain size and the martensite-start temperature. *Scripta Materialia, 60*(7), 493-495. doi:10.1016/j.scriptamat.2008.11.043.

Yi, H. L., Lee, K. Y., & Bhadeshia, H. K. D. H. (2011). Mechanical stabilisation of retained austenite in δ-TRIP steel. *Materials Science and Engineering: A, 528*(18), 5900-5903. doi:10.1016/j.msea.2011.03.111.

Yin, J. (2017). Formation of Bainite in Steels. *PhD Thesis*.

Yin, J., Hillert, M., & Borgenstam, A. (2017). Morphology of Upper and Lower Bainite with 0.7 Mass Pct C. *Metallurgical and Materials Transactions A, 48*(9), 4006-4024. doi:10.1007/s11661-017-4208-5.

Yoozbashi, M. N., Yazdani, S., & Wang, T. S. (2011). Design of a new nanostructured, high-Si bainitic steel with lower cost production. *Materials & Design, 32*(6), 3248-3253. doi:10.1016/j.matdes.2011.02.031.

Young, C. H., & Bhadeshia, H. K. D. H. (1995). Computer Modelling for the Yield Strength of the Mixed Micro-Structures of Bainite and Martensite. *Le Journal de Physique IV, 05*(C8), C8-267-C268-272. doi:10.1051/jp4:1995837.

Zhang, F. C., Yang, Z. N., & Kang, J. (2013). Research progress of bainitic steel used for railway crossing. *Journal of Yanshan University, 37*, 1-7. doi:10.1007/978-3-642-27758-0_1704-5.

Zhang, M., Wang, T. S., Wang, Y. H., Yang, J., & Zhang, F. C. (2013). Preparation of nanostructured bainite in medium-carbon alloy steel. *Materials Science and Engineering: A, 568*, 123-126. doi:10.1016/j.msea.2013.01.046.

Zhang, M., Wang, Y. H., Zheng, C. L., Zhang, F. C., & Wang, T. S. (2014a). Austenite deformation behavior and the effect of ausforming process on martensite starting temperature and ausformed martensite microstructure in medium-carbon Si–Al-rich alloy steel. *Materials Science and Engineering: A, 596*, 9-14. doi:10.1016/j.msea.2013.11.097.

Zhang, M., Wang, Y. H., Zheng, C. L., Zhang, F. C., & Wang, T. S. (2014b). Effects of ausforming on isothermal bainite transformation behaviour and microstructural refinement in medium-carbon Si–Al-rich alloy steel. *Materials & Design 62*, 168-174. doi:10.1016/j.matdes.2014.05.024.

Zhang, M. X., & Kelly, P. M. (1998). Determination of Carbon Content in Bainitic Ferrite and Carbon Distribution in Austenite by Using CBKLDP. *Materials Characterization, 40*(3), 159-168. doi:10.1016/s1044-5803(98)00005-9.

Zhao-Dong Li , Z.-G. Y., Chi Zhang, Zhen-Qing Liu. (2010). Influence of austenite deformation on ferrite growth in a Fe–C–Mn alloy. *Materials Science and Engineering A*.

Zhao, J., Jia, X., Guo, K., Jia, N. N., Wang, Y. F., Wang, Y. H., & Wang, T. S. (2017). Transformation behavior and microstructure feature of large strain ausformed low-temperature bainite in a medium C - Si rich alloy steel. *Materials Science and Engineering: A, 682*, 527-534. doi:10.1016/j.msea.2016.11.073.

Zhao, J., Liu, D., Li, Y., Yang, Y., Wang, T., & Zhou, Q. (2020). Microstructure and Mechanical Properties of Tempered Ausrolled Nanobainite Steel. *Crystals, 10*(7), 573. Retrieved from https://www.mdpi.com/2073-4352/10/7/573.

Zhao, J. Z., Fucheng; Lv, Bo; Yang, Zhinan; Chen, Chen; Long, Xiaoyan; Zhao, Xiaojie; Chu, Chunhe. (2019). Inconsistent effects of austempering time within transformation stasis on monotonic and cyclic deformation behaviors of an ultrahigh silicon carbide-free nanobainite steel. *Materials Science and Engineering: A, 751*, 80-89. doi:10.1016/j.msea.2019.01.100.

Zhao, L., Qian, L., Liu, S., Zhou, Q., Meng, J., Zheng, C., & Zhang, F. (2016). Producing superfine low-carbon bainitic structure through a new combined thermo-mechanical process. *Journal of Alloys and Compounds, 685*, 300-303. doi:10.1016/j.jallcom.2016.05.281.

Zhao, L., Qian, L., Meng, J., Zhou, Q., & Zhang, F. (2016). Below-Ms austempering to obtain refined bainitic structure and enhanced mechanical properties in low-C high-Si/Al steels. *Scripta Materialia, 112*, 96-100. doi:10.1016/j.scriptamat.2015.09.022.

Zhao, L., Qian, Lihe, Zhou, Qian, Li, Dongdong, Wang, Tongliang, Jia, Zhigeng, Zhang, Fucheng, Meng, Jiangying. (2019). The combining effects of ausforming and below-Ms or above-Ms austempering on the transformation kinetics, microstructure and mechanical properties of low-carbon bainitic steel. *Materials & Design, 183*. doi:10.1016/j.matdes.2019.108123.

Zhi, C., Zhao, A., He, J., Yang, H., & Qi, L. (2016). *Effects of the multi-step ausforming process on the microstructure evolution of nanobainite steel.* Paper presented at the International Conference on Advanced Materials, Structures and Mechanical Engineering, ICAMSME 2015, May 29, 2015 - May 31, 2015, Incheon, Korea, Republic of.

Zhou, M.-x., Xu, G., Wang, L., Xue, Z.-l., & Hu, H.-j. (2015). Comprehensive analysis of the dilatation during bainitic transformation under stress. *Metals and Materials International, 21*(6), 985-990. doi:10.1007/s12540-015-2348-y.

Zhou, M., Xu, G., Hu, H., Yuan, Q., & Tian, J. (2018). Kinetics model of bainitic transformation with stress. *Metals and Materials International, 24*(1), 28-34. doi:10.1007/s12540-017-7261-0.

Zhou, M., Xu, G., Wang, L., & Yuan, Q. (2016). The Varying Effects of Uniaxial Compressive Stress on the Bainitic Transformation under Different Austenitization Temperatures. *Metals, 6*(5). doi:10.3390/met6050119.

Zorgani, M., Garcia-Mateo, C., & Jahazi, M. (2020). The role of ausforming in the stability of retained austenite in a medium-C carbide-free bainitic steel. *Journal of Materials Research and Technology, 9*(4), 7762-7776. doi:10.1016/j.jmrt.2020.05.062.